New System Control Methodologies: Adapting AGC and Other Generator Controls to the Restructured Environment

Final Project Report

Power Systems Engineering Research Center

A National Science Foundation
Industry/University Cooperative Research Center
since 1996

Power Systems Engineering Research Center

New System Control Methodologies: Adapting AGC and Other Generator Controls to the Restructured Environment

Final Project Report

Report Compiled and Edited by:

Christopher L. DeMarco
University of Wisconsin-Madison

Faculty Contributors:

M.A. Pai
University of Illinois, Urbana/Champaign;
C.L. DeMarco, I. Hiskens and I. Dobson
University of Wisconsin-Madison

Graduate Student Contributors:

V. Donde, A.S. Nayak,
University of Illinois, Urbana/Champaign;
B. Huber, S. Tiptipakorn
University of Wisconsin-Madison

PSERC Publication 05-64

November 2005

Information about this project

For information about this project contact:

Christopher L. DeMarco
Electrical and Computer Engineering
University of Wisconsin-Madison
1415 Engineering Drive
Madison, WI 53706
Phone: 608-262-5546
Fax: 608-262-1267
Email: demarco@engr.wisc.edu

Power Systems Engineering Research Center

This is a project report from the Power Systems Engineering Research Center (PSERC). PSERC is a multi-university Center conducting research on challenges facing a restructuring electric power industry and educating the next generation of power engineers. More information about PSERC can be found at the Center's website: http://www.pserc.org.

For additional information, contact:

Power Systems Engineering Research Center
Cornell University
428 Phillips Hall
Ithaca, New York 14853
Phone: 607-255-5601
Fax: 607-255-8871

Notice Concerning Copyright Material

Acknowledgements

This is the final report for the Power Systems Engineering Research Center project “New System Control Methodologies” (PSERC project S-6). This is a System Research Stem project.

We express our appreciation for the support provided by the PSERC industrial members and by the National Science Foundation under grant NSF EEC-0119230 received from the Industry / University Cooperative Research Center program.

Executive Summary

As the US moves towards competitive markets in electric power generation, the shift of ownership and operational control of generation from the vertically integrated utilities to independent, for-profit generation owners has raised a number of fundamental issues regarding grid control. Questions concerning appropriate generator control loop functionality to meet grid-wide objectives, while simultaneously enabling full profit potential for individual generator owners, have not been fully answered more than a decade into North America's experience in electric utility restructuring.

Generators remain the fundamental control resource for achieving system-wide frequency regulation, stable electromechanical dynamic response, and, to a lesser degree, voltage control. In working toward appropriate functionality, the goal should be to develop practical generator feedback controls that maximize a generator's contributions to the system-wide control objectives while minimally conflicting with that generator's profit-making, energy production activities. Remaining issues relate to the creation of generator control designs that are more appropriate to the new operational objectives of a restructured power network. Generator control designs needs to address (1) regulation of bilateral transactions, (2) the interplay of generation controls with grid congestion management, and (3) the need for large numbers of distributed, potentially intermittently-connected generators to "do no evil" with respect to stable, system-wide electromechanical response.

In this project, we modified the traditional "Automatic Generation Control (AGC)" to accommodate bilateral transactions. Specific reconfiguration of the area control area functionality in AGC was developed so that area interchange error signals could be supplemented to account for imbalances in multiple, point-to-point bilateral transactions. As might be expected, the finer granularity required to maintain regulation on multiple bilateral transactions requires monitoring of a greater number of control error signals along with greater diversity in generation setpoint-update capability. However, our design demonstrated that the functionality of tracking bilateral transactions can successfully be incorporated in an "AGC-like" control structure. We anticipate that such functionality could be added to existing control center software with fairly minimal modifications. In general, the designs developed in the project provide a practical roadmap for specifying this enhanced functionality to software vendors.

We also developed an algorithm to automate a generator's contribution to relieving grid congestion. The algorithm is based upon control signals that supplement direct market prices as incentives for redispatch of generation. The redispatch signals are based on the gradient directions that are locally optimal in "backing off" from active line flow constraints in an Optimal Power Flow (OPF). While this approach is conceptually straightforward, it was still necessary to develop a computationally efficient method for extracting such information in an operational time frame. We demonstrate our approach using the IEEE 14-bus test system. The new algorithm could be further developed for implementation in control center software.

There is an implementation issue of the OPF-based congestion relief algorithm in a very large-scale, interconnected control area. Even with the advanced computational approach developed in the congestion relief algorithm, its OPF-based approach might become computationally impractical in very large-scale control areas being considered for North American operations under Regional Transmission Operators. Anticipating this challenge, we developed a partitioning scheme for decomposing the OPF-based computations into a sequence of computations over smaller portions of the network. Building upon existing coherency and

synchrony-based partitioning techniques that focus on frequency, angle, and active power deviations, we developed an extension for partitioning that incorporated reactive power flows and bus voltage magnitude variations. Given the very novel nature of this approach, we conducted a computational demonstration of the partitioning algorithm's effectiveness. A research-grade software package was created in the MATLAB environment, building on *MATPOWER*, Power Systems Engineering Research Center's MATLAB-based power flow and OPF code. Full source code and documentation for this OPF-partitioning software is provided in the final project report.

In the years to come there will be a growing need for small-scale generators (i.e., distributed generation) to have controllers that will allow the generators to participate in meeting system stability objectives . We created a framework for standardized design of fast-time scale governor controllers for such generators. The approach was to develop controllers for small-scale generators so that the generators would not degrade the network's small-signal electromechanical stability as the number of on-line generators grows. The approach uses the well-established Linear-Quadratic-Regulator (LQR) controller design methodology, with an added constraint placed on the controllers to guarantee that their interconnection with generator dynamics is passive. We simulated use of the controllers with the IEEE 14-bus test system. This initial investigation suggested that a relatively small degree of frequency regulation performance is sacrificed in exchange for this standardized, guaranteed stable behavior. This contribution of the project is an initial feasibility study into a new class of controller designs for distributed generation. More development work could proceed to more thorough simulation of the governor control designs, with subsequent progression to hardware implementation and testing on grid-connected, small-scale, distributed generation units.

Table of Contents

Table of Contents (continued)

Table of Contents (continued)

List of Figures

List of Figures (continued)

List of Tables

List of Tables (continued)

1. Generation Control in a Restructured Environment

1.1 Background and Motivation

As the US moves towards competitive markets in electric power generation, the shift of ownership and operational control of generation from the vertically integrated utilities to independent, for-profit generation owners has raised a number of fundamental questions regarding grid control. Some of the questions relating to appropriate generator control loop functionality are still not completely answered, more than a decade into North America's experience in electric utility restructuring. Generators remain the fundamental control resource for achieving system wide goals of frequency regulation, stable electromechanical dynamic response, and to a lesser degree, voltage control. In broad terms, the goal is development of practically implementable feedback controls that maximize a generator's contributions to these system-wide control objectives, while minimally conflicting with generators' primary profit making activity of producing energy. Key questions relate to the creation of generator control designs that are more appropriate to the new operational objectives of a restructured power network, including the control of bilateral transactions, the interplay of generation controls with congestion relief in the grid, and the need for large numbers of distributed, potentially intermittently connected generators to "do no evil" with respect to stable system-wide electromechanical response.

Contributions Reported in this Work

The first area of investigation concerned modification to traditional "Automatic Generation Control (AGC)" to accommodate bilateral transactions. In this aspect of the work, specific reconfiguration of the area control area functionality in AGC is proposed, in such a way that area interchange error signals can be supplemented to account for imbalances in multiple point-to-point, bilateral transactions. As might be expected, the finer granularity required to maintain regulation on multiple bilateral transactions requires a greater number control error signals to be monitored, with greater diversity in generation setpoint update capability. However, the design proposed here demonstrates that the functionality of tracking bilateral transactions can successfully be incorporated in an "AGC-like" control structure.

The report next turns to methodologies to automate generators' contributions to network congestion relief. The approach employed is based upon control signals to supplement direct market price outcomes, where these signals seek to incentive redispatch of generation. The direction of redispatch is obtained from gradient directions that are locally optimal in "backing off" from active line flow constraints in an Optimal Power Flow (OPF). While conceptually straightforward, this work demonstrates a computationally efficient method for extracting such information in an operational timeframe. The approach is demonstrated in the context of the IEEE 14 bus test system. However, even with the advanced computational approach advocated, there remains concern that an OPF-based approach for congestion relief might become computationally impractical in the very large scale ISO's and RTO being considered for North American operations. Anticipating this challenge, work under this project also considered a partitioning scheme for decomposing the OPF-based computations into a sequence of computations over smaller portions of the network. Building upon existing coherency and synchrony based partitioning techniques, an extension to incorporate consideration of reactive power flows and bus voltage magnitude variations was developed.

The final contribution of the report addresses a problem we anticipate to become increasingly relevant with penetration of large numbers of small-scale generators; e.g., distributed generation. We develop a framework for standardized design of fast-time scale governor controllers. The basic premise is to develop controllers with the property that successive additions of any number of such small generators with these designs can be guaranteed not to detract from the small-signal electromechanical stability of the network. The approach uses the standard Linear-Quadratic-Regulator (LQR) linear controller design methodology, with an added constraint placed on the controllers to guarantee that their interconnection with generator dynamics is passive. Our sample designs for the IEEE 14 bus test system suggest that a relatively small degree of regulation performance is sacrificed in exchange for this standardized, guaranteed stable behavior.

1.2 Organization of the Report

The report is organized into five chapters, representing each of the major thrusts of contribution in the work. Chapter Two addresses the redesign of traditional AGC to accommodate bilateral transactions. Chapter Three describes the use of generation redispatch for automated congestion relief, based upon price signals obtained from an optimal power flow (OPF) formulation. Anticipating the challenges in employing an OPF-based control methodology in the operation of very large scale ISO's and RTO's, Chapter Four addresses the extension of coherency-based methods of network partitioning to account for reactive power flows and bus voltage magnitude variations, with the goal of partitioning into smaller sub-problems the calculations necessary for Chapter Three's techniques. Finally, Chapter Five considers the impact of generation controls on network-wide electromechanical dynamics. Recognizing concerns that increasing penetration of distributed generation will mean large numbers of smaller units that may connect and disconnect from the grid intermittently, this chapter's premise is that such distributed generators' governors will need a standardized design. In particular, we anticipate such units should possess faster time scale controls such that connecting/disconnecting any set of units can be guaranteed to "do-no-evil" with regard to electromechanical stability. The approach described in that chapter examines modification of well-known LQR design techniques, applied to generator governor design, with the novelty that passivity constraints are imposed on the resulting generator/controller input/output characteristic, to guarantee that connection to the network should not undermine system-wide electromechanical small-signal stability.

2. Automatic Generation Control (AGC) Adapted to a Restructured Power Systems Operating Environment

2.1 The Need for AGC Redesign

In a restructured power system environment, allowing independent, competitive generating units the flexibility to enter into bilateral contracts raises new engineering issues in planning and operation, even though the underlying physical behavior of units and the operational goals for the system operator remain essentially the same. With the emergence of the distinct identities of GENCOs, TRANSCOs, DISCOs and the ISO, many of the ancillary services of a vertically integrated utility will have a different role to play and hence have to be modeled differently. Among these ancillary services is the automatic generation control (AGC). In the new scenario, a DISCO can contract individually with a GENCO for power and these transactions are done under the supervision of the ISO.

In this chapter, we formulate the two area dynamic model following the ideas presented by Kumar et al [1], [2]. Specifically we focus on the dynamics and trajectory sensitivities. The concept of a DISCO participation matrix (DPM) is proposed which helps the visualization and implementation of the contracts. The information flow of the contracts is superimposed on the traditional AGC system and the simulations reveal some interesting patterns. The trajectory sensitivities are helpful in studying the effects of parameters as well as in optimization of the ACE parameters viz. tie line bias and frequency bias parameters K and B respectively. The traditional AGC is well discussed in the papers of Elgerd and Fosha [3], [4] as well as in text-books [5], [6], [7]. Research work in deregulated AGC is contained in [1], [2], [8], [9].

This chapter is organized as follows. In section 2, we explain how the bilateral transactions are incorporated in the traditional AGC system leading to a new block diagram. Simulation results are presented in section 3. In section 4, we discuss trajectory sensitivities and the optimization of K and B parameters using these sensitivities. Section 5 presents conclusions.

2.2 Traditional Versus New AGC

There is a wealth of analyses available in the literature on traditional AGC. In a traditional power system structure, the generation, transmission and distribution is owned by a single entity called 'Vertically Integrated Utility' (VIU) which supplies power to the customers at regulated rates. The definition of a control area is somewhat determined by the pooling arrangements of utilities. Sometimes the physical boundaries of a VIU define a control area. All such control areas are interconnected by tie lines.

It is a primary goal of the AGC to control the tie line power flow at the scheduled value defined by the contracts among various VIUs, to maintain a generation equal to the local load, thus controlling the frequencies of the control areas as close to the nominal value as possible during normal load changes. In cases of loss of generation in an area the neighboring utility will come to help it. In the classical AGC system, this balance is achieved by detecting the frequency and tie line power deviations to generate the ACE (area control error) signal which is in turn utilized in the integral feedback control strategy as shown in the block diagram (Figure 1) for a two-area system. It should be noted that this is a linearized model of the AGC, hence is based on an assumption that the frequency and tie line power deviations are small.

During a sudden load change within an area, the frequency of that area experiences a transient drop. A generator in each area is designated to be on regulation to meet this change in load in steady state. In the transient state there will be power flows from other areas to this area to supply excess load. Here, the feedback mechanism comes into play and generates appropriate raise/lower signals to the turbines to make generation follow the load. In the steady state, the generation is exactly matched with the load, driving the tie line power and frequency deviations to zero. The area control error (ACE) vanishes in the steady state. This system has performed exceedingly well in the past.

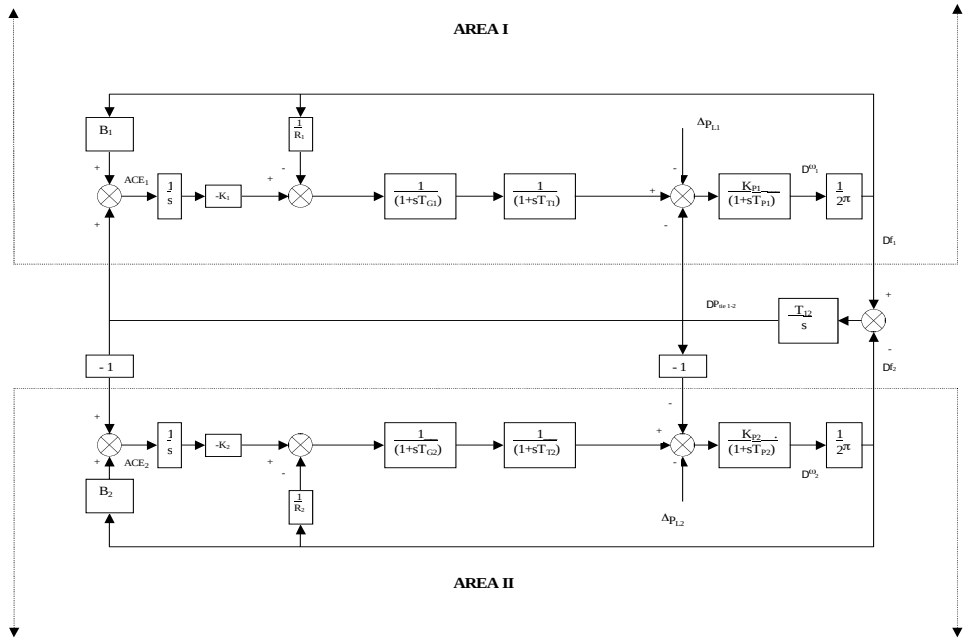

Figure 2-1: Two area system (traditional scenario)

In a competitive market structure, vertically integrated utilities no longer exist. The utilities do not own generation-transmission-distribution any more, instead there are three different entities viz. GENCOs (generation companies), TRANSCOs (transmission companies) and DISCOs (distribution companies). GENCOs can be imagined to be at par with 'independent power producers' (IPPs) and they compete with each other to sell the power they produce. TRANSCOs are accessible to any GENCO or DISCO for wheeling of power. Again, a control area is defined by physical boundaries as before, but now, a DISCO has the freedom to contract with any GENCO, in its own area or otherwise for a transaction of power with a GENCO in another area. This is called a 'bilateral transaction'. All the transactions have to be cleared by the ISO [10].

There can be various combinations of contracts between DISCOs and GENCOs which can be conveniently visualized by the concept of a 'DISCO participation matrix' (DPM). The rows of a DPM correspond to GENCOs and columns to DISCOs which contract power. Each entry in this matrix can be thought as a fraction of a total load contracted by a DISCO (column) towards a GENCO (row). The sum of all the entries in a column in this matrix is unity e.g. for a two-area system, DPM will have the structure that follows.

$$
\begin{array}{cc}
 & \begin{array}{cccc} \mathbf{1} & \text{DISCO} & & \mathbf{4} \end{array} \\
\begin{array}{c} \\ 1 \\ 2 \\ 3 \\ 4 \end{array} & \left[\begin{array}{c:ccc} cpf_{11} & cpf_{12} & cpf_{13} & cpf_{14} \\ cpf_{21} & cpf_{22} & cpf_{23} & cpf_{24} \\ cpf_{31} & cpf_{32} & cpf_{33} & cpf_{34} \\ \hdashline cpf_{41} & cpf_{42} & cpf_{43} & cpf_{44} \end{array}\right] \begin{array}{l} \\ \\ \\ \\ \text{GENCO} \end{array}
\end{array}
$$

Area 1

Area 2

where cpf_{jd} = Contract Participation factor of j^{th} GENCO in the load following of d^{th} DISCO. DPM shows the participation of a DISCO in a contract with any GENCO, hence the name Disco Participation Matrix.

As any entry in a DPM corresponds to a contracted load by a DISCO, it must be demanded from the corresponding GENCO involved in the contract and should be reflected in the control loop. Whenever a load change takes place in this new restructured system, it is felt in its own area as in the traditional case, but *as defined by the contractual agreement* (hence DPM), only a particular GENCO must follow the load change demanded by a particular DISCO. Thus, information signals must flow from the DISCOs to the GENCOs specifying corresponding demands. This introduces new information signals which were absent in the traditional scenario. These signals carry information as to '*which* GENCO has to follow a load demanded by *which* DISCO'. Also, for those DISCOs having a contract with GENCOs *NOT* in their area, demand signals must adjust the scheduled flow over the tie lines. This change in scheduled flow produces a tie line power error which is used to derive ACEs for the control areas involved. Based on all abovementioned ideas, a block diagram for an AGC in a deregulated system can be conceptualized and depicted as in Figure 2. Structurally it is based upon the idea of [1]. Dashed lines show the demand signals.

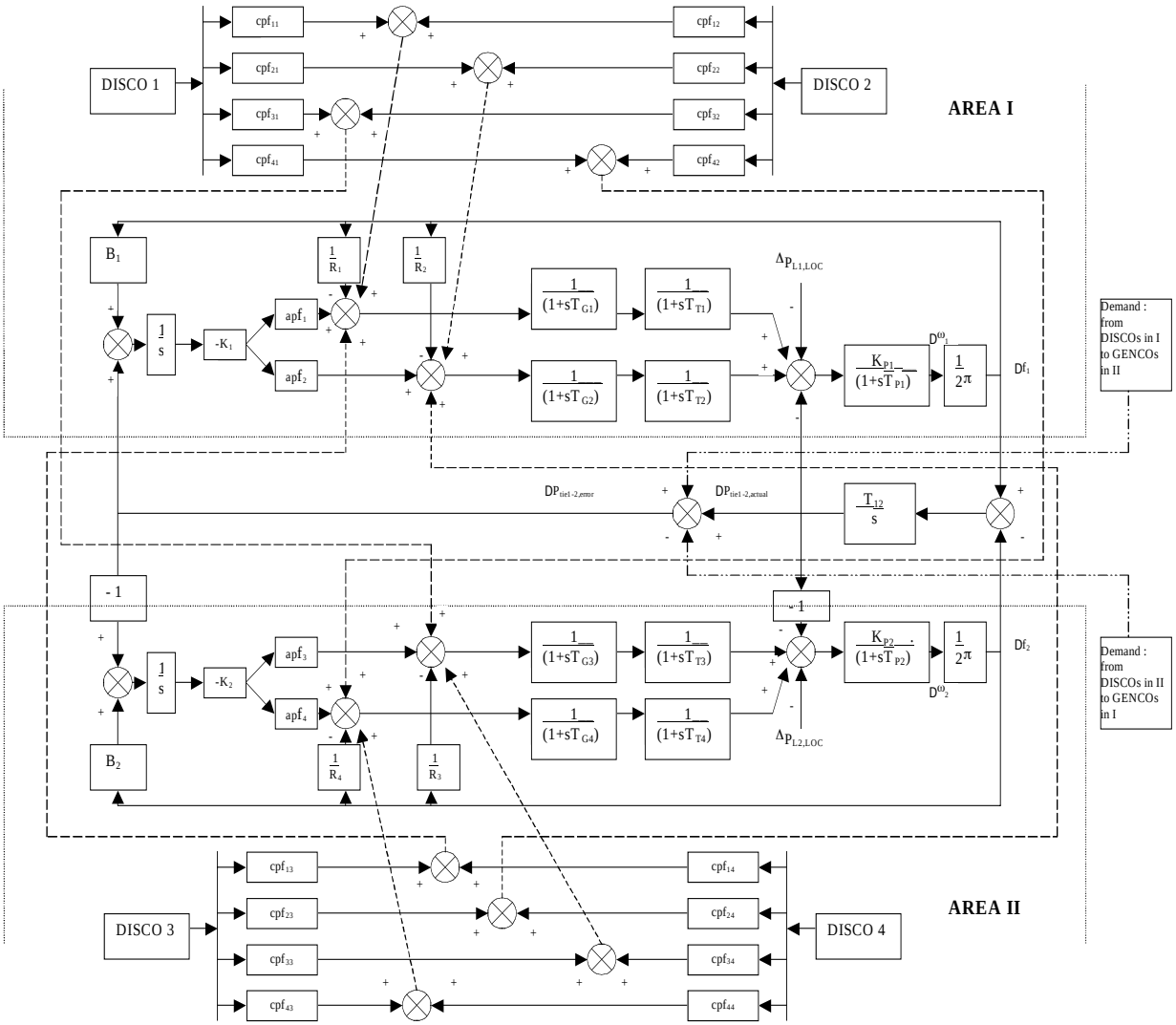

Figure 2-2: Two area system (deregulated scenario)

2.3 Simulation Results of Two-Area System in the Deregulated Environment

A two-area system is used to illustrate the behavior of the proposed AGC scheme. The data for this system is taken from [3].

2.3.1 Case 1: Base case

Consider a case where the GENCOs in each area participate equally in AGC, i.e., ACE participation factors are $apf_1 = 0.5$, $apf_2 = 1 - apf_1 = 0.5$; $apf_3 = 0.5$, $apf_4 = 1 - apf_3 = 0.5$.

Assume that the load change occurs only in area I. Thus, the load is demanded only by $DISCO_1$ and $DISCO_2$. Let the value of this load perturbation be 0.1 pu MW for each of them.

$$\mathbf{DPM} = \left[\begin{array}{cc:cc} 0.5 & 0.5 & 0 & 0 \\ 0.5 & 0.5 & 0 & 0 \\ 0 & 0 & 0 & 0 \\ \hdashline 0 & 0 & 0 & 0 \end{array}\right]$$

Note that as $DISCO_3$ and $DISCO_4$ do not demand from any GENCOs, corresponding participation factors (columns 3 and 4) are zero. $DISCO_1$ and $DISCO_2$ demand identically from their local GENCOs viz. $GENCO_1$ and $GENCO_2$. The frequency deviations in area I and II, actual tie line power flow in a direction from area I to area II and the generated powers of various GENCOs following a step change in the loads of $DISCO_1$ and $DISCO_2$ are shown in figures 2.3.A, 2.3.B and 2.3.C respectively.

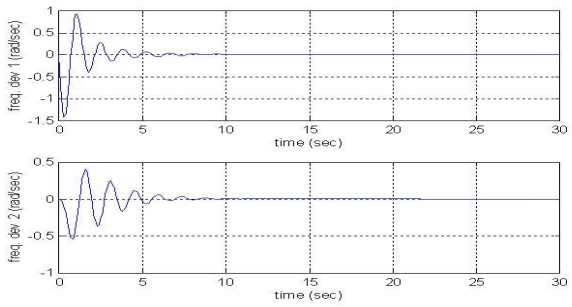

Figure 2.3.A

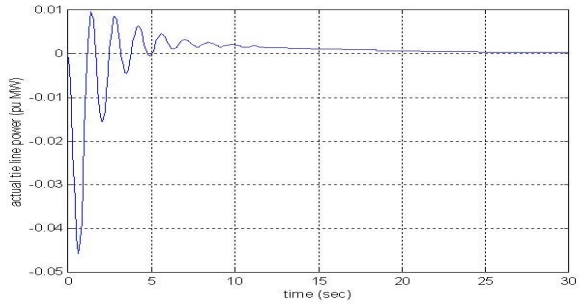

Figure 2.3.B

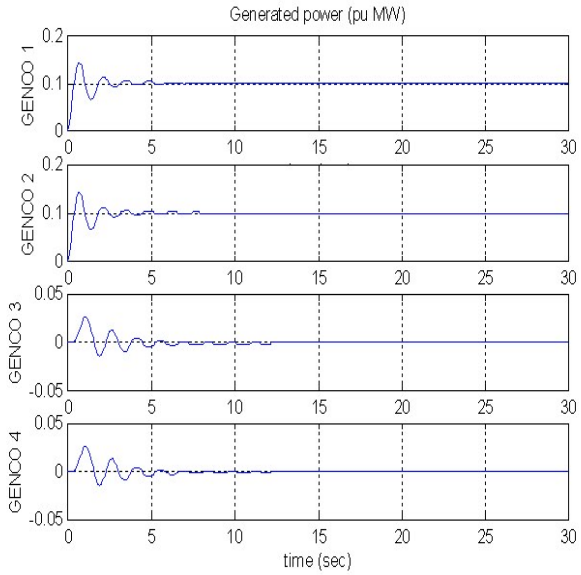

Figure 2.3.C

Figure 2-3: Base case simulation

The tie line power goes to zero in the steady-state as there are no contracts of the DISCOs in one area with the GENCOs in other areas. In the steady state, the generation of each GENCO matches the demand of the DISCOs in contract with it. e.g. $GENCO_1$ generates

$$\sum_{d=1}^{4} (pu\_MW\_load\_of\_DISCO\_'d')*cpf_{1,d} = 0.1pu$$

As $GENCO_3$ and $GENCO_4$ are not contracted by any DISCOs, their generation change is zero in the steady state.

2.3.2 Case 2: Individual DISCO Contratcs

Consider a case where all the DISCOs contract with the GENCOs for power as per the following DPM,

$$\mathbf{DPM} = \left[\begin{array}{cccc} 0.5 & 0.25 & 0 & 0.3 \\ 0.2 & 0.25 & 0 & 0 \\ 0 & 0.25 & 1 & 0.7 \\ \hdashline 0.3 & 0.25 & 0 & 0 \end{array}\right]$$

Assume that the total load of each DISCO is perturbed by 0.1 pu and each GENCO participates in AGC as defined by following apfs:

$$apf_1=0.75, apf_2=1-apf_1=0.25;\ apf_3=0.5,\ apf_4=1-apf_3=0.5$$

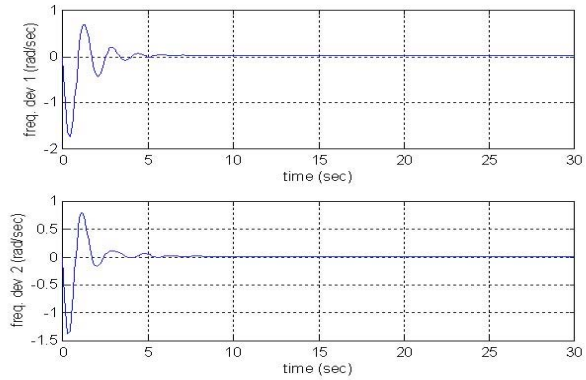

Figure 2.4.A

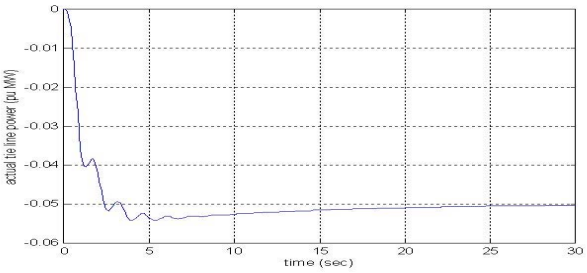

Figure 2.4.B

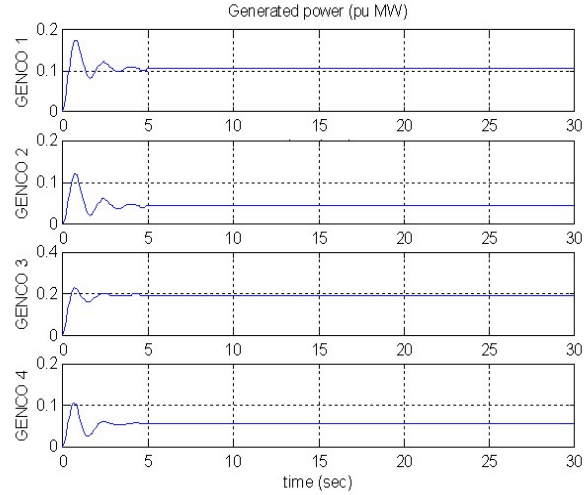

Figure 2.4.C

Figure 2-4: Simulation with demand from DISCOs

DISCOs in area I demand 0.08 pu MW from the GENCOs in area II. (This is obtained by summing the entries in the lower left block of the DPM matrix.) Likewise, DISCOs in area II demand 0.03 pu MW from the GENCOs in area I. (This is given by the top right block of the DPM matrix.) The tie line power settles down to the net scheduled value viz. 0.05 pu MW from

area II to area I (Figure 4.B). Again, as in the base case, GENCOs generate power equal to the contracted demands of the DISCOs. (Figure 4.C).

2.3.3 Case 3: Contract violation

Consider case 2 again except that $DISCO_1$ demands an additional 0.1 pu MW which is not contracted out to any GENCO.

The uncontracted load of $DISCO_1$ reflects in the generations of $GENCO_1$ and $GENCO_2$. Thus, this excess load is taken up by the GENCOs in the same area as that of the DISCO making the uncontracted demand. $GENCO_3$ and $GENCO_4$ generate to satisfy their own demands as in case 2 and are not affected by this excess load (Figure 2.5).

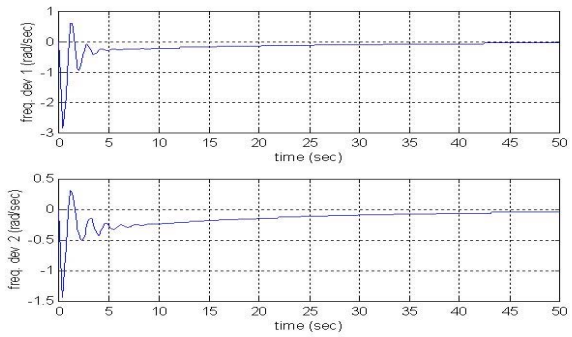

Figure 2.5.A

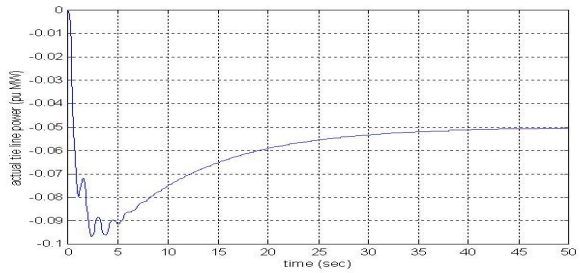

Figure 2.5.B

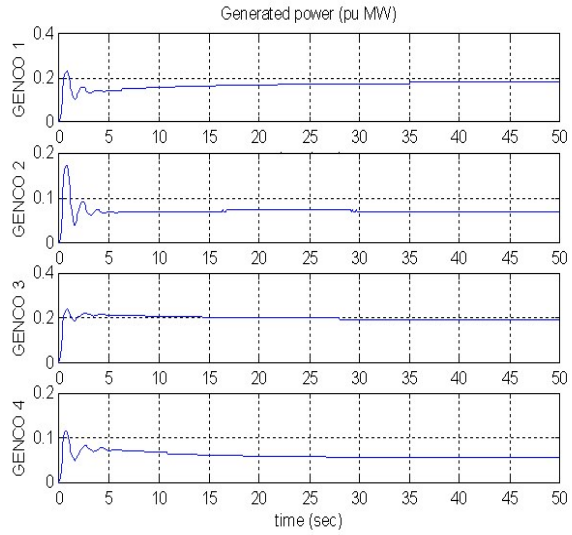

Figure 2.5.C

Figure 2-5: Two area system (deregulated scenario)

2.4 Trajectory Sensitivities and Optimization

The two-area system in the deregulated case with identical areas can be optimized with respect to system parameters to obtain the best response. Figure 2.2 showed a closed loop system with feedback that is derived from the states of frequency deviations and the tie line power flow deviation. The parameters involved in the feedback are the integral feedback gains (K_1=K_2=K) and the frequency bias (B_1=B_2=B). The optimal values of K and B depend on the cost function used for optimization [11]. The integral of square error criterion is chosen for this case [3],

$$C = \int_0^\infty [\alpha(\Delta P_{tie,error})^2 + \beta(\Delta f_1^{\,2})]dt$$

The 'equi-B' cost curves can be plotted as shown in Figure 2.6 assuming α=1 and β=1. The optimum values of K and B correspond to the point where the curves reach the minimum.

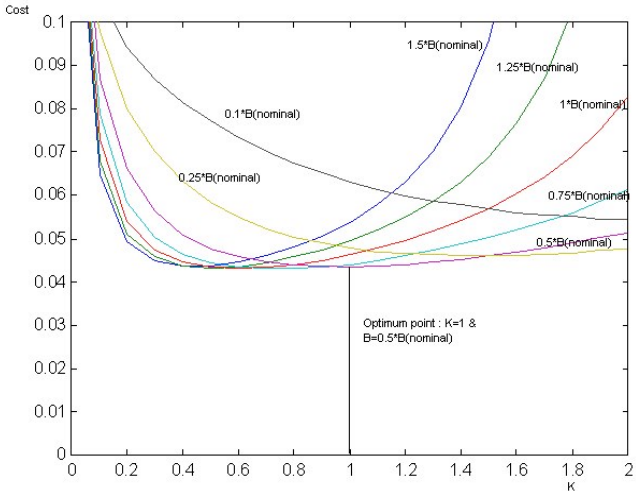

Figure 2-6: 'Equi-B' cost curves

The cost curves in Figure 2.6 correspond to the case of AGC in the deregulated environment where $DISCO_1$ and $DISCO_2$ contract to have 0.05 pu MW equally from the local GENCOs. Thus, the contracted load perturbation in area I is 0.1 pu MW. $DISCO_1$ demands an excess (uncontracted) load of 0.1 pu MW. $DISCO_3$ and $DISCO_4$ do not have contracts with any GENCO. The cost function is plotted against K for various values of B to obtain equi-B curves as shown in Figure 6. It is found that the optimum values of the parameters K and B are consistent with those obtained from the optimization of the case of two-area traditional AGC

system i.e., the two-area system in the 'Vertically Integrated Utility' environment with only one generating unit in each area [3].

The optimal parameter values given above were obtained by evaluating the cost function for many sets of parameter values. A more systematic approach to the optimization can be achieved by using trajectory sensitivities in conjunction with a gradient type Newton algorithm.

The closed loop system of the form in Figure 1 or Figure 2 can be characterized in the state-space as follows.

$$\dot{x} = A^{cl} x + B^{cl} u \tag{2.1}$$

where

x: states
A^{cl}: closed loop A matrix
B^{cl}: closed loop B Matrix
u: pu MW load change of DISCOs

Differentiating with respect to a parameter λ,

$$\dot{x}_{\lambda} = (A^{cl})_{\lambda} x + A^{cl} (x)_{\lambda} + (B^{cl})_{\lambda} u \tag{2.2}$$

where the subscript 'λ' denotes a derivative. Equations (2.1) and (2.2) can be solved simultaneously to obtain trajectory sensitivities x_{λ}.

2.4.1 Gradient type Newton algorithm

Optimization of the deregulated AGC system used trajectory sensitivities in the following way:

$$\lambda = [\ K \quad B\ ]^T \qquad \text{(parameter vector)}$$

$$C = \int_0^{\infty} [\alpha(\Delta P_{tie,error})^2 + \beta(\Delta f_1^{\ 2})] dt \qquad \text{(the cost function)}$$

$$\lambda_o = [\ K_o \quad B_o]^T \qquad \text{(guess values)}$$

Do until converged with required accuracy:

1. Using the latest λ, simulate the system along with trajectory sensitivities i.e.,

   $$\frac{\partial \Delta P_{tie,error}}{\partial K}, \frac{\partial \Delta f_1}{\partial K}, \frac{\partial \Delta P_{tie,error}}{\partial B}, \frac{\partial \Delta f_1}{\partial B}$$

   to obtain

   $$\frac{\partial C}{\partial K} = 2\int_0^\infty (\alpha.\Delta P_{tie,error}.\frac{\partial \Delta P_{tie,error}}{\partial K} + \beta.\Delta f_1.\frac{\partial \Delta f_1}{\partial K})dt$$
   $$\frac{\partial C}{\partial B} = 2\int_0^\infty (\alpha.\Delta P_{tie,error}.\frac{\partial \Delta P_{tie,error}}{\partial B} + \beta.\Delta f_1.\frac{\partial \Delta f_1}{\partial B})dt$$

2. Form,

   $$\nabla f(\lambda) = \left[\frac{\partial C}{\partial K} \quad \frac{\partial C}{\partial B}\right]^T$$
   $$H_f(\lambda) = \begin{bmatrix} \frac{\partial^2 C}{\partial K^2} & \frac{\partial}{\partial B}(\frac{\partial C}{\partial K}) \\ \frac{\partial}{\partial K}(\frac{\partial C}{\partial B}) & \frac{\partial^2 C}{\partial B^2} \end{bmatrix}$$

3. Update parameters,

   $$\lambda = \lambda - [H_f(\lambda)]^{-1}.\nabla f(\lambda)$$

End

When this procedure is applied to the two-area system in the deregulated case, the optimum values of the parameters match with those obtained by plotting 'equi-B' cost curves. This 'trajectory sensitivity approach' to optimization will be useful for any general control strategy, particularly when nonlinearities are involved.

2.5 Conclusions on AGC Redesign for a Restructured Environment

AGC provides a relatively simple, yet extremely effective method of adjusting generation to minimize frequency deviations and regulate tie-line flows. This important role will continue in restructured electricity markets. However some important modifications are necessary to cater for bilateral contracts that span control areas.

Bilateral contracts can exist between DISCOs in one control area and GENCOs in other control areas. The scheduled flow on a tie-line between two control areas must exactly match the net sum of the contracts that exist between market participants on opposite sides of the tie-line (taking account of contract directions). If a contract is adjusted, the scheduled tie-line flow must be adjusted accordingly.

A key concept in the work here is that of the ‘DISCO Participation Matrix’ (DPM. The DPM provides a compact yet precise way of summarizing bilateral contractual arrangements. The modeling of AGC in a restructured environment must take account of the information flow relating to bilateral contracts. Clearly, contracts must be communicated between DISCOs and GENCOs. As demonstrated here, it is also important that information regarding contracts is taken into account in establishing/adjusting the tie-line setpoints.

3. Congestion Management in the Restructured Power Systems Environment – An Optimal Power Flow Framework

3.1 Problem Motivation and Chapter Organization

The restructuring of the electric power industry has involved paradigm shifts in the real-time control activities of the power grids. Managing dispatch is one of the important control activities in a power system. Optimal power flow (OPF) has perhaps been the most significant technique for obtaining minimum cost generation patterns in a power system with existing transmission and operational constraints. The role of an independent system operator in a competitive market environment would be to facilitate the complete dispatch of the power that gets contracted among the market players. With the trend of an increasing number of bilateral contracts being signed for electricity market trades, the possibility of insufficient resources leading to network congestion may be unavoidable. In this scenario, congestion management (within an OPF framework) becomes an important issue. Real-time transmission congestion can be defined as the operating condition in which there is not enough transmission capability to implement all the traded transactions simultaneously due to some unexpected contingencies. It may be alleviated by incorporating line capacity constraints in the dispatch and scheduling process. This may involve redispatch of generation or load curtailment. Other possible means for relieving congestion are operation of phase-shifters or FACTS devices.

In this chapter we look at a modified OPF whose objective is to minimize the absolute MW of rescheduling. In this framework, we consider dispatching the bilateral contracts too in case of serious congestion, with the knowledge that any change in a bilateral contract is equivalent to modifying the power injections at both the buyer and the seller buses. This highlights the fact that, in a restructured scenario, contracts between trading entities must be considered as system decision variables (in addition to the usual generation, loads and flows). Figure 1.1 shows a transaction network [12] in a typical deregulated electricity system. It displays links of data and cash flow between various market players. In the figure, G stands for generator-serving entities (or GENCOs), D for load or demand-serving entities (LSEs or discos), E for marketers, and ISO for the independent system operator.

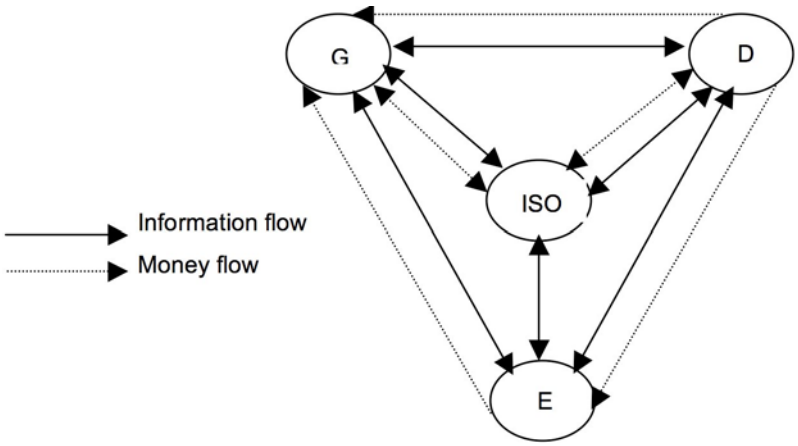

Figure 3-1: Transaction network

The dispatch problem has been formulated with two different objective functions: cost minimization and minimization of transaction deviations. Congestion charges can be computed in both the cases. In a pool market mode, the sellers (competitive generators) may submit their incremental and decremental bidding prices in a real-time balancing market. These can then be incorporated in the OPF problem to yield the incremental/decremental change in the generator outputs. Similarly, in case of a bilateral market mode, every transaction contract may include a compensation price that the buyer-seller pair is willing to accept should its transaction be curtailed. This can then be modeled as a prioritization of the transactions based on the latter's sensitivities to the violated constraint in case congestion occurs.

In this chapter, we also seek to develop an OPF solution incorporating FACTS devices in a given market mode (pool or bilateral dispatch). FACTS devices assume importance in the context of power system restructuring since they can expand the usage potential of transmission systems by controlling power flows in the network. FACTS devices are operated in a manner so as to ensure that the contractual requirements are fulfilled as far as possible by minimizing line congestion.

Various optimization techniques have been used to solve OPF problems. These may be classified as sequential, quadratic, linear, nonlinear, integer and dynamic programming methods, Newton-based methods, interior point methods, etc. Nonlinear programming methods involve nonlinear objective and constraint equations. These make up the earliest category of OPF techniques as they can closely model electric power systems. The benchmark paper by Dommel and Tinney [13] discusses a method to minimize fuel costs and active power loss using the penalty function

optimization approach. Divi and Kesavan [14] use an adapted Fletcher's quasi-Newton technique for optimization of shifted penalty functions. Linear programming deals with problems with constraints and objective function formulated in linear forms. Sterling and Irving [15] solved an economic dispatch of active power with constraints relaxation using a linear programming approach. Chen et al. [16] developed a successive linear programming (SLP) based method for a loss minimization objective in an ac-dc system. In the SLP approach, the nonlinear OPF problem is approximated to a linear programming problem by linearizing both the objective function as well as the constraints about an operating state. At every iteration, a suboptimal solution is found and the variables are updated to get a new operating state. The process is then repeated until the objective function converges to an optimal level. Megahed et al. [17] have discussed the treatment of the nonlinearly constrained dispatch problem to a series of constrained linear programming problems. Similarly, Waight et al. [18] have used the Dantzig-Wolfe decomposition method to break the dispatch problem into one master problem and several smaller linear programming subproblems. Combinations of linear programming methods with the Newton approach have been discussed in the literature [19]. In [20], Burchett and Happ apply an optimization method based on transforming the original problem to that of solving a series of linearly constrained subproblems using an augmented Lagrangian type objective function. The subproblems are optimized using quasi-Newton, conjugate directions, and steepest descent methods. Quadratic programming is another form of nonlinear programming where the objective function is approximated by a quadratic function and the constraints are linearized. Nanda et al. [21] discuss an OPF algorithm developed using the Fletcher's quadratic programming method. Burchett et al. [22] discuss a successive quadratic programming (SQP) method where the approximation-solution-update process is repeated to convergence just as in the SLP method. In this method, a sequence of quadratic programs is created from the exact analytical first and second derivatives of the power flow equations and the nonlinear objective function. Interior point methods are fairly new entrants in the field of power system optimization problems. Vargas et al. [23] discussed an interior point method for a security-constrained economic dispatch problem. In [24], Momoh et al. present a quadratic interior point method for OPF problems, economic dispatch, and reactive power planning.

The chapter is organized as follows. In Section 2 we look at congestion management methodologies and how they get modified in the new competitive framework of electricity power markets. A simple example is given for the calculation of congestion charges in a scenario where the objective of optimization is to maximize societal benefit. In Section 3, we work out different OPF formulations. Objective functions that are treated include cost minimization and transaction curtailment minimization. Market models involving pool and bilateral dispatches are considered. The possibility of using these formulations in an open access system dispatch module and in real-time balancing markets is discussed. In Section 4, we treat the subject of including FACTS devices in the OPF framework. Various device models are considered and then applied in the problem formulation. The impact of these devices on minimizing congestion and transaction deviations is studied. In Section 5, the OPF results are displayed on two test systems and inferences are drawn from the same. Further areas of research in this field are then explored in the concluding section.

3.2 Congestion Management Methodologies

In this chapter, we look at congestion management methodologies and how they get modified in the new competitive framework of electricity power markets. A simple example is given for the calculation of congestion charges in a scenario where the objective of optimization is to maximize societal benefit.

The unbundling of the electric power market has led to the evolution of new organizational structures. *Unbundling* implies opening to competition those tasks that are, in a vertically integrated structure, coordinated jointly with the objective of minimizing the total costs of operating the utility. In such a traditional organizational structure, all the control functions, like automatic generation control (AGC), state estimation, generation dispatch, unit commitment, etc., are carried out by an energy management system. Generation is dispatched in a manner that realizes the most economic overall solution. In such an environment, an optimal power flow can perform the dual function of minimizing production costs and of avoiding congestion in a least-cost manner. Congestion management thus involves determining a generation pattern that does not violate the line flow limits. Line flow capacity constraints, when incorporated in the scheduling program, lead to increased marginal costs. This may then be used as an economic

signal for rescheduling generation or, in the case of recurring congestion, for installation of new generation/transmission facilities.

3.2.1 Unbundled operation

In a competitive power market scenario, besides generation, loads, and line flows, contracts between trading entities also comprise the system decision variables. The following pool and bilateral competitive structures for the electricity market have evolved/are evolving:

(1) Single auction power pools, where wholesale sellers (competitive generators) bid to supply power in to a single pool. Load serving entities (LSEs or buyers) then buy wholesale power from that pool at a regulated price and resell it to the retail loads.

(2) Double auction power pools, where the sellers put in their bids in a single pool and the buyers then compete with their offers to buy wholesale power from the pool and then resell it to the retail loads.

(3) In addition to combinations of (1) and (2), bilateral wholesale contracts between the wholesale generators and the LSEs without third-party intervention.

(4) Multilateral contracts, i.e., purchase and sale agreements between several sellers and buyers, possibly with the intervention of third parties such as forward contractors or brokers. In both (3) and (4) the price-quantity trades are up to the market participants to decide, and not the ISO. The role of the ISO in such a scenario is to maintain system security and carry out congestion management.

The contracts, thus determined by the market conditions, are among the system inputs that drive the power system. The transactions resulting from such contracts may be treated as sets of power injections and extractions at the seller and buyer buses, respectively. For example, in a system of *n* buses, with the generator buses numbered from 1 to *m*, the nodal active powers may be represented as [25]

$$P_i = P_{po,i} + \sum_{k \in K} P_{T_K,i} + \text{loss compensation},\ i = 1, 2, \ldots \text{m} \tag{3.1}$$

$$D_j = D_{po,j} + \sum_{k \in K} D_{T_K,j}\ ,\ j = m+1, \ldots n \tag{3.2}$$

where

P_i = active injected power at generator bus *i*`

D_j = active extracted power at load bus *j*

K = set of bilateral / multilateral transactions

$P_{po,I}$ = pool power injected at bus *i*

$D_{po,j}$ = pool power extracted at bus *j*

$P_{Tk,I}$ = power injected at bus i in accordance with transaction T_K

$D_{Tk,j}$ = power extracted at bus j in accordance with transaction T_K

Loss compensation = power supplied at bus i by all transaction participants to make good the transmission losses.

3.2.2 Congestion management methodologies

There are two broad paradigms that may be employed for congestion management. These are the *cost-free* means and the *not-cost-free* means [26]. The former include actions like outaging of congested lines or operation of transformer taps, phase shifters, or FACTS devices. These means are termed as *cost-free* only because the marginal costs (and not the capital costs) involved in their usage are nominal. The *not-cost-free* means include:

(1) Rescheduling generation. This leads to generation operation at an equilibrium point away from the one determined by equal incremental costs. Mathematical models of pricing tools may be incorporated in the dispatch framework and the corresponding cost signals obtained. These cost signals may be used for congestion pricing and as indicators to the market participants to rearrange their power injections/extractions such that congestion is avoided.

(2) Prioritization and curtailment of loads/transactions. A parameter termed as *willingness-to-pay-to-avoid-curtailment* was introduced in [25]. This can be an effective instrument in setting the transaction curtailment strategies which may then be incorporated in the optimal power flow framework.

In the next chapter we look at OPF formulations incorporating both (1) and (2) above. These models can be used as part of a real-time open access system dispatch module [27]. The function

of this module is to modify system dispatch to ensure secure and efficient system operation based on the existing operating condition. It would use the dispatchable resources and controls subject to their limits and determine the required curtailment of transactions to ensure uncongested operation of the power system.

3.2.3 Example of congestion management in an economic dispatch framework

We now look at an example for calculating optimal bus prices and congestion costs for a power system, wherein an independent company (ISO) controls the transmission network and sets nodal prices that are computed as part of a centralized dispatch. A simple power system is considered here for the calculation of congestion charges. A three-bus system is shown in Figure 3.2.1 with generator cost/marginal cost and load benefit/marginal benefit functions as shown. Also shown in the figure are the maximum line flow limits and line susceptances.

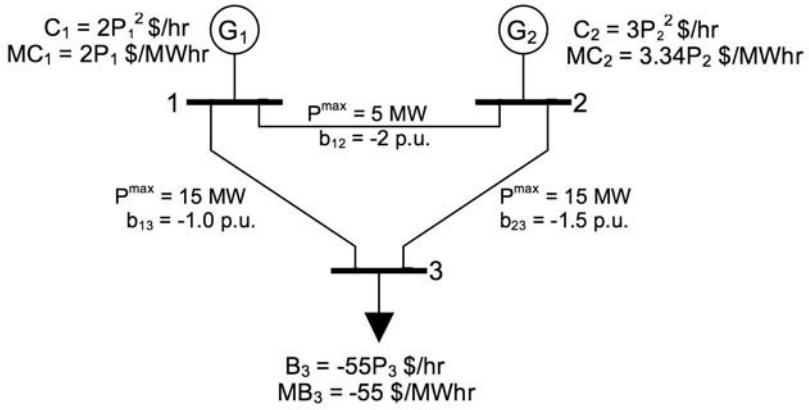

Figure 3-2: Sample power system

For simplicity we make the following approximations:

(1) Each transmission line is represented by its susceptance b_{ij}.

(2) A lossless DC power flow model is assumed; i.e., the bus voltage angular differences are assumed to be small and the voltage magnitudes approximately 1.00 p.u.

The real power flow on each line is given by

$$P_{ij} = b_{ij} \cdot (\delta_i - \delta_j) \tag{3.3}$$

where δ_i and δ_j represent the voltage angles at buses *i* and *j*, respectively.

The total power injection at bus *i* is given by

$$P_i = \sum_j P_{ij} \tag{3.4}$$

As mentioned above, we solve this problem in a centralized dispatch framework where the objective is to maximize social benefit. This optimization problem thus seeks to minimize the system operating costs minus the consumer benefit, subject to the binding line flow inequality constraints and the power flow equality constraints. The problem involves solving a quadratic Lagrangian (quadratic in the decision variables and multipliers).

The variables are given by

$$z = [\underline{P}, \underline{\delta}, \underline{\lambda}, \underline{\mu}] \tag{3.5}$$

where

$\underline{P}$ denotes the net power injections at all the buses

$\underline{\delta}$ denotes the voltage angles

$\underline{\lambda}$ denotes the Lagrangian multipliers for the equality constraints

$\underline{\mu}$ denotes the multipliers for the inequality constraints.

The problem may be thus stated as

$$\min_{P,\delta}\{C_1(P_1) + C_2(P_2) - B_3(P_3)\} \tag{3.6}$$

subject to

$$P_1 = -2\delta_2 - \delta_3 \tag{3.7}$$

$$P_2 = 3.5\delta_2 - 1.5\delta_3 \tag{3.8}$$

$$P_3 = -1.5\delta_2 + 2.5\delta_3 \tag{3.9}$$

$$\left|P_{12}\right| \le P_{12}^{\max}, \left|P_{23}\right| \le P_{23}^{\max}, \left|P_{13}\right| \le P_{13}^{\max} \tag{3.10}$$

In this example, the inequality constraint limiting the flow on line 1-2 is taken as binding. The Lagrangian function for this problem may be given as

$$\ell = 2P_1^2 + 3P_2^2 + 55P_3 + \lambda_1(-2\delta_2 - \delta_3 - P_1) + \lambda_2(3.5\delta_2 - 1.5\delta_3 - P_2) + \lambda_3(-1.5\delta_2 + 2.5\delta_3 - P_3) + \mu_{12}(-2\delta_2 - 5) \tag{3.11}$$

The optimality condition is given by

$$\frac{\partial \ell}{\partial z} = 0 \tag{3.12}$$

and

$$\ell(z) = \frac{1}{2} z^T \cdot \frac{\partial^2 \ell}{\partial z^2} \cdot z + \left[\frac{\partial \ell}{\partial z}\bigg|_{z=0} \right]^T \cdot z \tag{3.13}$$

From equations (2.12) and (2.13), it can be seen that the optimal value of z may be obtained by solving

$$\frac{\partial^2 \ell}{\partial z^2} \cdot z = -\frac{\partial \ell}{\partial z}\bigg|_{z=0} \tag{3.14}$$

Solving the problem in the above example yields the following optimal values:

$$z = [16.21\ 8.06\ -24.27\ |\ -2.5\ -11.21\ |\ 64.86\ 48.42\ 55|\ -21.36]^T \tag{3.15}$$

The Lagrange multipliers $\underline{\lambda} = [64.86\ 48.42\ 55]^T$ can be interpreted as the optimal nodal prices at each of the three buses in \$/MWhr. In other words, if these had been used as the bus prices, the

generator and load responses to these prices would have been the same as what was obtained in the above optimal dispatch.

We now compute the congestion charges (for the flow on each transmission line). The congestion charge may be looked upon as the inherent cost of transmitting power across the line. A simple way to compute this is given here. The congestion charge c_{ij} for line ij is the difference in the congestion costs c_i and c_j at buses i and j, respectively; i.e.,

$$c_{ij} = c_j - c_i, \tag{3.16}$$

Now, each bus nodal price λ_i is made up of three components, viz., the marginal cost of generation at the slack bus, the marginal cost of losses, and the congestion cost. Hence,

$$\lambda_i = -\frac{\partial C_1(P_1)}{\partial P_1} \cdot \frac{\partial P_1}{\partial P_i} + c_i \tag{3.17}$$

where $C_1(P_1)$ is the cost function at bus 1, which has been considered as the slack bus in this example.

We have considered the lossless case in this example. Hence we have,

$$c_{ij} = \lambda_j - \lambda_i, \tag{3.18}$$

Thus the congestion charge for any line ij may be computed as the difference in the nodal prices between buses i and j. The values obtained in this problem are c_{12} = -16.43 \$/MWhr, c_{23} = 6.58 \$/MWhr, c_{13} = -9.86 \$/MWhr.

3.2.4 Congestion Management Using Pricing Tools

In [26], Glavitsch and Alvarado discuss congestion pricing as may be done by an ISO in the absence of information on the marginal costs of the generators. The methodology suggested involves observing the behavior of generators under a variety of conditions, based on which quadratic coefficients for all generators may be inferred.

In [28], Bhattacharya et al. discuss the method of market splitting to alleviate transmission congestion. The basic principle of this method lies in sending price signals that either exceed or are less than the marginal costs to generators and thereby effecting a change in the generation pattern. The market is "split" into different bid areas and the area-prices are calculated for each bid area using a "capacity fee."

In the next section we work out different OPF formulations in the various market modes discussed earlier.

3.3 Optimal Dispatch Methodologies in Different Market Structures

3.3.1 Market structure issues and section organization

In this section, we look at ways of managing the power dispatch problem in the emerging electricity market structures. The operating strategies that may be used by the ISO in different market modes have been explored and test cases have been studied to determine the compatibility of the strategies with the market environment. Emphasis is placed on dealing with congestion management.

The conventional OPF problem comprises scheduling the power system controls to optimize a given objective function under a set of nonlinear inequality constraints and equality constraints. Under a deregulated environment, mechanisms for competition and trading are created for the market players. This leads to the introduction of new OPF controls. In this chapter we look at how to deal with these controls.

The fundamental entity in all competitive market structures is an ISO. "Successful" trading requires that the ISO match the power bids from the supply side (GENCOs) with the offers from the demand side (discos). This is true for all market structures. The important way in which market structures differ is in the manner of the main contractual system that is followed by the market players on both the supply and demand sides. We look at two different market modes, viz., pool dispatch and bilateral dispatch.

3.3.2 Pool dispatch

Interconnected system operation becomes significant in a deregulated environment. This is because the market players are expected to treat power transactions as commercial business instruments and seek to maximize their economic profits. Now when several GENCOs decide to interchange power, complications may arise. An economic dispatch of the interconnected system can be obtained only if all the relevant information, viz., generator curves, cost curves, generator limits, commitment status, etc., is exchanged among all the GENCOs. To overcome this complex data exchange and the resulting non-optimality, the GENCOs may form a power pool regulated by a central dispatcher. The latter sets up the interchange schedules based on the information submitted to it by the GENCOs. While this arrangement minimizes operating costs and facilitates system-wide unit commitment, it also leads to several complexities and costs involved in the interaction with the central dispatcher. Conventionally, the optimal operation of a power system has been based on the economic criterion of loss minimization, i.e., maximization of societal benefit. Pool dispatch follows the same criterion but with certain modifications necessitated by the coexistence of the pool market with a short-term electricity spot market. Namely, these effects are demand elasticities and the variation in the spot price with the purchaser's location on the grid. The existence of the spot market or bilateral market behind the scene does not explicitly affect the operation of the ISO.

3.3.3 Pool dispatch formulation

Neglecting the effects of price elasticities and location, the dispatch formulation may be stated as

$$\min_{P_{Gi},P_{Dj}} \sum_i C_i(P_{Gi}) - \sum B_j(P_{Dj}) \tag{3.19}$$

subject to

$$\begin{aligned} g(x,u) &= 0 \\ h(x,u) &\le 0 \end{aligned} \tag{3.20}$$

where

g and *h* are the sets of system operating constraints, including system power flow equations and line flow limits

u is the set of control variables, viz., active powers at the generator and load buses

x is the set of dependent variables

i and *j* are the set of GENCOs and discos, respectively

This OPF uses the bids and offers submitted by the participants and sets the nodal prices (that are obtained as the Lagrangian multipliers), which are in turn used to charge for the power consumption at every node. The vectors of generation and load are denoted as P_{Gi} and P_{Dj}, respectively. The nodal prices applied to the generation and load controlled by players *i* and *j* are obtained as a byproduct of the OPF and are represented as λ_i and λj, respectively. The cost and benefit functions of each generator and load are denoted by C_i and B_j, respectively. The cost and benefit functions are assumed to be well described by quadratic functions.

$$C_i(P_{G_i}) = a_{G,i} \cdot P_{G_i}^2 + b_{G,i} \cdot P_{G_i} + c_{G,i}, \ i \in G \tag{3.21}$$

$$B_j(P_{D_j}) = a_{D,i} \cdot P_{D_j}^2 + b_{D,j} \cdot P_{D_j} + c_{D,j}, \ j \in D \tag{3.22}$$

where *G* represents the set of all GENCOs and *D* represents the set of discos.

The equality constraint may be written as

$$\sum_j P_{D_j} - \sum_i P_{G_i} + L = 0 \tag{3.23}$$

where *L* is the transmission loss function.

The capacity constraint (inequality) may be given as

$$P_{G_i} - P_{G_i,\max} \leq 0 \tag{3.24}$$

Problem (3.1) leads to the solution and Kuhn-Tucker conditions given as

$$\frac{\partial B_j}{\partial P_{D_j}} - p_j - \lambda_j (1 + \frac{\partial L}{\partial P_{D_j}}) + \sum_k \pi_k \frac{\partial h_k}{\partial P_{D_j}} = 0$$

$$\frac{\partial C_i}{\partial P_{G_i}} - \lambda_i (1 - \frac{\partial L}{\partial P_{G_i}}) - \mu_i - \sum_k \pi_k \frac{\partial h_k}{\partial P_{G_i}} = 0$$

$$\mu_i (P_{G_i} - P_{G_i,\max}) = 0 \quad \text{and} \quad \mu_i \geq 0$$

$$\pi_k h_k = 0 \quad \text{and} \quad \pi_k \geq 0 \tag{3.25}$$

where λ represents the system incremental cost (dual multiplier on the equality constraint) and μ and π represent the sets of Kuhn-Tucker dual variables on the capacity and operating constraints, respectively.

3.3.4 Example of corrective rescheduling in pool dispatch

When the system is insecure and there are violations in the system, the objective of the pool central dispatcher is to eliminate the system overload and come up with the corrective rescheduling to eliminate the violations as fast as possible. Minimum operating cost, minimum number of controls, or minimum shift from the optimum operation may be used as the objective function. We now look at an OPF example where the objective function is to minimize the rescheduling of generation. Consider a five-bus system as shown in Figure 3.3. The system data is given in Table 3.1

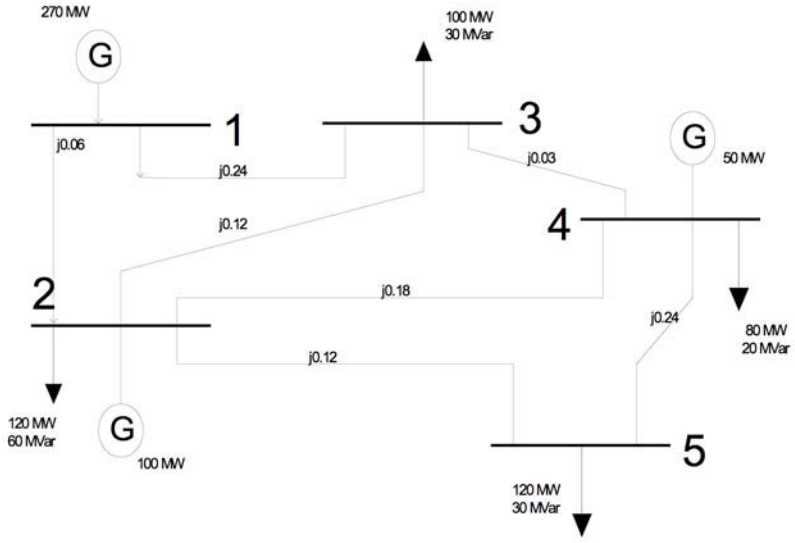

Figure 3-3: Three-generator five-bus system

Table 3.1: Data for Figure 3.3

Table 3.1A: Bus data

Bus number	Load MW	MVar	Gen MW	Gen min MW	Gen max MW	Voltage setpoint	Cost ($/MWhr)
1 (slack)	0	0	270	0	1000	1.05	15
2	120	60	100	100	400	1.02	17
3	100	30	-	-	-	-	-
4	80	20	50	50	300	1.02	19
5	120	30	-	-	-	-	-

Table 3.1B: Bus data

From bus	To bus	p.u. impedance	MVA rating	Base case power flow(MW)
1	2	j0.06	150	197.27
1	3	j0.24	100	72.72
2	3	j0.12	50	46.39
2	4	j0.18	100	34.29
2	5	j0.12	120	96.60
3	4	j0.03	100	19.12
4	5	j0.24	100	23.40

The base case power flow for the system shows (Table 3.1B) that congestion occurs on line 1-2. The aim is to reschedule generation to remove this congestion and any other induced congestion. We first compute the sensitivities of line flow Pjk to changes in generation PG1, PG2, PG4. For that we use the chain rule:

$$\frac{\partial P_{jk}}{\partial P_{Gi}} = \left[\frac{\partial P_{jk}}{\partial \theta}\right]^{T} \left[\frac{\partial f^{P}}{\partial \theta}\right]^{-1} \left[\frac{\partial f^{P}}{\partial P_{Gi}}\right] \tag{3.26}$$

where f_i^{p} represents the power flow equation at bus i, which is given as

$$\sum \frac{1}{x_{ij}}(\theta_i - \theta_j) - (P_{Gi} - P_{Di}) = 0 \tag{3.27}$$

In matrix formulation the power flow equation is $\theta = -B^{-1}P$, where B is the bus susceptance matrix computed from the line impedance data. Fixing bus 1 as the slack, we can then get the equations for line flows and the line flow sensitivities to generation. The sum of all the products

of line flow sensitivities with changes in generation (rescheduling) gives the overload in that particular line.

In this particular example, the objective is to minimize the rescheduling of generation required to limit the flow on line 1-2 to 150 MVA. The OPF problem can then be given as

$$\min(\Delta P_{G_1}^{+} + \Delta P_{G_1}^{-} + \Delta P_{G_2}^{+} + \Delta P_{G_2}^{-} + \Delta P_{G_4}^{+} + \Delta P_{G_4}^{-}) \tag{3.28}$$

subject to

$$\Delta P_{G_1}^{+} - \Delta P_{G_1}^{-} + \Delta P_{G_2}^{+} - \Delta P_{G_2}^{-} + \Delta P_{G_4}^{+} - \Delta P_{G_4}^{-} = 0 \tag{3.29}$$

and

$$\frac{\partial P_{12}}{\partial P_{G_2}}\left[\Delta P_{G_2}^{+} - \Delta P_{G_2}^{-}\right] + \frac{\partial P_{12}}{\partial P_{G_4}}\left[\Delta P_{G_4}^{+} - \Delta P_{G_4}^{-}\right] = -0.47 \tag{3.30}$$

where 0.47 is the overload on line 1-2.

This OPF problem can be solved to minimize the rescheduling of generation. We get the result that bus 1 must drop its generation by 56.2 MW, bus 2 must raise its generation by 52.37 MW, and bus 4 must raise its generation by 3.88 MW;

$$\Delta P_{G_1}^{-} = 56.2 \text{ MW}$$
$$\Delta P_{G_2}^{+} = 52.37 \text{ MW}$$

$$\Delta P_{G_4}^{+} = 3.88 \text{ MW} \tag{3.31}$$

3.3.5 Bilateral dispatch

The conceptual model of a bilateral market structure is that GENCOs and discos enter into transaction contracts where the quantities traded and the prices are at their own discretion and not a matter for the ISO; i.e., a bilateral transaction is made between a GENCO and a DISCO

without third party intervention. These transactions are then submitted to the ISO. In the absence of any congestion on the system, the ISO simply dispatches all the transactions that are requested, making an impartial charge for the service.

3.3.6 Bilateral dispatch formulation

In a bilateral market mode, the purpose of the optimal transmission dispatch problem is to minimize deviations from transaction requests made by the market players. The goal is to make possible all transactions without curtailments arising from operating constraints. The new set of rescheduled transactions thus obtained will be closest to the set of desired transactions, while simultaneously satisfying the power flow equations and operating constraints. One of the most logical ways of rescheduling transactions is to do it on the basis of rationing of transmission access. This may be modeled as a user-pay scheme with "willingness-to-pay" surcharges to avoid transmission curtailment. The mathematical formulation of the dispatch problem may then be given as

$$\min f(x,u)$$

where

$$f(u,x) = [(u - u^o)^T \cdot A] \cdot W \cdot [(u - u^o)^T \cdot A]^T \tag{3.32}$$

subject to

$$g(x,u) = 0$$
$$h(x,u) \leq 0$$

where

W is a diagonal matrix with the surcharges as elements

A is a constant matrix reflecting the curtailment strategies of the market participants

u and u^o are the set of control variables, actual and desired

x is the set of dependent variables

g is the set of equality constraints, viz., the power flow equations and the contracted transaction relationships,

h is the set of system operating constraints including transmission capacity limits

The bilateral case can be modeled in detail. We consider transactions in the form of individual contracts where a seller i injects an amount of power T_{ij} at one generator bus and the buyer j extracts the same amount at a load bus. Let the power system consist of n buses with the first m assumed to be seller buses and the remaining n-m as buyer buses. One particular bus (bus 1) may be designated as the slack, to take into account transmission losses. The total power injected/extracted at every bus may be given by the summation of all individual transactions carried out at those buses. Thus,

for $i = 2$ *to* m, $P_i = \sum_j T_{ij}$, and

$$\text{for } j = m+1 \text{ to } n,\ P_j = \sum_i T_{ij} \tag{3.33}$$

The transactions T_{ij} also appear in the power flow equality constraints since they act as the control variables along with the usual generator bus voltages. The set of control variables can thus be represented as $u = \{\sum T_{ij}\ , V\}^T$, where V is the vector of generator bus voltages.

The real and reactive power flow equations can be written in the usual form represented by $g(x,u) = 0$.

The transaction curtailment strategy is implemented by the ISO in collaboration with the market participants. In the case of bilateral dispatch, this strategy concerns the individual power contracts. One such strategy is such that, in case of an individual contract, the curtailment of the transacted power injected at the GENCO bus must equal the curtailment of the transacted power extracted at the DISCO bus.

In this case, we may rewrite the dispatch formulation as

$$\min f(x,u)$$

where

$$f(x,u) = \sum_{i=2}^{m} \sum_{j=m+1}^{n} w_{ij} \cdot (T_{ij} - T_{ij}^{0})^2 \tag{3.34}$$

where

w_{ij} = the willingness to pay factor to avoid curtailment of transaction

T_{ij}^{0} = the desired value of transaction T_{ij}

3.3.7 Test results

We consider a six-bus system (Figure 3.4) representing a deregulated market with bilateral transactions. An OPF will be solved for this system to determine the optimal generation schedule that satisfies the objective of minimizing deviations from the desired transactions.

Table 3.2A provides the system data pertaining to generation and load. Table 3.2B provides the system network data. Figure 3.2 shows the system network configuration. Buses 1 and 2 are GENCO buses and, being PV buses, the voltages here are specified exactly. At the other buses, the allowable upper and lower limits of voltage are specified. The losses are assumed to be supplied only by the generator at bus 1.

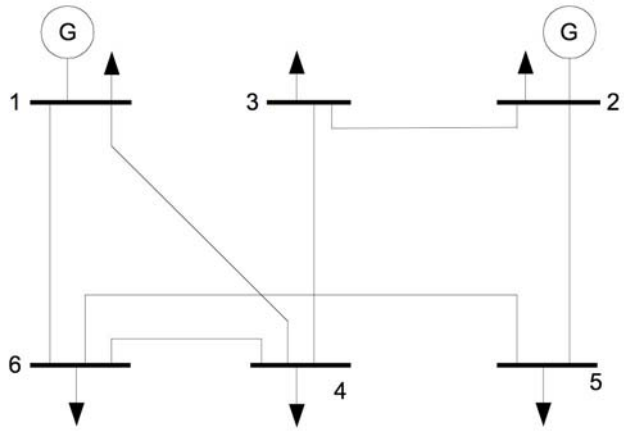

Figure 3-4: Two-generator six-bus system

Table 3.2A: System Data

Bus	Generation capacity, MW	Generator cost characteristic, $/hr	Voltage, pu
1	$100 \le P_1 \le 400$	$P_1^2 + 8.5P_1 + 5$	1.05
2	$50 \le P_2 \le 200$	$3.4P_2^2 + 25.5P_2 + 9$	1.06
3	-	-	$0.9 \le V_3 \le 1.1$
4	-	-	$0.9 \le V_4 \le 1.1$
5	-	-	$0.9 \le V_5 \le 1.1$
6	-	-	$0.9 \le V_6 \le 1.1$

Table 3.2B: System Network Data

From bus – to bus	Resistance, pu	Reactance, pu	Line charging admittance, pu
1-4	0.0662	0.1804	0.003
1-6	0.0945	0.2987	0.005
2-3	0.0210	0.1097	0.004
2-5	0.0824	0.2732	0.004
3-4	0.1070	0.3185	0.005
4-6	0.0639	0.1792	0.001
5-6	0.0340	0.0980	0.004

In this case, bilateral contracts have been considered between each GENCO and each DISCO. Table 3.3 shows the desired power transactions.

Table 3.3: Desired Transactions Before Curtailment

Bus #	Desired transactions, MW
1	20.0
2	30.0
3	35.0
4	50.0
5	42.0
6	55.0

Three strategies for the curtailment of transactions are adopted for congestion management:

1. The curtailment on the DISCO loads is assumed to be linear. In this case, all the willingness to pay factors are taken to be equal.
2. Same as case (1), except that the willingness to pay price premium of loads on buses 1 to 3 is assumed to be twice that of loads on buses 4 to 6.
3. In this case, the price premium of loads on buses 4 to 6 is assumed to be twice that of loads on buses 1 to 3.

The OPF problem is solved using the MINOS-5.0 nonlinear programming solver in the Generalized Algebraic Modeling Systems (GAMS) programming environment [29].

Table 3.4 shows the constrained generation and load data obtained from the OPF solution. It can be seen that the willingness to pay and the participants' curtailment strategy are two factors that significantly affect the constrained dispatch. The higher the willingness to pay, the less is the curtailment of that particular transaction. The curtailment strategies implemented have complex effects. These factors not only affect the curtailment of its own transaction, but will also impact that of other transactions.

Table 3.4: Constrained generation and load data after running OPF

Bus #	Constrained generation and load, MW		
	Case (1)	Case (2)	Case (3)
1	109.63	109.62	109.68
2	124.24	124.41	123.60
3	34.72	34.93	33.95
4	48.87	48.86	48.94
5	40.74	40.72	40.81
6	53.99	53.97	54.05

3.3.8 Treatment of transaction-based groups

In a competitive market scenario, relationships among market players may develop over time and may lead to the formation of electricity supply and consumption groups. The concept of a group as a collection of buyers, sellers, and market brokers functioning together in a cohesive manner has to be dealt with. The formation of such transaction-based groups in a power system

necessitates changes in power dispatch. In the following sections we look at dispatch formulations taking into account the group concept.

3.3.9 Dispatch formulations

Here the concern is to make possible a group transfer without curtailment, even if the individual generators within the group or utility have to be rescheduled. The objective function is

$$\min f(x,u)$$

where

$$f(u,x) = \sum_{k=1}^{K}[w_k \cdot (\sum_{i=2}^{m} T_{ik} - \sum_{i=2}^{m} T_{ik}^0)^2] \tag{3.35}$$

where

w_k = the willingness to pay factor to avoid curtailment of the *k*th group transaction

T_{ik}^0 = the desired value of transaction T_{ij}

In this group curtailment dispatch formulation, there is the need to develop a strategy to allocate the total group power curtailment among all the group participants. That is, if the GENCO powers within a group need to be curtailed, the resulting shortfall has to be allocated to all the group discos in accordance with some predetermined strategy.

Another way of implementing curtailment of group transactions is by minimizing the change to every injected or extracted power transaction at the generator bus and load bus of a group based on the willingness to pay factors. In this case, the objective function may be expressed as

$$\min f(x,u)$$

where

$$f(u,x) = \sum_{k=1}^{K}\sum_{i=2}^{m}[w_{ik} \cdot (T_{ik} - T_{ik}^0)^2] \tag{3.36}$$

where w_{ik} = the willingness to pay factor to avoid curtailment of the injected power block T_{ik} .

In this optimal transmission dispatch problem, all power transactions are required to be as close as possible to the initial desired power transfers, and the curtailment decisions are based on the market players' willingness to pay to avoid curtailment, their preferred curtailment strategies, and on the system security conditions. The dispatch procedure starts with the market participants submitting their multilateral transactions to the ISO. If the operating and capacity constraints are satisfied while all the desired transactions are dispatched, there is no need to go through the curtailment routine. Otherwise the optimal dispatch models described above (Sections 3.2.2, 3.3.2, 3.4.1) are used to curtail the requested power transfers. Finally, the original/curtailed power transfers are dispatched and the ISO buys the required regulating power at bus 1 to compensate for transmission losses.

3.3.10 Test Case

We now look at an optimal transmission dispatch problem in a deregulated market having transaction-based groups. We consider the IEEE 14-bus system here (Figure 3.5).

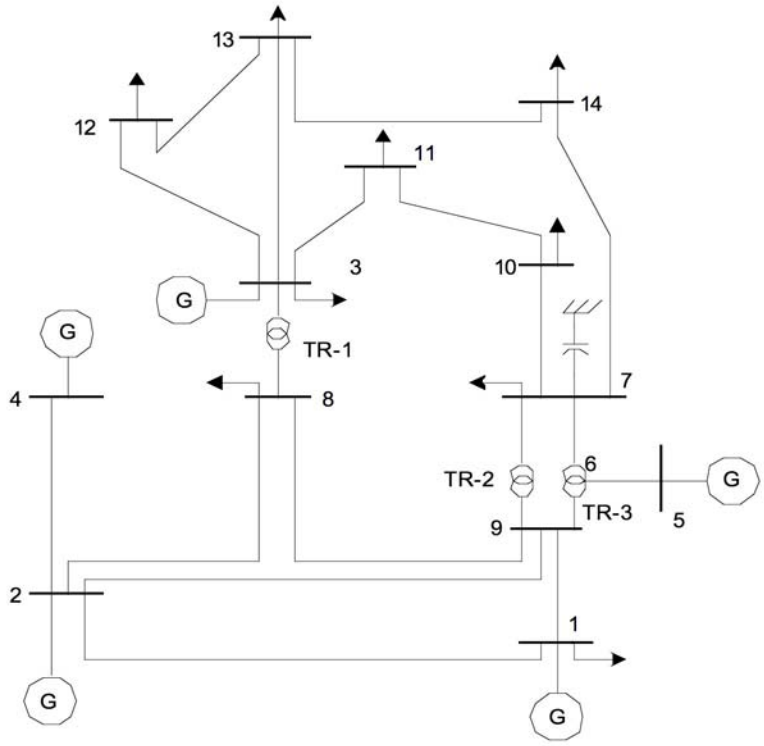

Figure 3-5: IEEE five-generator fourteen-bus system

Some slight modifications are made. Bus 4 is renumbered as bus 1 and it is assumed that this bus is contracted by the system ISO to provide for the transmission losses; i.e., bus 1 is the system slack bus. This bus, in addition to bus 5, is usually shown connected to a synchronous condenser. But in this problem, we treat bus 1 as a generator bus owned by a GENCO. Similarly, bus 5 is treated as a PV-bus in the problem.

Table 3.5A provides the generation bus data. Table 3.5B provides the system network data. The voltages at the GENCO buses are specified since they are P-V buses, whereas at the DISCO buses, the allowable upper and lower limits of voltage are specified.

Table 3.5: Generation and System Network Data

Table 3.5A Generation Bus Data

Bus	Generation capacity, MW	Generator cost characteristic, $/hr	Voltage, pu
1	-	-	1.01
2	$20 \le P_2 \le 100$	$0.5P_2^2 + 3.51P_2 + 44.4$	1.045
3	$20 \le P_3 \le 100$	$0.5P_3^2 + 3.89P_3 + 40.6$	1.07
4	$50 \le P_4 \le 200$	$0.5P_4^2 + 2.45P_4 + 105.0$	1.06
5	-	-	1.09

Table 3.5B: System Network Data

From bus – to bus	Resistance, pu	Reactance, pu	Line charging admittance, pu
4-8	0.05403	0.22304	0.0246
2-8	0.05695	0.17388	0.0170
1-9	0.06701	0.17103	0.0173
9-8	0.01335	0.04211	0.0064
4-2	0.01938	0.05917	0.0264
2-1	0.04699	0.19797	0.0219
5-6	0.00000	0.17615	0.0000
2-9	0.05811	0.17632	0.0187
6-7	0.00000	0.11001	0.0000
7-10	0.03181	0.08450	0.0000
3-11	0.09498	0.19890	0.0000
3-12	0.12291	0.25581	0.0000
3-13	0.06615	0.13027	0.0000
7-14	0.12711	0.27038	0.0000
10-11	0.08205	0.19207	0.0000
12-13	0.22092	0.19988	0.0000
13-14	0.17093	0.34802	0.0000

We now assume that there are two groups in this power system: Group 1 consists of buses 2 and 3 and makes transfers to DISCO buses 7, 9, 11, and 14. Group 2 consists of the single GENCO

bus 4 and makes tranfers to DISCO buses 8, 10, 12, and 13. Table 3.6 shows the desired power generation and load for both groups.

Table 3.6: Desired Generation and Load Before Curtailment

Bus #	Pre-curtailment MW
1	38.1
2	138.4
3	92.6
4	213.5
5	0.0
6	0.0
7	54.3
8	155.4
9	91.5
10	16.8
11	56.6
12	13.1
13	28.2
14	28.6

It is seen from the power flow solution that the dispatch of the contracted transactions without any curtailment leads to overloading of the lines between buses 3 and 11, and buses 7 and 9. Therefore, to remove this congestion and to ensure that the system security limits are not violated, the ISO needs to curtail the power transactions

The following four strategies for the curtailment of transactions are adopted for congestion management. The results are shown in Table 3.7.

(1) Both groups 1 and 2 employ the group curtailment formulation as described by (3.35). The curtailment on the DISCO loads is assumed to be linear. The total group power curtailment is taken as a linear combination of the individual DISCO curtailments. In this case, all the willingness to pay factors are taken to be equal to unity.

(2) Same as case (1), except that the willingness to pay price premium of the players in group 2 is assumed to be twice that of the players in group 2.

(3) In this case, group 1 employs the curtailment strategy given in (3.35), whereas group 2 adopts the curtailment formulation described in (3.34). Willingness to pay premiums are maintained at unity.

(4) Same as case (3), except that the willingness to pay premiums on the transactions between buses 4 and 10, and buses 4 and 12, are doubled.

Table 3.7 shows the constrained generation and load data obtained from the OPF solutions using the four curtailment strategies.

Table 3.7: Constrained Generation and Load Data after Running OPF

Bus #	Constrained generation and load, MW			
	Case (1)	Case (2)	Case (3)	Case (4)
(group #1)				
2 (GENCO)	138.42	138.40	138.51	138.47
3 (GENCO)	78.53	79.76	87.20	84.73
7	52.11	52.33	53.58	53.04
9	86.37	87.20	89.71	88.33
11	53.10	53.24	55.13	54.75
14	25.40	25.42	27.32	27.11
(group #2)				
4 (GENCO)	204.10	197.31	207.01	210.75
8	149.62	144.36	155.20	155.22
10	15.53	14.96	12.84	15.32
12	12.62	12.25	11.25	12.81
13	26.37	25.81	27.78	27.65
(loss compensator)				
1 (GENCO)	35.41	35.23	35.62	36.27

The optimal dispatch gives an uncongested system solution (Table 3.7); i.e., all the line overloads are removed. In case (1), both the groups use the same curtailment strategies with identical willingness-to-pay factors, and this results in all power transactions getting curtailed in varying degrees. In case (2), the willingness to pay of group 1 is increased. This does not lead to a proportionate reduction in the curtailment of the transactions in group 1 or a proportionate increase in the curtailment of transactions in group 2. In case (3), the use of two different

curtailment strategies for the two groups seems to affect some transactions more than others. For instance, the transaction between buses 4 and 10, and buses 4 and 12, get relatively heavily curtailed. This is remedied in case (4) where the willingness to pay for both these pairs of players is doubled.

3.4 Optimal Dispatch Using FACTS Devices in Competitive Market Structures

In the previous sections of this chapter, we have looked at congestion management in competitive power systems using models that include pricing tools such as prioritization and curtailment of transactions. In this chapter we look at treating congestion management with the help of flexible AC transmission (FACTS) devices. We consider an integrated approach to incorporate the power flow control needs of FACTS in the OPF problem for alleviating congestion. Two main types of devices are considered here, namely, thyristor controlled series compensators (TCSC) and thyristor controlled phase angle regulators (TCPAR).

The concept of flexible AC transmission systems (FACTS) was first proposed by Hingorani [30]. FACTS devices have the ability to allow power systems to operate in a more flexible, secure, economic, and sophisticated way. Generation patterns that lead to heavy line flows result in higher losses, and weakened security and stability. Such patterns are economically undesirable. Further, transmission constraints make certain combinations of generation and demand unviable due to the potential of outages. In such situations, FACTS devices may be used to improve system performance by controlling the power flows in the grid. Studies on FACTS so far have mainly focused on device developments and their impacts on the power system aspects such as control, transient and small signal stability enhancement, and damping of oscillations [31]-[34]. Here we look at solving the OPF problem in a power system incorporating FACTS devices. As we have seen in the earlier chapters, different solution approaches are possible to solve the OPF problem. The main conventional control variables are the generation MWs when the DC power flow model is used. With the increased presence of independent GENCOs in the deregulated scenario, the operation of power systems would require more sophisticated means of power control. FACTS devices can meet that need.

3.4.1 Static modeling of FACTS devices

For the optimal power dispatch formulation using FACTS controllers, only the static models of these controllers have been considered here [35]. It is assumed that the time constants in FACTS devices are very small and hence this approximation is justified.

3.4.1 Thyristor-controlled series compensator (TCSC)

Thyristor-controlled series compensators (TCSC) are connected in series with the lines. The effect of a TCSC on the network can be seen as a controllable reactance inserted in the related transmission line that compensates for the inductive reactance of the line. This reduces the transfer reactance between the buses to which the line is connected. This leads to an increase in the maximum power that can be transferred on that line in addition to a reduction in the effective reactive power losses. The series capacitors also contribute to an improvement in the voltage profiles.

Figure 3.6 shows a model of a transmission line with a TCSC connected between buses *i* and *j*. The transmission line is represented by its lumped π-equivalent parameters connected between the two buses. During the steady state, the TCSC can be considered as a static reactance $-jx_c$. This controllable reactance, x_c, is directly used as the control variable to be implemented in the power flow equation.

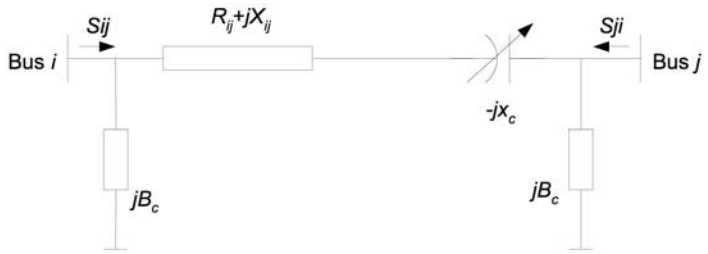

Figure 3-6: Model of a TCSC

Let the complex voltages at bus *i* and bus *j* be denoted as $V_i\angle\delta_i$ and $V_j\angle\delta_j$, respectively. The complex power flowing from bus *i* to bus *j* can be expressed as

$$S_{ij}^{*} = P_{ij} - jQ_{ij} = V_i^{*} I_{ij}$$

$$= V_i^{*}[(V_i - V_j)Y_{ij} + V_i(jB_c)]$$

$$= V_i^{2}[G_{ij} + j(B_{ij} + B_c)] - V_i^{*}V_j(G_{ij} + jB_{ij}) \tag{3.37}$$

where

$$G_{ij} + jB_{ij} = 1/(R_L + jX_L - jX_C) \tag{3.38}$$

Equating the real and imaginary parts of the above equations, the expressions for real and reactive power flows can be written as

$$P_{ij} = V_i^{2}G_{ij} - V_iV_jG_{ij}\cos(\delta_i - \delta_j) - V_iV_jB_{ij}\sin(\delta_i - \delta_j) \tag{3.39}$$

$$Q_{ij} = -V_i^{2}(B_{ij} + B_c) - V_iV_jG_{ij}\sin(\delta_i - \delta_j) + V_iV_jB_{ij}\cos(\delta_i - \delta_j) \tag{3.40}$$

Similarly, the real and reactive power flows from bus *j* to bus *i* can be expressed as

$$P_{ji} = V_j^{2}G_{ij} - V_iV_jG_{ij}\cos(\delta_i - \delta_j) + V_iV_jB_{ij}\sin(\delta_i - \delta_j) \tag{3.41}$$

$$Q_{ij} = -V_j^{2}(B_{ij} + B_c) + V_iV_jG_{ij}\sin(\delta_i - \delta_j) + V_iV_jB_{ij}\cos(\delta_i - \delta_j) \tag{3.42}$$

These equations are used to model the TCSC in the OPF formulations.

3.4.2 Thyristor-controlled phase angle regulator (TCPAR)

In a thyristor-controlled phase angle regulator, the phase shift is achieved by introducing a variable voltage component in perpendicular to the phase voltage of the line. The static model of a TCPAR having a complex tap ratio of 1:a$\angle\alpha$ and a transmission line between bus *i* and bus *j* is shown in Figure 3.7

Figure 3-7: Model of TCPAR

The real and reactive power flows from bus *i* to bus *j* can be expressed as

$$P_{ij} = \mathrm{Re}\{V_i^*[(a^2V_i - a^*V_j)Y_{ij}]\} = a^2V_i^2G_{ij} - aV_iV_jG_{ij}\cos(\delta_i - \delta_j + \alpha) - aV_iV_jB_{ij}\sin(\delta_i - \delta_j + \alpha) \quad (3.43)$$

and

$$Q_{ij} = -\mathrm{Im}\{V_i^*[(a^2V_i - a^*V_j)Y_{ij}]\}$$

$$= -a^2V_i^2G_{ij} - aV_iV_jB_{ij}\cos(\delta_i - \delta_j + \alpha) - aV_iV_jG_{ij}\sin(\delta_i - \delta_j + \alpha) \quad (3.44)$$

Similarly, real and reactive power flows from bus *j* to bus *i* can be written as

$$P_{ji} = \mathrm{Re}\{V_j^*[(V_j - aV_i)Y_{ij}]\}$$

$$= V_j^2G_{ij} - aV_iV_jG_{ij}\cos(\delta_i - \delta_j + \alpha) + aV_iV_jB_{ij}\sin(\delta_i - \delta_j + \alpha) \quad (3.45)$$

and

$$Q_{ji} = -\mathrm{Im}\{V_j^*[(V_j - aV_i)Y_{ij}]\}$$

$$= -V_j^2B_{ij} + aV_iV_jB_{ij}\cos(\delta_i - \delta_j + \alpha) + aV_iV_jG_{ij}\sin(\delta_i - \delta_j + \alpha) \quad (3.46)$$

The real and reactive power loss in the line having a TCPAR can be expressed as

$$P_l = P_{ij} + P_{ji}$$

$$= a^2V_i^2G_{ij} + V_j^2G_{ij} - 2V_iV_jG_{ij}\cos(\delta_i - \delta_j + \alpha) \quad (3.47)$$

$$Q_l = Q_{ij} + Q_{ji}$$

$$= -a^2 V_i^2 B_{ij} - V_j^2 B_{ij} + 2V_i V_j B_{ij} \cos(\delta_i - \delta_j + \alpha) \quad (3.48)$$

This mathematical model makes the Y-bus asymmetrical. In order to make the Y-bus symmetrical, the TCPAR can be simulated by augmenting the existing line with additional power injections at the two buses. The injected active and reactive powers at bus *i* (ΔP_i, ΔQ_i) and bus *j* (ΔP_j, ΔQ_j) are given as

$$\Delta P_i = -a^2 V_i^2 G_{ij} - aV_i V_j [G_{ij} \sin(\delta_i - \delta_j) - B_{ij} \cos(\delta_i - \delta_j)] \quad (3.49)$$

$$\Delta P_j = -aV_i V_j [G_{ij} \sin(\delta_i - \delta_j) + B_{ij} \cos(\delta_i - \delta_j)] \quad (3.50)$$

$$\Delta Q_i = a^2 V_i^2 B_{ij} + aV_i V_j [G_{ij} \cos(\delta_i - \delta_j) + B_{ij} \sin(\delta_i - \delta_j)] \quad (3.51)$$

$$\Delta Q_j = -aV_i V_j [G_{ij} \cos(\delta_i - \delta_j) - B_{ij} \sin(\delta_i - \delta_j)] \quad (3.52)$$

These equations will be used to model the TCPAR in the OPF formulation.

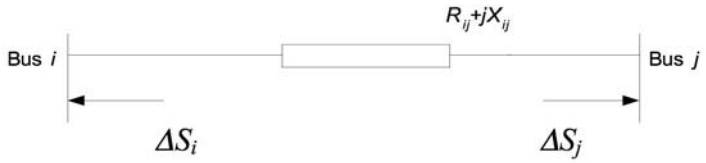

The injection model of the TCPAR is shown in Figure 3.8

Figure 3-8: Injection model of TCPAR

3.4.3 Static VAr compensator (SVC)

The static VAr compensator (SVC) is generally used as a voltage controller in power systems. It can help maintain the voltage magnitude at the bus it is connected to at a desired value during load variations. The SVC can both absorb as well as supply reactive power at the bus it is connected to by control of the firing angle of the thyristor elements. It is continuously controllable over the full reactive operating range as determined by the component ratings.

We can model the SVC as a variable reactive power source. Figure 3.9 shows the schematic diagram of a SVC and Figure 3.10 shows its control characteristics.

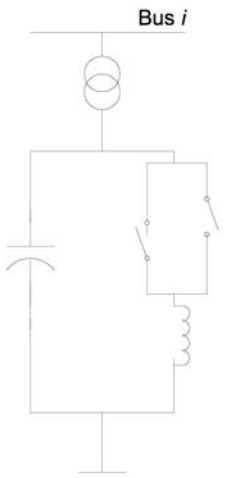

Figure 3-9: Schematic diagram of a SVC

The slope of the SVC voltage control characteristics can be represented as X_{SL}, the equivalent slope reactance in p.u. The limiting values of the SVC inductive and capacitive reactances are given by X_L and X_C, respectively. V and V_{ref} are the node and reference voltage magnitudes, respectively. Modeling the SVC as a variable VAr source, we can set the maximum and minimum limits on the reactive power output Q_{SVC} according to its available inductive and capacitive susceptances B_{ind} and B_{cap}, respectively. These limits can be given as

$$Q_{\max} = B_{ind} \cdot V_{ref}^2 \tag{3.53}$$

$$Q_{\min} = B_{cap} \cdot V_{ref}^2 \tag{3.54}$$

where $B_{ind} = 1/X_L$ and $B_{cap} = 1/X_C$.

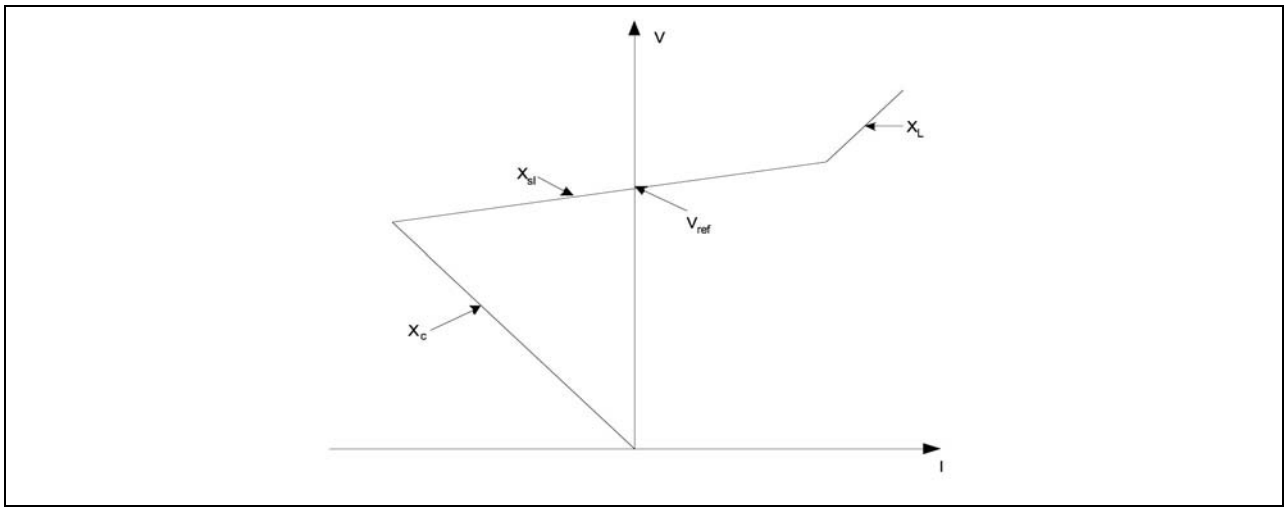

Figure 3-10: Control characteristics of a SVC

3.4.4 Problem formulation for OPF with FACTS devices

As seen in Chapter 2, the transmission dispatch in a deregulated environment may be a mix of pool and bilateral transactions. The optimal dispatch is comprised of complete delivery of all the transactions and the fulfillment of pool demand at least cost subject to non-violation of any security constraint. It may be assumed that the ISO provides for all loss compensation services and dispatches the pool power to compensate for the transmission losses, including those associated with the delivery of contracted transactions. The normal dispatch problem is rewritten here as

$$\min_{P_{Gi},P_{Dj}} \sum_i C_i(P_{Gi}) - \sum B_j(P_{Dj}) \tag{3.55}$$

subject to

$$g(P_G, P_D, T_k, Q, V, \delta, F) = 0 \tag{3.56}$$

$$h(P_G, P_D, T_K, Q, V, \delta, F) \leq 0 \tag{3.57}$$

where P_{G_i} and P_{D_j} are the active powers of pool generator i with bid price C_i and pool load j with offer price B_j, respectively, and $P_G, P_D, T_k, Q, V, \delta,$ and F are the vectors of pool power injections, pool power extractions, bilateral contracts, reactive powers, voltage magnitudes,

voltage angles, and control parameter of FACTS devices placed in the line concerned. Equation (3.56) is a set of equality constraints comprising of the set of contracted transaction relationships and power balance equations. Equation (3.57) is a set of inequality constraints comprising of the system operating constraints.

If only bilateral transactions are considered, we may rewrite the dispatch formulation as

$$\min f(x,u)$$

where

$$f(x,u) = \sum_{i=2}^{m} \sum_{j=m+1}^{n} w_{ij} \cdot (T_{ij} - T_{ij}^{0})^2 \tag{3.58}$$

subject to the real and reactive power balance equations

$$P_{G_i} + P_{i(inj)}^{F} + (P_{C_i} - P_{D_i}) - P_i = 0 \tag{3.59}$$

$$Q_{G_i} + Q_{i(inj)}^{F} + (Q_{C_i} - Q_{D_i}) - Q_i = 0 \tag{3.60}$$

and the inequality constraints,

where

n= number of buses in the power system, with the first m buses being GENCOs and the rest, discos

w_{ij}= the willingness to pay factor to avoid curtailment of transaction

T_{ij}^{0} = the desired value of transaction T_{ij}

P_{G_i}, Q_{G_i} are the real and reactive power generation at GENCO i

P_{D_i}, Q_{D_i} are the real and reactive load demand at DISCO i

P_{C_i}, Q_{C_i} are the real and reactive load curtailment at DISCO i

P_i, Q_i are the real and reactive power injection at bus i

$P^{F}_{i(inj)_i}, Q^{F}_{i(inj)}$ are the real and reactive power injection at bus *i*, with the installation of FACTS device

The modified OPF is different from the conventional OPF due to the FACTS related control variables. If it is desired to use the conventional linear programming based technique to solve the modified OPF problem, the solution strategy needs to be changed. This is because, with the introduction of the FACTS related control variables, the OPF no longer remains a linear optimization problem. One such strategy would be to separate the modified OPF problem into two subproblems, viz., the power flow control subproblem and the normal OPF problem. The power flow of the system can be obtained from the initial operation values of the power system. Using the power flow and constraint equations, the power flow control subproblem may be solved, thereby yielding the controllable FACTS devices' parameters. These parameters may then be used to solve the main OPF to obtain the conventional control variable values. Then if the solution of the power flow problem with the new control variables does not satisfy the constraint equations, this entire process is iteratively repeated until the mismatch falls below some predefined tolerance.

3.4.5 FACTS device locations

We look at static considerations here for the placement of FACTS devices in the power system. The objectives for device placement may be one of the following:

1. reduction in the real power loss of a particular line
2. reduction in the total system real power loss
3. reduction in the total system reactive power loss
4. maximum relief of congestion in the system.

For the first three objectives, methods based on the sensitivity approach may be used. If the objective of FACTS device placement is to provide maximum relief of congestion, the devices may be placed in the most congested lines or, alternatively, in locations determined by trial and error.

3.4.6 Reduction of total system VAr power loss via FACTS devices

Here we look at a method based on the sensitivity of the total system reactive power loss (Q_L) with respect to the control variables of the FACTS devices. For each of the three devices considered in Section 3.4 we consider the following control parameters: net line series reactance (X_{ij}) for a TCSC placed between buses *i* and *j*, phase shift (α_{ij}) for a TCPAR placed between buses *i* and *j*, and the VAr injection (Q_i) for an SVC placed at bus *i*. The reactive power loss sensitivity factors with respect to these control variables may be given as follows:

Loss sensitivity with respect to control parameter X_{ij} of TCSC placed between buses *i* and *j*,

$$a_{ij} = \frac{\partial Q_L}{\partial X_{ij}}$$

1.Loss sensitivity with respect to control parameter θ_{ij} of TCPAR placed between buses *i* and *j*,

$$b_{ij} = \frac{\partial Q_L}{\partial \theta_{ij}}$$

2.Loss sensitivity with respect to control parameter Q_i of SVC placed at bus *i*,

$$c_i = \frac{\partial Q_L}{\partial Q_i}$$

These factors can be computed for a base case power flow solution. Consider a line connected between buses *i* and *j* and having a net series impedance of X_{ij}, that includes the reactance of a TCSC, if present, in that line. θ_{ij} is the net phase shift in the line and includes the effect of the TCPAR. The loss sensitivities with respect to X_{ij} and θ_{ij} can be computed as

$$\frac{\partial Q_L}{\partial X_{ij}} = [V_i^2 + V_j^2 - 2V_iV_j\cos(\delta_i - \delta_j)] \cdot \frac{R_{ij}^2 - X_{ij}^2}{(R_{ij}^2 + X_{ij}^2)^2} \tag{3.61}$$

and

$$\frac{\partial Q_L}{\partial \theta_{ij}} = -2aV_iV_jB_{ij}\sin\theta_{ij} \tag{3.62}$$

3.4.7 Selection of optimal placement of FACTS devices

Using the loss sensitivities as computed in the previous section, the criteria for deciding device location might be stated as follows:

1. TCSC must be placed in the line having the most positive loss sensitivity index $a_{ij.}$
2. TCPAR must be placed in the line having the highest absolute value of loss sensitivity index b_{ij}.

3.4.8 FACTS-enhanced system test cases

In this section we again consider the transmission dispatch problems treated in Sections 3.3.3 and 3.4.2. Here, the presence of FACTS devices in the power system is accounted for in the optimal power dispatch model.

3.4.9 Six-bus example system

We consider the same six bus system that as was treated earlier in this chapter. In this case, we solve the OPF with TCSC devices installed on two of the most congested lines in the system. To determine the optimal placement of the TCSC devices, we first perform the reactive power loss sensitivity analysis as developed in Section 3.4. The sensitivity index a_{ij} is computed for each line in the system and the result shown in Table 3.8

Table 3.8: VAr Loss Sensitivity Index

Line	From bus	To bus	Sensitivity index
1	1	4	a_{14} = -0.179
2	1	6	a_{16} = -0123
3	2	3	a_{23} = -0.23
4	2	5	a_{25} = -0.15
5	3	4	a_{34} = -0.0189
6	4	6	a_{46} = -0.0184
7	5	6	a_{56} = -0.044

The lines having the most positive loss sensitivity index must be chosen for placement of the TCSC devices. For this we select lines 5 and 6 from Table 3.8.

When TCSC devices in the inductive mode of operation are connected in series with these two lines, with inductive reactances of 53.6% and 48.2% of the line reactances, respectively, it is seen that the line overloads are removed. The effect of optimal power dispatch with the TCSC devices installed on the line flows is shown in Table 3.9.

Table 3.9: Line Flows

Line	From bus	To bus	Line flow (in p.u.)		
			Rated	Without FACTS devices	With TCSCs in lines 5 and 6
1	1	4	0.50	0.138	0.176
2	1	6	0.50	0.383	0.386
3	2	3	0.50	0.480	0.494
4	2	5	0.80	0.132	0.162
5	3	4	0.57	0.62	0.483
6	4	6	0.55	0.562	0.418
7	5	6	0.30	0.025	0.027

The constrained generation and load data may be obtained after running the OPF with the TCSCs installed. Table 3.10 shows a comparison between the data obtained with and without FACTS devices in the system for one particular curtailment strategy employed by the ISO (Case (1)).

Table 3.10: OPF Results with and without TCSC

Bus #	Constrained generation and load, MW, Case (1) of 3.3.3	
	Without FACTS	With FACTS
1	109.63	109.72
2	124.24	124.41
3	34.72	34.96
4	48.87	49.14
5	40.74	41.32
6	53.99	53.99

This integrated framework covers the scenario where, even after putting the FACTS devices into operation, there is a need for the ISO to curtail the initial power transactions in order to maintain the system operation within security limits. The OPF result shows that the individual power transactions suffer less curtailment when FACTS devices are included in the system.

3.4.10 FACTS-enhanced fourteen-bus example system

We consider the same fourteen-bus example system that was treated earlier. Here, we solve the OPF for three different cases. In each case, one of the three FACTS controllers, viz., TCSC, TCPAR, and SVC, is included in the problem formulation. The static models of these devices, as developed in Section 3.4, are considered, i.e., a TCSC is represented as a static impedance, a TCPAR as a transformer with a complex tap ratio, and an SVC as a reactive power source with limits. The optimal locations for placing each of these devices can be determined by sensitivity analysis. In this problem we consider these three cases:

1. A TCSC placed between buses 3 and 11, operated with an inductive reactance of 59.3% of the line reactance
2. A TCPAR placed between buses 3 and 11, operated with a phase shift of –0.039 radians and unity tap ratio.
3. An SVC connected at bus 10, operating as a reactive power source of 0.13 p.u. within limits of ±3.5 p.u., at a voltage of 1.05 p.u.

Here we consider only the Case (4). Table 3.11 shows the results of the OPF with Cases (A), (B) and (C) referring to the results obtained with TCSC, TCPAR, and SVC, respectively.

Table 3.11: OPF Results with TCSC, TCPAR, and SVC

Bus #	Pre-curtailment MW	Constrained generation and load, MW		
		Case (A)	Case (B)	Case (C)
(group #1)				
2 (GENCO)	138.4	136.08	135.73	136.54
3 (GENCO)	92.6	90.29	91.36	90.60
7	54.3	53.76	53.81	53.46
9	91.5	89.93	90.67	90.31
11	56.6	55.31	55.20	55.25
14	28.6	27.37	27.40	28.12
(group #2)				
4 (GENCO)	213.5	208.31	210.81	210.52
8	155.4	155.26	155.30	155.25
10	16.8	13.36	14.97	15.36
12	13.1	11.87	12.71	12.07
13	28.2	27.81	27.83	27.82
(loss compensator)				
1 (GENCO)	38.1	36.85	37.32	36.22

3.5 Conclusions and Future Directions for OPF-Based Congestion Management

The operational aspects of power systems pose some of the most challenging problems encountered in the restructuring of the electric power industry. In this chapter we looked at one such problem. This work focuses on congestion management within an OPF framework in a deregulated electricity market scenario. The conventional OPF problem is modified to create a mechanism that enables the market players to compete and trade and simultaneously ensures that the system operation stays within security constraints. The pool and bilateral dispatch functions of an ISO are dealt with. This chapter then focused on the use of FACTS devices to alleviate congestion. An integrated approach that includes FACTS devices in a bilateral dispatch framework to maintain system security and to minimize deviations from contractual requirements is then proposed. The approach is validated through numerical examples.

OPF is increasingly being used for transmission pricing and transaction evaluation in open access transmission systems. From the case studies carried out in this chapter, it was apparent that the interactions between market players are complex. Future work in this field may focus on quantifying the economic risk faced by market players due to differences in their willingness to pay to avoid curtailment. Research may also be carried out on designing different dispatch and curtailment strategies.

The sensitivity approach for determining optimal locations of FACTS devices can at best give an approximate idea about the optimal location for those devices in a deregulated environment. More reliable methods need to be developed for this.

4. Network Partitioning Schemes for Facilitating OPF-Based Control Algorithms in Large Scale ISO's and RTO's

Use of OPF-based methods in power systems models of a scale appropriate to emerging ISO's and RTO's involve a huge number of state variables, which present barriers both to intuitive understanding of behavior and practical on-line computations. To reduce the computational burden, and to gain qualitative insight, it is often useful to partition the original model into several reduced sub-networks. Such an approach will allow focus on smaller-scale study area and simplify other sub-networks into equivalent models. Extensive research seeking reduced-order models to improve numeric efficiency, while accurately representing the physical behavior of the original systems, has been developed from many perspectives, over several decades. Our work will begin from the foundation of equivalents developed in the context of models for electromechanical oscillations. The work here seeks to extend the underlying rationale of such techniques to models that account for voltage magnitude variation and reactive power flow.

4.1 Background and Related Literature

One of the popular aggregation methods based on "coherency" exploits the observation that in multi-machines transients after a disturbance, some synchronous machines have the tendency to "swing together". Such coherent machines are grouped into "coherent areas" which are then represented by "equivalent machines" [39], [40] and [48]. The approach exploits the two-times-scale properties of the power systems in a linear, time-invariant (LTI) dynamic model. The swing modes of the system are categorized into 2 classes, slow inter-area modes and fast intra-area modes. The small parameter to denote the separation of the time-scales is the ratio of the sparseness of the connections between the coherent machines to the stiffness of the connections within the coherent machines [40]. Thus, when there is a disturbance to these slow inter-area modes, the generator angles in each sub-network will move closely coherently together. The fast intra-area modes are localized within these strongly connected regions.

More flexible area clustering called "synchrony", which is an extension of the concept of coherency, is suggested in [57], [58], and [59]. It is argued in those literatures that the synchrony

recognition and aggregation algorithm has advantages over the slow-coherency algorithm based on Gaussian elimination. The authors define the term “chord” as a selected subset of modes of a linearized model. In their works, groups of generators are said to be exactly or approximately synchronic in a chord ν, or are ν-synchronic, if their angular variations are exactly or approximately in constant proportion for any transient in which only the modes in ν are excited. This is different from the earlier ν - coherency that requires exact or approximate equality of the angular variations.

As an alternative to the singular perturbation approaches for characterizing coherency, [41] iteratively uses the sensitivity of the smallest non-zero eigenvalue to the removal of lines to identify weak cutsets that will partition the network into coherent groups. The advantage of this method is that it provides partitions indicating both generators and load buses within a coherent area, while many of the previously mentioned researches identify only generator buses within an area. This additional information of load buses in the network decomposition is useful because it shows the boundaries of weak links between coherent areas in more details. On the other hand, work in [63] modifies the slow coherency technique in [39] and augments the eigenbasis matrix in [39] to also include the information of load buses. For [63], the approach identifies indices of buses within the coherent groups by measuring the closeness of each bus to each area reference generator. The closeness is the cosine of the angle between the two row vectors of the corresponding eigenbasis matrix. Yet, the criteria for setting a closeness tolerance to assign bus indices into coherent areas are arbitrary. Although the work in [41] shares certain features with algorithms based on locating weak cutsets within the network [50], it has the advantage of explicitly using the interaction of network topology, branch admittances, and machine inertias in determining the electromechanical modes in an unreduced, generalized eigenvalue formulation of the linearized dynamics [41]. However, the literature on that method to date simplifies the analysis to the flat start operating point, treating an operating point at which all the bus voltage magnitudes and bus voltage angles are equal to 1 and 0, respectively. Losses of the system are ignored in this case.

Work in [60] studies the partitioning of the electrical networks using 3 different types of the weighted Laplacian matrix from the network graph and extends the algorithm in [41] to include a set of the smallest eigenvalues as a direct approach to simultaneously, instead of recursively,

partitioning a system into multiple areas. That work also proposes a second method, namely the eigenvector component correlation partitioning, which modifies the correlation function suggested in [63] for the steps in excluding lines between generators. The authors mention that the research is in its initial stage, so that work does not yet offer numerical results comparing quality between these two methods. Moreover, the algorithms require uniform node weights, or equality in all bus voltages, to yield the symmetric Laplacian structure. This analytically desirable structure is lost in the case of a lossy network.

In contrast to the previous works that focused on partitioning the network in dynamic models, this chapter will focus on network partitioning applications in the optimal power flow (OPF). Without considering this OPF aspect, the resulting decomposed sub-networks from all previously mentioned techniques may not be functional under the system's various security constraints. A different strategy will be introduced to obtain the system weighted Laplacian matrix, which accounts for the real topological network structures including losses at the optimal operation point. We notice from our new formulation of the optimal power flow Jacobian that a certain sub-block of this matrix is in the form of graph Laplacian, and could be processed in our network partition. This Laplacian matrix formulation also involves all relevant inequality constraints that limit the system to sustain its security while in the optimal operation. We will apply the concept of the recursive spectral graph bisection (RSB) presented in [38], [S11, and [56] as our basis to formulate the network decomposition scheme. The RSB method is proven in [38] to be optimal among various graph-partitioning techniques.

Although the ties between the areas are weak, they should not be completely disregarded during the steps of network partition. For a higher degree of accuracy in the simulation of the reduced sub-networks, we present here in this research the notion in replacing these ties with the equivalent fixed demands or injections between the links.

This chapter will be organized as follows. In the section 2, we include some graph theoretic terminology, and notation that we will use for our further discussion. The background material on the spectral properties of Laplacian matrices and their relevance to graph partition will be explained in the early of the section 3. The fundamental concepts of the optimal power flow and system topology that apply to the RSB network partitioning will follow. Here, the key properties

of the block matrix $\frac{\partial \mathbf{P^N}}{\partial a}$ of the system optimal power flow Jacobian are exhibited. This block matrix has a form that may be interpreted as weighted graph Laplacian, and the system losses are accounted in this computation. We test our algorithm in the IEEE 9 and 30-buses to demonstrate the performance of our method in preserving the optimal cost of generation for the decomposed sub-networks and in the deviations of the bus nodal prices in scenarios in which their active load demands are significantly increased. In addition, in the IEEE 30-bus case, we arbitrarily partition this network to examine its characteristics comparing with our RSB approach as evidence that the desirable properties produced by RSB are not generic to any partition. The final section contains our conclusions and some directions for future work.

4.2 Terminology and Notation

To start, readers should be familiar with some basic graph theory terminology and notations used in our discussion. We excerpt some of these basic definitions from [45] and [61] for readers' reference:

> A **graph** G with n **vertices** and m **edges** consists of a **vertex set** $V(G)=\{v_1,\ldots,v_n\}$, and an **edge set** $E(G)=\{e_1,\ldots,e_m\}$. A **weighted graph** is a graph for which a value w_i is associated with each vertex v_i, and a nonzero weight w_{ij} is associated with each edge (v_i,v_j). We consider a zero edge weight to indicate the lack of an edge. Note that graph G is also a weighted graph where all edge weights are 1.

A **subgraph** of a graph G is a graph H such that $V(H) \subseteq V(G)$ and $E(H) \subseteq E(G)$; we write this as $H \subseteq G$ and say that "G contains H". A graph G is **connected** if it has a u,v-path for each pair $u,v \in V(G)$ (otherwise it is disconnected). For a connected graph G, an **edge separator** is a set S of edges such that if removed would break the graph into components G_1 and G_2 with no edges between G_1 and G_2. A **vertex separator** is a set S of vertices such that if these vertices and all incident edges are removed, the graph is broken in to components G_1 and G_2 with no edges between G_1 and G_2 (such separators will be assumed to be minimal sets with respect to the particular G_1 and G_2).

The **adjacency matrix** of G, written $A(G)$, whose entry a_{ij} is the number of copies of the edge v_iv_j in G. The **incidence matrix** of a graph G, written $M(G)$, has rows indexed by $V(G)$ and columns indexed by $E(G)$, with m_{ij}=1 if vertex v_i is the tail of e_j, and m_{ij} = -1 if v_i is the head e_j.

4.3 Background

4.3.1 Recursive Spectral Bisection (RSB)

Work in [37] and references therein explain various important applications of graph partitioning: VLSI circuit layout, image processing, solving spare linear systems, computing fill-reducing orderings for sparse matrices, and distributing workloads for parallel computation. Generally, the objective of graph partitioning is to separate the graph's vertices into a predetermined number sub-graphs, in which each sub-graph has an equal number of vertices and the cutset links among these sub-graphs are minimized.

Pothen, Simon, and Liou introduce an approach in [56] to partition the input graph using the spectral information of the Laplacian matrix, *L*; this technique is referred to as **recursive spectral bisection (RSB)**.

Work in [36] exhibits a proposition of the Laplacian matrix *L* that this matrix *L* should satisfy:

$$L = MM^t = \Delta - A \tag{4.1}$$

where *M* is the incidence matrix of graph *G*, *A* is the adjacency matrix of *G*, and Δ is the diagonal matrix whose i^{th} entry is the degree of the vertex v_i ($1 \le i \le n$). Thus, *L* is independent of the orientation given to *G*.

For a connected graph, *L* has the property that its smallest eigenvalue is equal to zero, and each element of the corresponding eigenvector is equal to one; all other eigenvalues are greater than zero. Miroslav Fiedler proved several properties of the second smallest eigenvalue and its corresponding eigenvector of this Laplacian matrix in his famous works [43] and [44]. These second smallest eigenvalue and eigenvector have now become known as "Fiedler value" and "Fiedler vector," respectively, in recognition for his contribution. The RSB method that we mentioned is based on the Fiedler vector of this Laplacian matrix *L*. 1

Holzerichter and Oliveria clearly illustrate in [47] to show how finding a partition of a graph, which minimizes the number of edge-cuts, can be transformed into an eigenvalue problem involving the graph Laplacian. In their analysis, they use Lagrange multipliers to solve

optimization problem setting the objective function to minimize the number of edges between the two parts. The non-linear equality constraints are stipulated in the first condition that the number of vertices in each part be equal, and second condition that every vertex be assigned to one of the partitions.

Chan, and Szeto in [38] show the size of the cutsets can be minimized by using, specifically, the corresponding second smallest eigenvalue, the Fiedler value, of the Laplacian matrix, *L*. They introduce the concept of median cut RSB method that maps indices of vertices which have values above the median value of Fiedler vector to one part and below the median value of Fiedler vector to the other. They prove that this median cut method is the optimal in the sense that partition vector induced by this method is the partition vector closest to the Fiedler vector in any l_s norm, for $s \geq 1$. The partitions are then further partitioned by recursive application of the same procedure. The multiplicity of zero eigenvalues of *L* indicates the number of connected sub-graphs in *G*. The magnitude of the Fiedler value is proved in [53] as a measure of the connectivity among these sub-graphs, and the magnitude of each element of the Fiedler vector as a measure of an approximated vertex-distance from the other vertices. If any 2 values of elements in the Fiedler vector are closed together, the corresponding vertices connecting path will be short.

4.3.2 Power system network modeling

Previous work in power systems network modeling in [41], with minor enhancements, will be shown in this section. We consider here a power network, with shunts neglected, as the interconnection structure of a directed graph *G*. The original power network has *n* buses and *l* branches, or hereby *n* vertices and *l* edges. Assume each branch has weight *b*, thus, the admittance matrix of the network is $Y(b) := A\text{diag}\{b\}A^T$ where matrix *A* is an unreduced incidence matrix for this graph. The equilibrium system frequency is equal to a known value of ω_0. With no coupled lines, no phase shifting transformers, “primitive” per phase admittance matrix will be diagonal. We assume, in our first illustration, reactive equations are normalized by voltage magnitude as in [55] to yield a symmetric power flow Jacobian.

Let

$V \in \Re^{n-m}$, V:= vector of variable bus voltage magnitudes;

$\ddot{a} \in \Re^{n}$, $\ddot{a}$:= vector of bus voltage phase angles relative to an arbitrary synchronous reference frame of frequency $\grave{u}_0$;

$\grave{u} \in \Re^{m}$, $\grave{u}$:= vector of generator frequency deviations, relative to synchronous frequency $\grave{u}_0$;

$A \in \Re^{nxl}$, A:= the full bus incidence matrix for the network, (no elimination of a reference bus);

$|A|$ is constructed by taking component-wise absolute value.

$b_l \in \Re^{l}$, b_l:= vector of transmission line susceptances;

$P^I \in \Re^{n}$, P^I:= vector of net active power injection at each bus. For indices j ranging from *1* to (through) m, P_j^I is a constant equal to the mechanical power input to machine j. For j ranging from $m+1$ to through n, component P_j^I is a constant equal to the negative value of active load demand.

$Q^{I:}\ \Re^{n-m} \rightarrow \Re^{n-m}$, $Q^I(V)$:= vector valued function of net reactive power injections at load buses, normalized by voltage magnitude. Each component Q_j^I is a function of voltage magnitude at that bus only.

L:= rows $m+1$ through n of an nxn identity matrix (e.g., projection operator selecting components $m+1$ through n of an n-vector);

Under the above simplified assumption, active and (voltage-normalized) reactive power absorbed by the network at each bus may be written to follow MATLAB[1] format as below. In particular

$P^N(\ddot{a}, V)$: = vector-valued function of active power absorbed by network at each bus

$$= A\,\mathrm{diag}\{b_l\}\,\mathrm{diag}\{exp(|A|^{T}\ln(V))\}(sin(A^{T}\ddot{a}) \qquad (4.2)$$

[1] MATLAB is a highly efficient matrix computational program developed by MathWorks [51].

$[\text{diag}(V)]^{-1} Q^N(\ddot{a}, V)$: = vector-valued function of reactive power absorbed by network at each load bus, normalized by bus voltage magnitude

$$= L\text{diag}\{|A|\, b_l\}V - [\text{diag}\{V_L\}^{-1} L_2 |A| \text{diag}\{\, b_l\}\text{diag}\{exp(|A|^T ln(V)\} cos(A^T \ddot{a}) \quad (4.3)$$

Its corresponding power Jacobian is:

$$J : \Re^n \times \Re^{n-m} \rightarrow \Re^{(2n-m)\times(2n-m)}$$

$$J = \begin{bmatrix} \dfrac{\partial P^N}{\partial \ddot{a}} & \dfrac{\partial P^N}{\partial V_L} \\ \dfrac{\partial Q^N}{\partial \ddot{a}} & \dfrac{\partial Q^N - Q^I}{\partial V_L} \end{bmatrix} \quad (4.4)$$

where

$$\begin{aligned} \frac{\partial P^N}{\partial \ddot{a}} &= A\text{diag}\{b_l\}\text{diag}\{\exp(|A|^T \ln(V))\}\text{diag}\{\cos(A^T \ddot{a})\}A^T \\ \frac{\partial P^N}{\partial V_L} &= A\text{diag}\{b_l\}\text{diag}\{\exp(|A|^T \ln(V))\}\text{diag}\{\sin(A^T \ddot{a})\}|A|^T L^T [\text{diag}\{V_L\}]^{-1} \\ \frac{\partial Q^N}{\partial \ddot{a}} &= [\text{diag}\{V_L\}]^{-1} L|A|\text{diag}\{b_l\}\text{diag}\{\exp(|A|^T \ln(V))\}\text{diag}\{\sin(A^T \ddot{a})\}A^T \\ \frac{\partial Q^N - Q^I}{\partial V_L} &= L\text{diag}\{|A| b_l\}L^T + H - \text{diag}\{\text{diag}(H)\} + \text{diag}\{Q\}[\text{diag}\{V_L^{\,2}\}]^{-1} \end{aligned} \quad (4.5)$$

$$H = LA\text{diag}\{b_l\}\text{diag}\{\cos(A^T \ddot{a})\}A^T L^T$$

4.3.3 Role of optimal power flow concepts in partitioning

In this section, we will explain some fundamental concepts of the optimal power flow (OPF) before we proceed further. We summarize some OPF concepts from [62] as below:

Basic OPF will seek the operating point of a power system with the objective to reach a minimum active power generating cost while balancing the entire power flow, and satisfying other sets of security constraints. The limits on $P_{gi}^- \le P_{gi} \le P_{gi}^+$, $Q_{gi}^- \le Q_{gi} \le Q_{gi}^+$, $|V_i|^- \le |V_i| \le |V_i|^+$, and flows on transmission lines will allow the dispatch of the generation while not allowing the

transmission system to violate a limit while achieving the minimum cost of generation. "Bus incremental costs" or (BICs) from OPF solution can be used in power systems economic analyses to set the marginal cost of power at any bus in the system.

From a standard OPF formulation, one approaches the general optimization problem:

$$\text{Min} \sum_{i=1}^{m} C_i(P_{gi}) \qquad \text{(total cost of active power generation)}$$

subject to

$$\underline{f}(\underline{\delta},\underline{v}) + \begin{bmatrix} -\underline{P_g} \\ \underline{P_d} \\ \underline{0} \end{bmatrix} = \underline{0} \text{ (active power balance equations)}$$

$$\underline{g}(\underline{\delta},\underline{v}) - \underline{Q_d} = \underline{0} \text{ (reactive power balance equations)}$$

$$P_{gi}^{-} \le P_{gi} \le P_{gi}^{+} \text{ (active power generation limits)}$$

$$Q_{gi}^{-} \le Q_{gi} \le Q_{gi}^{+} \text{ (reactive power generation limits)}$$

Line flow limits and other inequality constraints (4.6)

For convenience, we underline some of the above variables to emphasize their vector or matrix structures. The state vectors, $\underline{\delta}$, and $\underline{v}$, are the voltage angles at all buses (including the slack bus) and the non-generator bus voltage magnitudes respectively. The above $\underline{f}(\underline{\delta},\underline{v})$ denotes the real power absorbed into the network at all buses; $\underline{g}(\underline{\delta},\underline{v})$ denotes the reactive power absorbed into the network at all non-generator buses; and $C_i(P_{gi})$ in the objective function denotes the variable cost of operation for each generator.

To solve the above OPF problem, we construct the following Lagrange equation:

$$L(\underline{P_g},\underline{P_d},\underline{\delta},\underline{v}) = \sum_{i=1}^{m} C_i(P_{gi}) + \underline{\lambda}^T \underline{F}(\underline{P_g},\underline{P_d},\underline{\delta},\underline{v}) + \underline{\gamma}^T \underline{\phi}(\underline{P_g},\underline{P_d},\underline{\delta},\underline{v}) \tag{4.7}$$

In equation (4.7), $\underline{F}(\underline{P_g}, \underline{P_d}, \underline{\delta}, \underline{v})$ and $\underline{\phi}(\underline{P_g}, \underline{P_d}, \underline{\delta}, \underline{v})$ represent the real and reactive power balance equality constraints and all inequality constraints from (6) respectively.

A candidate optimal solution can then be determined by solving for the Kuhn-Tucker conditions [49]:

$$\lambda_{gi} - \frac{\partial C_i}{\partial P_{gi}} - \gamma^T \frac{\partial \phi}{\partial P_{gi}} = 0, \quad i = 1,\ldots,m$$

$$\gamma^T \frac{\partial \phi}{\partial P_{dj}} - \lambda_{dj} = 0, \quad j = 1,\ldots,n$$

$$\underline{\lambda}^T \begin{bmatrix} \frac{\partial \underline{f}}{\partial \underline{\delta}} & \frac{\partial \underline{f}}{\partial \underline{v}} \\ \frac{\partial \underline{g}}{\partial \underline{\delta}} & \frac{\partial \underline{g}}{\partial \underline{v}} \end{bmatrix} + \underline{\gamma}^T \begin{bmatrix} \frac{\partial \underline{\phi}}{\partial \underline{\delta}} & \frac{\partial \underline{\phi}}{\partial \underline{v}} \end{bmatrix} = \underline{0}^T$$

$$\underline{F}(\underline{P_g}, \underline{P_d}, \underline{\delta}, \underline{v}) = \underline{0}$$

$$\underline{\phi}(\underline{P_g}, \underline{P_d}, \underline{\delta}, \underline{v}) \le \underline{0}$$

$$\underline{\gamma}^T \phi = 0$$

$$\underline{\gamma}^T \ge \underline{0}^T \qquad (4.8)$$

Each element of the vector $\underline{\gamma}^T$ in (4.8) indicates whether the inequality constraints are binding. If the element of γ is zero, the corresponding inequality constraint is free to be non-binding; if the element of γ is positive, then the corresponding inequality constraint must be binding. We refer these last 2 equations of (4.8) as **the complimentary slackness conditions**.

4.3.4 Median cut spectral bisection power systems network partitioning

We can observe that the block matrix $\frac{\partial P^N}{\partial \ddot{a}}$ in (4) is in the form of Laplacian matrix associated with the weighted graph whose voltage magnitude weight V_i is assigned to each vertex v_i, and branch admittance weight b_{ij} is assigned to each edge (v_i,v_j). Thus, we can directly apply any property of the weighted Laplacian matrix, L to the block $\frac{\partial P^N}{\partial \ddot{a}}$. Specifically by the RSB method, we can use this $\frac{\partial P^N}{\partial \ddot{a}}$ block to partition the power systems network into smaller sub-systems.

As an alternative to formulating the Jacobian matrix in (4), and (5), we can use another technique to account for the losses of the study system. This derivation is described in [42] and will be repeated below. We will use bus voltage phasors and external current injections as intermediate variables during the Jacobian matrix construction. The overbar of the form "$\vec{\ }$" is used to emphasize a complex valued quality.

Let

$\delta \in \Re^n$, δ:= vector of bus voltage phase angles relative to an arbitrary synchronous reference frame of frequency (reference angle is **not** deleted);

$V \in \Re^n$, V:= vector of variable bus voltage magnitudes;

$\vec{V} \in \boldsymbol{C}^n$, $\vec{V}$:= vector of complex bus voltages; note that $\vec{V} = V.*\exp(j\delta)$

$\vec{Y} \in \boldsymbol{C}^{nxn}$, $\vec{Y}$:= full bus admittance matrix (reference bus rows and column not eliminated);

$\vec{I} \in \boldsymbol{C}^n$, $\vec{I}$:= vector of currents absorbed into network at each bus;

note that $\vec{I} = \vec{Y} * \vec{V}$

$\vec{S} \in \boldsymbol{C}^n$, $\vec{S}$:= vector of complex powers absorbed into network at each bus;

note that $\vec{S} = \vec{V}.*\text{conj}(\vec{I}) = \text{conj}(\vec{I}).*(\vec{V})$

$$\frac{\partial \vec{V}}{\partial \delta} = \frac{\partial\{V.*\exp(j\delta)\}}{\partial \delta} = \text{diag}\{V\} * \frac{\partial\{\exp(j\delta)\}}{\partial \delta}$$

$$= j * \text{diag}\{V\} * \text{diag}\{\exp(j\delta)\} \qquad = j * \text{diag}\{\vec{V}\}$$

$$\frac{\partial \vec{I}}{\partial \delta} \quad = \vec{Y} * \frac{\partial\{V .* \exp(j\delta)\}}{\partial \delta} \qquad = \vec{Y} * \text{diag}\{V\} * \frac{\partial\{\exp(j\delta)\}}{\partial \delta}$$

$$= j * \vec{Y} * \text{diag}\{V\} * \text{diag}\{\exp(j\delta)\} = j * \vec{Y} * \text{diag}\{\vec{V}\}$$

$$\frac{\partial\{\text{conj}(\vec{I})\}}{\partial \delta} = \text{conj}(j * \vec{Y}) * \text{diag}\{\text{conj}(\vec{V})\} = \text{conj}(j * \vec{Y} * \text{diag}\{\vec{V}\})$$

$$\frac{\partial \vec{V}}{\partial V} \quad = \frac{\partial\{\exp(j\delta) .* V\}}{\partial V} \qquad = \text{diag}\{\exp(j\delta)\} * \frac{\partial\{V\}}{\partial V}$$

$$= \text{diag}\{\exp(j\delta)\}$$

$$\frac{\partial \vec{I}}{\partial V} \quad = \vec{Y} * \frac{\partial\{\exp(j\delta) .* V\}}{\partial V} \qquad = \vec{Y} * \text{diag}\{\exp(j\delta)\}$$

$$\frac{\partial\{\text{conj}(\vec{I})\}}{\partial V} = \text{conj}(\vec{Y}) * \text{diag}\{\exp(-j\delta)\} \tag{4.9}$$

Thus,

$$\frac{\partial \vec{S}}{\partial \delta} = j * \text{diag}\{\text{conj}(\dot{\text{I}}) .* \vec{V}\} - j * \text{diag}\{\vec{V}\} * \text{conj}(\vec{Y}) * \text{conj}(\vec{V})\}$$

$$\frac{\partial \vec{S}}{\partial V} = j * \text{diag}\{\text{conj}(\dot{\text{I}}) .* \exp(j\delta)\} + j * \text{diag}\{\vec{V}\} * \text{conj}(\vec{Y}) * \text{diag}(\exp(-j\delta)\} \tag{4.10}$$

Blocks of the power flow Jacobian in a standard form are easily recovered from the above expressions by selecting the appropriate rows and columns of the real or imaginary parts of $\frac{\partial \vec{S}}{\partial \delta}$ or $\frac{\partial \vec{S}}{\partial V}$. The block $\frac{\partial P^N}{\partial \ddot{a}}$ obtained from this derivation will still preserve the properties of the weighted Laplacian matrix, and we will use this block matrix in our next steps of the network partitioning.

Given a power systems study network, first, we predetermine a desired number of final sub-networks. We solve OPF to find its optimal operating point of this system. As a result, we will obtain the un-reduced network OPF Jacobian (no deletion of the associated slack generator components during the matrix construction). Next, we will apply RSB technique to this weighted Laplacian matrix $\frac{\partial P^N}{\partial \ddot{a}}$ block Jacobian. Its smallest eigenvalue is 0, and every element of the corresponding eigenvector is one. We will map indices of vertices of their magnitudes above the median value of the Fiedler vector to one part and below the median value of the Fiedler vector to the other. For a higher degree of accuracy in the simulation of the reduced sub-networks, we replace the ties that link between these new decomposed areas with the equivalent fixed demands or injections of values equal to OPF line power flows. The branch flows "from" the relating buses will be assigned positive values, and the flows "to" buses will be assigned negative values. If a larger number of sub-networks is required, we will then recursively partition further, using the same approach, in the sub-network that has smaller Fiedler value of the OPF sub-network Jacobian.

4.4 Optimal Power Flow (OPF) Solver

In our OPF computation of the nonlinear optimization with constraints, we will use *fmincon* command that is a newer release than *constr* used in MATPOWER-OPF solver developed by PSERC [64]. The command *fmincon* is included in the Optimization Toolbox (available with MATLAB 5.3 Release 11). It uses a successive quadratic programming technique with a quasi-Newton approximation for the Hessian matrix [54]. The performance of *fmincon* to solve the OPF depends on numerous factors, i.e., *fmincon* has its limitations in solving the sparse non-linear constrained minimization problem as our case, so our study networks are inherently limited to medium-sized power systems. For a very large-scale power systems network, there are several commercial constrained optimization solvers available, e.g. TOMLAB [46]. These packages do exploit sparsity and claim to be more robust and more efficient, but were not tested in this work.

4.5 Numerical Analysis

4.5.1 IEEE 9-bus network example

In our initial presentation, we will use the 9-bus power systems data obtained from the MATPOWER-OPF solver of PSERC. This network contains 3 generators (buses 1, 2, and 3) injecting power to the system feeding 3 loads at buses 5, 7, and 9.

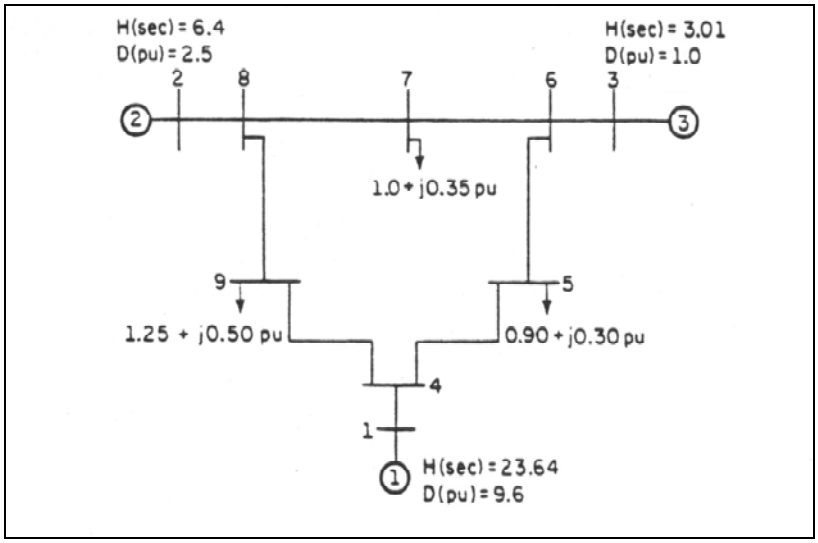

Figure 4-1: 9-Bus power systems test network

Our goal here is to separate this 9-bus network into the 2 smaller sub-networks. In computing the Fiedler eigenvector during the RSB routine, the MATLAB *eigs* function (finding a few eigenvalues and eigenvectors of a sparse matrix) will be employed.

The polynomial characteristic cost functions of these 3 generators are shown in Table 4.1. The relationship of a power generating cost (in \$/hr) and a specific active power output (in MW) is in the quadratic form: $C_i(P_{gi}) = c_{2i}P_{gi}^2 + c_{1i}P_{gi} + c_{0i}$.

Table 4.1: The Polynomial Characteristic Cost Coefficients of the 9-Bus Network

Generator at Bus	c2	c1	c0
1	0.1100	5.0	150
2	0.0850	1.2	600
3	0.1255	1.0	335

The security constraints on generating active power outputs, bus voltage magnitudes, and transmission line flows are presented in Tables 4.2 to 4.4 respectively. Note that the base voltage for each bus is 345 KV.

Table 4.2: The Limits of Generating Active Power Outputs

Generator at Bus	Minimum Active Power Output (MW)	Maximum Active Power Output (MW)
1	10	250
2	10	300
3	10	270

Table 4.3: The Limits of Bus Voltage Magnitudes - Base Voltage for Each Bus = 345 KV

Bus No.	Lower Boundary (p.u.)	Upper Boundary (p.u.)
1	0.90	1.10
2	0.90	1.10
3	0.90	1.10
4	0.90	1.10
5	0.90	1.10
6	0.90	1.10
7	0.90	1.10
8	0.90	1.10
9	0.90	1.10

Table 4.4: The Limits of Transmission Line Flows

Between Buses	Maximum Active Line Flow (MW)
1 - 4	250
4 - 5	250
5 - 6	150
3 - 6	300
6 - 7	150
7 - 8	250
8 - 2	250
8 - 9	250
9 - 4	250

Table 4.5: The Complex Power Demands – Base Case Load Demands (MW/MVar)

Bus No.	Pd	Qd
5	90	30
7	100	35
9	125	50

We run our OPF solver to find the system's optimal operating point at the base load demands as in Table 4.5. The results are the optimal bus voltage magnitudes and angles, the complex power branch flows, the active power injected from each generator, and the active power nodal price at each bus (see Tables 6 to 9).

Table 4.6: The Resulting Optimal Bus Voltage Magnitude and Angle at Each Bus

Bus#	V p.u.	Angle-degrees
1	1.1000	0.2919
2	1.0974	5.1852
3	1.0866	3.5411
4	1.0942	-2.1711
5	1.0844	-3.6902
6	1.1000	0.8945
7	1.0895	-0.9047
8	1.1000	1.1972
9	1.0718	-4.3235

Table 4.7: The Associated Branch Flows (*100 MW)

"From"-Bus	"To"-Bus	Line Power (pu) "From" Bus Side	Line Power (pu) "To" Bus Side
1	4	0.8980 + 0.1297i	-0.8980 - 0.0905i
4	5	0.3522 - 0.0389i	-0.3504 - 0.1388i
5	6	-0.5496 - 0.1612i	0.5597 - 0.2219i
3	6	0.9419 - 0.2263i	-0.9419 + 0.2729i
6	7	0.3822 - 0.0510i	-0.3807 - 0.1868i
7	8	-0.6193 - 0.1632i	0.6221 + 0.0082i
8	2	-1.3432 + 0.0933i	1.3432 + 0.0003i
8	9	0.7211 - 0.1015i	-0.7072 - 0.1892i
9	4	-0.5428 - 0.3108i	0.5458 + 0.1294i

Table 4.8: The Optimal Active Power Output from Each Generator

Generator at Bus number	Pg (MW)
1	89.8020
2	134.3182
3	94.1864

Table 4.9: The Lagrange Multipliers (The Active Power Nodal Prices in $/MWhr) of the IEEE 9-Bus Network – Unreduced Network (Base Case Load Demands)

Bus No.	Nodal price ($/MWhr)
1	2475.6
2	**2403.5**
3	2407.6
4	2475.6
5	2499.9
6	2407.6
7	2425.4
8	2403.5
9	**2499.9**
average	2444.3

When we substitute the values of the active power outputs from Table 4.8 to their corresponding polynomial characteristic cost coefficients in Table 4.1, the summation of the optimal power generating cost of this 9-bus network at the base case will be $5,296.69/hr.

The voltage magnitudes at buses 1, 6, and 8 reach their upper boundaries (1.10 p.u. volts, see Table 4.3 and Table 4.6). Each transmission line flow limit and each generating active power

output limit has a rating of approximately 250MW, which is much higher than the values in Table 4.7 and Table 4.8. As a result, none of other inequality constraints is active. From Table 4.9, the active power nodal price is the highest at bus number 9 ($2,499.9/MWhr), and the lowest at bus number 2 ($2,403.5/MWhr). The average of all active nodal prices is $2,444.3/MWhr.

The right eigenvectors relating to the two smallest eigenvalues of the $\frac{\partial P^N}{\partial \ddot{a}}$ block are shown in Table 4.10.

Table 4.10: The Right Eigenvectors Corresponding to the Two Smallest Eigenvalues of the $\frac{\partial P^N}{\partial \ddot{a}}$ block of the OPF Jacobian

Row	First	Second
1	0.3333	0.5282
2	0.3333	-0.3393
3	0.3333	-0.3198
4	0.3333	0.4097
5	0.3333	0.2440
6	0.3333	-0.2463
7	0.3333	-0.3031
8	0.3333	-0.2568
9	0.3333	0.2403

From Table 4.10, the median value of its Fiedler vector is -0.2463. We will assign the bus indices whose corresponding Fiedler vector element greater than this median value to one sub-network, and the rest to the other sub-network. Figure 2 shows the graphic bisection partitioning after our final MATLAB computation. The bus numbers 1, 4, 5, and 9 are grouped together forming a sub-network, and the bus numbers 2, 3, 6, 7, and 8 are grouped into the other set. The branches connected between buses 5-6, and buses 8-9 are the edge-separators between these two sub-networks. The corresponding eigenvalues of Table 4.10 are 0.0000, and 4.6812 respectively. As mentioned earlier, the Fiedler value can be used to indicate the connectivity of the 2 sub-networks. Thus, the large value of 4.6812 from this solution indicates a relatively high degree of coupling between the resulting 2 sub-networks.

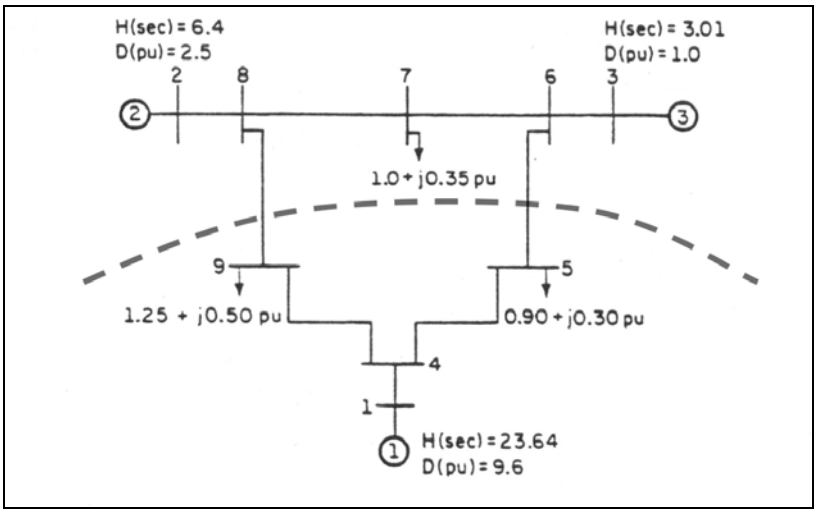

Figure 4-2: The final bisection result of the spectral bisection partitioning

Next, we need to replace each cutset-link with the equivalent fixed complex (active, and reactive) demand or injection at both connected buses, as in Fig 3. The value of each complex OPF branch flow for this replacement is obtained from Table 4.7, and will be repeated in Table 4.11.

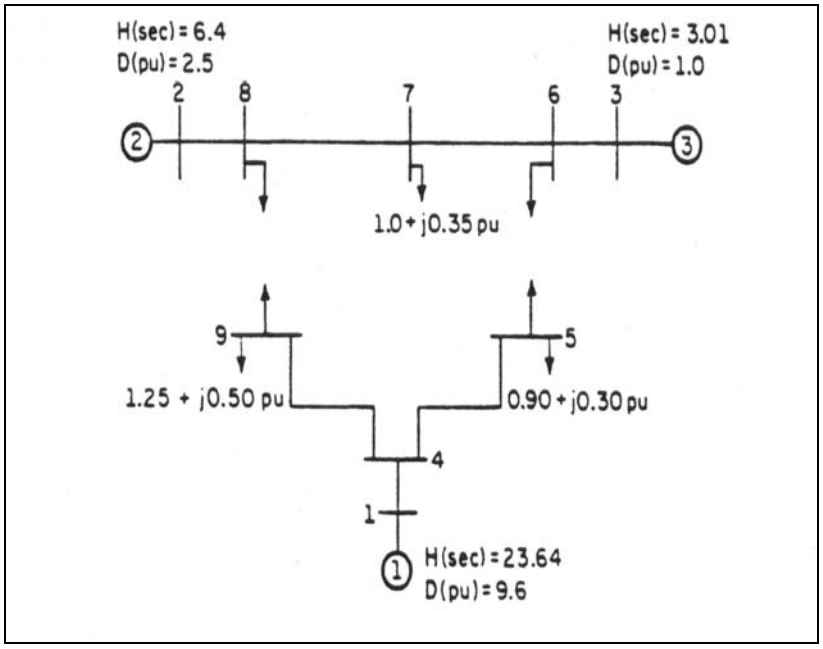

Figure 4-3: Two separate independent sets after replacing each branch flow by fixed complex load demands

Table 4.11: The Equivalent Fixed Complex Power Demands or Injections of the Buses Forming the Edge Separators (MW/MVar)

Bus Number	Pd	Qd
5	-54.9579	-16.1180
6	55.9676	-22.1907
8	72.1091	-10.1513
9	-70.7155	-18.9245

The accuracy of these 2 reduced sub-networks can be measured by running the OPF in each decomposed sub-network (see Table 4.12 and Table 4.13).

Table 4.12: The Optimal Active Power Output from Each Generator - 2 Decomposed Sub-Networks (Base Load Demands)

Generator Number	in Part	Pg (MW)
1	1	89.8020
2	2	134.3182
3	2	94.1864

Table 4.13: The Lagrange Multipliers (Active Power Nodal Prices in $/MWhr) of the RSB Partitioning Network – 2 Decomposed Sub-Networks (Base Demands)

Bus No.	Part	Nodal prices ($/MWhr)	The magnitudes of errors from the unreduced network	% errors from the unreduced network
1	1	2475.6	0.0	0.0000
2	2	**2403.9**	-0.4	-0.0166
3	2	2406.9	**0.7**	**0.0291**
4	1	2475.7	-0.1	-0.0040
5	1	**2501.0**	**-1.1**	**-0.0440**
6	2	2406.9	0.7	0.0291
7	2	2425.3	0.1	0.0041
8	2	**2403.9**	-0.4	-0.0166
9	1	2499.4	0.5	0.0200
average		2444.3	0.0	0.0001

The resulting total OPF generating cost from Table 4.12 is $5,296.69/hr, which as expected, is exactly the same as the total cost obtained from the unreduced network in Table 4.8. In addition, the errors of the active power nodal prices in Table 4.13 are very small comparing with the values in Table 4.9.

Next, we increase active loads in all load buses (buses 5, 7, and 9) as high as 130% of their original values, and then test the accuracy of the resulting reduced sub-networks using the same approach. Consequently, the generating active power outputs of the unreduced network will be as shown in Table 4.14, and the system active power nodal prices will be as shown in Table 4.15. In this case, the voltage magnitudes at buses 1, 2, and 6 reach their upper boundaries (1.10 p.u. volts). The line flow limits and the generating power output limits are still much higher than the resulting branch flows and the generating power outputs from OPF solutions. Accordingly, none of these inequality constraints is active.

Table 4.14: The Optimal Active Power Output of Each Generator – Unreduced Network (130% Active Load Demands)

Generator at Bus Number	Pg (MW)
1	121.4108
2	172.6415
3	120.9157

Table 4.15: The Lagrange Multipliers (The Active Power Nodal Prices in $/MWhr) – Unreduced Network (130% Active Load Demands)

Bus No.	Nodal prices ($/MWhr)
1	3171.0
2	**3054.9**
3	3062.4
4	3171.2
5	3214.3
6	3062.4
7	3092.4
8	3055.5
9	**3214.7**
average	3122.1

As a result, the total OPF generating cost now is raised to $7,966/hr. The system's lowest active power nodal price is still at bus 2 ($3,054.9/MWhr); the highest is at bus 9 ($3,214.7/MWhr).

In the above decomposed sub-network case, if we run the OPF in each reduced sub-network separately again, we will obtain the results as shown in Table 4.16 and Table 4.17.

Table 4.16: The Optimal Active Power Output from Each Generator – 2 Decomposed Sub-networks (130% Active Load Demands)

Generator at Bus Number	in Part	Pg (MW)
1	1	155.1871
2	2	145.4134
3	2	109.9601

Table 4.17: The Lagrange Multipliers (The Active Power Nodal Prices in $/MWhr) – 2 Decomposed Sub-networks (130% Active Load Demands)

Bus No.	Part	Nodal prices ($/MWhr)	The magnitudes of errors from the unreduced network	% errors from the unreduced network
1	1	3914.1	-743.1	-23.4342
2	2	2673.2	381.7	12.4947
3	2	**2664.2**	**398.2**	**13.0029**
4	1	3914.6	-743.4	-23.4422
5	1	**3987.8**	**-773.5**	**-24.0643**
6	2	**2664.2**	**398.2**	**13.0029**
7	2	2702.1	390.3	12.6213
8	2	2672.7	382.8	12.5282
9	1	3980.3	-765.6	-23.8156
average		3241.5	-119.4	-3.4563

Consequently, the summation of the OPF generating costs from both parts will be $8,073/hr. The error from the unreduced network is $\left(\frac{7{,}966 - 8{,}073}{7{,}966}\right) \times 100$ = -2.598 %. From Table 4.17, the highest active power nodal price of these 2 decomposed sub-networks is at bus 5 ($3,987.8/MWhr), and the lowest is at buses 3 and 6 ($2,664.2/MWhr). Buses 3 and 6 are connected next to each other. The average of all bus nodal prices is $3,241.5/MWhr. The lowest magnitude of errors comparing with the value from the unreduced network is at bus 5 ($-773.5/MWhr) and the highest is at buses 3 and 6 ($398.2/MWhr). The average of all error magnitudes is $-119.4/MWhr or -3.4563%. The above analysis in OPF generating cost errors and active nodal price errors indicates a relatively high degree of accuracy of the decomposed sub-network OPF solution relative to the unreduced network, even when we have increased every load demand by 130%.

Instead of the 2 sub-networks, if we need to partition further to focus our study on a smaller scale in 3 separated parts, we can proceed using the same technique as we did previously. Starting from the earlier reduced 2 sub-networks, we choose to partition a sub-network with the smaller Fiedler value, which means that sub-network will display the lower degree of the connectivity within its own elements. The Fiedler value obtained during this third sub-network partitioning routine is 5.6835. The Fiedler values of 4.6812 and 5.6835 indicate these sub-networks are highly connected. If the resulting 3 sub-networks had been completely disconnected, their corresponding Fiedler values of the second and the third partitioning should be both 0.

The voltage magnitudes at buses 1 and 8 reach their upper boundaries. None of other inequality constraints is active. The graphic partitioning after the final RSB partitioning procedures is shown in Figure 4. Buses 1, 4, 5, and 9 are grouped in the first independent set, buses 2, 7, and 8 in the second, and buses 3, and 6 in the third. Now, the branches connecting between buses 5-6, 6-7, and 8-9 are the edge separators between these three groups.

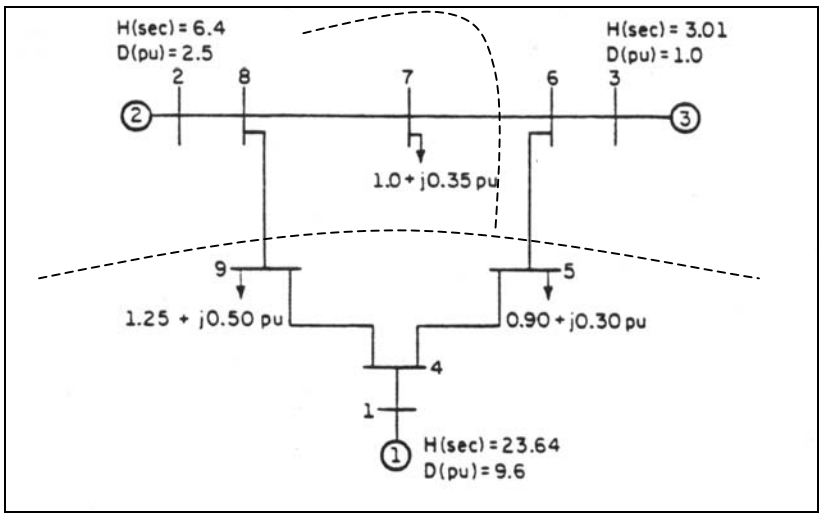

Figure 4-4: The final 3 RSB partitioning of the 9-bus network

Similarly, we delete each edge-cut and replace it with the equivalent fixed complex (active, and reactive) demand or injection at both ends with the corresponding OPF branch flow. The final graphic representation of these decomposed sub-networks are displayed in Figure 5. The value of the complex OPF branch flow for each edge-cut replacement is shown in Table 4.18.

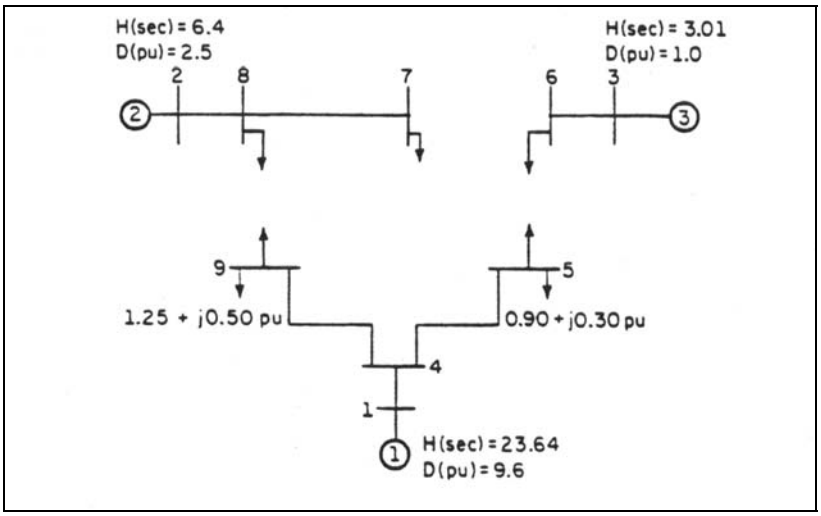

Figure 4-5: Three separate independent sets after replacing each branch flow in edge separators with fixed complex load demands

Table 4.18: The Equivalent Fixed Complex Power Demands or Injections of the Buses Forming the Edge Separators (MW/MVar)

Bus Number	Pd	Qd
5	-54.9579	-16.1180
6	94.1596	-27.2888
7	-38.0430	-18.6878
8	72.1091	-10.1513
9	-70.7155	-18.9245

We run the OPF in each sub-network separately and check the resulting active power output from each generator and each bus active nodal price. The solutions are shown in Table 4.19 and Table 4.20.

Table 4.19: The Optimal Active Power Output from Each Generator - 3 Decomposed Sub-networks (Base Load Demands)

Generator Number	in Part	Pg (MW)
1	1	89.8020
2	2	134.3450
3	3	94.1596

Table 4.20: The Lagrange Multipliers (Active Power Nodal Prices in $/MWhr) – 3 Decomposed Sub-networks (Base Load Demands)

Bus No.	Part	Nodal prices ($/MWhr)	The magnitudes of errors from the unreduced network	% errors from the unreduced network
1	1	2475.6	0.0	0.0000
2	2	2403.9	-0.4	-0.0166
3	3	2406.9	**0.7**	**0.0291**
4	1	2475.7	-0.1	-0.0040
5	1	**2501.0**	-1.1	-0.0440
6	3	2461.0	**-53.4**	**-2.2180**
7	2	2425.3	0.1	0.0041
8	2	**2403.9**	-0.4	-0.0166
9	1	2499.4	0.5	0.0200
average		2450.3	-6.0	-0.2496

In this base load demand case, the total OPF generating cost of the decomposed sub-networks is $5,296.70/hr, which is also almost the same as the total cost obtained from the unreduced network, $5,296.69/hr. The magnitudes of errors comparing with the corresponding magnitudes from the unreduced network are very small. However, when we compare with the previous results of the 2-sub-network case (Table 4.13), the magnitudes and the percentages of errors in Table 4.20 (3 decomposed sub-networks) are higher.

When we increase the active power load demands in buses 5, 7, and 9 to 130% of their original values, we will obtain the generating active power output and the bus active nodal prices as shown in Table 4.21 and Table 4.22.

Table 4.21: The Optimal Active Power Output of Each Generator - 3 Decomposed Sub-networks (130% Active Load Demands)

Generator Number	in Part	Pg (MW)
1	1	155.1871
2	2	164.6798
3	3	94.1596

Table 4.22: The Lagrange Multipliers (Active Power Nodal Prices in $/MWhr) – 3 Decomposed Sub-networks (130% Active Load Demands)

Bus No.	Part	Nodal prices ($/MWhr)	The magnitudes of errors from the unreduced network	% errors from the unreduced network
1	1	3914.1	-743.1	-23.4342
2	2	2919.6	135.3	4.4290
3	3	**2406.9**	**655.5**	**21.4048**
4	1	3914.6	-743.4	-23.4422
5	1	**3987.8**	**-773.5**	**-24.0643**
6	3	2461.0	601.4	19.6382
7	2	2959.2	133.2	4.3073
8	2	2919.8	135.7	4.4412
9	1	3980.3	-765.6	-23.8156
average		3273.7	-151.6	-4.5040

The total optimal cost of generation now becomes $8,193. Comparing with the unreduced network case, the optimal cost percentage error will be $\left(\frac{7{,}966 - 8{,}193}{7{,}966}\right)\times 100$ = -2.849 %. This percentage error is a little higher than the percentage error of the 2 sub-network case (-2.598 %).

From Table 4.22, the highest active power nodal price of these 3 decomposed sub-networks is at bus 5 ($3,987.8/MWhr), and the lowest is at bus 3 ($2,406.9/MWhr). The average of all bus nodal prices is $3,273.7/MWhr. The magnitude of the highest error, comparing with the results from the unreduced network, is at bus 5 ($-773.5/MWhr) and the lowest is at bus 3 ($655.5/MWhr). The average of all error magnitudes is ($-151.6/MWhr) or -4.5040%.

The above results show that the OPF solutions from the 2 decomposed sub-networks are more accurate than the solutions from the 3 sub-networks (both in the base load demands and in 130% demands). The huge magnitude of the Fiedler value in the third sub-network partitioning routines (5.6835) predicts this larger error in the case of three partitions. In general, the higher number of partitioning of the decomposed sub-networks, the lower degree of accuracy of the OPF solutions relative to the unreduced sub-network.

4.5.2 IEEE 30-bus network example

Next, we test the accuracy of our partitioning method in a larger network, the IEEE 30-bus system in Figure 6. This network contains 6 generators (at buses 1, 2, 5, 8, 11, and 13) injecting

power to the system feeding 20 loads. The generators' polynomial characteristic cost coefficients are presented in Table 4.23.

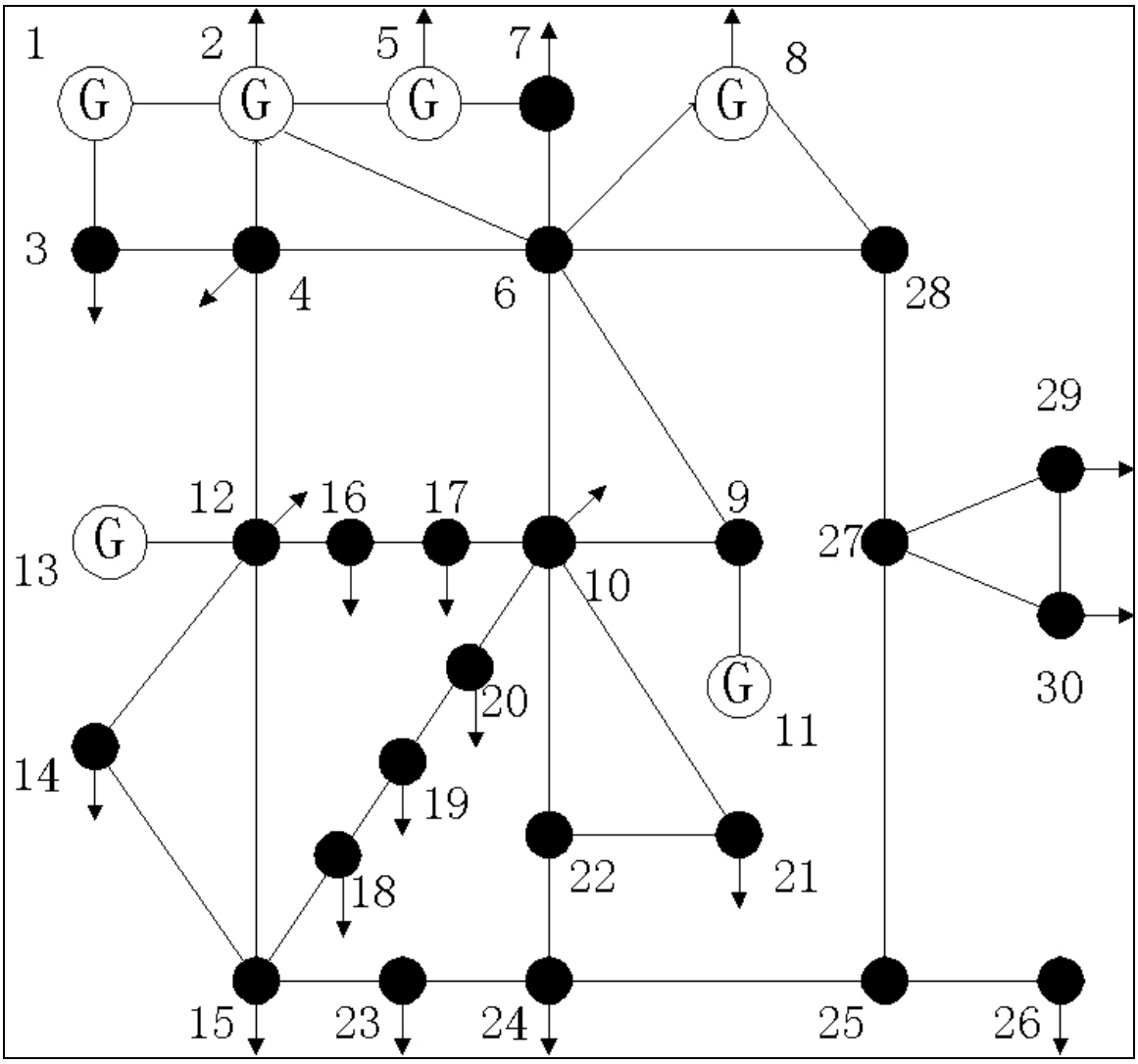

Figure 4-6: IEEE 30-bus power systems test network

Table 4.23: The Polynomial Characteristic Cost Coefficients of the IEEE 30-Bus Network

Generator at Bus Number	c2	c1	c0
1	0.0200	2.00	0
2	0.0175	1.75	0
5	0.0625	1.00	0
8	0.0083	3.25	0
11	0.0250	3.00	0
13	0.0250	3.00	0

For this IEEE-30 bus system, we cannot perturb the active power load demands too high to test the accuracy of the resulting decomposed sub-networks, as we did in the previous IEEE 9-bus case, using the original security constraint values from MATPOWER data. This is one of the disadvantages of our OPF based RSB network partitioning. The OPF decomposed sub-networks sometimes could have no solution when the margins of system's inequality constraints are too narrow comparing with their corresponding OPF solutions, or when the system's load demands are too heavy.

For readers' conceptual understanding, we modify some of the MATPOWER IEEE-30 bus inequality constraints (presented in Tables 24 to 26) and use them as the limits for our further OPF computations. The base voltage for each bus is 135 KV. The base complex power demands are shown in Table 4.27.

Table 4.24: The Limits of Generating Active Power Outputs

Generator at Bus No.	Minimum Active Power Output (MW)	Maximum Active Power Output (MW)
1	0	80
2	0	100
5	0	150
8	0	155
11	0	130
13	0	140

Table 4.25: The Limits of Bus Voltage Magnitudes - Base Voltage for Each Bus = 135 KV

Bus No.	Lower Boundary (p.u.)	Upper Boundary (p.u.)
1	0.85	1.25
2	0.85	1.25
3	0.85	1.25
4	0.85	1.25
5	0.85	1.25
6	0.85	1.25
7	0.85	1.25
8	0.85	1.25
9	0.85	1.25
10	0.85	1.25
11	0.85	1.25
12	0.85	1.25
13	0.85	1.25
14	0.85	1.25
15	0.85	1.25
16	0.85	1.25
17	0.85	1.25
18	0.80	1.25
19	0.80	1.25
20	0.80	1.25
21	0.80	1.25
22	0.80	1.25
23	0.80	1.25
24	0.80	1.25
25	0.80	1.25
26	0.80	1.25
27	0.85	1.25
28	0.85	1.25
29	0.80	1.25
30	0.80	1.25

Table 4.26: The Limits of Transmission Line Flows

Between Buses	Maximum Active Line Flow (MW)
1 - 2	130
1 - 3	130
2 - 4	165
3 - 4	130
2 - 5	130
2 - 6	165
4 - 6	190
5 - 7	170
6 - 7	130
6 - 8	130
6 - 9	165
6 - 10	130
9 - 11	165
9 - 10	165
4 - 12	165
12 - 13	165
12 - 14	130
12 - 15	130
12 - 16	130
14 - 15	160
16 - 17	160
15 - 18	160
18 - 19	160
19 - 20	130
10 - 20	130
10 - 17	130
10 - 21	130
10 - 22	130
21 - 22	130
15 - 23	160
22 - 24	160
23 - 24	160
24 - 25	160
25 - 26	160
25 - 27	160
28 - 27	165
27 - 29	160
27 - 30	160
29 - 30	160
8 - 28	160
6 - 28	130

Table 4.27: The Complex Power Demands – Base Case Load Demands (MW/MVar)

Bus No.	Pd	Qd
2	21.7	12.7
3	2.4	1.2
4	7.6	1.6
7	22.8	10.9
8	30.0	30.0
10	5.8	2.0
12	11.2	7.5
14	6.2	1.6
15	8.2	2.5
16	3.5	1.8
17	9.0	5.8
18	3.2	0.9
19	9.5	3.4
20	2.2	0.7
21	17.5	11.2
23	3.2	1.6
24	8.7	6.7
26	3.5	2.3
29	2.4	0.9
30	10.6	1.9

The OPF solutions of the unreduced network show that the voltage magnitudes at buses 1 and 11 reach their upper boundaries (1.25 p.u. volts). None of other inequality constraints is active. The active OPF generating power and the bus nodal prices for this base case operating point are presented in Tables 28 and 29.

Table 4.28: The Optimal Active Power Output of Each Generator of the IEEE 30-Bus Network - Unreduced Network (Base Case Load Demands)

Generator at Bus number	Pg (MW)
1	43.5079
2	57.3270
5	22.1133
8	35.0871
11	16.7068
13	16.2977

Table 4.29: The Lagrange Multipliers (The Active Power Nodal Prices in $/MWhr) of the IEEE 30-Bus Network – Unreduced Network (Base Case Load Demands)

Bus No.	Nodal price ($/MWhr)
1	**374.0416**
2	375.6500
3	381.0403
4	382.3525
5	376.4216
6	383.2506
7	382.8410
8	383.2444
9	383.5451
10	383.7384
11	383.5254
12	381.4709
13	381.4709
14	386.0133
15	387.3401
16	384.0404
17	384.8718
18	389.9821
19	390.3573
20	388.9525
21	386.4065
22	386.3546
23	389.6348
24	390.3501
25	388.5869
26	393.5271
27	385.4257
28	384.7125
29	392.8559
30	**397.9208**
average	385.3308

All above bus incremental costs are slightly different because of the transmission losses. Bus 1 is the generator bus and has the cheapest nodal price ($374.0416/MWhr) contrasting with the load bus number 30 which is the most expensive ($397.9208/MWhr). The average of all active nodal prices is $385.3308/MWhr. The optimal cost of generation in this base case is $572.26/hr.

At this time, we will apply our RSB network partitioning method to seek the optimal 3 decomposed sub-networks. The graphic representation of these resulting 3 sub-networks is shown in Figure 7. Hence, we will group buses 1, 2, 3, 4, 5, 6, and 7 into the first sub-network, buses 8, 24, 25, 26, 27, 28, 29, and 30 into the second, and buses 9, 10, 11, 12, 13, 14, 15, 16, 17,

18, 19, 20, 21, and 22 into the third. The branches connecting between buses 4-12, 6-8, 6-9, 6-10, 6-28, 22-24, and 23-24 are the edge separators among all these three groups. The Fiedler values obtained during the partitioning routines of the second and third sub-networks are relatively small, i.e., 0.9545 and 0.6741 respectively, which indicate the network has low degree of coupling between elements across these 3 separated groups.

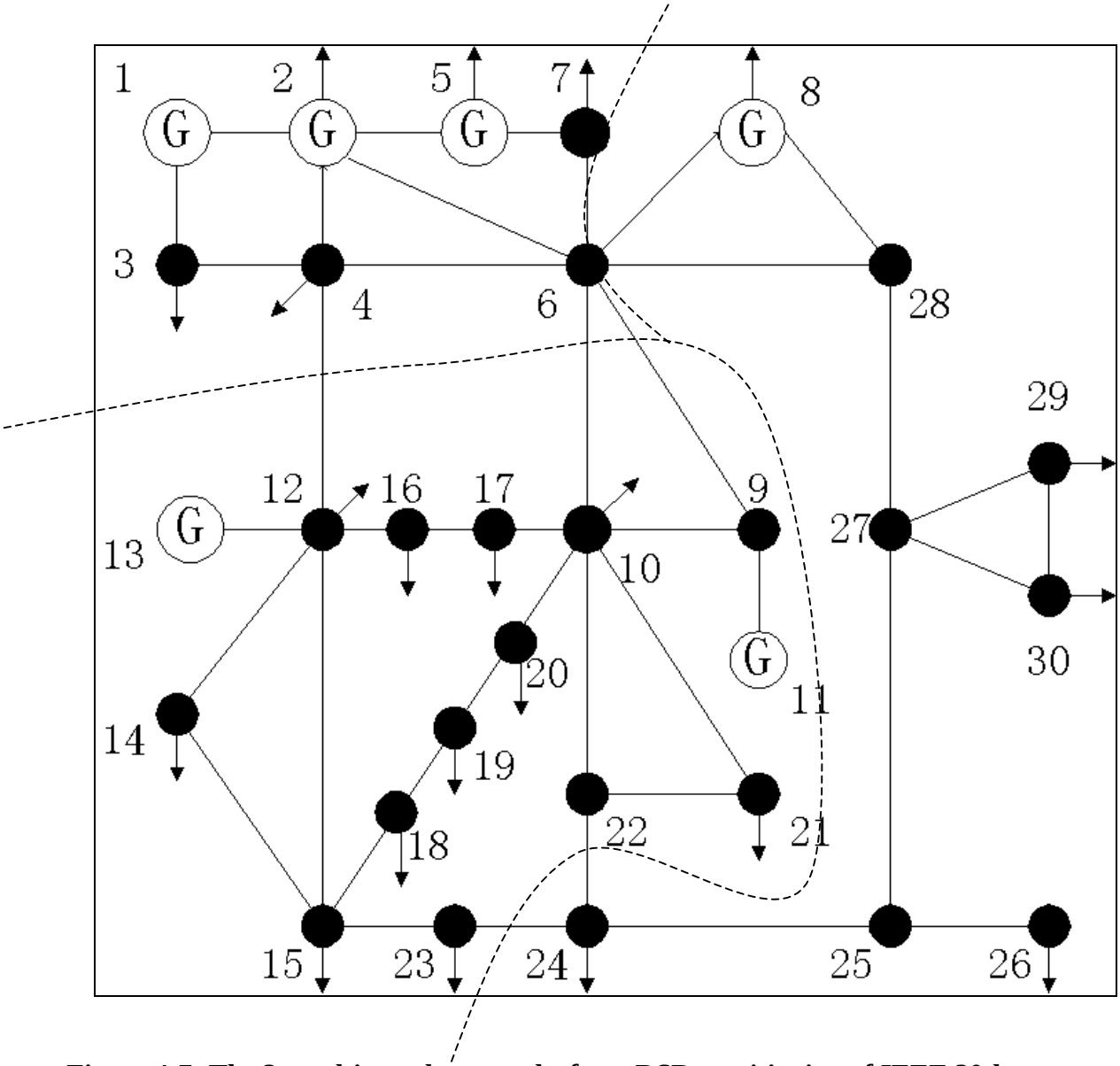

Figure 4-7: The 3 resulting sub-networks from RSB partitioning of IEEE 30-bus network

Figure 4.8 shows the result after we delete each branch connecting between these groups and replace this cutset-link with the equivalent fixed complex power demand or injection at both ends (see Table 4.30).

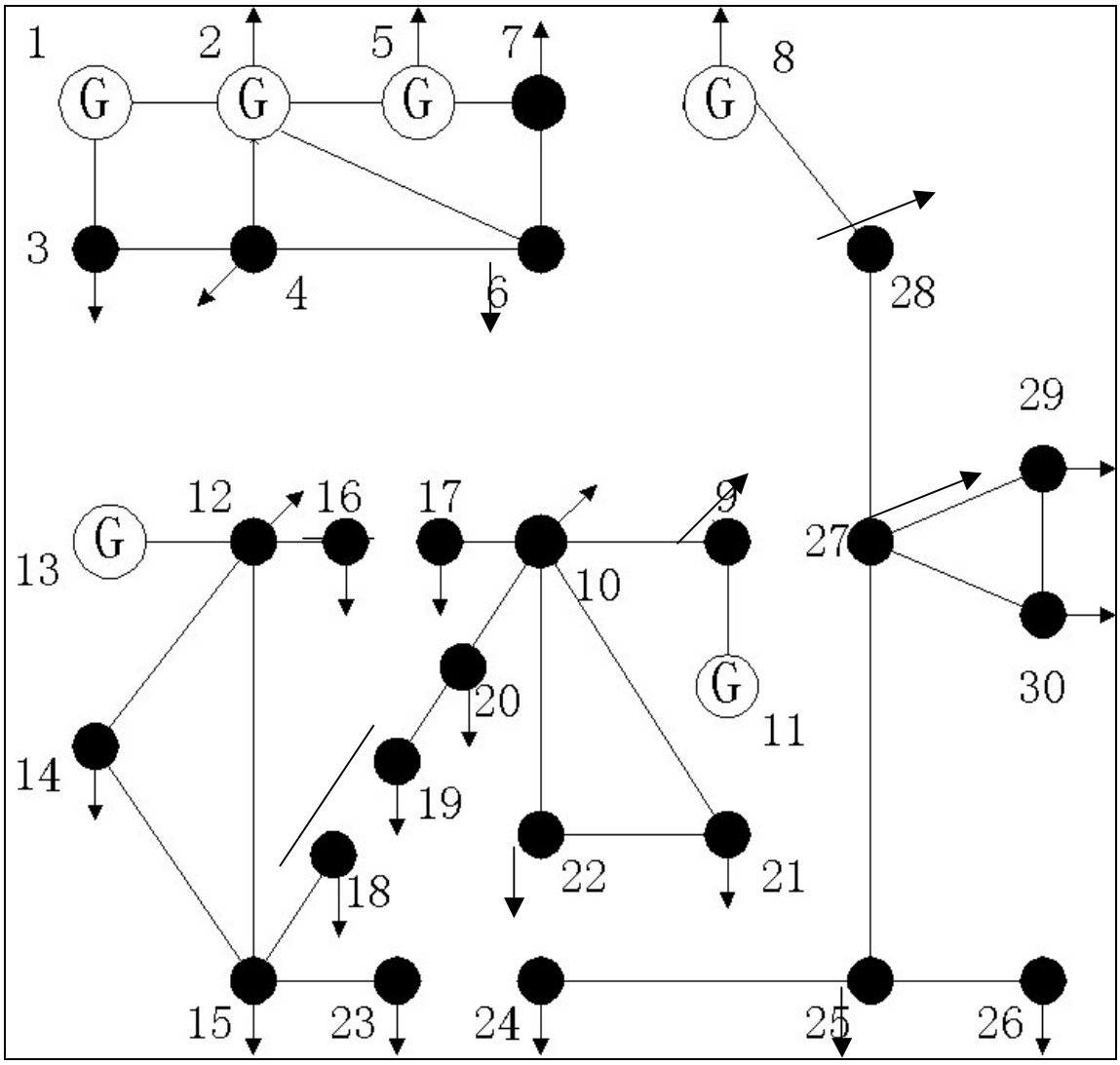

Figure 4-8: Three separated independent sets of IEEE 30-bus network after replacing each branch flow in edge separators with fixed complex load demand or injection

Table 4.30: The Equivalent Fixed Complex Power Demands

Bus Number	Pd	Qd
4	25.7729	5.8852
6	41.6694	-3.9331
8	0.6773	14.2295
9	-16.2073	-3.9637
10	-12.5022	-4.5119
12	-25.7729	-4.6925
22	6.1142	0.1582
23	1.3947	0.4064
24	-7.4760	-0.5141
28	-13.5994	-2.1522

With the same base load demands, the OPF solutions of the real power production and the network marginal prices of the decomposed RSB sub-networks are presented in Table 4.31 and Table 4.32 respectively.

Table 4.31: The Optimal Active Power Output from Each Generator - Decomposed Sub-networks (Base Load Demands)

Generator at Bus Number	in Part	Pg (MW)
1	1	43.5220
2	1	57.3359
5	1	22.1114
8	2	35.0639
11	3	16.8267
13	3	16.1717

Table 4.32: The Lagrange Multipliers (Active Power Nodal Prices in $/MWhr) of the RSB Partitioning Network – Decomposed Sub-networks (Base Load Demands)

Bus No.	Part	Nodal Prices ($/MWhr)	The magnitudes of errors from the unreduced network	% error from the unreduced network
1	1	**374.0803**	-0.0387	-0.0103
2	1	375.6687	-0.0187	-0.0050
3	1	381.1132	-0.0729	-0.0191
4	1	382.4337	-0.0812	-0.0212
5	1	376.3993	0.0223	0.0059
6	1	383.1834	0.0672	0.0175
7	1	382.7893	0.0517	0.0135
8	2	383.2060	0.0384	0.0100
9	3	384.1385	-0.5934	-0.1547
10	3	384.1723	-0.4339	-0.1131
11	3	384.1262	**-0.6008**	**-0.1567**
12	3	380.8619	0.6090	0.1596
13	3	380.8619	0.6090	0.1596
14	3	385.5514	0.4619	0.1197
15	3	387.0164	0.3237	0.0836
16	3	383.8867	0.1537	0.0400
17	3	385.1373	-0.2655	-0.0690
18	3	389.9478	0.0343	0.0088
19	3	390.4838	-0.1265	-0.0324
20	3	389.1571	-0.2046	-0.0526
21	3	386.8590	-0.4525	-0.1171
22	3	386.8093	-0.4547	-0.1177
23	3	389.5454	0.0894	0.0229
24	2	388.9243	**1.4258**	**0.3653**
25	2	387.6074	0.9795	0.2521
26	2	392.4399	1.0872	0.2763
27	2	384.7744	0.6513	0.1690
28	2	384.6173	0.0952	0.0247
29	2	392.0520	0.8039	0.2046
30	2	**397.0095**	0.9113	0.2290
average		385.1618	0.1690	0.0431

From the resulting nodal prices of the RSB method at the base case load demands, we can observe a high degree of accuracy in this decomposed OPF solutions compared with the OPF solutions from the unreduced network. The highest active power nodal price of these 3 decomposed sub-networks is at bus 30 ($397.0095/MWhr), and the lowest is at bus 1 ($374.0803/MWhr) with the average of all bus nodal prices equal to $385.1618/MWhr. The highest magnitude of errors comparing with the corresponding magnitudes of the unreduced network is at bus 24 in part 2 ($1.4258/MWhr) and the lowest is at bus 11 in part 3 ($-0.6008/MWhr). The average of all error magnitudes is $0.1690/MWhr or 0.0431%. The summation of the optimal power generating costs from these 3 separated networks is $572.23/hr, which is also almost the same (0.0052% error) as that of unreduced network, $572.26/hr.

Next, to measure the quality of the RSB method in maintaining the original network properties, we will boost the active power demands in all 20 load buses as high as 170% of their base values for both unreduced and RSB decomposed sub-network cases. For the unreduced network, the voltage magnitudes of the buses 1 and 11 reach their upper boundaries (1.25 p.u. volts); buses 1, 8, and 11 do for the RSB decomposed sub-network. None of other inequality constraints is active. The resulting real power production of both cases will be increased as shown in Table 4.33 and Table 4.34, respectively.

Table 4.33: The Optimal Active Power Output from Each Generator – Unreduced IEEE 30-Bus Network (170% Active Load Power Increase)

Generator at Bus Number	Pg (MW)
1	63.4543
2	80.5785
5	28.7145
8	85.9350
11	33.9441
13	33.1296

Table 4.34: The Optimal Active Power Output from Each Generator - Decomposed Sub-networks (170% Active Load Power Increase)

Generator at Bus Number	in Part	Pg (MW)
1	1	59.0196
2	1	75.4128
5	1	27.2462
8	2	74.5636
11	3	45.3007
13	3	44.0522

The summation of the optimal power generating costs from Table 4.34 is \$1,149.20/hr. It deviates from the total cost of the unreduced network in Table 4.33, \$1,140.40/hr, by $\left(\frac{1{,}140.40 - 1{,}149.20}{1{,}140.40}\right) \times 100 = -0.7717\%$, which is very small even in this case for which we have greatly boosted their active load demand consumptions. Note that the percentage of this error is much smaller than that of the 9-bus RSB network partitioning. We hypothesize that this is because the 30-bus network has the smaller Fiedler values (degree of coupling among each separated part). For a highly coupled network, the resulting decomposed sub-networks may not preserve the original network properties well.

Tables 35 and 36 present the bus active nodal prices from both cases at the new operating point.

Table 4.35: The Lagrange Multipliers (Active Power Nodal Prices in $/MWhr) of the IEEE 30-Bus Network – Base Case (170% load increased)

Bus No.	Nodal price ($/MWhr)
1	**453.8142**
2	457.0242
3	458.9324
4	467.6545
5	469.7157
6	465.6489
7	465.7421
8	467.9373
9	469.0944
10	469.7807
11	469.7915
12	470.3024
13	465.6517
14	475.1732
15	478.0598
16	470.9923
17	472.7137
18	483.7188
19	484.5255
20	481.4941
21	475.9807
22	475.8773
23	483.0019
24	484.5781
25	481.0175
26	491.8170
27	474.2775
28	471.8815
29	490.6819
30	**502.0765**
average	474.2986

Table 4.36: The Lagrange Multipliers (Active Power Nodal Prices in $/MWhr) – Decomposed Sub-Networks (170% Load Demands)

Bus No.	Part	Nodal prices ($/MWhr)	The magnitudes of errors from the unreduced network	% error from the unreduced network
1	1	436.0848	17.7294	3.9068
2	1	438.9367	18.0875	3.9577
3	1	446.4086	12.5238	2.7289
4	1	448.2860	19.3685	4.1416
5	1	440.5854	**29.1303**	**6.2017**
6	1	449.4016	16.2473	3.4892
7	1	450.4271	15.3150	3.2883
8	2	448.7813	19.1560	4.0937
9	3	526.6231	-57.5287	**-12.2638**
10	3	526.8433	-57.0626	-12.1466
11	3	526.5052	-56.7137	-12.0721
12	3	520.2594	-49.9570	-10.6223
13	3	520.2594	-54.6077	-11.7272
14	3	531.0012	-55.8280	-11.7490
15	3	534.0990	-56.0392	-11.7222
16	3	526.7901	-55.7978	-11.8469
17	3	529.2835	-56.5698	-11.9670
18	3	540.8786	-57.1598	-11.8167
19	3	542.0711	**-57.5456**	-11.8767
20	3	538.8510	-57.3569	-11.9123
21	3	532.5884	-56.6077	-11.8929
22	3	532.2651	-56.3878	-11.8492
23	3	539.3136	-56.3117	-11.6587
24	2	479.6238	4.9543	1.0224
25	2	469.2478	11.7697	2.4468
26	2	480.2263	11.5907	2.3567
27	2	458.7626	15.5149	3.2713
28	2	457.5107	14.3708	3.0454
29	2	475.0806	15.6013	3.1795
30	2	486.4198	15.6567	3.1184
average		494.4472	-20.1486	-4.2292

Comparing Table 4.36 with Table 4.35, the highest magnitude of errors is at bus 5 ($29.1303/MWhr) and the lowest is at bus 19 ($-57.5456/MWhr). The average of all error magnitudes is $-20.1486/MWhr or -4.2292%. We can see that the RSB reduced sub-networks can still very well preserve the OPF solutions of the original unreduced network.

To compare the quality of this Fiedler vector based partitioning with other arbitrary network partitionings, we exhibit one network example that produces a larger number of branches in the three cutsets in Figure 4.9. This case contains 12 branch-cuts comparing with 7 in our RSB

method. Buses 1, 2, 3, 4, 10, 12, 13, 14, 16, 17, 18, 19, and 20 are grouped in part 1. Buses 5, 6, 7, 9, and 11 are grouped in part 2, and buses 8, 15, 21, 22, 23, 24, 25, 26, 27, 28, 29, and 30 are grouped in part 3.

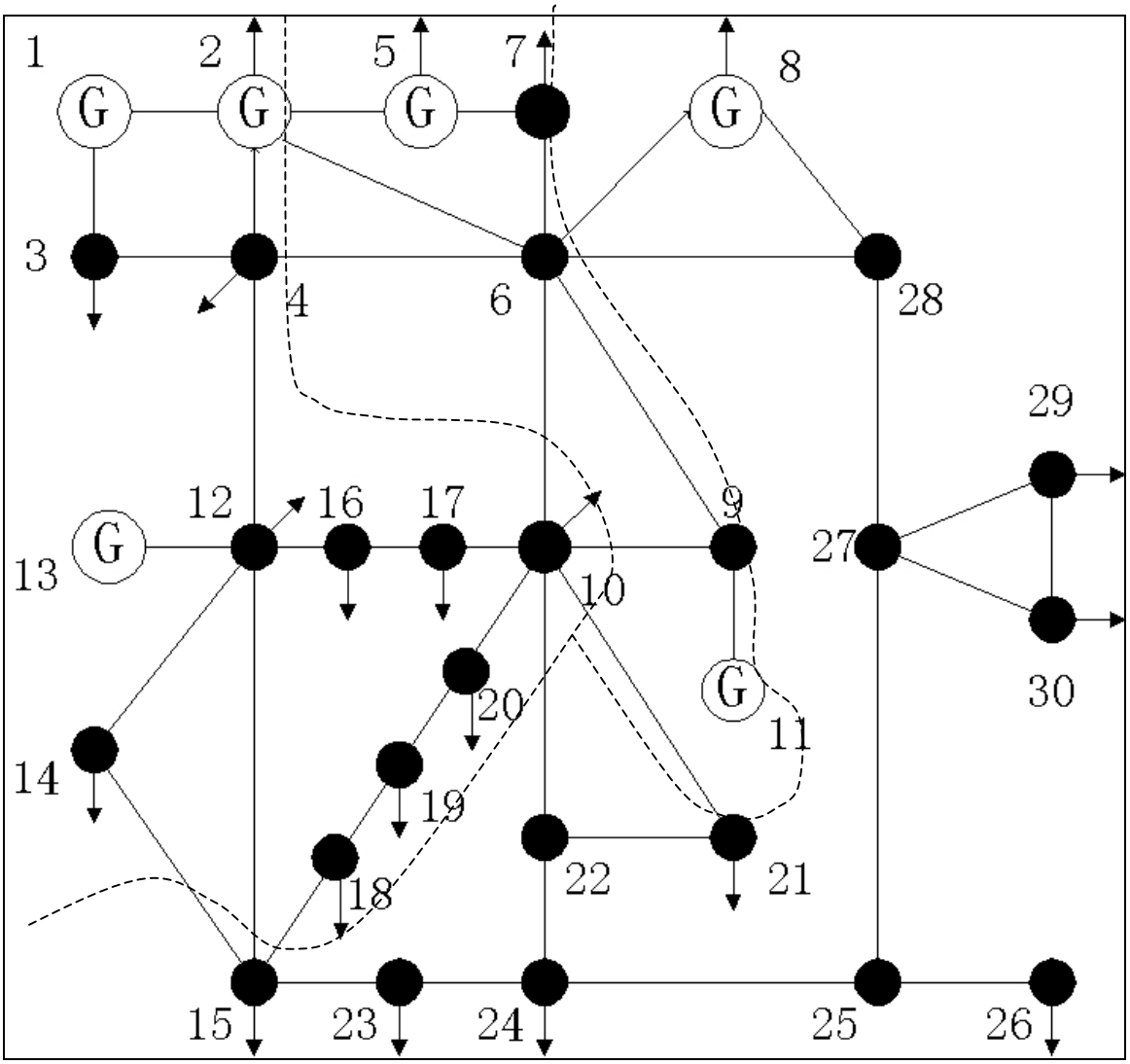

Figure 4-9: The arbitrary partitioning 3 sub-networks of the IEEE 30-bus network

Figure 10 shows the resulting 3 separated sub-networks after the deletion of each branch-cut connecting among these 3 groups. The value of each equivalent fixed complex demand or injection is presented in Table 4.37.

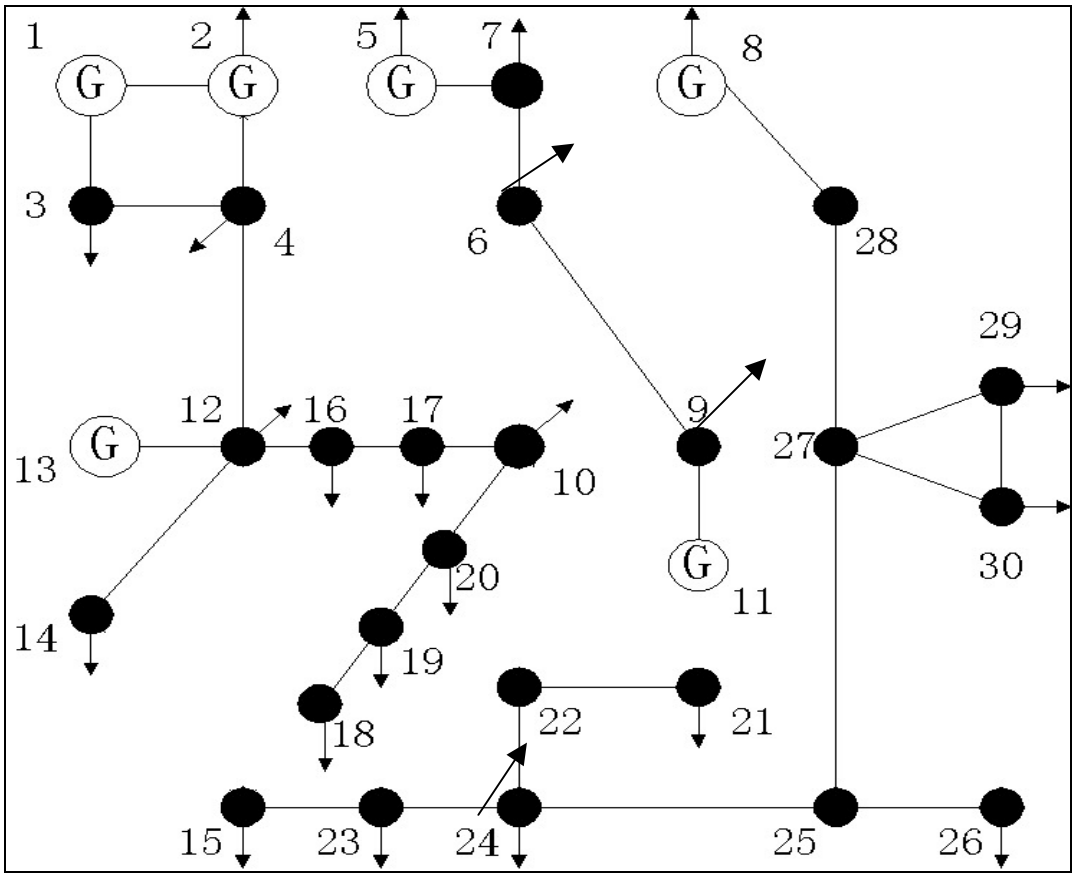

Figure 4-10: Three separated independent sets of IEEE 30-bus network after replacing each branch flow in edge separators with equivalent fixed complex demand or injection – arbitrary partitioning

Table 4.37: The Equivalent Fixed Complex Power Demands of the Buses Forming the Edge Separators – Arbitrary Partitioning (MW/MVar

Bus Number	Pd	Qd
2	30.8017	-2.2235
4	12.0698	-2.2345
5	-5.0711	-0.6142
6	-12.0798	-8.1854
8	0.6944	13.9017
9	32.915	17.2583
10	-21.703	-9.1738
12	17.0906	6.1084
14	1.3521	0.7173
15	-12.8113	-4.5393
18	-5.4481	-1.9456
21	-16.204	-8.2222
22	-7.4112	-3.1390
28	-13.6003	-2.2077

In this case, when we operate these 3 decomposed sub-networks at the base load operating point, the voltage magnitudes at buses 1, 8, 11, and 13 reach their upper boundaries (1.25 p.u. volts); none of other inequality constraints is active. Their OPF solutions will be as shown in Tables 38 and 39.

Table 4.38: The Optimal Active Power Output from Each Generator – Arbitrary Partitioning (Base Load Demands)

Generator at Bus Number	in Part	Pg (MW)
1	1	43.4706
2	1	57.2835
13	1	16.3742
5	2	22.1044
11	2	16.7137
8	3	35.0775

Table 4.39: The Lagrange Multipliers (Active Power Nodal Prices in $/MWhr) – Arbitrary Partitioning Decomposed Sub-networks (Base Load Demands)

Bus No.	Part	Nodal prices ($/MWhr)	The magnitudes of errors from the unreduced network	% error from the unreduced network
1	1	**373.8786**	0.1630	0.0436
2	1	375.4947	0.1553	0.0413
3	1	380.6005	0.4398	0.1154
4	1	381.8522	0.5003	0.1308
5	2	376.3054	0.1162	0.0309
6	2	383.5537	-0.3031	-0.0791
7	2	382.9646	-0.1236	-0.0323
8	3	383.2304	0.0140	0.0037
9	2	383.5730	-0.0279	-0.0073
10	1	384.9490	**-1.2106**	**-0.3155**
11	2	383.5677	-0.0423	-0.0110
12	1	381.8787	-0.4078	-0.1069
13	1	381.8758	-0.4049	-0.1061
14	1	386.5854	-0.5721	-0.1482
15	3	385.6518	**1.6883**	**0.4359**
16	1	384.7865	-0.7461	-0.1943
17	1	385.9473	-1.0755	-0.2794
18	1	390.0218	-0.0397	-0.0102
19	1	390.7637	-0.4064	-0.1041
20	1	389.5619	-0.6094	-0.1567
21	3	385.2014	1.2051	0.3119
22	3	385.1325	1.2221	0.3163
23	3	388.0933	1.5415	0.3956
24	3	389.0458	1.3043	0.3341
25	3	387.6685	0.9184	0.2363
26	3	392.4885	1.0386	0.2639
27	3	384.7990	0.6267	0.1626
28	3	384.6492	0.0633	0.0165
29	3	392.0612	0.7947	0.2023
30	3	**397.0122**	0.9086	0.2283
average		385.1065	0.2244	0.0573

In the base load demand operating point, the highest active power nodal price of these 3 decomposed sub-networks is at bus 30 ($397.0122/MWhr) and the lowest is at bus 1 ($373.8786/MWhr). The average of all bus nodal prices is $385.1065/MWhr. The highest magnitude of errors comparing with the unreduced network is at bus 15 ($1.6883/MWhr) and the lowest is at bus 10 ($-1.2106/MWhr). The average of all error magnitudes is $0.2244/MWhr or 0.0573%. The summation of the optimal costs of generation from these 3 separated networks is $572.21/hr or 0.0096% error from that of the un-reduced network ($572.26/hr).

As we did earlier, we will increase the active load demand in each bus of this decomposed sub-network case by the same 170% of its base load. The voltage magnitudes at buses 1, 5, 8, 11, and 13 reach their upper boundaries (1.25 p.u. volts). None of other inequality constraints is active. The optimal power productions and the bus active nodal prices at this new operating point will be as shown in Table 4.40 and Table 4.41.

Table 4.40: The Optimal Active Power Output from Each Generator – Arbitrary Partitioning Decomposed Sub-networks (170% Load Demands)

Generator at Bus Number	in Part	Pg (MW)
1	1	63.1000
2	1	80.0046
13	1	33.5333
5	2	26.6699
11	2	28.2027
8	3	98.2901

Table 4.41: The Lagrange Multipliers (Active Power Nodal Prices in $/MWhr) – Arbitrary Partitioning (170% Load Demands)

Bus No.	Part	Nodal prices ($/MWhr)	The magnitudes of errors from the unreduced network	% error from the unreduced network
1	1	452.4010	1.4132	0.3114
2	1	455.0086	2.0156	0.4410
3	1	465.1339	-6.2015	-1.3513
4	1	467.5034	0.1511	0.0323
5	2	**433.3736**	**36.3421**	**7.7370**
6	2	441.0206	24.6283	5.2890
7	2	442.3612	23.3809	5.0201
8	3	488.1613	-20.2240	-4.3219
9	2	441.0277	28.0667	5.9832
10	1	502.7701	-32.9894	-7.0223
11	2	441.0134	28.7781	6.1257
12	1	467.7012	2.6012	0.5531
13	1	467.6632	-2.0115	-0.4320
14	1	477.0171	-1.8439	-0.3880
15	3	**665.3681**	**-187.3083**	-39.1809
16	1	486.4638	-15.4715	-3.2849
17	1	500.7654	-28.0517	-5.9342
18	1	521.1987	-37.4799	-7.7483
19	1	521.2085	-36.6830	-7.5709
20	1	517.1835	-35.6894	-7.4122
21	3	663.1313	-187.1506	**-39.3189**
22	3	660.8830	-185.0057	-38.8768
23	3	663.5023	-180.5004	-37.3705
24	3	649.3352	-164.7571	-34.0001
25	3	571.6571	-90.6396	-18.8433
26	3	590.2068	-98.3898	-20.0054
27	3	524.5294	-50.2519	-10.5955
28	3	511.8329	-39.9514	-8.4664
29	3	548.8923	-58.2104	-11.8632
30	3	565.9198	-63.8433	-12.7159
average		520.1411	-45.8426	-9.5070

With this 12-branch cut arbitrary network partitioning, in 170% active load demands, the highest and lowest active power nodal prices are at bus 15 ($665.3681/MWhr) and bus 5 ($433.3736/MWhr) respectively. The average of all bus nodal prices is $520.1411/MWhr. The highest magnitude of errors comparing with the unreduced network is at bus 5 ($36.3421/MWhr) and the lowest is at bus 15 ($-187.3083/MWhr). Note that these values are much higher than the errors from our RSB approach. The average of all error magnitudes in this arbitrary partitioning is $-45.8426/MWhr or -9.5070%, which is about 2 times larger than the results from the RSB

partitioning. The optimal cost of generation from all 3 decomposed parts will be $1,161.80/hr, which is different from the unreduced network by

$$\left(\frac{1{,}140.40 - 1{,}161.80}{1{,}140.40}\right)\times 100 = -1.8765\%.$$

Even though this arbitrary partitioning preserved the optimal power flow solution characteristics for the base load demand, it could not do so when we significantly changed the operating points. The large magnitudes of the errors in the marginal price indicate this incapability. The huge errors of the system marginal prices are noticeable in part 3 because the large number of load buses locate far from the only one generator of that sub-network, bus 8. The higher number of branch-cuts also contribute to this loss of computational accuracy when boosting the active load demands. In our RSB network partitioning, the algorithm will minimize these undesirable factors. The method will try to balance and optimize the bus and branch configurations among all sub-networks. It will also seek to minimize the number of branch-cuts of the system, which in turn will diminish the coupling between the sub-networks, and as a result, will improve the accuracy of the OPF solution relative to the unreduced network.

Thus, we conclude that the reduced sub-networks produced by our RSB method can maintain a higher degree of accuracy during the OPF calculation. Our motivation for this research is to suggest an alternative approach to save the computational time of the large-scale power systems simulation. If we want to consider only some small portions in such a large-scale grid, we do not need to take the whole network model into our computation. We can apply the RSB network partitioning mentioned in this research to limit our focus on the smaller areas of interest. In practice, the RSB network partitioning could be applied as a preliminary measurement of network variables in the routine operations of the large-scale power systems.

4.6 Conclusions Regarding Network Partitioning for OPF

We propose a network partitioning technique to separate a large-scale power systems grid into the predetermined number of reduced order sub-networks. We use the concept of recursive spectral bisection (RSB) from the graph theory as the heart of our algorithm. The RSB network partitioning will locate the weak ties among these interconnections that produce the minimal

cutset-links and will seek to equate the size of each sub-network. We exercise our method in the IEEE 9 and 30-bus systems to test our method's performance. The results are very promising.

However, our method still has some disadvantages. If the load demands in a study network are too heavy, the OPF decomposed sub-networks could have no solution. Moreover, the current implementation of the algorithms makes use of the MATLAB Optimization Toolbox version 2.0, which unlike other elements of MATLAB is not designed to employ sparse matrices. In a power systems context, this is a significant disadvantage that adds significantly to the computational cost. However, the prospect of a transparent update to this toolbox that would allow sparsity to be exploited is quite probable. As an outlook for our future work, a key concept to reduce the computational burden may lie in the idea to include a set of smallest eigenvalues for the network partitioning, as reported in [60].

5. Passivity-Based Standardized Governor Control Design

5.1 Background and Motivation for Passivity-Based Controllers

Among the future trends perceived (correctly or incorrectly) as being encouraged by restructuring is that of growing penetration of smaller-scale generation, owned or leased either by individual customers, or by distribution companies operating micro-grids "downstream" from the substation. More broadly, restructuring does make it very probable that the mix of generation stock connected to the grid at any moment in time will become more volatile, and the nature of the interconnected generator types more varied. This clearly presents a challenge to the faster time scale controls that are expected to contribute to stable electromechanical response, as it remains true that generators are overwhelmingly the vehicle by which such control is exercised. In the era of the vertically integrated utility, feedback controller design for stability enhancing loops on generating units could be carried out in an environment where the designers had available full knowledge of both the machine's characteristics, and that of the grid to which it would connect. Moreover, for major units, the pattern of unit commitment was fairly predictable season-by-season. This allowed careful controller design, that for large or otherwise stability-critical generating units, could be tailored carefully to fairly predictable operating conditions. The loss of this degree of predictability regarding patterns of unit commitment, and the growing volatility of operating conditions in general, suggests a new control design paradigm may be needed. Particularly for smaller units, such as those that might be classified as "distributed generation," one might seek a design of feedback control (e.g., governor loops, power system stabilizer loops) that ideally could be guaranteed "stability enhancing" for any operating condition, or pattern of commitment among other units on the network. If such an ideal scenario is unobtainable, one might a least seek designs with the property that they could be expected not to contribute to a lessening of stability.

In control system analysis techniques, "passivity" is an input-output property associated with a subsystem that generally provides that such a subsystem will not degrade stability of a larger system upon interconnection. Applying this concept as a design guideline must be approached with care, as it is dependent upon the properties of the existing system (the power grid) to which

the subsystem (a generator with appropriate feedback controls) is connected. For a thorough treatment of these topics in passivity-based control design, the reader is referred to [65]. The goal of the work to be presented in this chapter is to formulate a design methodology to yield passive controllers for generator control loops, while staying within the framework of a very well-known (and well-supported by software design tools) design method. In particular, this chapter will approach the design of governor control loops using standard Linear-Quadratic-Regulator (LGR) techniques, while adding a novel enhancement that the problem will be formulated to ensure the controllers produced are passive. Our premise is that this may provide an attractive technique for design of governor control loops for small-scale generators that connect to the grid in unpredictable patterns.

5.2 Modeling Electromechanical Dynamics for Governor Control

The work presented here seeks to apply passivity based control and model reduction to power system electromechanical dynamics. A power system as analyzed here will be assumed to consist of a large number power sources that are *generating plants* or *generators*, power end users, at *loads*, and a transmission network that connects them. The transmission systems of the most electric utilities are interconnected and the systems operate as members of power pools. The primary objective of the interconnection is improved service reliability; a loss of generation in one area can be made up by utilizing spare capacity in another area. However, the end result is a very large system of enormous complexity that can impede reliable control design. The principles of power system modeling relevant to electromechanical dynamics are elementary, but are reviewed in the following section for completeness.

5.2.1 Brief review of relevant principles in power system modeling

In a power system the fundamental power flow variables are the voltage *(V* [Volt]) and the current *(I* [Ampere]). In the normal operation, most power system voltages and currents are (at least approximately) sinusoidal functions of time, all with the same frequency, i.e., the current and the voltage have the form

$$v(t) \qquad V_{max}\ \cos(\omega_0\, t + \delta_v(t)) \tag{5.2.1}$$

$$i(t) \qquad I_{max}\ \cos(\omega_0\, t + \delta_i(t)). \tag{5.2.2}$$

In this formulation ω_0 represents the frequency and δ the phase shift of the considered system. *Vmax* and *Imax* are real numbers denoting the *amplitudes.* The time dependent voltage *v(t)* and current *i(t)* are complex quantities. The phase shift δ is defined by being the phase angle of the complex variable; e.g., for *v(t)*

$$\delta_i(t) \ = \ \angle v(t). \tag{5.2.3}$$

The instantaneous power supplied to a one-port having terminal voltage *v(t)* and injected current *i(t)* is

$$p(t) = v(t) \cdot i(t) = V_{max} I_{max} \cos(\omega_0\, t + \delta_v(t))\ \cos(\omega_0\, t + \delta_i(t)). \tag{5.2.4}$$

Suppose

$$\Phi = \delta_v(t) \Leftrightarrow \delta_i(t), \tag{5.2.5}$$

with P constant over the time interval [0, *T*].

Introducing

$$V = \frac{1}{\sqrt{2}} V_{max}, \quad I = \frac{1}{\sqrt{2}} I_{max} \tag{5.2.6}$$

Since transmission system will be modeled by linear admittances the voltage and the current are related through linear algebraic constraints. Hence it is only necessary to consider either one of the variables. As is the common practice, the voltage will be the variable that is used in this work. For easier handling of the model, the given system is transformed with a Fourier transformation. The associated fundamental Fourier-component are

$$\vec{v} \ = \ V\, e^{j\,\delta_i}, \qquad \vec{i} \ = \ I\, e^{j\,delta_i}. \tag{5.2.7}$$

With the so called complex *admittance* matrix *Y* the relation between current and voltage is given by a matrix admittance relation (see, e.g. [6]):

$$Y \cdot \vec{v} \;=\; \vec{i}. \tag{5.2.8}$$

The admittance matrix contains all the network information.

5.2.2 Modeling of generator and load buses

The fourteen-bus example network has been employed in previous chapters; here we expand the model to include the electromechanical dynamics of generators. The parameter values for this extended version of the fourteen bus system are described in Appendix B. The states variables of the dynamics will be associated with the generators of the system. The modeling for electromechanical dynamics is the subject of widely available textbook treatments; see, for example, [6].

$$M \times \begin{pmatrix} \text{rotational} \\ \text{acceleration} \end{pmatrix} \;=\; \underbrace{\text{Net torque on generator shaft}}_{\underbrace{\tau_m}_{\substack{\text{applied} \\ \text{mechanical} \\ \text{torque}}} \;-\; \underbrace{\tau_e}_{\substack{\text{torque created} \\ \text{by magnetic} \\ \text{field in} \\ \text{the machine}}}} \tag{5.2.9}$$

in which *M* is the effective rotational inertia of the generator-turbine set. The injected power *P* is

$$P \;=\; Torque \;\times\; rotated\, speed.$$

Since the range of speed variation in normal operation is very small (typically less than 1.0%) the mechanical power *P* can be approximated by the product of the torque $\boldsymbol{\tau}_{\mathrm{m}}$ and the constant rotated speed ω_0; i.e.

$$P \approx \tau_m \omega_0 \Leftrightarrow \tau_m \approx \frac{P}{\omega_0}.$$

Assuming lossless performance of the generator in transforming applied mechanical power to electrical output, it is straightforward that the electrical torque $\boldsymbol{\tau}_{\mathrm{e}}$ is given by

$$\tau_e \approx \frac{\Re(\vec{v}\cdot\vec{i})}{\omega_0}$$

in which

$$\Re(\vec{v}\cdot\vec{i}) = \frac{1}{T}\int_0^T v(t)i(t)\mathrm{dt}.$$

The mechanical shaft angle δ_m and the electrical phase angle δ_e can be related by (see [6])

$$\underbrace{\frac{\mathrm{d}\delta_m}{\mathrm{d}t}}_{\substack{\text{normalized}\\ \text{mechanical}}}\quad\underbrace{\frac{\mathrm{d}\delta_m}{\mathrm{d}t}}_{\substack{\text{normalized}\\ \text{mechanical}}} \Leftrightarrow\omega_0 = \frac{\mathrm{d}\delta_e}{\mathrm{d}t}. \tag{5.2.10}$$

speed

$$\text{Defining } \Delta\omega \text{ as}$$
$$\Delta\omega = \frac{\mathrm{d}\delta_m}{\mathrm{d}t} \Leftrightarrow\omega_0 \tag{5.2.11}$$

then the mechanical acceleration may be expressed either in terms of the time derivative of ω or $\Delta\omega$: i.e.,

$$\frac{\mathrm{d}\omega}{\mathrm{d}t} = \frac{\mathrm{d}\Delta\omega}{\mathrm{d}t}. \tag{5.2.12}$$

Using the approximations and equivalences above, the resulting equation for the rotational dynamics at generator *#k* is

$$M\cdot\frac{\mathrm{d}\Delta\omega_k}{\mathrm{d}t} = \tau_m \Leftrightarrow\frac{\Re(V_k\cdot I_k)}{\omega_0} \tag{5.2.13}$$

in which, by equation (5.2.10), we have

$$\frac{\mathrm{d}\delta_k}{\mathrm{d}t} = \Delta\omega \qquad \frac{\mathrm{d}\Delta\omega_k}{\mathrm{d}t} = \frac{\mathrm{d}^2\delta_k}{\mathrm{d}t^2}. \tag{5.2.14}$$

Also with equation (5.2.8) and equation (5.2.7) the product defining active power can be rewritten as a function of the voltage and the phase angle

$$\Re(\vec{v}_k \cdot \vec{i}_k^*) = f_k(v, \delta). \tag{5.2.15}$$

This leads to a set of differential equations, indexed by *k* for each node with a generator attached. At generator nodes, there is a control system which attempts to hold the voltage magnitude of each generator constant. The nodes *j* without a generator attached and their voltage V_j and phase deviation δ_j yield to another set of equations. The current delivered, i_j satisfies the equation

$$i_j = \mathcal{Y}_j v_j \tag{5.2.16}$$

in which Y_j represents admittance of an admittance load. Equation (5.2.16) can be rewritten as

$$v_j i_j^* \Leftrightarrow P_j^0 \Leftrightarrow i \cdot Q_j^0 = 0 \tag{5.2.17}$$

in which $P_{j,0}$ and $Q_{j,0}$ are known constants. Equation (5.2.17) imposes two constraints at each node that yields an additional vector constraint

$$g(v, \delta) = 0. \tag{5.2.18}$$

Using the index "*g"* for node attached to a generator bus and "*l"* for nodes attached to a load bus, the following set of variables are given to model the power system:

$$\left.\begin{bmatrix} \delta_g \\ \delta_l \end{bmatrix}, \begin{bmatrix} v_g \\ v_l \end{bmatrix}\right\} \text{total number of nodes } n \tag{5.2.19}$$

The set of quantities given in (5.2.19) define the (complex) vector *V* and the associated (complex) vector *1= Y. V.* The admittance matrix *Y* is known. This yields the following structure of the equations:

$$\left.\ddot{\delta}_g = \frac{1}{\omega_0} M^{-1} \left[\tau_g \Leftrightarrow \frac{1}{\omega_0} f(\delta, v)\right] \right\} m \text{ equations} \tag{5.2.20}$$

$$0 = v_g \Leftrightarrow \underbrace{v_g^{setpoint}}_{known} \Big\} \; m \text{ equations} \tag{5.2.21}$$

$$0 = g(\delta, v) \quad \Big\} \; 2\,(n \Leftrightarrow m) \text{ equations} \tag{5.2.22}$$

5.2.3 Overall linearized state-space model

The equations (5.2.20) - (5.2.22) are linearized around the equilibrium δ^0, V^0. This equilibrium satisfies the equations

$$f(\delta^0, v^0) = \tau_g \cdot \omega_0 \tag{5.2.23}$$

and

$$g(\delta^0, v^0) = 0 \tag{5.2.24}$$

if the set point v_g^0 is chosen as

$$v_g^0 = v_g^{setpoint} \Longleftrightarrow \Delta v_g = v_g^0 \Leftrightarrow v_g^{setpoint} = 0.$$

The linearized equations are then given by

$$\Delta\ddot{\delta}_g = \Leftrightarrow \frac{1}{\omega_0} M^{-1} \left[\frac{\partial f}{\partial \delta_g} \cdot \Delta\delta_G + \frac{\partial f}{\partial \delta_L} \cdot \Delta\delta_l + \frac{\partial f}{\partial v_l} \cdot \Delta v_l \right] \Leftrightarrow D_{damp} \Delta\omega_g \tag{5.2.25}$$

$$0 = \frac{\partial g}{\partial \delta_g} \cdot \Delta\delta_g + \left[\frac{\partial g}{\partial [\delta_l \; v_l]} \right] \cdot \begin{bmatrix} \Delta\delta_l \\ \Delta v_l \end{bmatrix}. \tag{5.2.26}$$

The term (D_{damp}) is the rotational damping, appearing as a diagonal matrix. Since the second Jacobian matrix appearing in (5.2.26) is a square matrix, and may be assumed invertible in the vicinity of equilibria that define normal operating points, equation (5.2.26) can be solved to yield

$$\begin{bmatrix} \Delta\delta_l \\ \Delta v_l \end{bmatrix} = \Leftrightarrow \left[\frac{\partial g}{\partial [\delta_l \; v_l]} \right]^{-1} \frac{\partial g}{\partial \delta_g} \cdot \Delta\delta_g. \tag{5.2.27}$$

Combining equation (5.2.27) with equation (5.2.25) results in

$$\Delta\ddot{\delta}_g = \Leftrightarrow\frac{1}{\omega_0} M^{-1} \left[\frac{\partial f}{\partial \delta_g} \Leftrightarrow \left[\begin{array}{c|c} \frac{\partial f}{\partial \delta_l} & \frac{\partial f}{\partial v_l} \end{array} \right] \cdot \left[\frac{\partial g}{\partial [\delta_l \; v_l]} \right]^{-1} \frac{\partial g}{\partial \delta_g} \right] \cdot \Delta\delta_g + \underbrace{M^{-1} \Delta\tau_m}_{\Delta P_m} \Leftrightarrow D_{damp} \Delta\omega_g \tag{5.2.28}$$

with the output given by

$$\Delta\omega_g = \Delta\delta_g. \tag{5.2.29}$$

The applied control will measure the output frequency $\Delta\omega_g$ and produce at the generator the control input $\Delta\tau_m$. A diagram with the principle structure is shown in Figure 2.1. Introducing state space formulation yields a system of differential equations given by

$$\Delta\dot{\omega}_g = \Leftrightarrow\frac{1}{\omega_0} M^{-1} A_1 \, \Delta\delta_g \Leftrightarrow D_{damp} \, \Delta\omega_g \tag{5.2.30}$$

$$\Delta\dot{\delta}_g = \Delta\omega_g \tag{5.2.31}$$

which is equivalent to

$$\left[\begin{array}{c} \Delta\dot{\omega}_g \\ \Delta\dot{\delta}_g \end{array} \right] = \left[\begin{array}{cc} \Leftrightarrow D_{damp} & \Leftrightarrow\frac{1}{\omega_0} M^{-1} A_1 \\ I & 0 \end{array} \right] \left[\begin{array}{c} \Delta\omega_g \\ \Delta\delta_g \end{array} \right] + \left[\begin{array}{c} \Leftrightarrow\frac{1}{\omega_0} M^{-1} \\ \hline 0 \end{array} \right] \Delta P_m \tag{5.2.32}$$

Note that the term ΔP_{m} is input in units of mechanical power to the system. The values of the matrices used for the IEEE14 bus network are in Appendix B.1. Conceptually, the passing of input/output quantities between the power system, viewed as plant, and our feedback to be designed, as controller, is illustrated in Figure 5.1.

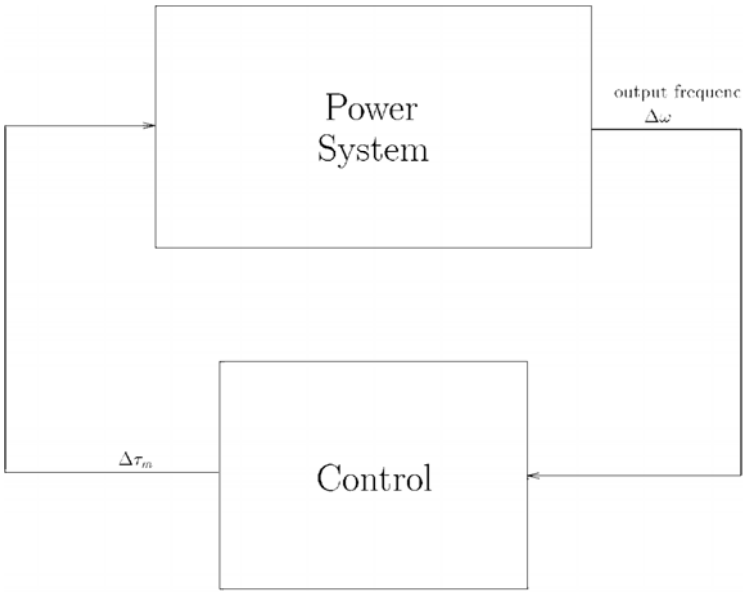

Figure 5-1: Signal Exchange between Power System and Controller

5.2.4 Dynamic model development summary

In this section the principles of power system modeling have been derived. A state space system for a power system has been formulated. This model will serve as the numerical example for further investigations to` be carried out in subsequent sections.

In this section the principles of power system modeling have been derived. A state space system for a power system has been formulated. This model will serve as the numerical example for further investigations to be carried out in subsequent sections.

5.3 The Quadratic Storage Function of the IEEE 14 Bus Network

In this Chapter a quadratic storage function for the IEEE 14-bus network will be determined. The storage function will serve as the state dependent term in the cost function for design of a Linear Quadratic Regulator (LQR). The numerical solution for the LQR problem applied to our example will be computed using the MATLAB [51] tool *lqr*. The result is a feedback matrix with the property that it minimizes the cost function; our subsequent development will modify this standard controller design approach in such a way as to produce controllers that are passive.

5.3.1 The cost function

The cost function *J(t)* of LQ-problems is defined by

$$J(t) = \int_t x(t)^T Q x(t) + u(t)^T R u(t) \mathrm{dt}. \tag{5.3.1}$$

The term < *x, Qx* > determines the stored energy in the system. The use of the control *u(t)* is penalized by the term < *u, Ru* >; here *R* will be chosen such that this penalty is negligible. For the IEEE14 bus network the dimensions of the matrix *Q* are 10 x 10, and *R*'s are 5 x 5, where R is selected as $10^{-5} \bullet I$, with *I* representing a 5 x 5 identity matrix.

5.3.2 Interpretation of the storage function

In a dissipative dynamical system, the book-keeping of energy is done via the supply rate and the storage function, as reviewed here in Appendix A. The supply rate is the rate of energy going into the system and the storage function measures the amount of energy stored inside the system.

These two functions are related via the dissipation inequality (A.8), which states that along time trajectories of the dynamical system the supply rate is not less then the increase in storage. This correlates to the assumption that no system can increase its stored energy by more than the amount of energy that is supplied to it from the outside. The difference between the internally stored and the supplied energy is the dissipated energy.
As described in chapter A the storage function is quite important to determine whether a dynamical system (FDLS) is dissipative or not. Furthermore, the storage function measures the amount of energy that is stored inside the system at any instant of time.

5.3.3 Determination of a storage function for the IEEE 14 bus network

Since our numerical example of the IEEE14 bus network is given in state space formulation, it is reasonable to adopt this state space formulation given in 2. The IEEE14 bus network swing dynamics are linearized, yielding the state space formulation (2.32). Introducing the state variable $\tilde{x}$ as

$$\tilde{x} = \begin{bmatrix} \Delta\omega_g \\ \Delta\delta_g \end{bmatrix} \tag{5.3.2}$$

And the matrix A as

$$\tilde{A} = \begin{bmatrix} \Leftrightarrow D_{damp} & \Leftrightarrow M^{-1}A_1 \\ I & 0 \end{bmatrix}, \tag{5.3.3}$$

with the input matrix $\tilde{B}$ for the input $u = \Delta P_m$

$$\tilde{B} = \begin{bmatrix} M^{-1} \\ \hline 0 \end{bmatrix} \tag{5.3.4}$$

and the output matrix $\tilde{C}$ for the output $y = \Delta\delta_\gamma$

$$\tilde{C} = \left[\, I \,\middle|\, 0 \,\right] \tag{5.3.5}$$

yields the dynamical system

$$\tilde{G}(s) \begin{cases} \dot{\tilde{x}} &= \tilde{A}\,\tilde{x} + \tilde{B}\,u \\ \tilde{y} &= \tilde{C}\,\tilde{x} + \tilde{D}\,\tilde{u} \end{cases} \tag{5.3.6}$$

with $\tilde{D} = 0$.

To apply the principle of passivity-based control, we must first establish whether our system is indeed passive. If a system is dissipative it is also passive ([74]). Thus it will be easier to determine whether the system is dissipative, since this implies passivity. A necessary condition for Dissipativity (and hence passivity) is that the considered dynamical system is a minimal realization. A system *G (s)* is given by

$$G = \left(\begin{array}{c|c} A & B \\ \hline C & D \end{array}\right), \qquad G \in \mathbb{R}^{n\times m} \tag{5.3.7}$$

Standard results (e.g., Theorem 2.4-6 of [84]) yields to the criteria for a system in equation (5.3.7) to be a minimal realization; these require:

- the matrices *(A, B)* are controllable, and
- the matrices *(C, A)* are observable.

Controllability and observability means the matrices

$$U = \left[\, B \ldots A^{n-1}B \,\right] \tag{5.3.8}$$

and

$$V = \begin{bmatrix} C \\ \dots \\ CA^{n-1} \end{bmatrix} \tag{5.3.9}$$

have the rank *n* with

$$A \in \mathbb{R}^{n \times n}.$$

For the IEEE14 bus network *G(s)* in equation (5.3.6) this can easily be verified by using the MATLAB functions *ctrb(A,B)* and *obsv(A,C)*. Since

$$rank(U) = 10 = n \tag{5.3.10}$$

$$rank(V) = 9 \neq n \tag{5.3.11}$$

the system G*(s)* is *not* a minimal realization and the method proposed in [88] cannot be applied to this system in its present form. To apply this algorithm the system (5.3.7) has to be transformed into a minimal realization. This is done in the next section.

5.3.4 Transformation to a minimal realization

The state space used for the model of the IEEE14 network will be modified through the introduction of a reference angle. The angle deviations are defined in reference to the first angle

$$\begin{bmatrix} \Delta\delta_1 \\ \vdots \\ \Delta\delta_5 \end{bmatrix} = \begin{bmatrix} \delta_1 \\ \vdots \\ \delta_5 \end{bmatrix} \Leftrightarrow \begin{bmatrix} \delta_1 \\ \vdots \\ \delta_1 \end{bmatrix}. \tag{5.3.12}$$

This means that within the overall vector of states, the state variable $\Delta\delta_1$ will always be zero, which yields a zero eigenvalue and associated unobservability. The system can be reduced by elimination of this reference angle from the state space formulation. To eliminate this state one uses the following dimension reducing transformation

$$\Delta\delta_{red} = T_1 \, \Delta\delta_g \tag{5.3.13}$$

with

$$T_1 = \left[\begin{array}{c|c} \Leftrightarrow 1 & \\ \vdots & \\ \Leftrightarrow 1 & I_{m-1\times m-1} \\ \vdots & \\ \Leftrightarrow 1 & \end{array}\right], \qquad T_1 \in \mathbb{R}^{\mathrm{m-1\times m}}, \qquad \Delta\delta_{\mathrm{g}} \in \mathbb{R}^{\mathrm{m}}.$$

Note that $\Delta\delta_G \in \mathbb{R}^5$ may be recovered from $\Delta x \in \mathbb{R}^4$ via the relation

$$\Delta\delta_G = T_2\,\Delta x \tag{5.3.14}$$

with

$$T_2 \in \mathbb{R}^{\mathrm{m\times m-1}}, \qquad T_2 = \left[\begin{array}{ccc|ccc} 0 & \dots & 0 & \dots & 0 \\ \hline & & I_{m-1\times m-1} & & \end{array}\right].$$

To reconstruct the complete state vector one has the relation

$$\Delta x = \underbrace{\left[\begin{array}{c|c} I_{n-m\times n-m} & 0_{m\times m} \\ \hline 0 & T_1 \end{array}\right]}_{:=\tilde{T}_1} \Delta\tilde{x}$$

and

$$\Delta\tilde{x} = \underbrace{\left[\begin{array}{c|c} I_{n-m\times n-m} & 0_{m-1\times m} \\ \hline 0 & T_2 \end{array}\right]}_{:=\tilde{T}_2} \Delta x.$$

Using these transformation yields

$$\underbrace{T_1\,\Delta\tilde{x}}_{\Delta x} \;=\; \tilde{T}_1\,A\,\underbrace{\tilde{T}_2\,\Delta x}_{\Delta\tilde{x}}. \tag{5.3.15}$$

So the reduced system matrix is given by

$$A = A_{red} = T_1 A T_2, \qquad \text{with } A \in \mathbb{R}^{9\times 9}. \tag{5.3.16}$$

The matrices B (C, D, respectively) are determined by eliminating the appropriate row or column. Now the observability and controllability tests are applied to the resulting 9 state dynamical system. The rank of the controllability and observability matrices are

$$rank(U) = 9 \tag{5.3.17}$$

$$rank(V) = 9 \tag{5.3.18}$$

Hence, the new system

$$G(s) = \left(\begin{array}{c|c} A & B \\ \hline C & D \end{array}\right) \tag{5.3.19}$$

is minimal and the design in [87], [88] for the matrix Q can be applied. The size of the matrices is shown in Table 3.1.

Table 5.1: Dimensions for MATRICES in Reduced System G

A	$\in \mathbb{R}^{9\times 9}$
B	$\in \mathbb{R}^{9\times 5}$
C	$\in \mathbb{R}^{5\times 9}$
D	$\in \mathbb{R}^{5\times 5}$
x	$\in \mathbb{R}^{9}$
y, u	$\in \mathbb{R}^{5}$

All further examinations will be done for the IEEE14 bus network as represented by this G(s).

5.3.5 Determination of a storage function

When applying the lqr algorithm to develop a feedback control, it is necessary to obtain first an appropriate quadratic storage function. As mentioned above, the storage function will be chosen, such that it is a quadratic function in the states, such given by

$$S(x) =< x, Qx > .$$

Assuming the IEEE14 bus network is dissipative, then the given definition of Dissipativity (MIE) in Theorem A.3.3 holds for an appropriate Q. Instead using a matrix Q and checking for the Dissipativity, one approach is going all the way around. Interpreting the inequality (MIE) as an optimization problem leads to an appropriate storage function Q. In this approach the passivity constraints are applied on the storage function Q. As a second approach to select Q, a formulation using the (partial) derivatives of the power flow equations to determine an appropriate Q is discussed later in this chapter. Additionally the matrix Q of the storage function can just be taken as an identity matrix. The controls based on these three possible Q choices are developed and investigated in Section 5.4.

First, various possible choices for the matrix Q of the storage function S(x) =< x, Qx > in the IEEE14 bus network are determined.

5.3.6 Optimization approach to selection of design matrix Q

The determination of the matrix *Q* via the optimization approach is based on the definition of Dissipativity for quadratic storage functions. The associated definition of Dissipativity for the optimization approach is given by [88], [89]. A dynamical system is therefore dissipative, if the matrix

$$\underbrace{\begin{bmatrix} A^T Q \Leftrightarrow Q A & Q B \Leftrightarrow C^T \\ B^T Q \Leftrightarrow C & \Leftrightarrow D \Leftrightarrow D' \end{bmatrix}}_{:=F(Q)} \leq 0 \tag{5.3.20}$$

with

$$Q \geq 0 \tag{5.3.21}$$

$$Q = Q^T. \tag{5.3.22}$$

This can be restated as an optimization problem. The objective function is minimizing the maximal eigenvalue of the matrix function *F(Q)*

$$z = \min_{Q} \left(\max(\lambda(F(Q)))\right) \tag{5.3.23}$$

with the constraint that the matrix *Q* is symmetric, positive definite. With this optimization algorithm, storage functions of several examples are determined. To illustrate the concept in simple systems familiar to most readers, we begin with examples of linear RLC-networks, which of course are inherently dissipative. This class of examples is developed in the next section.

5.3.7 Examples of determining the matrix Q by optimization

In this section this approach of determining the storage function via the Dissipativity inequality (MIE) is applied on several examples. The inequality is applied on some simple RCL-circuits to determine its validity and its precision. For the circuits it is known apriori that they are dissipative. In this way the algorithm and its implementation will be tested to see if a solution *Q* that confirms passivity can be reliably computed.

Example circuit #1

The first used RCL-circuit is shown in Figure 5.2. This simple network consists of inductors, capacitors, and resistors. Hence this RCL~network has to be a dissipative system (energy is "destroyed" in the resistors and dissipated in form of heat). The voltage *u(t)* is used as input variable. The output variable is the voltage at the resistor *R* parallel to the capacitor C.

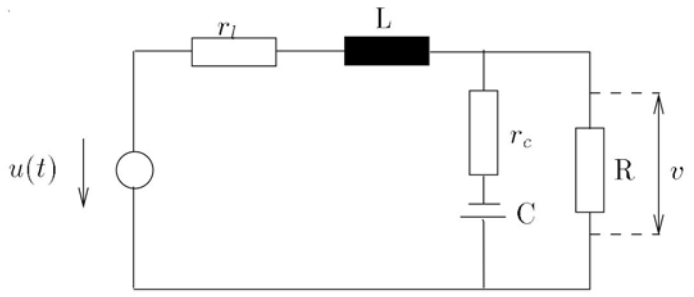

Figure 5-2: Passive example RCL-circuit #1. Input is the voltage u(t), output the voltage at the resistor R.

The dynamics of this RCL-circuit is described by systems equations given by

$$\dot{x} = \begin{bmatrix} \Leftrightarrow\frac{Rr_c + Rr_l + r_c r_l}{L(R+r_c)} & \Leftrightarrow\frac{R}{L(R+r_c)} \\ \frac{R}{C(R+r_c)} & \Leftrightarrow\frac{1}{C(R+r_c)} \end{bmatrix} x + \begin{bmatrix} \frac{1}{L} \\ 0 \end{bmatrix} u(t) \qquad (5.3.27)$$

$$y = \begin{bmatrix} \frac{Rr_c}{R+r_c} & \frac{R}{R+r_c} \end{bmatrix} x \qquad (5.3.28)$$

with $x = [\, i_L \, v_C \,]$ as the state variables. The numeric parameter values used for this system are given in Appendix D.

Applying the optimization algorithm to this system should lead to a square, symmetric positive definite matrix Q. For the numeric parameter values employed here, the result one obtains is

$$Q = 10^{-4} \cdot \begin{bmatrix} 0.01817147437353 & \Leftrightarrow 0.05253395510361 \\ \Leftrightarrow 0.05253395510361 & 0.34216072309434 \end{bmatrix} \qquad (5.3.28)$$

$$\lambda(F(Q)) = \begin{bmatrix} 0.00017041629317 \\ 0.00024971295098 \\ \Leftrightarrow 1.65999090525947 \end{bmatrix} \qquad (5.3.29)$$

$$\lambda(Q) = \begin{bmatrix} 0.00986614347705 \\ 0.35046605399082 \end{bmatrix}. \qquad (5.3.30)$$

Apparently the criterion of positive definiteness of the matrix *Q* is fulfilled, but the criteria of negative definiteness of the matrix *F(Q)* is violated. The location of the eigenvalues is shown in the Figures 5.3 and 5.4.

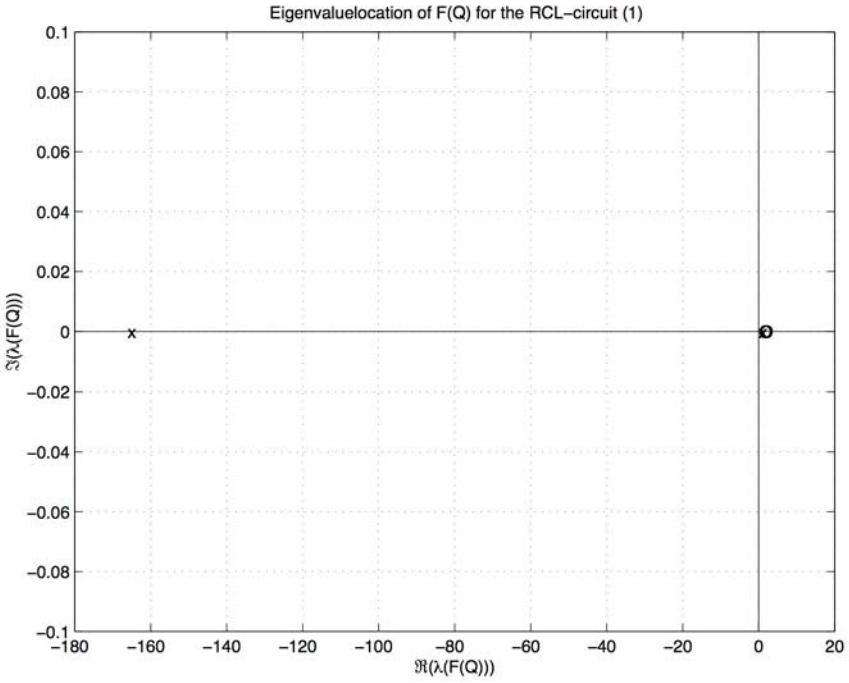

Figure 5-3: Location of the eigenvalues for example circuit #1.

Obviously two of three eigenvalues of *F(Q)* are positive. But if one considers their relative magnitude in the relation to the third eigenvalue, one observes that

$$\frac{|\lambda_1(F(Q))|}{|\lambda_3(F(Q))|} \approx \frac{|\lambda_2(F(Q))|}{|\lambda_3(F(Q))|} \approx 10^{-4}. \tag{5.3.31}$$

Since the eigenvalues λ_1 and λ_2 are much smaller than λ_3, we will assumed that these eigenvalues may be treated as essentially zero. If one accepts this premise, the dynamical system can be classified as dissipative and the concept of dissipative control will be applied.

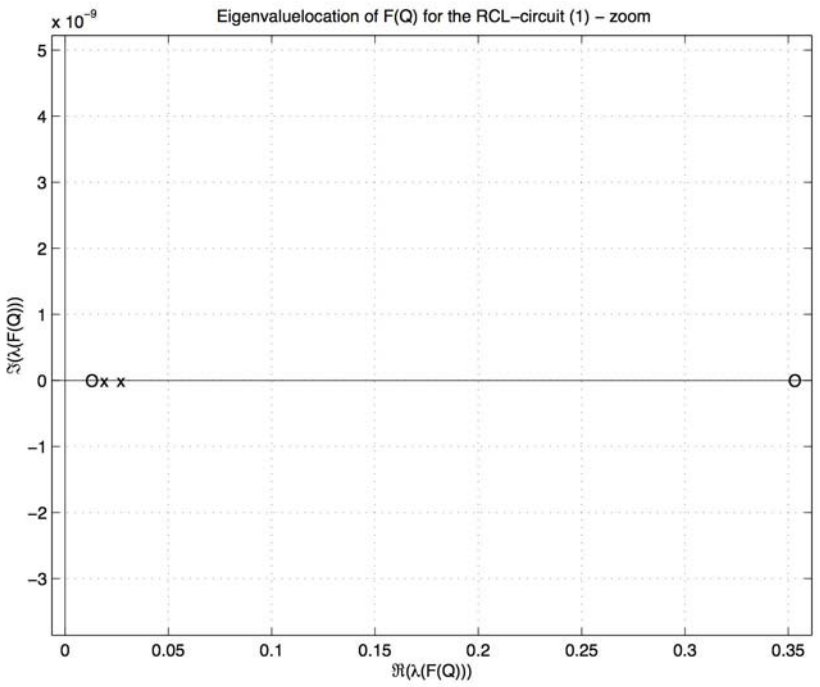

Figure 5-4: Detailed picture of the location of the eigenvalues for example circuit (1).

Example circuit #2

Again a simple RCL-circuit is used. The circuit is shown in 3.4. Due to its construction

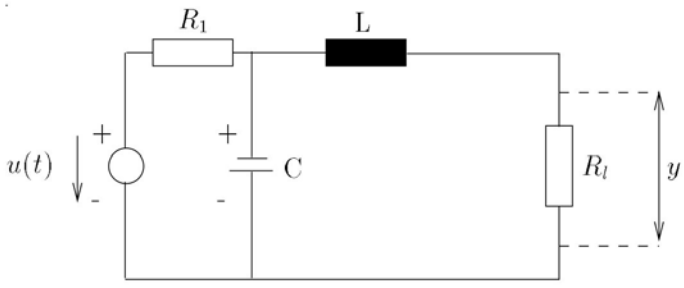

Figure 5-5: Passive RCL~circuit #2.

this RCL-circuit is only passive and not strictly passive, which is a challenge for the proposed algorithm.

The dynamics of this RCL-circuit is described by systems equations given by

$$\dot{x} = \begin{bmatrix} \Leftrightarrow\frac{R}{L} & \frac{1}{L} \\ 0 & \Leftrightarrow\frac{1}{C} \end{bmatrix} x + \begin{bmatrix} 0 \\ \frac{1}{R_l} \end{bmatrix} u(t) \quad (5.3.32)$$

$$y = [R \mid 0]\, x \quad (5.3.33)$$

again with $x = [\, i_L\, v_C\,]$ as the state vector. The parameters used are shown in Appendix D. Here, the algorithm converges and the conditions in equation (5.3.20) are satisfied[2]

$$\lambda(F(Q)) \leq \underline{0} \quad (5.3.34)$$

$$\lambda(Q) \geq \underline{0} \quad (5.3.35)$$

$$Q = Q^T \quad (5.3.36)$$

The results are shown in Appendix C.

Knowing that the algorithm works, the IEEE14 bus system has been examined and a matrix Q for storage function $< x, Qx >$ can be derived.

5.3.8 The energy matrix Q determined for the IEEE14 system

The MATLAB routine *simsys2* is applied on the IEEE14 example system. As in the case of our simple circuit example above, one finds a wide range of magnitudes for the relevant eigenvalues, with not all maintaining a single sign. However, since the critical eigenvalues (the eigenvalues at the right side of the imaginary axis) are very small compared to the other eigenvalues, as a heuristic, we will proceed as if these values were zero. Hence the conditions for Dissipativity of the IEEE14 bus network will be treated as being "practically" satisfied, and we will consider the quality of control design that results.

The matrices *F(Q)* and *Q* are shown in Appendix C. The associated eigenvalues of the matrices *F(Q)* ands *Q* are

[2] As a matter of fact, the same approximation error appears in this dynamical system. But again,we will accept the heuristic of classifying the system as passive to within a numerical tolerance.

$$\lambda(F(Q)) = \begin{bmatrix} 0.07331395722946 \\ 0.07331395722946 \\ 0.07202031479281 \\ 0.06123868588640 \\ \Leftrightarrow 0.00367694563201 \\ \Leftrightarrow 0.00152923139098 \\ \Leftrightarrow 0.00975405097283 \\ \Leftrightarrow 0.01645200579705 \\ 0.02821816735109 \\ \Leftrightarrow 0.03285589748382 \\ \Leftrightarrow 0.09020432179642 \\ \Leftrightarrow 0.14821035586885 \\ \Leftrightarrow 0.33506846099789 \\ \Leftrightarrow 0.72848705227267 \end{bmatrix} \approx \begin{bmatrix} 0 \\ 0 \\ 0 \\ 0 \\ \Leftrightarrow 0.00367694563201 \\ \Leftrightarrow 0.00152923139098 \\ \Leftrightarrow 0.00975405097283 \\ \Leftrightarrow 0.01645200579705 \\ 0 \\ \Leftrightarrow 0.03285589748382 \\ \Leftrightarrow 0.09020432179642 \\ \Leftrightarrow 0.14821035586885 \\ \Leftrightarrow 0.33506846099789 \\ \Leftrightarrow 0.72848705227267 \end{bmatrix}$$

and

$$\lambda(Q) = \begin{bmatrix} 1.02309319440031 \\ 1.03174104209236 \\ 0.99176986499408 \\ 0.97123858370697 \\ 0.95030038580541 \\ 2.39701285091361 \\ 6.63156054088885 \\ 8.10467005810500 \\ 30.19246060693700 \end{bmatrix}.$$

In the further developments of the control we will use the determined approximated storage function Q as one exact storage function of the dynamical system (5.3.19). Since there is another approach for determining a energy matrix Q (to be described in the following section), the energy matrix as derived in this section will be labeled as Q^{opt}.

5.3.9 Observations regarding the approach via optimization

Since the optimization did not yield to an unique result for Q in the sense of Dissipativity in (MIE), an approximation of the objective function

$$z = \min_{Q} \left(\max(\lambda(F(Q)))\right)$$

based on the Gershgorin-circles was investigated. Here in the main text we will comment only that this approach did not improve the effectiveness of the algorithm. For completeness this investigation is briefly summarized in Appendix D.

5.3.10 Determining the matrix Q via the approach of the partial derivatives of the power flow functions

Another approach determining the energy matrix Q is the possibility via the partial derivatives of the power flow function which then yields a quadratic approximation to the potential function routinely used in power system Lyapunov functions. The energy matrix of the storage function can be approximated by

$$Q = \left[\begin{array}{c|c|c|c} M & 0 & 0 & 0 \\ \hline 0 & \frac{\partial P_G}{\partial \delta_G} & \frac{\partial P_G}{\partial \delta_L} & \frac{\partial P_G}{\partial v_L} \\ \hline 0 & \frac{\partial P_L}{\partial \delta_G} & \frac{\partial P_L}{\partial \delta_L} & \frac{\partial P_L}{\partial v_L} \\ \hline 0 & \frac{\partial Q_L}{\partial \delta_G} & \frac{\partial Q_L}{\partial \delta_L} & \frac{\partial Q_L}{\partial v_L} \end{array}\right]. \tag{5.3.37}$$

This is the matrix Q of a storage function for the power system dynamic equations. The power system equations are given by equations:

$$\Delta\dot{\omega} = M^{-1} \cdot \{P_G(\delta_G, \delta_L, v_L) \Leftrightarrow D\,\Delta\omega\} + u \tag{5.3.38}$$

$$\Delta\dot{\delta_G} = \Delta\omega_G \tag{5.3.39}$$

$$0 = P_L(\delta_G, \delta_L, v_L) \tag{5.3.40}$$

$$0 = Q_L(\delta_G, \delta_L, v_L). \tag{5.3.41}$$

The quadratic storage function *S (Q)* then is given by

$$S(Q) = \frac{1}{2}(\hat{x}^T\, Q\, \hat{x}) \tag{5.3.42}$$

with

$$\hat{x}^T = \begin{bmatrix} \Delta\omega^T & \Delta\delta_G^T & \Delta\delta_L^T & \Delta v_L^T \end{bmatrix}. \tag{5.3.43}$$

With the given constraints (5.3.40) and (5.3.41) one can solve the system (5.3.38)~(5.3.41) for $\Delta\delta_L$ and Δv_L in terms of $\Delta\delta_G$.

$$\begin{bmatrix} \Delta\delta_G \\ \Delta\delta_L \\ \Delta v_l \end{bmatrix} = \underbrace{\begin{bmatrix} I_{m\times m} \\ \Leftrightarrow \begin{bmatrix} \frac{\partial P_L}{\partial \delta_L} & \frac{\partial P_L}{\partial v_L} \\ \frac{\partial Q_L}{\partial \delta_L} & \frac{\partial Q_L}{\partial v_L} \end{bmatrix}^{-1} \cdot \begin{bmatrix} \frac{\partial P_L}{\partial \delta_G} \\ \frac{\partial Q_L}{\partial \delta_G} \end{bmatrix} \end{bmatrix}}_{:= N} \cdot \Delta\delta_G \tag{5.3.44}$$

The storage function expressed in terms of the state variables $\Delta\omega$ and $\Delta\delta_G$ is given by

$$S(Q) = \frac{1}{2}(x^T\, Q_{red}^{pd}\, x) \tag{5.3.45}$$

with

$$x^T = \begin{bmatrix} \Delta\omega^T & \Delta\delta_G^T \end{bmatrix} \tag{5.3.46}$$

$$Q_{red}^{pd} = \begin{bmatrix} I & 0 \\ 0 & N^T \end{bmatrix} \cdot Q \cdot \begin{bmatrix} I & 0 \\ 0 & N \end{bmatrix} \tag{5.3.47}$$

Note that the matrix *N* is *not* a square matrix. This method, applied on the IEEE14 bus system, yields a reduced system

$$\tilde{x} \in \mathbb{R}^9. \tag{5.3.48}$$

The matrix Q^{pd} created by this approach is not inherently symmetric. To force the desired symmetry, the following standard step is performed

$$Q_T^{pd} = \frac{1}{2} \cdot (Q_{red}^{pd} + (Q_{red}^{pd})^T)$$

The maximum magnitude component-wise error introduced by using the symmetric approximation is quite small. For our IEEE14 bus system example this error is

$$\varepsilon_{approx} = 2.6\%.$$

Unfortunately the matrix *F(QTd)* in (MIE) is also not negative definite. The eigenvalues

$$\lambda(F(Q_T^{pd})) = \begin{bmatrix} \Leftrightarrow 0.0100 \\ \Leftrightarrow 0.0426 \\ 0.0326 \\ \Leftrightarrow 0.1078 \\ 0.0978 \\ \Leftrightarrow 0.1546 \\ 0.1446 \\ \Leftrightarrow 0.2064 \\ 0.1964 \\ 0 \\ 0 \\ 0 \\ 0 \\ 0 \end{bmatrix}$$

are positive and negative. And the ratio between the minimum and maximum eigenvalue is 10. Comparing the eigenvalues of the matrix *QPd* and the eigenvalues of the matrix *Qopt* shows, that the eigenvalues of these matrices are very close to each other. This yields the assumptions the developed controls will not be very different if they are based on *Qopt* or *QTd.* For simplification in the notation in the following sections the matrix *QPd* = *QTd*, if not otherwise stated.

5.3.11 Summary of storage function development

Associating a quadratic storage function with passive systems, we have demonstrated a means by which the constraints of passivity can be imposed on an optimization problem, such as that employed in LQR design. Upon careful examination, the model for the IEEE14 bus network is shown to fails a rigorously imposed passivity test, since the matrix function *F(Q)* is not strictly negative definite. This may be explainable with the complexity of the numerical algorithms employed for the optimization and their sensitivity to initial conditions. The derived matrix *Qopt* can be possibly better optimized in regard the function *F(Q).* Nonetheless, the derived *Qopt* was not strictly negative definite, yet was the best derivable *Q.*

Via this approach, the two problems have been solved in one step ~ the Dissipativity (and therefore the passivity) of the system is established to hold within an acceptable (heuristically determined) numeric threshold, and the storage function *Q* is simultaneously determined. Based on a choice of matrix *Q* a LQR based control can now be designed. Various designed control can be compared to controls, can be compared, based on differing choices of the matrix *Q.*

In the next section of this chapter the controls based on this method are computed and implemented, and their performance bears out the acceptance of a heuristic criterion of “near passivity” as being acceptable for design purposes.

5.4 Results of the Control Design

In this section the quality of the control produced by our design method will be discussed. The quality of a control is on the one hand judged by the nature of its dynamic response, and on the other hand by the used amount of control energy. The cost function is given by

$$J(t) = \int_t x(t)^T Q^{\zeta} x(t) + u(t)^T R u(t) + 2x(t)^T N u(t)\ dt. \tag{5.4.1}$$

The matrix *Q* is the matrix assigning the amount of energy stored in the system, while the matrix *R* "penalizes" use of a control, i.e., the more control effort is necessary the higher is the energy consumption. The importance in choosing the matrices *Q* and *R* will be shown in the next sections. For the matrix *Q,* three different approaches are made

$$Q^{\zeta} = \begin{cases} Q \\ Q^{pd} \\ Q^{id} \end{cases}$$

The matrices Q and Q^{Pd} were derived earlier in Chapter 3.5 and 3.7. In more investigations the influence of the matrix R is examined. The first case discussed, is the control designed with the assumption of $R = 0$. Since the numeric implementation of the *lqr* algorithm in MATLAB does not allow a choice of R identically zero, $R = 10^{-16} * I$ is chosen. This is quite small compared to the magnitude of nonzero elements of the matrices Q. To make this examination into a fair comparison between the designed, controls, the difference in relative magnitude of elements between the matrices Q, Q^{Pd} and the matrix Q^{id} has to be confronted, and the problem of output normalization must be solved.

5.4.1 Dimensionality Issues

In order to have a fair comparison, the influence of the different dimensions in the used matrices *Q(* has to be eliminated. Therefore the condition

$$1 \leq \max(\lambda(Q^{\zeta})) \leq 10 \tag{5.4.2}$$

has to be satisfied. This is easily done by multiplying the matrices *Q, Qid* with a constant 0:. In this case, *O:Q*, $O{:}Q^{Pd} = 0.1$ and $O{:}Q^{id} = 1$. So the maximum eigenvalues of the normed matrices are

$$\max(\lambda(Q^{opt})) = 3.019 \tag{5.4.3}$$

$$\max(\lambda(Q^{pd})) = 3.022 \tag{5.4.4}$$

$$\max(\lambda(Q^{id})) = 1. \tag{5.4.5}$$

In the future simulations, these matrices are used.

5.4.2 Output normalizing via /LQR-gain

To examine the system the step or impulse response for the system are computed. Since these functions are not normalized, i.e., their output is not fixed on a certain value, the direct results cannot be compared to each other. Therefore, an output of the step response has to fixed on a

certain value. This has to be done for all the designed controls. The approach is to normalize the step response of the transfer function such that

$$\bar{H}(s) = \frac{1}{\mu_{dc}} \cdot H(s) \tag{5.4.6}$$

in which *fldc* is the gain at *s* = o. The transfer function is given by

$$H(s) = C^T \left[sI \Leftrightarrow (A \Leftrightarrow BK)\right]^{-1} B$$

The associated block-diagram is shown in the upper part of Figure 5.4.1. As can be seen the in this figure, the transfer function can be rewritten in the following form

$$H(s) = C^T \left[sI \Leftrightarrow (A \Leftrightarrow B^f K)\right]^{-1} B^i. \tag{5.4.7}$$

The associated block-diagram is shown in the lower part of Figure 5.4.1. To compute the required dc gain, the system is viewed as a sequence of SISO systems. This is done by selecting one column of Bi and one row of C. Computing the dc-gain at (i.e., $s = 0$) yields

$$\mu_{dc}(i,j) = C^T_{row\,i} \left[sI \Leftrightarrow (A \Leftrightarrow B^f K(Q^{\zeta}))\right]^{-1} B^i_{column\,j}$$

$$\bar{B}^i = \frac{1}{\mu_{dc}(i,j)} \cdot B^i \tag{5.4.8}$$

with *(i,j)* corresponding to the SISO system *{Yi, Uj}.* As can be seen in the Figures 5.7 and 5.8 after scaling by *fldc* the control reaches the same output value in the step response after the rescaling. This now allows a consistent comparison to the control effort expended in each design.

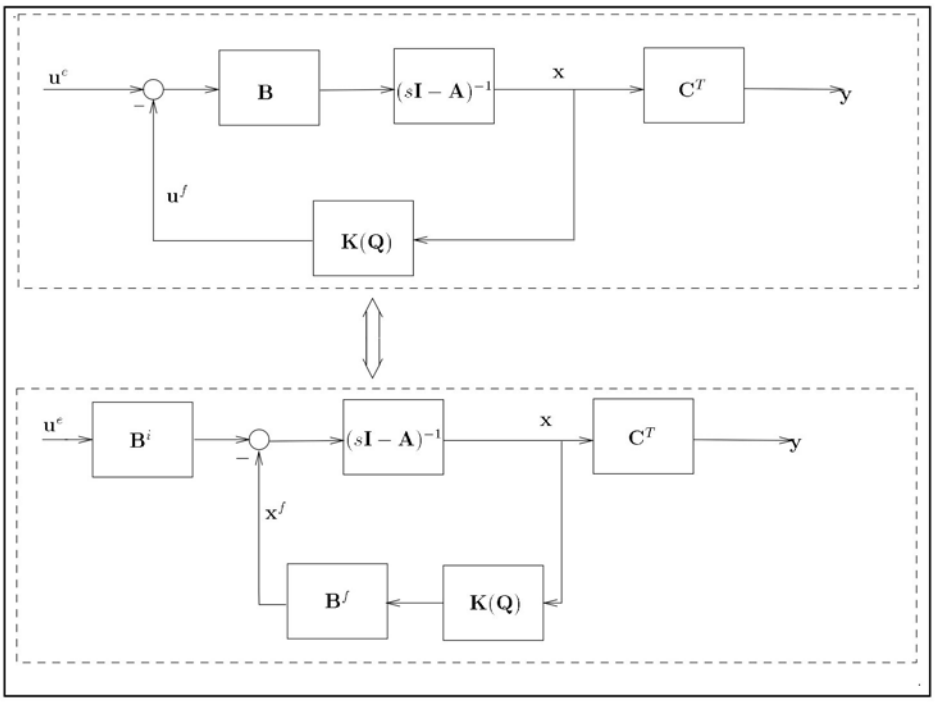

Figure 5-6: Block diagram of the feedback system. The lower part of the diagram shows the system split into the external input and into the feedback.

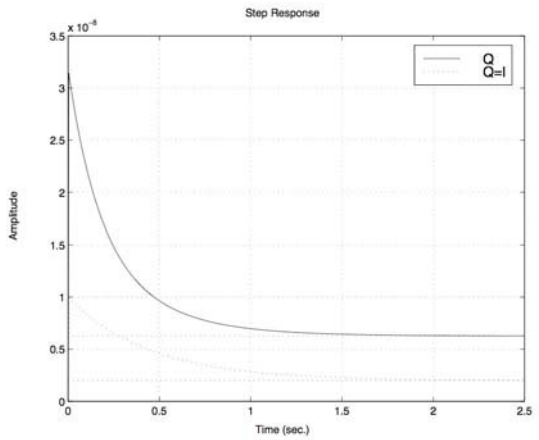

Figure 5-7: Step response of the SISO system without rescaling.

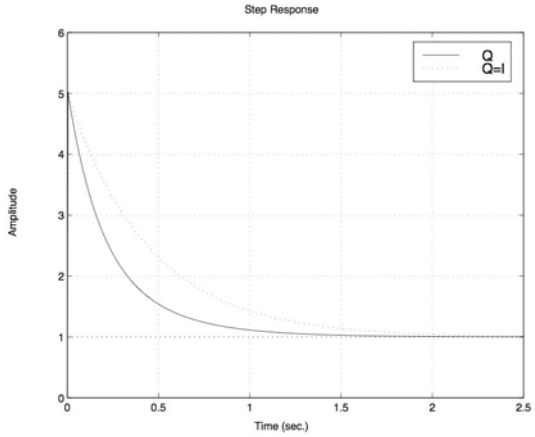

Figure 5-8: Corrected response of the SISO system appropriate rescaling

Table 5.2: Norm of the Output

Output	Q	Q^{pd}	Q^{id}
$\|y_1\|_2$	1.37300816903771	1.38266772040191	4.51183709756009
$\|y_2\|_2$	0.00430043627975	0.00010253279725	0.00002015129389
$\|y_3\|_2$	0.00358836676767	0.00002645322245	0.00002017510737
$\|y_4\|_2$	0.00035521324325	0.00002022959594	0.00002017462944
$\|y_5\|_2$	0.00040455703086	0.00001650392399	0.00002017531606
$\sum_{i=1}^{5} \|y_i^u\|_2^2$	1.38165674235924	1.38283343994155	4.51191777390684

5.4.3 Comparison of control effort expended between designs

In this section the effort of the different controls to reach the same output value on a step response is investigated. One possibility in which to rate the control energy is to consider the new output

$$y_{new}^{\zeta} = \Leftrightarrow K(Q^{\zeta})\, x.$$

The graph of the step response of the SIMO system with selected single input and vector of outputs is shown in Figure 5.4.4. Regarding the Figure 5.4.4 the control based on Q^{id} is the control using the most effort. This means it is the control with the worst properties. To make a statement about the quality of the control of the SIMO system, it is necessary to compute the *L2* norm of the output, given by (see [65]):

$$\|f\|_2 = \left[\sum_{i=1}^{n} \|f_i\|_2^2\right]^{\frac{1}{2}}. \tag{5.4.9}$$

The results, obtained by the MATLAB-function *normit1* are shown in the Table 5.2. Now the question is: In what way does the matrix *R*, previously assumed to be of negligible magnitude, influence the control effort? Therefore, the following ratios

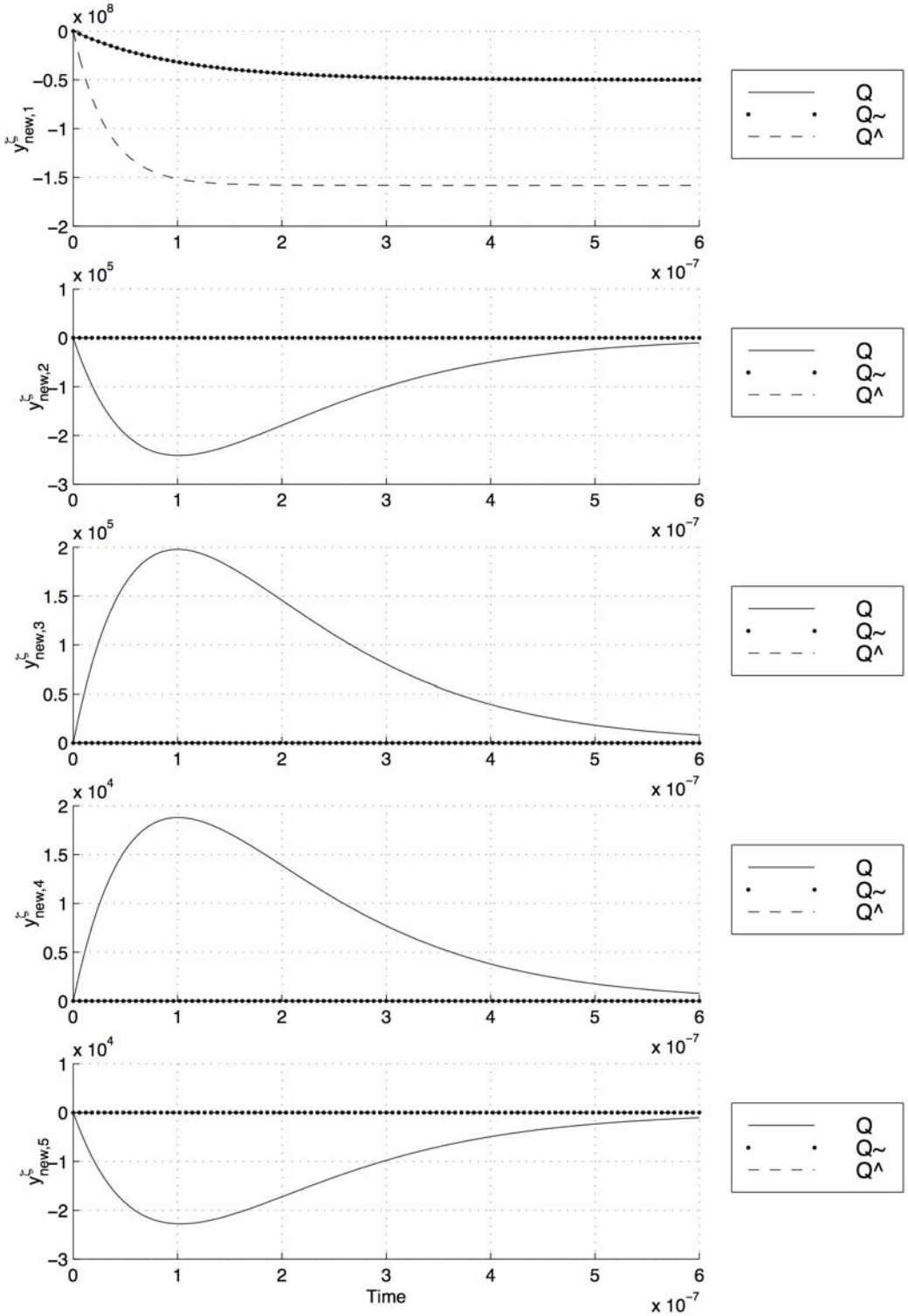

Figure 5-9: Control Effort Summary Results

$$\xi_1 = \frac{\|y(Q^{pd})\|}{\|y(Q)\|}$$

and

$$\xi_2 = \frac{\|y(Q^{id})\|}{\|y(Q)\|}$$

are of interest, and have been computed and plotted in Figure 5.10. This ratio has been computed with several different values for *R*, successively chosen of order 10^{-16}, 10^{-17}, $\cdots$ 10^{-20} magnitude.

The x-axis in Figure 5.10 is the power in the control signal. That is, Figure 5.10 shows the progression of the ratio depending on *R.* The reader should note that the ratio is constant and stays approximately 1**,** indicating both that the magnitude of *R* has little effect, and the choice of *Q* or Q^{Pd} does not make significant difference regarding the overall control energy expended. The authors must frankly state that this outcome was surprising, and remains without an intuitive explanation. Nonetheless, the pragmatic conclusion drawn is that the control based on the matrix Q^{id} is not nearly as good as the other two controls.

In the subsequent investigations, the control based on Q^{id} will no longer considered.

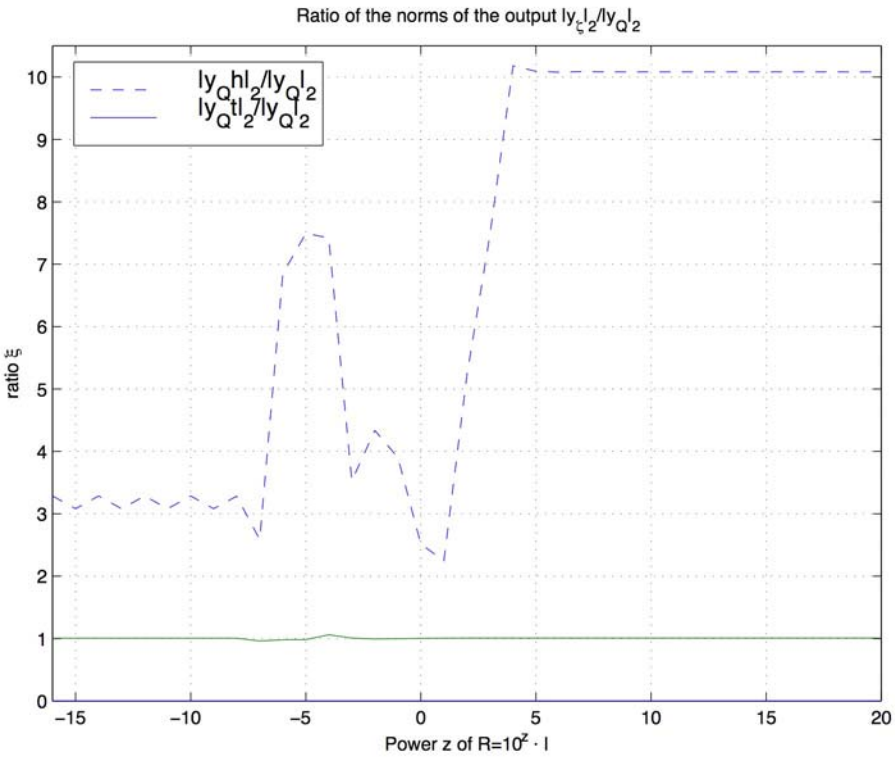

Figure 5-10: Ratios of Output Norms

5.5 Construction of a State Observer to Feed the LQR Controller

In this chapter a state observer for the IEEE14 bus system is developed. Since the whole system has to be regarded as an interconnected network of generators spread over a large area, restrictions have to be introduced to make the assumed controller design, which includes a full state observer, fit to reality. In particular, it is wildly unrealistic to require that each generator's local control logic implement a full dynamic model for the electromechanical dynamics of the network, which is implicit in the full state observer assumption. Therefore our goal in this section will be to investigate the feasibility of reduced dimension observers, which produce the local state estimates to "feed" each generator's LQR controller.

5.5.1 Additional constraints on the IEEE14 system

Due to the problem of real-time transfer of data, it is quite unrealistic, that *all* of the states can be observed in reality. Actually the only directly measurable states available to me as the operator of a given machine are the state variables associated with "my" plant or generator. In

the IEEE14 example system, the only observable state is the state X_1 if we define the generator #1 as the generator of "my" plant[3]. Using this knowledge, the new matrix *Cr* is[4]

$$C_r = \begin{bmatrix} 1 & 0 & \dots & 0 \end{bmatrix}.$$

Computing the rank of the observability matrix

$$rank(V) = rank([C_r \; C_r A \; \dots \; C_r A^{n-1}]^T)$$

shows that the system is fully observable by this choice of *Cr*. With the same reasoning of problems in the real-time transfer of data the choice for the matrix *B:* and in the same moment *B;* is

$$B_r^e = B_r^i = \begin{bmatrix} 1 & 0 & \dots & 0 \end{bmatrix}^T.$$

The only state (=generator) which can influence the behavior of the system is the generator of "my" plant. With these restriction a state-observer is constructed. The questions which have to be answered are, if it is possible to create a state observer which shows a "sufficiently good" behavior, i.e., the estimated states are sufficiently close to the true values of the states to enable the control to operate. Additionally is the dynamics of the observer fast enough. Furthermore, can a feedback control be designed in which the feedback input to the system is only based on the first estimated state. In addition to that, it is very important to know, is it possible to reduce the system?

5.5.2 Construction of the observer

The goal of an observer is to create its error dynamics faster than the dynamics of the feedback control system. The dynamics of the error

$$\tilde{x} = x \Leftrightarrow \hat{x} \tag{5.5.1}$$

[3] Consider the IEEE14 bus network as representative of a large network, with multiple generators playing the role of “plants.” In this scenario, as an owner of such a plant, one has control and knowledge about one’s own unit(s) only.

[4] Note that the starting formulation here maintains the reference angle as a state. This state is, as shown before, neither observable nor controllable and eliminated from the system. Nonetheless which generator stands for "my" plant it does make sense to use the associated angle of the "my" plant as a reference angle and eliminate the mode correlating to the reference angle from the system.

are described by the equation

$$\dot{\tilde{x}} = (A \Leftrightarrow LC)\,\tilde{x} \tag{5.5.2}$$

(e.g. [67]).

Since the choice of *L* is arbitrary, it is reasonable to choose the matrix *L* such that

$$\lambda(A \Leftrightarrow LC_r) \leq \lambda(A \Leftrightarrow B_r K). \tag{5.5.3}$$

Table 5.3: *Lopt* and *Kopt* and the Eigenvalues of the Feedback Matrices

L^{opt}	$(K^{opt})^T$	$\lambda(A \Leftrightarrow LC)$	$\lambda(A \Leftrightarrow BK)$
$1.9875e+08$	$9.9376e+07$	$\Leftrightarrow 1.9875e+08$	$\Leftrightarrow 9.9376e+07$
$9.2365e+08$	$1.2563e+08$	$\Leftrightarrow 1.9424e \Leftrightarrow 01$	$\Leftrightarrow 1.8052e+00+5.4661e+00i$
$\Leftrightarrow 1.5632e+09$	$4.3204e+07$	$\Leftrightarrow 2.6424e \Leftrightarrow 01$	$\Leftrightarrow 1.8052e+00 \Leftrightarrow 5.4661e+00i$
$\Leftrightarrow 1.9465e+09$	$\Leftrightarrow 9.6266e+06$	$\Leftrightarrow 1.1622e+00$	$\Leftrightarrow 1.7267e+00+1.5981e+00i$
$2.3972e+09$	$\Leftrightarrow 3.4619e+07$	$\Leftrightarrow 1.1922e+00$	$\Leftrightarrow 1.7267e+00 \Leftrightarrow 1.5981e+00i$
$3.8262e+08$	$\Leftrightarrow 5.1189e+08$	$\Leftrightarrow 3.8203e+00$	$\Leftrightarrow 4.7612e \Leftrightarrow 01+2.6109e+00i$
$1.8601e+09$	$\Leftrightarrow 1.3930e+08$	$\Leftrightarrow 3.7704e+00$	$\Leftrightarrow 4.7612e \Leftrightarrow 01 \Leftrightarrow 2.6109e+00i$
$\Leftrightarrow 8.2338e+09$	$\Leftrightarrow 1.4029e+08$	$\Leftrightarrow 3.7033e+00$	$\Leftrightarrow 5.2122e \Leftrightarrow 02+2.6540e+00i$
$6.2606e+09$	$\Leftrightarrow 5.5296e+06$	$\Leftrightarrow 3.6934e+00$	$\Leftrightarrow 5.2122e \Leftrightarrow 02 \Leftrightarrow 2.6540e+00i$

This can be realized by the MA TLAB function *place.* Since the choices of *B;* and *B:* are restricted to a vector, the eigenvalues turn out to be complex in the given system. To make the dynamics of the observer fast enough, the eigenvalues are chosen as

$$\lambda(A \Leftrightarrow LC_r) \leq 2 \cdot \Re(\lambda(A \Leftrightarrow B_r K)).$$

Since the rank of the matrix *Cr* is **1,** the maximum multiplicity of the eigenvalues is 1. Hence, small terms are added to the pole locations. The results are shown in Table 5.3.

5.5.3 Open loop response of the observer model

To judge the quality of the observer model, the open loop response of the observer is computed. The model equations are

$$\underbrace{\begin{bmatrix} \dot{x} \\ \dot{\hat{x}} \end{bmatrix}}_{\dot{\xi}} = \begin{bmatrix} A & 0 \\ LC_r & A \Leftrightarrow LC_r \end{bmatrix} \begin{bmatrix} x \\ \hat{x} \end{bmatrix} + \begin{bmatrix} B_r^i \\ B_r^e \end{bmatrix} u \qquad (5.5.4)$$

$$y = \bar{C} \begin{bmatrix} x \\ \hat{x} \end{bmatrix} \qquad (5.5.5$$

with

$$\bar{C} = \begin{bmatrix} 1 & 0 & 0 & 0 & 0 & 0 & 0 & 0 & 0 & 0 & 0 & 0 & 0 & 0 & 0 & 0 & 0 & 0 \\ 0 & 0 & 0 & 0 & 0 & 0 & 0 & 0 & 0 & 1 & 0 & 0 & 0 & 0 & 0 & 0 & 0 & 0 \end{bmatrix}.$$

The choice of C allows us to compare the estimated state with the actual state. The results are shown in Figure 5.5.1.

5.5.4 Step response of the closed control loop

The dynamics of the closed control loop is given by

$$x = (A \Leftrightarrow B_r K)x + B_r\, u \qquad (5.5.6)$$

$$y = C_r\, x + D\, u$$

Regarding now the step response of the closed loop system shows for each of the determined *Kopt* and *KPd* a rather unexpected behavior a the very beginning. The amplitude is far overshooting than the designated value of 1 (see Figures 5.12 and 5.13).
This can be explained considering the bode-plot of the feedback system. The diagram is show in Figure 5.14. As can be seen in Figure 5.14 there exists an eigenvalue which is dominating in the high frequency band. This eigenvalue is responsible for the "odd" behavior of the step response done to the feedback system. One mode may be attributed as causing the overshooting at the beginning.

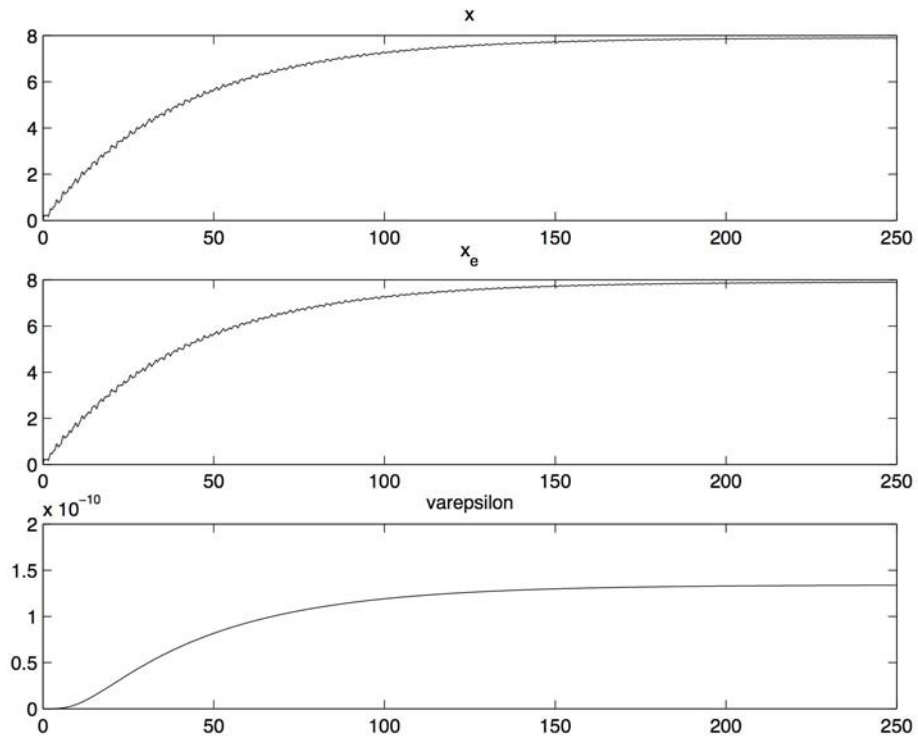

Figure 5-11: Plot of the state 6 and the state 60. As is obvious, that the estimated states follows almost optimal the state 6. The error of the state and the estimated state is marginal.

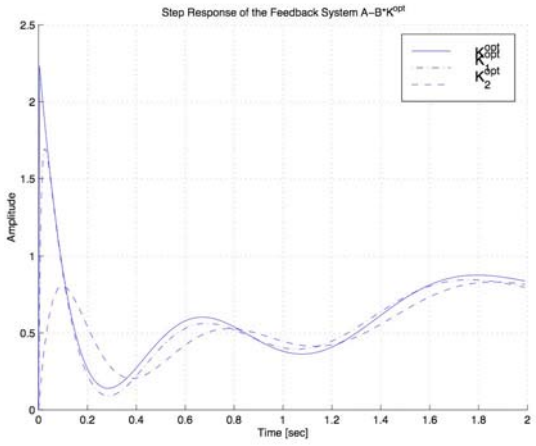

Figure 5-12: Step response of the first Feedback System with different locations of the eigenvalue. Relevant design values are given in Table 5.2

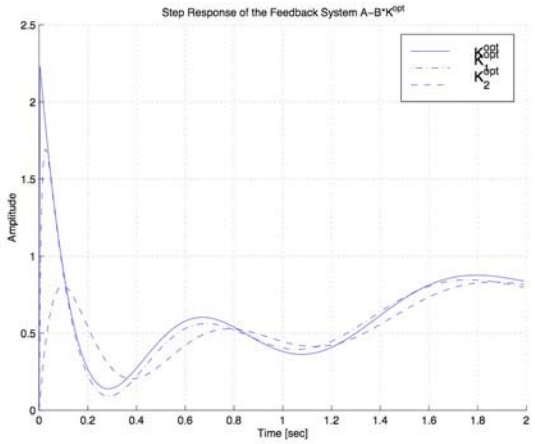

Figure 5-13: Step response of the second Feedback System with different locations of the eigenvalue. Relevant design values are given in Table 5.2.

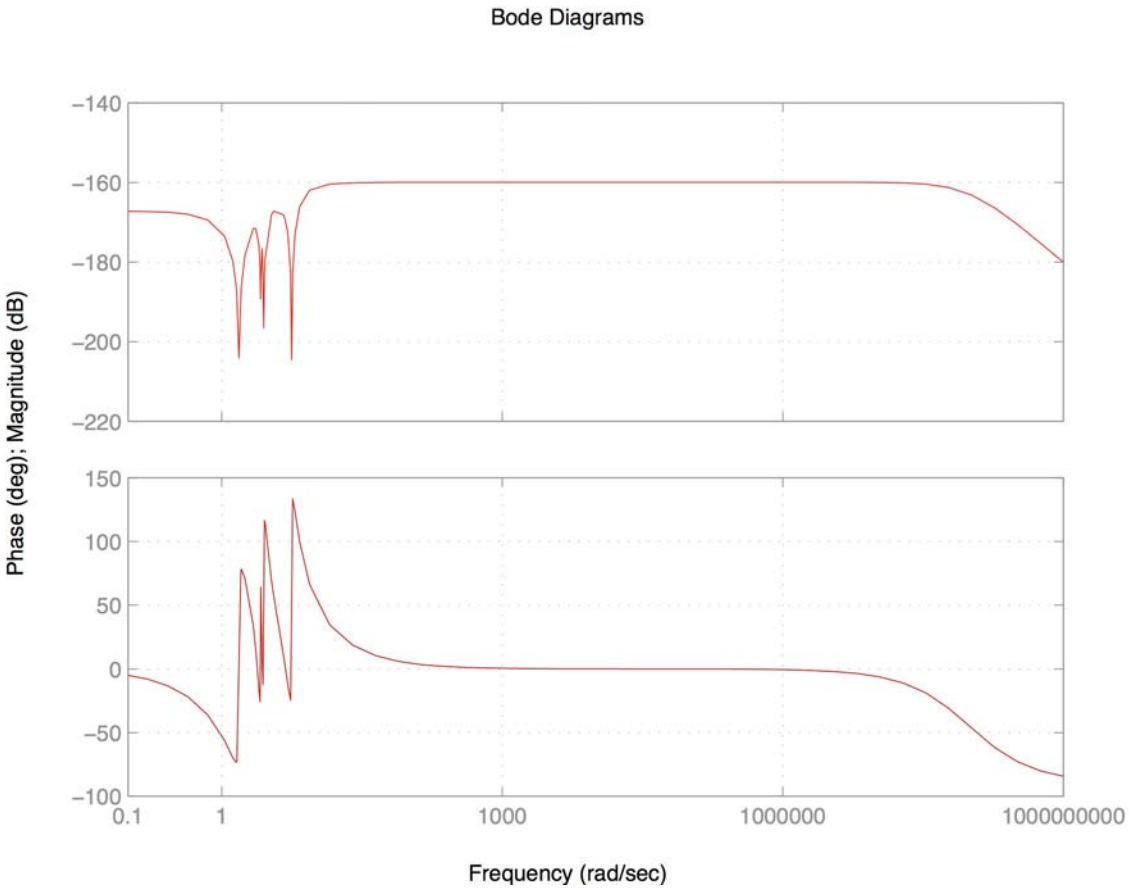

Figure 5-14: Bode-plot of the feedback system. It shows a clear dominance of the fastest eigenvalue (the eigenvalue located on the very left) in the high frequency band.

Table 5.4: Values used in Eigenvalue Computation

	$\lambda_1(A \Leftrightarrow B_r K^{opt})$	$\lambda_1(A \Leftrightarrow B_r K^{pd})$
K^{ζ}	$\Leftrightarrow 9.9376e+07$	$\Leftrightarrow 1.0000e+08$
K_1^{ζ}	$\Leftrightarrow 9.9376e+01$	$\Leftrightarrow 1.0000e+02$
K_2^{ζ}	$\Leftrightarrow 9.9376e+00$	$\Leftrightarrow 1.0000e+01$

This overshooting could cause some trouble in the overall design and so it has to be reduced in some way. Since the main interest in this investigation is concentrated on the lower frequency band, there are two possibilities to remove this unintended progression of the step response.

1. Removing the mode associated with high frequency band.
2. The mode associated with the high frequency band is dominated by the one troublesome eigenvalue. Hence moving this eigenvalue to a more "reasonable" value more right decreases this influence and smoothes the step response.

In this work the *2nd* approach has been chosen. Hereby the MATLAB routine *place* been used to create the new feedback matrices

$$K_i^{\zeta} = place(A, B, E_i^{\zeta}) \; i = 1.2. \tag{5.5.7}$$

Hereby the vector *E;* is the vector of the eigenvalues of interest. only with a change in the first eigenvalue given by Table 5.4. The improvement of the step response of the feedback system can be seen in the Figures 5.12 and 5.13. The more the first eigenvalue of the feedback matrix is moved to the right, the lower becomes the peak until finally at an eigenvalue

$$\lambda_1(A \Leftrightarrow BK^{\zeta}) \propto \Leftrightarrow 10$$

3. The system considered here is of course a power system example. The state variables are the frequency of the generators and the deviation of their angles. Neglecting shaft torsional dynamics (as we do here), the bandwidth of the transfer function of a generator is quite limited. Hence there is no possible high frequency influence on the generators' rotational dynamics.

The system shows a "nice" behavior. This can also be seen in the root-locus diagram given in Figures 5.12-5.14. In these plots the Evans root locus of the SISO open-loop model

$$\begin{aligned} x &= A\,x + B^i\,u \\ y &= K_i^{\zeta}\,x. \end{aligned}$$

is shown. Using the MATLAB function *rlocus* it is necessary to determine a feedback gain *k.* For the purposes in this work, *k* has to be

$$0 \leq k \leq 1$$

that denotes in the case of $k = 0$ no feedback control, and in the case of $k = 1$ full feedback control. In principle there is no major difference between the approaches. By changing the pole location in the feedback, a major change in the control matrix *KC*, is done. The change in the control matrices are shown in Table 5.5.3.

A major question is, in which way this change in the control matrices *K;* influences the needed control energy. Since the values of *K;* are smaller than the values of *KC,* it is quite reasonable to assume, that the needed control energy of the control matrices *K;* is smaller. Additionally the question is raised, how is the observer influenced by these changes and in which way the system can be reduced.

4 Since only one state is considered being observable and controllable, the control matrix *K* is reduced to a vector. The values of the matrices designed by placing the eigenvalues *(Kf* 2) are from a lower dimension than the matrices *KC,* designed by the LQR algorithm.

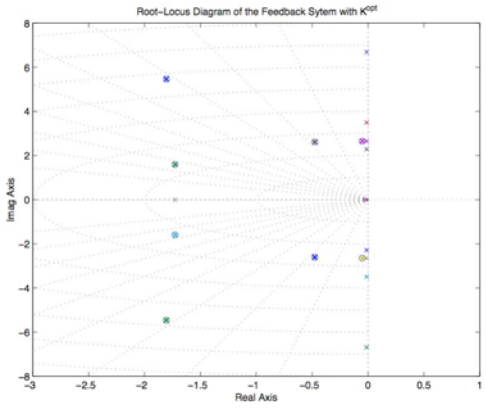

Figure 5-15: Root-Locus diagram for the feedback system 1

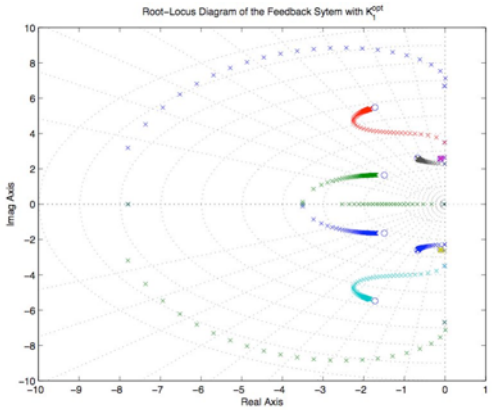

Figure 5-16: Root-Locus diagram for the feedback system 2

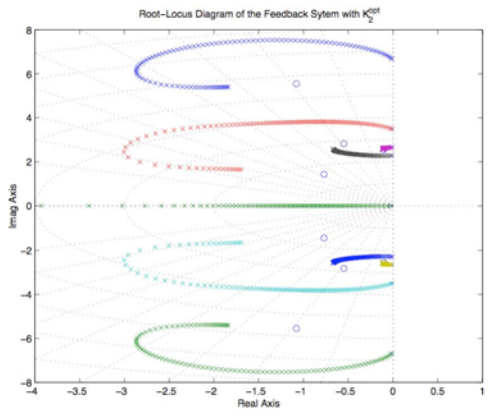

Figure 5-17: Root-Locus diagram for the feedback system 3

Table 5.5: Matrices K of the Feedback Control

$(K^{opt})^T$	$(K_1^{opt})^T$	$(K_2^{opt})^T$	$(K^{pd})^T$	$(K_1^{pd})^T$	$(K_2^{pd})^T$
$9.9376e{+}07$	$1.0789e{+}02$	$1.8448e{+}01$	$1.0000e{+}08$	$1.0883e{+}02$	$1.8827e{+}01$
$1.2563e{+}08$	$1.3994e{+}02$	$9.2535e{+}00$	$1.1816e{+}08$	$1.5550e{+}02$	$1.0811e{+}01$
$4.3204e{+}07$	$8.9862e{+}01$	$6.6491e{+}00$	$3.5213e{+}07$	$1.4334e{+}02$	$1.1901e{+}01$
$-9.6266e{+}06$	$-1.6201e{+}02$	$-1.7768e{+}01$	$-1.1232e{+}07$	$-3.5182e{+}02$	$-3.9417e{+}01$
$-3.4619e{+}07$	$3.2624e{+}01$	$4.2001e{+}00$	$-1.8140e{+}07$	$1.3995e{+}02$	$1.7415e{+}01$
$-5.1189e{+}08$	$-5.3988e{+}02$	$-7.2105e{+}01$	$-5.5898e{+}08$	$-5.4564e{+}02$	$-7.5273e{+}01$
$-1.3930e{+}08$	$-2.5480e{+}02$	$-2.4633e{+}01$	$-9.7722e{+}07$	$-2.7030e{+}02$	$-3.0337e{+}01$
$-1.4029e{+}08$	$-1.6288e{+}02$	$-3.5536e{+}00$	$-6.8913e{+}07$	$-4.5213e{+}02$	$-2.0843e{+}01$
$-5.5296e{+}06$	$1.0379e{+}02$	$9.8892e{+}00$	$-6.8517e{+}07$	$3.7561e{+}02$	$3.0639e{+}01$

5.5.5 Control energy expended by the new controls

In this section the amount of used control energy is examined. Therefore the closed loop model is employed, constructed as:

$$\begin{bmatrix} \dot{x} \\ \dot{\hat{x}} \end{bmatrix} = \begin{bmatrix} A & \Leftrightarrow BK \\ LC & (A \Leftrightarrow LC \Leftrightarrow BK) \end{bmatrix} \begin{bmatrix} \dot{x} \\ \dot{\hat{x}} \end{bmatrix} + \begin{bmatrix} B^i \\ B^e \end{bmatrix} u \qquad (5.5.8)$$

$$\begin{bmatrix} x \\ \hat{x} \end{bmatrix}$$

$$y = C \qquad (5.5.9)$$

with

$$\tilde{C} = \begin{bmatrix} 1 & 0 & \dots & \dots & \dots & 0 \\ 0 & \dots & 0 & K^{\zeta}_{i_{1,1}} & \dots & K^{\zeta}_{i_{1,n}} \end{bmatrix}$$

To examine use of control energy, a step input is applied to excite the system. The results are shown in the following sections. Since the cases *Kopt* and *KPd* are very similar to each other here only the case *KC,* = *Kopt* is considered.

5.5.5.1 Case: *Kopt*

For the feedback matrix *K* in the observer system (5.5.6) is chosen to be the matrix *Kopt* based on the matrix *Qopt* derived by the passivity constraints. The step response of this system is given in the Figure 5.18. To reach the control goal, a very high amount of control energy is needed.

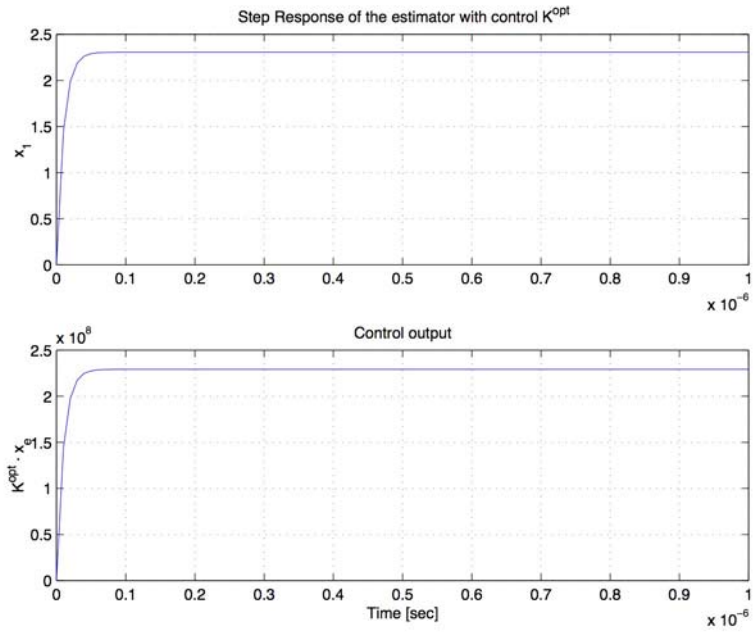

Figure 5-18: Plot of the state variable x_1 and the control feedback $Kopt \cdot x_e$ of the observer system.

The bode diagrams of the observer systems based on *Kopt* and *KPd* in Figures 5.19 and 5.20 show the dominance of an eigenvalue in the high frequency band. This finally leads the controller failing, and makes the system unstable as seen in its step response.

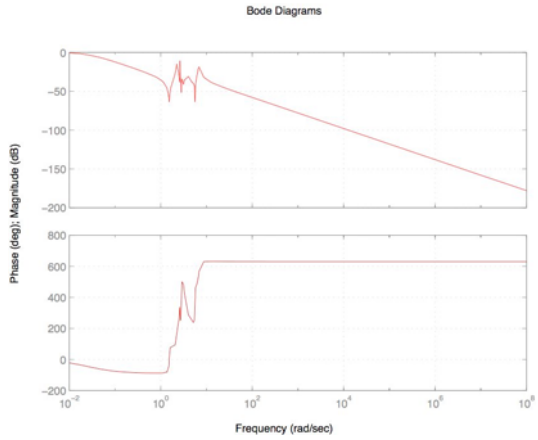

Figure 5-19: Bode-diagram of the observer system based on the control matrix Kopt.

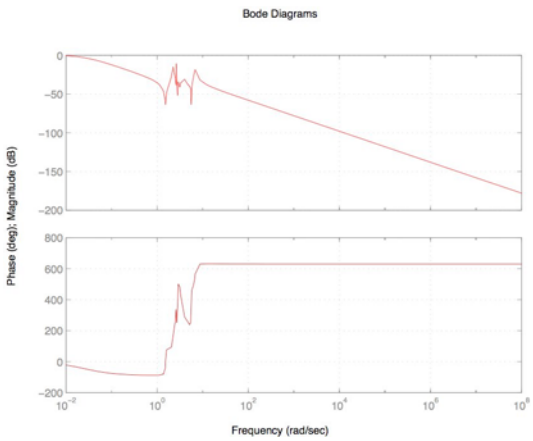

Figure 5-20: Bode-diagram of the observer system based on the control matrix Kopt.

5.5.5.2 Performance for Other Gain Selections

In this section the modified matrices are the basis for the observer model. Again, the step a given onto the system. The overall output of the system is the state X_l and the control output. With the second output the control can be judged since the amount of used control energy is a sign for the quality of the control. The result of the step response is visualized in the Figure 5.21 and 5.22. As can be seen, both controls are able to stabilize the system. As expected, the used control energy in the model based on *K2* is much less than the used control energy in the case based on *KI*.

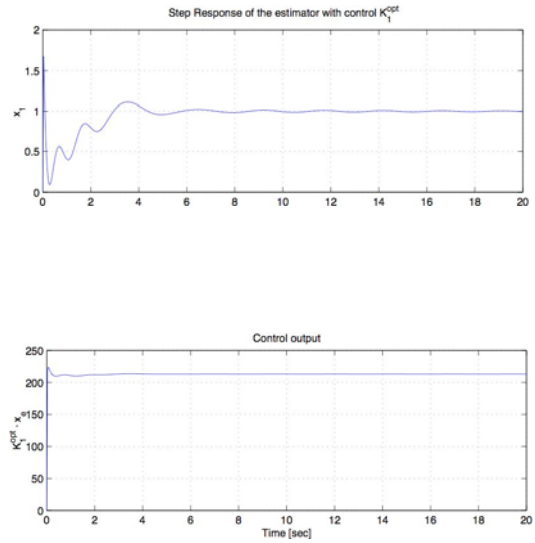

Figure 5-21: Step response of the observer system based on first gain selection

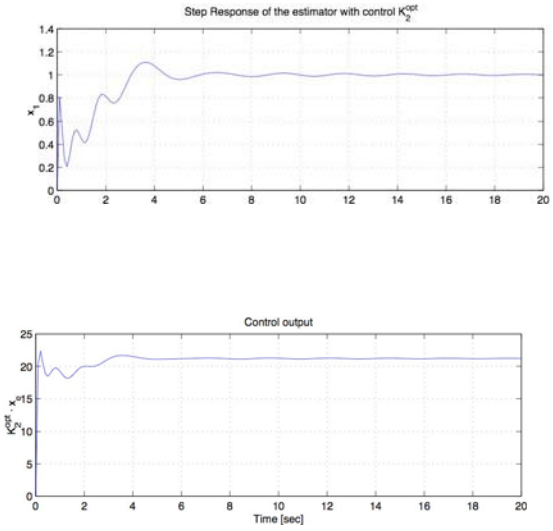

Figure 5-22: Step response of the observer system based the second gain selection

5.5.6 Conclusions Regarding Construction of the State Observer

In this section the observer model has been constructed. The feedback matrices have been determined and implemented. Certain difficulties in the control design have been investigated and (if possible) eliminated. The constructed state-space observer is the new model in next examinations and can be treated as a "black box".

The remaining question to be addressed relates to reduction of the order of the "black box" observer system. The motivation is that in real applications a very large number of states (> 700) is involved. The goal is to reduce these large-scale systems to a much smaller dimensional system. This question will be examined in the next section of this chapter.

5.6 Dimensionality Reduction to Allow Practical Implementation of the State Observer

Consider the nature of the control design described thus far: each generator locally implements a ***state*** feedback control, based on LQR design, that assumes avaialability of the full state vector to "feed" this control. Clearly, the full state vector is not available as a measurement. So as a first step towards practical implementation, we have examined the construction of an observer, or dynamic state estimator, to be coupled with each controller. Such an observer reconstructs an estimate of the state vector from available measurements local to the generator. However, even with the use of an observer, a critical shortcoming remains with regard to any practical implementation: the required state observer that is part of the design has the same dimension as the overall system to be controlled. In other words, the computational power employed at each controller would have to be such that the full, linearized electromechanical state space model of the power system was implemented in software. This is obviously impractical. Considering a large-scale power system problem, this raises the obvious need to reduce the observer dimension. In other words, we seek to create a observer with a ***much*** lower number of internal states, which has the same (or approximately the same) input/output properties. To this end, in this section the balanced realization of the observer model is examined. The idea is to use the balanced realization of the observer, ranking the states in order with regard to their impact on input/output behavior, and thereby make an intelligent choice as to reduction of its number of states. This yields to a lower dimensional observer with the approximate input/output behavior of the original system. The procedure employed here follows the algorithms of [80], [81]. A balanced realization of the observer system is obtained. Then it is simply truncated by discarding those parts relating to the state variables that are most weakly coupled to the inputs and outputs.

5.6.1 The balanced realization

The balanced realization algorithm is described in [80]. For a continuous-time and asymptotically stable system

$$G(s) = \left(\begin{array}{c|c} A & B \\ \hline C & D \end{array}\right) \tag{5.6.1}$$

a balanced realization

$$g(s) = \left(\begin{array}{c|c} a & b \\ \hline c & d \end{array} \right) \tag{5.6.2}$$

is one for which the Lyapunov equations

$$aP + Pa^T + bb^T = 0 \tag{5.6.3}$$

and

$$a^T Q + Qa + c^T c = 0 \tag{5.6.4}$$

have a common solution

$$P = Q = \Sigma$$

and Σ is diagonal. *P* and *Q* are the controllability and observability gramians, respectively. The controllability gramian is defined by

$$P = \int_0^\infty e^{A\tau} B\, B^T e^{A^T \tau} \mathrm{d}\tau \tag{5.6.5}$$

and analogously the observability gramian

$$Q = \int_0^\infty e^{A^T \tau} C^T\, C e^{A\tau} \mathrm{d}\tau \tag{5.6.6}$$

In such a balanced realization the state variable is equally strongly coupled to the input and the output of the system. Solving the Lyapunov equations (5.6.3) and (5.6.4) for a dynamical system *(A, B,* C, *D)* gives solutions *P* and *Q.* The matrix is determined by

$$R\, R^T = Q \Leftrightarrow R = \sqrt{Q}.$$

With the matrix *R* a singular value decomposition can be done in the following form

$$R\, P\, R^T = U\, \Sigma^2\, U^T. \tag{5.6.7}$$

Then the balanced realization *(a, b,* c, *d)* of the system *(A, B,* C, *D)* is given by

$$a = T A T^{-1} \tag{5.6.8}$$

$$b = T B \tag{5.6.9}$$

$$c = C T^{-1} \tag{5.6.10}$$

$$d = D \tag{5.6.11}$$

where the transformation matrix is given by

$$T = \Sigma^{-\frac{1}{2}} U^T R \tag{5.6.12}$$

Considering the Gramian vector $g_{o,c}$. This vector $g_{o,c}$ is given by

$$g_{o,c} = diag(T P T^T) = diag(T^{-T} Q T^{-1}). \tag{5.6.13}$$

The vector $g_{o,c}$ is sorted. The first elements of $g_{o,c}$ correlate to the states with the most influence on the input/output behavior, the last elements correlate to the states with the least influence on the input/output behavior.

5.6.2 Balanced realization of the observer model

The goal is, determining a blanced realized model *(a, b,* c, *d)* of the open loop observer model *(A–LC, B*, K, D)* with

$$B^* = \left[\; L \;\middle|\; B^e \; \right]$$

as shown in Figure 5.23 on the following page. The new observer model *(a, b,* c, *d)* will then be reduced in its states and tested to determine how well the control behaves with the reduced observer.

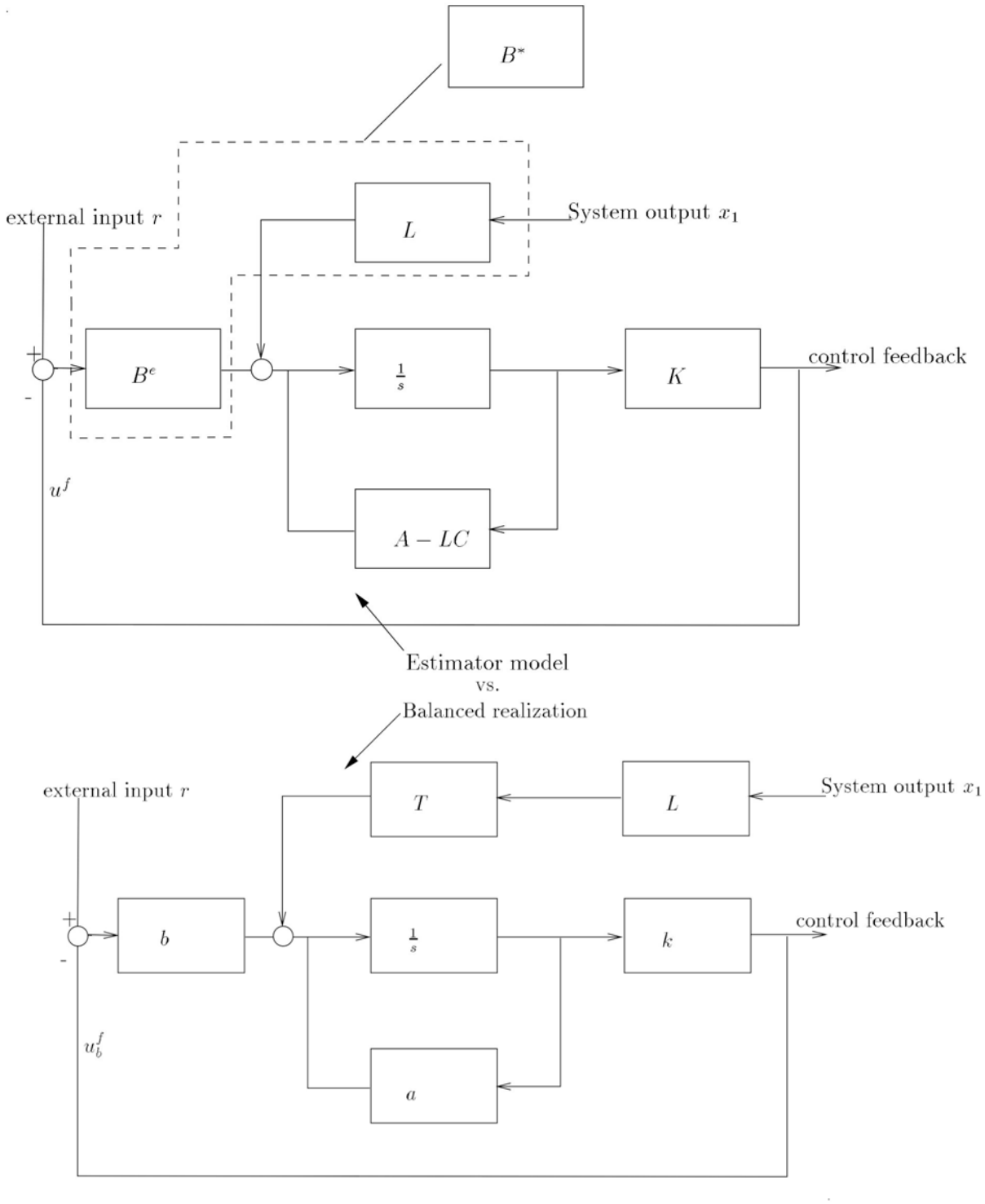

Figure 5-23: Observer VS. Balanced realization

The aggregate dynamics of the balanced realized model of the system and observer together is given by

$$\begin{bmatrix} \dot{x} \\ \dot{\hat{x}}_b \end{bmatrix} = \begin{bmatrix} A & Bk \\ TLC & a \end{bmatrix} \begin{bmatrix} x \\ \hat{x}_b \end{bmatrix} + \begin{bmatrix} B \\ b \end{bmatrix} u \tag{5.6.25}$$

As a proof, that the balanced realization observer behaves the same input/output property as the original observer, the step responses of the systems are shown in Figure 5.24. The output *Xl* of the combination system-original observer and system-balanced realization observer are identical. Additionally, the Bode diagrams of the two combined systems in Figure 5.25 demonstrate that the input/output behaviors of these two systems are very similar.

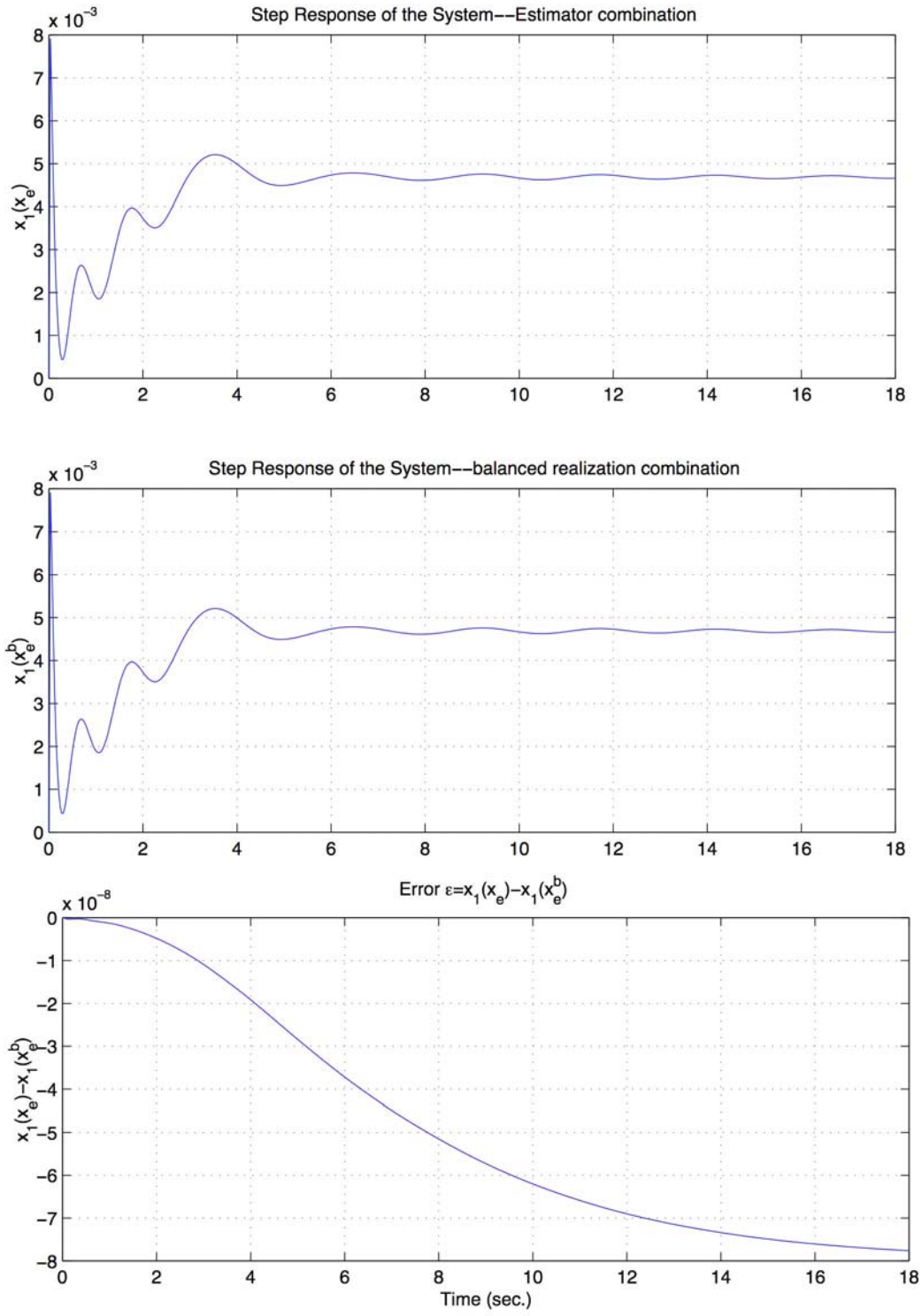

Figure 5-24: Output Xl based on the combination System-Observer vs. System-Balanced Realization. The error of the System-Balanced Realization is minimal.

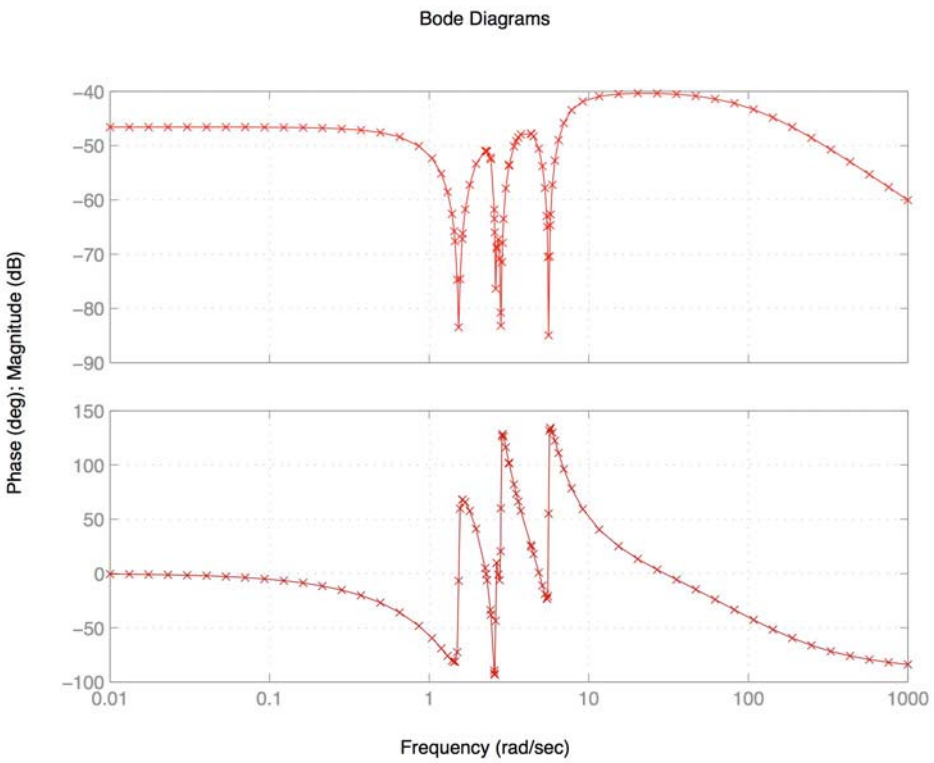

Figure 5-25: Bode diagrams of the system-observer combination vs. system-balanced realization combination

This means, the dynamics of the balanced realization based system is unchanged. Based on this knowledge, the observer (after applying the balanced realization) is reduced in its states by eliminating certain modes. Regarding the vector $g_{o,c}$ for the IEEE14 bus network

$$g_{o,c} = \begin{bmatrix} 4.3206e+05 \\ 2.9041e+05 \\ 1.3108e+05 \\ 3.3031e+04 \\ 8.5191e+03 \\ 7.9355e+03 \\ 6.9455e+03 \\ 2.1023e+03 \\ 1.7617e+03 \end{bmatrix}$$

The vector $g_{O,C}$ shows, that the biggest difference in dimension is about 102 between the first and the last element of $g_{O,C}$. Therefore the first try will be to eliminate the state, associated to the last element in $g_{O,C}$. This means the associated columns and rows will be eliminated from the formulation. To determine the quality of the approximation the bode-diagrams of the original observer and the reduced observer is computed. The results are shown in Figure 5.26.

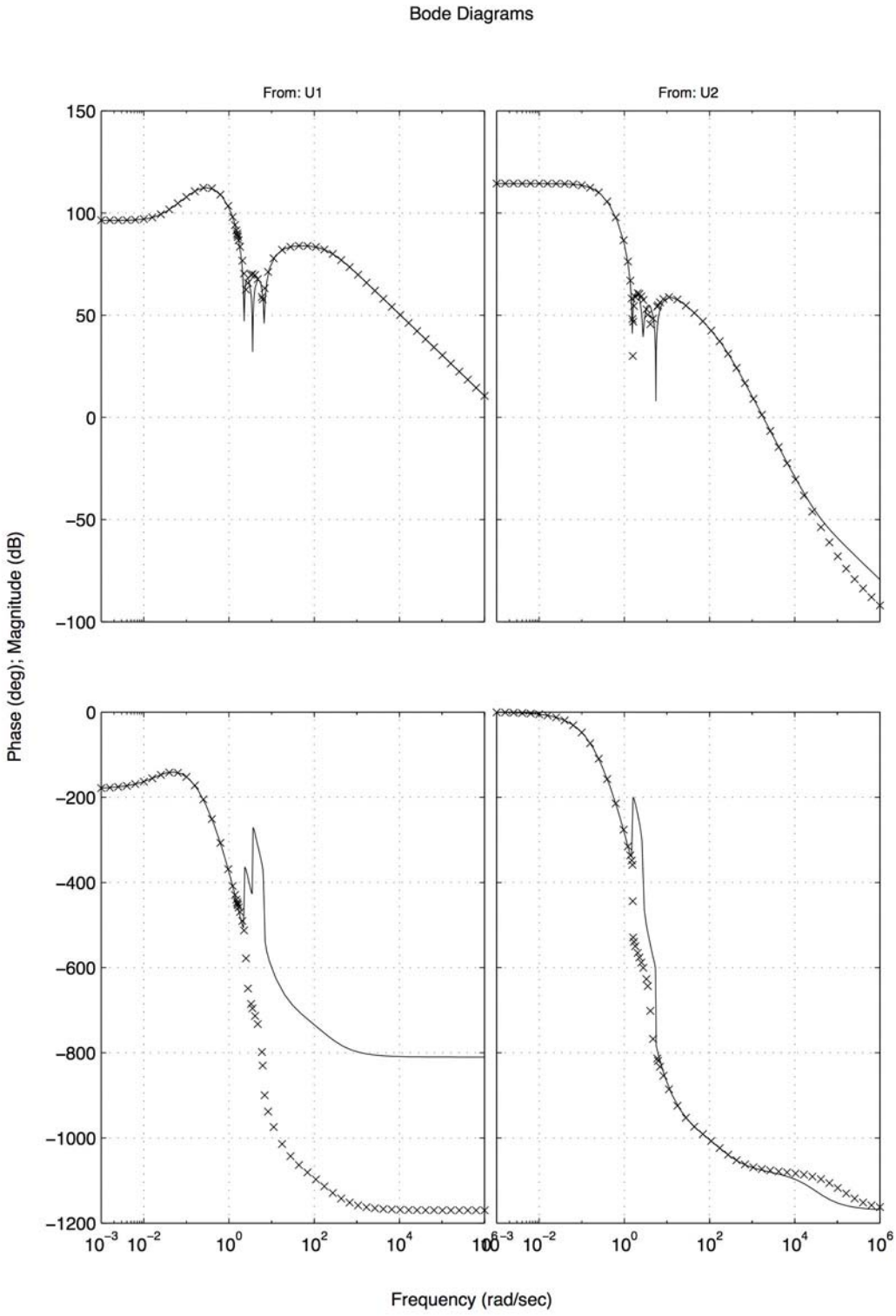

Figure 5-26: Bode diagrams of the open loop observers: Original observer (shown as line format -) and Reduced observer (shown as line format x).

After reducing the *9th* mode the step response to the system with the reduced observer is shown in Figure 5.24. Surprisingly the system is unstable, even if the reduced feedback observer has a very similar input/output behavior as the full state observer. The explanation is given by considering the bode diagrams. The bode diagrams of the reduced model vs. the full observer model are shown in Figure 5.25. In Figure 5.25 the unstable behavior of the reduced system is explained. Even if the open loop input/output behavior of the reduced observer is a good approximation to the full state observer, that closed loop with the reduced model changes the dynamics dramatically. This leads finally to the instability of the closed loop system.

This yields the conclusion, that the model reduction via the balanced realization can not be successfully applied to a dynamical system like the IEEE14 bus network in its present form I. There exist other approaches to reduce the model of a dynamical system, e.g. the approach of [83]. But this method does not yield to a successful solution either.

5.6.3 Sensitivity analysis

As shown in the previous section, a reduction of the system consisting of the IEEE14 bus network and an observer2 cannot be done by the here shown approach. This raises the question why this approach is not working. Therefore a sensitivity analysis has been done. In the sensitivity analysis the impact of parameter changes in the observer matrix L and the control matrix K to closed loop system has been examined.

The matrix of the closed loop is given by

$$\mathcal{A}(L,K) = \begin{bmatrix} A & \Leftrightarrow BK \\ LCA \Leftrightarrow LC & \Leftrightarrow BK \end{bmatrix}. \tag{5.6.26}$$

1 As a matter of fact, the IEEE14 bus network is a stable but poorly damped system. While not practically of interest, one notes that increasing the damping of the system in equation by increasing the entries in the matrix D_{damp} would yields a system which would be easier to reduce by the balanced realization (see Appendix E).

2 To avoid cumbersome repetition, if not mentioned explicitly, the composite system "IEEE14 bus network–observer" will be called simply "the system" .

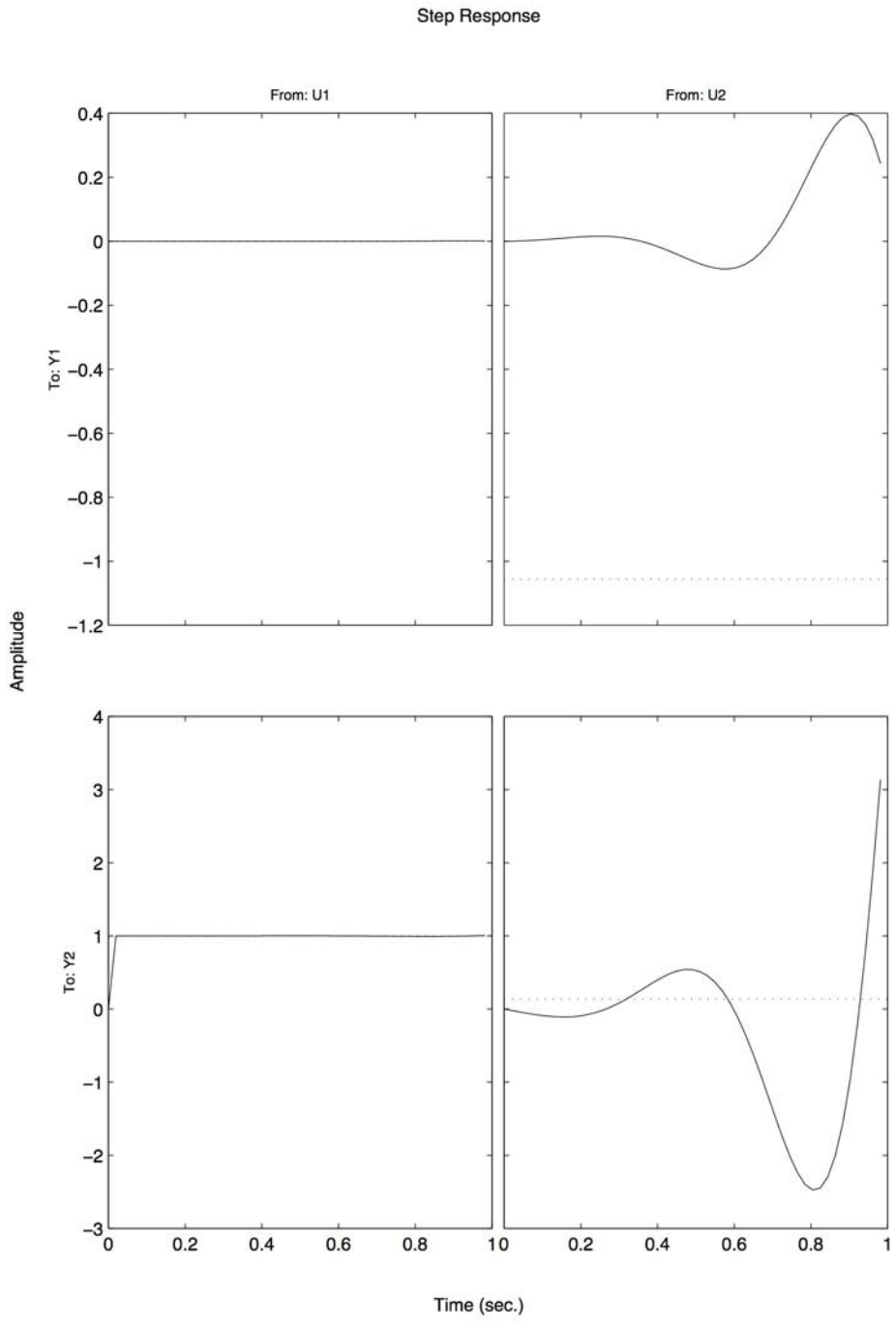

Figure 5-27: Step Response on the system with observer reduced by order 1. The system is instable, even if the reduced observer has almost the same input/output behavior as the full observer.

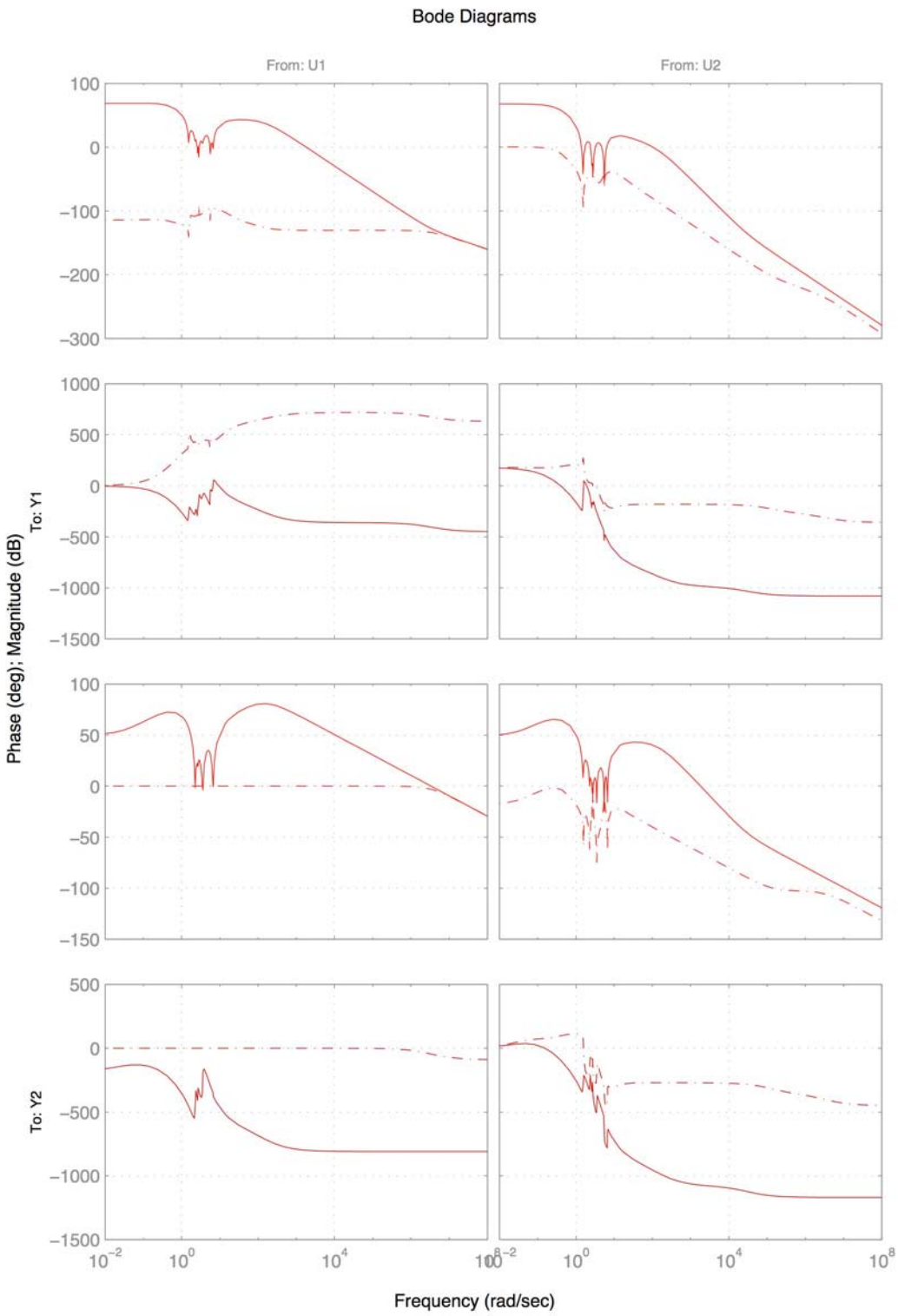

Figure 5-28: Bode Diagram of the full model and the by order 1 reduced model

The behavior of the system is determined by its eigenvalues. Since we are interested in the influence of parameter changes to the stability of *A(L, K)* we investigate the impact on the eigenvalues.

For given initial L_O, K_O the eigenvalues *A(A)* can be determined. Then the partial derivatives of the eigenvalue vector and either the observer vector *L* or *K* is computed such that

$$\Xi_{k,j}^{L} = \frac{\partial \lambda_k}{\partial L_j}, \qquad \Xi_{k,j}^{K} = \frac{\partial \lambda_k}{\partial K_j} \tag{5.6.27}$$

The eigenvalues of the system *A* are not sensitive due to parameter changes in *L, K* respectively, if the maximum value of the resulting matrix 2£, *2K* respectively is very small (if the maximum value of 2(is 0, there is not impact).

5.6.3.1 Sensitivity of A(*L, K*) due to changes in *L*

Provided that there are no repeated eigenvalues, the following approach the partial derivatives of *A(L, K)* can easily be determined.

With

$$W \cdot \mathcal{A} = \Lambda \cdot \mathcal{W} \tag{5.6.28}$$

where A is given by

$$Lambda = [\lambda_1 \ \ldots \ \lambda_n]^T \cdot I \tag{5.6.29}$$

the matrix of left eigenvectors can be determined. Analogously the matrix of right eigenvectors *V* can be derived from the equation

$$A \cdot V = V \cdot \Lambda. \tag{5.6.30}$$

Then the partial derivatives of the eigenvalues can be derived from

$$\frac{\partial \lambda_k}{\partial L_j} = \frac{w_k \left[\frac{\mathcal{A}}{L_j}\right] v_k}{w_k \cdot v_k} \tag{5.6.31}$$

Table 5.6: Matrix of Sensitivity of the Eigenvalues of A due to Parameter Changes in L

$\frac{\partial \lambda_k}{\partial L_j}$	L_1	L_2	L_3
λ_1	$-1.8199e-01-5.3135e-02i$	$2.3713e-01+6.9235e-02i$	$-4.2830e-02-1.2505e-02i$
λ_2	$-1.8199e-01+5.3135e-02i$	$2.3713e-01-6.9235e-02i$	$-4.2830e-02+1.2505e-02i$
λ_3	$3.0175e-15$	$2.1761e-16$	$-2.9015e-16$
λ_4	$-1.5242e-01-9.6917e-02i$	$-7.7830e-02-4.9487e-02i$	$2.1484e-01+1.3660e-01i$
λ_5	$-1.5242e-01+9.6917e-02i$	$-7.7830e-02+4.9487e-02i$	$2.1484e-01-1.3660e-01i$
λ_6	$-1.9779e-01$	$-1.9827e-01$	$-1.9484e-01$
λ_7	$-1.4630e-15+3.8231e-16i$	$1.0055e-17-3.9647e-15i$	$7.8498e-16+1.3767e-15i$
λ_8	$-1.4630e-15-3.8231e-16i$	$1.0055e-17+3.9647e-15i$	$7.8498e-16-1.3767e-15i$
λ_9	$-6.2012e-02-8.9175e-02i$	$-5.5626e-02-7.9991e-02i$	$-6.6172e-02-9.5157e-02i$
λ_{10}	$-6.2012e-02+8.9175e-02i$	$-5.5626e-02+7.9991e-02i$	$-6.6172e-02+9.5157e-02i$
λ_{11}	$-4.6803e-03-4.6952e-03i$	$-4.5434e-03-4.5579e-03i$	$-8.4182e-03-8.4449e-03i$
λ_{12}	$-4.6803e-03+4.6952e-03i$	$-4.5434e-03+4.5579e-03i$	$-8.4182e-03+8.4449e-03i$
λ_{13}	$8.1448e-17-1.0317e-15i$	$7.7046e-16-9.0707e-16i$	$1.6390e-15+2.9560e-17i$
λ_{14}	$8.1448e-17+1.0317e-15i$	$7.7046e-16+9.0707e-16i$	$1.6390e-15-2.9560e-17i$
λ_{15}	$2.8326e-16+1.4581e-15i$	$-1.0019e-15+1.4925e-15i$	$-3.0255e-15+2.8616e-16i$
λ_{16}	$2.8326e-16-1.4581e-15i$	$-1.0019e-15-1.4925e-15i$	$-3.0255e-15-2.8616e-16i$
λ_{17}	$-1.8234e-16+3.2291e-16i$	$-5.9830e-16+2.7264e-16i$	$-1.4504e-15+2.1913e-16i$
λ_{18}	$-1.8234e-16-3.2291e-16i$	$-5.9830e-16-2.7264e-16i$	$-1.4504e-15-2.1913e-16i$

$\frac{\partial \lambda_k}{\partial L_j}$	L_4	L_5	L_6
λ_1	$-6.7067e-03-1.9581e-03i$	$-5.6078e-03-1.6373e-03i$	$3.0337e-15+1.6527e+00i$
λ_2	$-6.7067e-03+1.9581e-03i$	$-5.6078e-03+1.6373e-03i$	$3.0337e-15-1.6527e+00i$
λ_3	$-2.6113e-16$	$-2.9015e-16$	$-9.2847e-15$
λ_4	$2.0084e-02+1.2770e-02i$	$-4.6709e-03-2.9699e-03i$	$2.7857e-16-3.2230e-01i$
λ_5	$2.0084e-02-1.2770e-02i$	$-4.6709e-03+2.9699e-03i$	$2.7857e-16+3.2230e-01i$
λ_6	$-2.0684e-01$	$-2.0226e-01$	$-1.2077e-15$
λ_7	$3.2601e-16+4.4245e-16i$	$2.5228e-16+3.7191e-16i$	$2.4660e-14-4.6614e-15i$
λ_8	$3.2601e-16-4.4245e-16i$	$2.5228e-16-3.7191e-16i$	$2.4660e-14+4.6614e-15i$
λ_9	$5.6555e-02+8.1328e-02i$	$1.2725e-01+1.8300e-01i$	$1.2763e-15-2.2251e-01i$
λ_{10}	$5.6555e-02-8.1328e-02i$	$1.2725e-01-1.8300e-01i$	$1.2763e-15+2.2251e-01i$
λ_{11}	$3.3488e-02+3.3594e-02i$	$-1.5846e-02-1.5896e-02i$	$6.0314e-16-1.7038e-02i$
λ_{12}	$3.3488e-02-3.3594e-02i$	$-1.5846e-02+1.5896e-02i$	$6.0314e-16+1.7038e-02i$
λ_{13}	$8.7979e-17+1.7363e-15i$	$-7.0762e-16+2.1473e-15i$	$2.1198e-15+2.9424e-15i$
λ_{14}	$8.7979e-17-1.7363e-15i$	$-7.0762e-16-2.1473e-15i$	$2.1198e-15-2.9424e-15i$
λ_{15}	$-1.6944e-16-2.1816e-15i$	$9.5567e-16-2.3372e-15i$	$-4.5613e-15-4.0262e-15i$
λ_{16}	$-1.6944e-16+2.1816e-15i$	$9.5567e-16+2.3372e-15i$	$-4.5613e-15+4.0262e-15i$
λ_{17}	$1.8927e-15-3.4014e-15i$	$1.4921e-16+1.9323e-15i$	$-1.1096e-15-1.5078e-15i$
λ_{18}	$1.8927e-15+3.4014e-15i$	$1.4921e-16-1.9323e-15i$	$-1.1096e-15+1.5078e-15i$

$\frac{\partial \lambda_k}{\partial L_j}$	L_7	L_8	L_9
λ_1	$-9.3618e-16-2.9850e-01i$	$-1.8072e-16-4.6742e-02i$	$-5.9252e-18-3.9083e-02i$
λ_2	$-9.3618e-16+2.9850e-01i$	$-1.8072e-16+4.6742e-02i$	$-5.9252e-18+3.9083e-02i$
λ_3	$-1.3927e-15$	$-1.5088e-15$	$-1.3927e-15$
λ_4	$-1.9753e-15+8.8967e-01i$	$-6.0779e-16+8.3170e-02i$	$-4.7642e-16-1.9343e-02i$
λ_5	$-1.9753e-15-8.8967e-01i$	$-6.0779e-16-8.3170e-02i$	$-4.7642e-16+1.9343e-02i$
λ_6	$1.4040e-15$	$-1.0568e-16$	$-1.5096e-16$
λ_7	$-4.7536e-15+4.8664e-15i$	$-4.2061e-16+1.6687e-15i$	$-1.4205e-16+1.2367e-15i$
λ_8	$-4.7536e-15-4.8664e-15i$	$-4.2061e-16-1.6687e-15i$	$-1.4205e-16-1.2367e-15i$
λ_9	$2.0123e-15-2.6470e-01i$	$1.2111e-15+2.2623e-01i$	$2.0496e-16+5.0904e-01i$
λ_{10}	$2.0123e-15+2.6470e-01i$	$1.2111e-15-2.2623e-01i$	$2.0496e-16-5.0904e-01i$
λ_{11}	$1.9178e-15-3.1568e-02i$	$-1.3086e-14+1.2558e-01i$	$6.4544e-15-5.9423e-02i$
λ_{12}	$1.9178e-15+3.1568e-02i$	$-1.3086e-14-1.2558e-01i$	$6.4544e-15+5.9423e-02i$
λ_{13}	$2.0322e-15+3.6225e-15i$	$-2.6214e-15+3.4548e-15i$	$-4.0935e-15+2.5535e-15i$
λ_{14}	$2.0322e-15-3.6225e-15i$	$-2.6214e-15-3.4548e-15i$	$-4.0935e-15-2.5535e-15i$
λ_{15}	$-4.3127e-15-6.5656e-15i$	$3.3210e-15-4.6225e-15i$	$4.9749e-15-2.7245e-15i$
λ_{16}	$-4.3127e-15+6.5656e-15i$	$3.3210e-15+4.6225e-15i$	$4.9749e-15+2.7245e-15i$
λ_{17}	$-2.8692e-15-2.6606e-15i$	$1.0033e-14-3.1007e-15i$	$-3.1419e-15+3.5021e-15i$
λ_{18}	$-2.8692e-15+2.6606e-15i$	$1.0033e-14+3.1007e-15i$	$-3.1419e-15-3.5021e-15i$

Table 5.7: Matrix of Sensitivity of the Eigenvalues of A due to Parameter Changes in K

$\frac{\partial \lambda_k}{\partial K_j}$	K_1	K_2	K_3
λ_1	$-2.5012e-030+2.2533e-030i$	$-2.5121e-030-2.4726e-030i$	$3.9323e-031+4.7355e-031i$
λ_2	$-2.5012e-030-2.2533e-030i$	$-2.5121e-030+2.4726e-030i$	$3.9323e-031-4.7355e-031i$
λ_3	$-3.0157e+001$	$-3.1503e+000$	$-3.2192e-001$
λ_4	$1.2073e-029-7.7784e-030i$	$1.0178e-029+1.1409e-030i$	$-1.8363e-029+2.6323e-030i$
λ_5	$1.2073e-029+7.7784e-030i$	$1.0178e-029-1.1409e-030i$	$-1.8363e-029-2.6323e-030i$
λ_6	$1.9558e-029$	$9.8612e-030$	$-6.2447e-031$
λ_7	$2.3921e+000+3.3801e-001i$	$6.5954e-002+2.0060e+000i$	$-2.3285e-001-3.8885e-001i$
λ_8	$2.3921e+000-3.3801e-001i$	$6.5954e-002-2.0060e+000i$	$-2.3285e-001+3.8885e-001i$
λ_9	$-1.5454e-029-4.4988e-030i$	$-2.5165e-030-3.6257e-030i$	$-9.3064e-031-4.8873e-030i$
λ_{10}	$-1.5454e-029+4.4988e-030i$	$-2.5165e-030+3.6257e-030i$	$-9.3064e-031+4.8873e-030i$
λ_{11}	$-8.2487e-029-1.5725e-028i$	$-1.0511e-029-1.0971e-028i$	$-1.0322e-029-1.7957e-028i$
λ_{12}	$-8.2487e-029+1.5725e-028i$	$-1.0511e-029+1.0971e-028i$	$-1.0322e-029+1.7957e-028i$
λ_{13}	$-4.2147e+000-1.0688e+001i$	$5.7465e-001-4.9450e+000i$	$3.2105e+000-3.6246e+000i$
λ_{14}	$-4.2147e+000+1.0688e+001i$	$5.7465e-001+4.9450e+000i$	$3.2105e+000+3.6246e+000i$
λ_{15}	$7.7086e+000+7.9278e+000i$	$9.2809e-001+4.9615e+000i$	$-2.8373e+000+5.0075e+000i$
λ_{16}	$7.7086e+000-7.9278e+000i$	$9.2809e-001-4.9615e+000i$	$-2.8373e+000-5.0075e+000i$
λ_{17}	$-3.1561e-002-9.9593e-002i$	$6.4604e-003-6.3848e-002i$	$2.0552e-002-1.0191e-001i$
λ_{18}	$-3.1561e-002+9.9593e-002i$	$6.4604e-003+6.3848e-002i$	$2.0552e-002+1.0191e-001i$

$\frac{\partial \lambda_k}{\partial K_j}$	K_4	K_5	K_6
λ_1	$-8.1950e-030-3.8950e-030i$	$-8.1215e-031-2.4402e-031i$	$3.9347e-030-2.7701e-030i$
λ_2	$-8.1950e-030+3.8950e-030i$	$-8.1215e-031+2.4402e-031i$	$3.9347e-030+2.7701e-030i$
λ_3	$6.2622e-001$	$-8.4416e-002$	$9.3909e+000$
λ_4	$-1.4110e-028-5.0012e-029i$	$-2.0431e-029-8.9682e-030i$	$-5.5675e-030+1.2955e-029i$
λ_5	$-1.4110e-028+5.0012e-029i$	$-2.0431e-029+8.9682e-030i$	$-5.5675e-030-1.2955e-029i$
λ_6	$1.8949e-028$	$1.8066e-029$	$-2.4367e-030$
λ_7	$1.7344e-001+2.2653e-001i$	$-1.7498e-002-3.4172e-002i$	$-2.8538e+000-1.4530e-001i$
λ_8	$1.7344e-001-2.2653e-001i$	$-1.7498e-002+3.4172e-002i$	$-2.8538e+000+1.4530e-001i$
λ_9	$3.5121e-028-9.0200e-029i$	$8.8320e-029-2.4587e-029i$	$1.5295e-029-2.5183e-030i$
λ_{10}	$3.5121e-028+9.0200e-029i$	$8.8320e-029+2.4587e-029i$	$1.5295e-029+2.5183e-030i$
λ_{11}	$-1.3958e-027-1.1728e-027i$	$-2.5763e-028-1.3649e-028i$	$1.2827e-028-1.3663e-030i$
λ_{12}	$-1.3958e-027+1.1728e-027i$	$-2.5763e-028+1.3649e-028i$	$1.2827e-028+1.3663e-030i$
λ_{13}	$-8.6127e+000-4.8785e+000i$	$9.4519e-001+3.0498e+000i$	$5.6076e+000+4.5140e+000i$
λ_{14}	$-8.6127e+000+4.8785e+000i$	$9.4519e-001-3.0498e+000i$	$5.6076e+000-4.5140e+000i$
λ_{15}	$8.7393e+000+2.7479e+000i$	$-7.6231e-001-2.2334e+000i$	$-7.5242e+000-2.1707e+000i$
λ_{16}	$8.7393e+000-2.7479e+000i$	$-7.6231e-001+2.2334e+000i$	$-7.5242e+000+2.1707e+000i$
λ_{17}	$-6.1318e-001-7.7480e-001i$	$-1.2318e-001-9.5210e-002i$	$7.4930e-002+1.6507e-002i$
λ_{18}	$-6.1318e-001+7.7480e-001i$	$-1.2318e-001+9.5210e-002i$	$7.4930e-002-1.6507e-002i$

$\frac{\partial \lambda_k}{\partial K_j}$	K_7	K_8	K_9
λ_1	$1.8729e-031+6.7808e-031i$	$2.6003e-032+3.0586e-031i$	$-5.6066e-031+3.7531e-031i$
λ_2	$1.8729e-031-6.7808e-031i$	$2.6003e-032-3.0586e-031i$	$-5.6066e-031-3.7531e-031i$
λ_3	$3.9321e+000$	$5.7195e-001$	$-1.6067e+000$
λ_4	$-1.9316e-029-1.6266e-029i$	$5.9125e-031+9.1700e-030i$	$2.7883e-030+1.9146e-029i$
λ_5	$-1.9316e-029+1.6266e-029i$	$5.9125e-031-9.1700e-030i$	$2.7883e-030-1.9146e-029i$
λ_6	$-6.3687e-030$	$-1.0037e-029$	$-4.3210e-030$
λ_7	$-5.0082e-002-7.5889e-001i$	$-2.4084e-002-8.2818e-002i$	$6.9292e-002+2.1850e-001i$
λ_8	$-5.0082e-002+7.5889e-001i$	$-2.4084e-002+8.2818e-002i$	$6.9292e-002-2.1850e-001i$
λ_9	$1.1038e-029-2.6177e-030i$	$-2.7306e-029-8.9543e-030i$	$-8.7962e-029-2.8965e-029i$
λ_{10}	$1.1038e-029+2.6177e-030i$	$-2.7306e-029+8.9543e-030i$	$-8.7962e-029+2.8965e-029i$
λ_{11}	$1.4271e-028-1.0224e-028i$	$8.1962e-030+1.5008e-028i$	$8.7577e-029+2.1361e-028i$
λ_{12}	$1.4271e-028+1.0224e-028i$	$8.1962e-030-1.5008e-028i$	$8.7577e-029-2.1361e-028i$
λ_{13}	$5.0074e+000+3.2257e+000i$	$2.2931e-001+1.3228e+000i$	$8.7571e-001-4.5573e+000i$
λ_{14}	$5.0074e+000-3.2257e+000i$	$2.2931e-001-1.3228e+000i$	$8.7571e-001+4.5573e+000i$
λ_{15}	$-7.0192e+000-1.7073e+000i$	$-4.8007e-001-1.1498e+000i$	$-1.7007e-001+3.6292e+000i$
λ_{16}	$-7.0192e+000+1.7073e+000i$	$-4.8007e-001+1.1498e+000i$	$-1.7007e-001-3.6292e+000i$
λ_{17}	$9.5803e-002-3.4559e-002i$	$-1.1137e-002+8.0416e-002i$	$2.8447e-002+1.1735e-001i$
λ_{18}	$9.5803e-002+3.4559e-002i$	$-1.1137e-002-8.0416e-002i$	$2.8447e-002-1.1735e-001i$

with V_k the *kth* column of V and W_k the *kth* row of W. The partial derivatives with respect to *L* are derived in a manner analogous to that in equation (5.6.31), replacing *L* by *K*. The sensitivity matrix for *L* is shown in Table 5.6, the sensitivity matrix for *K* is shown in Table 5.7.

The maximum values of the sensitivities with respect to *L* and *K* are:

$$\max_{i,j} \Xi^L = \underbrace{6.4975 \cdot 10^{-15}}_{\approx 0} + 1.6527i \qquad \max_{i,j} \Xi^K = \Leftrightarrow 30.157. \tag{5.6.32}$$

This shows, that perturbations in the control matrix *K* have a bigger impact on the stability of the system than variations in the observer matrix *L*. This is also the explanation for the fact that the model reduction presented in this chapter does not yield a practically feasible result. The elimination of one or more states influences the stability of the composite system such a way that it becomes unstable.

5.6.4 Summary Observations Regarding Use of a Reduced Order Observer

Application of the balanced realization technique to obtain a reduced observer has been described. This procedure has been applied at the IEEE14 bus network. The model approximation of the reduced observer was a very good approximation of the input/output behavior of the full state observer. But even since the input/output behavior is very much the same, the feedback system constructed out of the physical system and the reduced observer of the IEEE14 bus network is unstable.

A reduction of the observer by the balanced realization to a stable composite system with a reduced number of states is in this case not possible.

The sensitivity analysis showed that the composite system consisting of the physical system and the state observer is quite sensitive due to parameter changes in the control matrix *K*. A model development sequence in which the control matrix K is determined first, then followed by model order reduction, appears not to be practically feasible because of this high sensitivity.

Project References and Bibliography

[1] Kumar, K. Ng, G. Sheble, "AGC Simulator for Price-Based Operation: Part I", IEEE Transactions on Power Systems, Vol. 12, No. 2, May 1997.

[2] Kumar, K. Ng, G. Sheble, "AGC Simulator for Price-Based Operation: Part II", IEEE Transactions on Power Systems, Vol. 12, No. 2, May 1997.

[3] I. Elgerd, C. Fosha, "Optimum Megawatt-Frequency control of multiarea Electric Energy Systems", IEEE Transactions on Power Apparatus & Systems, Vol. PAS-89, No. 4, April 1970.

[4] Fosha, O. I. Elgerd, "The Megawatt-Frequency control Problem: A New approach via Optimal control Theory", IEEE Transactions on Power Apparatus & Systems, Vol. PAS-89, No. 4, April 1970.

[5] I. Elgerd, *Electric Energy Systems Theory: An Introduction*, McGraw Hill, New York, 1982.

[6] A. Bergen, V. Vittal, *Power Systems Analysis, Prentice Hall*, New Jersey 2000.

[7] J. Nagrath, D. P. Kothari, *Power Systems Engineering*, Tata McGraw-Hill, 1994.

[8] Christie, A. Bose, "Load-Frequency control Issues in Power Systems Operations After Deregulation", IEEE Transactions on Power Systems, Vol 11, Aug 1996, pp. 1191-1200.

[9] Nobile, A. Bose, K. Tomsovic, "Bilateral Market for Load Following Ancillary Services", *Proc. PES Summer Power Meeting, Seattle*, WA, July 15-21, 2000.

[10] M. Ilic, F. Galiana, L. Fink (Editors), *Power Systems Restructuring: Engineering & Economics*, Kluwer Academic Publishers, Boston 1998.

[11] J. L. Willems, "Sensitivity Analysis of the Optimum Performance of Conventional Load-Frequency control", Transactions on Power Apparatus & Systems. Vol 93 No. 6, Sept/Oct., pp. 1287-1291.

[12] M. Ilic, F. Galiana, and L. Fink (Editors), *Power Systems Restructuring: Engineering & Economics.* Boston: Kluwer Academic Publishers, 1998.

[13] H. Dommel and W. F. Tinney, "Optimal power flow solutions," *IEEE Transactions on Power Apparatus and Systems*, vol. 87, no. 10, pp. 1866-1876, October 1968.

[14] R. Divi and H. K. Kesavan, "A shifted penalty function approach for optimal power flow," *IEEE Transactions on Systems, Man and Cybernetics*, vol. 4, no. 2, pp. 765-773, August 1982.

[15] M. R. Irving and M. J. H. Sterling, "Economic dispatch of active power with constraint relaxation," *IEE Proceedings*, Pt. C., vol. 130, no. 4, pp. 172-177, July 1983.

[16] S. S. Chen, C. N. Lu, and C. M. Ong, "Reactive and DC power dispatch to minimize transmission losses of an AC-DC power system," in *CIGRE Symposium on AC/DC Transmission*, Boston, USA, paper No. 400-05, September 1987.

[17] I. Megahed, N. Abou-Taleb, E. Iskandrani, and A. Moussa, "A modified method for solving the economic dispatch problem," *IEEE Transactions on Power Apparatus and Systems*, vol. 96, no. 1, pp. 124-133, January/February 1977.

[18] J. G. Waight, A. Bose, and G. B. Sheble, "Generation dispatch with reserve margin constraints using linear programming," *IEEE Transactions on Power Apparatus and Systems*, vol. 100, no. 1, pp. 252-258, January 1981.

[19] G. A. Maria and J. A. Findlay, "A Newton optimal power flow program for Ontario Hydro EMS," *IEEE Transactions on Power Systems*, vol. 2, no. 3, pp. 576-584, August 1987.

[20] R. C. Burchett and H. H. Happ, "Large scale security dispatching: An exact model," *IEEE Transactions on Power Apparatus and Systems*, vol. 102, no. 9, pp. 2995-2999, September 1983.

[21] J. Nanda, D. P. Kothari, and S. C. Srivastava, "New optimal power dispatch algorithm using fletcher's quadratic programming method," *IEE Proceedings*, vol. 136, Pt. C, no. 3, pp. 153-161, May 1989.

[22] R. C. Burchett, H. H. Happ, and D. R. Vierath, "Quadratically convergent optimal power flow," *IEEE Transactions on Power Apparatus and Systems*, vol. 103, no. 11, pp. 3267-3276, November 1984.

[23] L. S. Vargas, V. H. Quintana, and A. Vannelli, "A tutorial description of an interior point method and its application to security-constrained economic dispatch," *IEEE Transactions on Power Systems*, vol. 8, no. 3, pp. 1315-1324, August 1993.

[24] J. A. Momoh, S. X. Guo, E. C. Ogbuobiri, and R. Adapa, "Quadratic interior point method for solving power system optimization problems," *IEEE Transactions on Power Systems*, vol. 9, no. 3, pp. 1327-1336, August 1994.

[25] R. S. Fang and A. K. David, "Transmission congestion management in an electricity market," *IEEE Transactions on Power Systems*, vol. 14, no. 3, pp. 877-883, August 1999.

[26] H. Glatvitsch and F. Alvarado, "Management of multiple congested conditions in unbundled operation of a power system," *IEEE Transactions on Power Systems*, vol. 13, no. 3, pp. 1013-1019, August 1998.

[27] D. Shirmohammadi et al., "Transmission dispatch and congestion management in the emerging energy market structures," *IEEE Transactions on Power Systems*, vol. 13, no. 4, pp. 1466-1474, November 1998.

[28] K. Bhattacharya, M. H. J. Bollen, and J. E. Daalder, *Operation of Restructured Power Systems.* Boston: Kluwer Academic Publishers, 2000.

[29] GAMS Release 2.25, *A User's Guide*, Washington: GAMS Development Corporation, 2000.

[30] N. G. Hingorani, "Flexible AC transmission," *IEEE Spectrum*, April 1993, pp. 40-45.

[31] E. J. de Oliveri, J. W. M. Lima, and J. L. R. Pereira, "Flexible AC transmission system devices: Allocation and transmission pricing," *International Journal of Electric Power and Energy Systems.*, vol. 21, no. 2, pp. 111-118, February 1999.

[32] R. Rajaraman, F. Alvarado, A. Maniaci, R. Camfield, and S. Jalali, "Determination of location and amount of series compensation to increase power transfer capability," *IEEE Transactions on Power Systems*, vol. 13, no. 2, pp. 294-300, May 1998.

[33] G. Wu, A. Yokoyama, J. He, and Y. Yu, "Allocation and control of FACTS devices for steady-state stability enhancement of large-scale power system," in *Proceedings of IEEE International Conference on Power System Technology*, vol. 1, pp. 357-361, August 1998.

[34] N. Martins and L. T. G. Lima, "Determination of suitable locations for power system stabilizers and static VAr compensators for damping electromechanical oscillations in large scale power systems," *IEEE Transactions on Power Systems*, vol. 5, no. 4, pp 1455-1469, November 1990.

[35] S. N. Singh and A. K. David, "Congestion management by optimizing FACTS device location," in *Proceedings of International Conference on Electric Utility Deregulation and Restructuring, and Power Technologies 2000*, London, pp. 23-28, April 2000.

[36] N. Biggs, *Algebraic Graph Theory,* Cambridge University Press, 1993.

[37] B.L. Chamberlain, "Graph Partitioning Algorithms for Distributing Workloads of Parallel Computations," *University of Washington Technical Report UW-CSE-98-10-03*, October 1998.

[38] T.F. Chan and W.K. Szeto, "On the Optimality of the Median Cut Spectral Bisection Graph Partitioning Method," *SIAM J. Sci. Comput*., 18(3):943--948, 1997.

[39] J.H. Chow, *Time Scale Modeling of Dynamic Networks with Applications to Power Systems*, Springer-Verlag, Berlin, 1982.

[40] J.H. Chow, "New Algorithms for Slow Coherency Aggregation of Large Power Systems," *Systems and Control Theory for Power System*, Springer-Verlag, New York 1995.

[41] C.L. DeMarco, and J. Wasser, "A Generalized Eigenvalue Perturbation Approach to Coherency," pp. 605-610, *Proc. IEEE Conference on Control Applications*, Albany, NY, Sep. 28-29 1995.

[42] C.L. DeMarco, T. Yong, J. Meng, and F.L. Alvarado, "Efficient Computation of Higher Order Derivatives of Power Flow and Line Flow Quantities," *13th Power System Computation Conference*, 1998.

[43] M. Fiedler. “Algebraic connectivity of graphs,” *Czechoslovak Mathematical Journal*, 23(98): 298-305, 1973.

[44] M. Fiedler. “A property of eigenvectors of non-negative symmetric matrices and its application to graph theory,” *Czechoslovak Mathematical Journal*, 25(100): 619-633, 1975.

[45] S. Guattery, and G.L. Miller, “On the Performance of Spectral Graph Partitioning Methods,” *SODA: ACM-SIAM Symposium on Discrete Algorithms (A Conference on Theoretical and Experimental Analysis of Discrete Algorithms)*, 1995.

[46] K. Holmström, *TOMLAB v2.0 User's Guide*, http://www.tomlab.net

[47] M. Holzrichter, and S. Oliveira, “A Graph Based Method for Generating the Fiedler Vector of Irregular Problems”, *IPPS/SPDP Workshops*, 978-985, 1999.

[48] P.V. Kokotovic, B. Avramovic, J.H. Chow, and J.R. Winkelman, “Coherecy Based Decomposition and Aggregation,” *Automatica*, 18(1): 47-56, 1982.

[49] H.W. Kuhn, and A.W. Tucker, “Nonlinear Programming,” *Proc. Second Berkeley Symposium on Mathematical Statistics and Probability*, University of California Press, 481-492, 1961.

[50] S.S. Lamba, and R. Nath, “Coherency Identification by the Method of Weak Coupling,” *Electrical Power and Energy Systems*, 7(4): 233-242, 1985.

[51] *MATLAB User’s Guide*, The MathWorks, Inc., Natick, MA 1996.

[52] J. Meng, “Stability of Power Systems Coupled with Market Dynamics,” *Phd. Dissertation*, The University of Wisconsin – Madison, 2001.

[53] B. Mohar, “The Laplacian Spectrum of Graphs,” *Sixth International Conference on Theory and Applications of Graphs*, 1988.

[54] *Optimization Toolbox – For Use with MATLAB*, The MathWorks, Inc., Natick, MA 1999.

[55] M.A. Pai, *Energy Function Analysis for Power System Stability*, Kluwer Academic Publishers, Boston, 1989.

[56] A. Pothen, H.D. Simon, and K. Liou, "Partitioning sparse matrices with eigenvectors of graphs," *SIAM J. Matrix Anal. Appl.*, 11(3): 430-452, July 1990.

[57] G.N. Ramaswamy, G.C. Verghese, C. Vialas, and C.L. DeMarco, "Going Beyond Coherency: Synchrony as a Basis for Dynamic Equivalencing in Power System Models," *North American Power Symposium, Howard University, Washington D.C.*, 579-588, October 1993.

[58] G.N. Ramaswamy, G.C. Verghese, L. Rouco, C. Vialas, and C.L. DeMarco, "Synchrony, Aggregation, and Multi-Area Eigenanalysis," *IEEE Transactions on Power Systems*, 10(4): 1986-1993, November 1995.

[59] G.N. Ramaswamy, L. Rouco, O. Filiatre, G.C. Verghese, P. Panciatici, B. Lesieutre, and D. Peltier, "Synchronic Modal Equvalencing (SME) for Structure-Preserving Dynamic Equivalents," *IEEE Transactions on Power Systems*, 11(1): 19-29, February 1996.

[60] S. Roy, and B. Lesieutre, "Studies in Network Partitioning Based on Topological Structure," *North American Power Symposium, University of Waterloo, Canada*, 13: 1-8, October 2000.

[61] D.B. West, *Introduction to Graph Theory*, Prentice-Hall, Inc., NJ, 1996.

[62] A.J. Wood, and B.F. Wollenberg, *Power Generation Operation and Control*, John Wiley & Sons, Inc., NY, 1996.

[63] S.B. Yosof, G.J. Rogers, and R.T.H. Alden, "Slow coherency based network partitioning including loads," *IEEE Transaction on Power Systems*, 8(3) 1375-1381, August 1993.

[64] R.D. Zimmerman, and D. Gan, *MATPOWER version 2.0 User's Manual*, Power Systems Engineering Research Center, NY 1997.

[65] A.J. van der Schaft. *L2-Gain and Passivity Techniques in Nonlinear Control.* Springer-Verlag, London/Berlin/Heidelberg/New York, 1996.

[66] LN. Bronstein and Semendjajew, K.A. *Taschenbuch der Mathematik.* Verlag Harri Deutsch, Frankfurt (Main), 1983.

[67] C-T. Chen. *Linear System Theory and Design.* Holt, Rinehart and Winston, Inc., New York - Chicago - San Francisco - Philadelphia - Montreal - Toronto London - Sydney - Tokyo - Mexico City - Rio de Janeiro - Madrid, 1970.

[68] C.L. DeMarco, J.V. Sarlashkar, and F.L. Alvarado. The potential for malicious control in a competitive power systems environment. In *Proc. IEEE Conference on Control Applications,* pages 462-467, Dearborn, MI, Sept 18-20 1996; first appeared as University of Wisconsin-Madison, Department of Electrical and Computer Engineering memorandum ECE-95-10, August 1995.

[69] C.L. DeMarco. Design of Predatory Generation Control in Electrical Systems. Project note University of Wisconsin-Madison, Department of Electrical and Computere Engineering.

[70] C.A. Desoer. *Notes For A Second Course On Linear Systems.* D. Van Nostrand Company, New York Cincinnati Toronto London Melbourne, 1975.

[71] C.A. Desoer and M. Vidyasagar. *Feedback Systems: Input-Output Properties.* Academic Press, New York San Francisco London, 1975.

[72] T. Gorski. Malicious control of a power system through eigenvector placement. Master's thesis, University of Wisconsin-Madison, Department of Electrical and Computer Engineering, 1415 Engineering Drive; Madison, WI 53706, 1995.

[73] H.L. Trentelmann and J.C. Willems. *Essays on control: Perspectives in the theory and its application.* Birkhauser, Boston Basel Berlin, 1993.

[74] H.Nijmeijer, A.J. van der Schaft. *Nonlinear dynamical control systems.* Springer Verlag, New York Berlin Heidelberg London Paris Tokyo Hong Kong, 1990.

[75] A. Isidori. *Nonlinear Control Systems;* 2. *Edition.* Springer-Verlag, Berlin, 1989.

[76] J.C.Willems. *Stability theory of dynamical systems.* NELSON, London Nairobi Dar es Salaam Accra San Fernando (Trinidad), 1971.

[77] J.C.Willems. *The analysis of feedback systems.* The M.I.T. Press, Cambridge, Massachusetts, and London, England, 1971.

[78] J. Raisch. *Mehrgrossenregelung im Frequenzbereich.* Munchen Wien. Munchen Wien. 1994. R.Oldenburg Verlag

[79] G.J. Kirwin and Stephen E. Grodzinsky. *Basic Circuit Analysis.* Houghton Mifflin Company, Dallas Geneva, IL Hopewell,NJ Palo Alto London, 1980.

[80] J.M. Maciejowski. *Multivariable Feedback Design.* Addison-Wesley Publishing Company, Wokingham, England - Reading, Massachusetts - Menlo Park, California - New York - Don Mills, Ontario - Amsterdam - Bonn - Sydney - Singapore - Tokyo - Madrid - San Juan, 1989.

[81] B.C. Moore. Principal component analysis in linear systems: controllability, observability, and model reduction. *IEEE Transactions on Automatic Control,* AC(27):17-27, 1981.

[82] R.D. Strum and J.R Ward. *Electric Circuits and Networks.* Quantum Publishers, Inc., 257 Park Avenue South, New York, NY 10010, 1973.

[83] Thomas E. Fortmann and Darrell Williamson. Design of low-order observers for linear feedback control laws. *IEEE Transactions on Automatic Control. 1972.*

[84] T. Kailath. *Linear Systems.* Prentice-Hall, Englewood Cliffs, 1980.

[85] E.D. Gilles und U. Knopp. *Skriptum zur Vorlesung Regelungstechnik II; Analyse und Synthese von Regelsystemen* im *Zustandsraum.* Universitat Stuttgart, Institut fur Systemdynamik und Regelungstechnik (ISR), Stuttgart, Germany, 1993.

[86] U. Helmke and J. B. Moore. *Optimization and Dynamical Systems.* SpringerVerlag, London Berlin Heidelberg New York Paris Tokyo Hong Kong Barcelona Budapest, 1994.

[87] J.C. Willems. Dissipative Dynamical Systems Part I: General Theory. *Archive for Rational Mechanics and Analysis,* 45(5):321-351, 1972.

[88] J.C. Willems. Dissipative Dynamical Systems Part II: Linear Systems with Quadratic Supply Rates. *Archive for Rational Mechanics and Analysis, 45(5):352*393, 1972.

[89] J.C. Willems, Bittanti, Laub, A. *The Ricatti Equation.* Springer-Verlag, London/Berlin/Heidelberg/New York, 1980.

[90] I. Dobson, "Strong Resonance Effects in Normal Form Analysis and Subsynchronous Resonance," *Proc. Of International Workshop on Bulk Power System Dynamics and Control V,* Aug. 2001, Onomichi, JAPAN.

[91] I. Dobson, E. Barocio "Scaling of normal form analysis coefficients under coordinate change*," IEEE Trans. Power Systems,* vol. 19, no. 3, August 2004, pp. 1438-1444.

Appendix A

Definition of Passivity and Dissipativity

A.1 Introduction

This sections introduces the idea of passivity (and dissipativity). Furthermore the definition of passivity and other definitions and theorems related to the subject of passivity are introduced. The fundamental work in passivity theory is [1]. Most of the definitions used in the here presented work are quoted from [1].

A.2 Passivity

A.2.1 Motivation for Passivity

The passivity theorem and the small gain theorem play an important role in the study of closed-loop stability ([1],[8]). The small gain theorem is defined as following (from [1]).

Definition A.2.1 *Consider the closed-loop system $\Sigma^f_{G_1,G_2}$ given in Figure A.1 and let $q \in \{1, 2, \ldots, \infty\}$. Suppose that both G_1 and G_2 have finite L_q–gain given as $\gamma_q(G_1)$,*

respectively $\gamma(G_2)$. *Then the closed–loop system* $\Sigma^f_{G_1,G_2}$ *is* L_q*–stable if*

$$\gamma_q(G_1) \cdot \gamma(G_2) \leq 1. \tag{A.1}$$

Equation (A.1) is also known as the *small gain condition.* This means that two stable systems G_1 and G_2 which are interconnected as shown in Figure A.1, result in a stable closed–loop system provided, that the "loop–gain" is "small" (i.e. less than 1) [1]. The passivity theorem is primarily concerned with the L_2–space, while the small gain

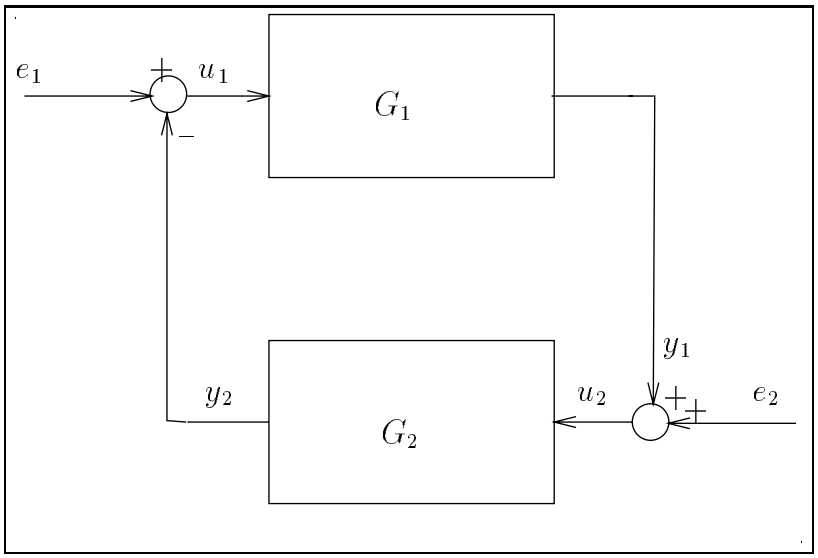

Figure A.1: Closed–loop configuration.

theorem can be formulated for all L_q–spaces.

An important definition which will be often used in this work, is the definition of the inner product of two functions in L_2.

Definition A.2.2 *The inner product of two vector fields is given by*

$$< f, g > = \int_0^\infty f(t)g(t)\mathrm{dt}, \qquad f, g \in L_2. \tag{A.2}$$

or more generally for the extended space L_{2e}^m

$$< f, g >_T = \int_0^\infty \sum_{i=1}^m f_i(t) g_i(t) \mathrm{dt} \tag{A.3}$$

with

$$f = (f_1, \ldots, f_m), \quad g = (g_1, \ldots, g_m) \in L_{2e}^m.$$

Definition A.2.3 *Let* $G : L_{2e}^m \to L_{2e}^m$. *Then* G *is* passive *if* $\exists$ *some constant* β *such that*

$$< G(u), u >_T \geq \beta \qquad \forall u \in L_{2e}^m, \quad \forall T \geq 0. \tag{A.4}$$

G *is* strictly input passive *if* $\exists\ \beta$ *and* $\exists\ \delta$ *such that*

$$< G(u), u >_T \geq \delta \|u_T\|_2^2 + \beta \qquad \forall u \in L_{2e}^m, \quad \forall T \geq 0. \tag{A.5}$$

and strictly output passive *if* $\exists\ \beta$ *and* $\exists\ \varepsilon > 0$ *such that*

$$< G(u), u >_T \geq \varepsilon \|(G(u))_T\|_2^2 + \beta \qquad \forall u \in L_{2e}^m, \quad \forall T \geq 0. \tag{A.6}$$

Next to these definitions of passivity an important role plays the theorem of interconnection of passive systems:

Theorem A.2.1 *(from [1]) Consider the closed–loop system* Σ_{G_1,G_2}^f *in Figure A.1. Assume that for any* e_1, e_2 *in* L_{2e}^m *there are solutions* u_1, u_2 *in* L_{2e}^m. *If* G_1 *and* G_2 *are passive, then* Σ_{G_1,G_2}^f *with the inputs* (e_1, e_2) *and outputs* (y_1, y_2) *is passive, and strictly output passive if both* G_1 *and* G_2 *are strictly output passive.*

The proof for this Theorem can be found in e.g. [1]. These definition can now be applied on an electrical circuit. Considering a One–port in Figure A.2. The power delivered to the one–port is

$$p(t) = v(t) i(t).$$

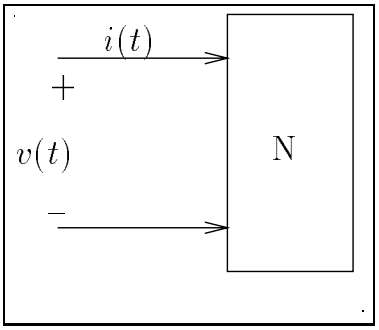

Figure A.2: One–port.

If $S(t_0)$ represents the energy stored in the system at the initial time t_0, then the one–port is passive if

$$S(t_0) + \int_{t_0}^{t} v(t)i(t)\mathrm{dt} \geq 0, \qquad \forall v, i; \quad \forall t \geq t_0. \tag{A.7}$$

The nonnegative function $S : X \to \mathbb{R}^+$ is called the *Storage function*. The inner product $w =< v, i >$ is called the *Supply rate* of the dynamical system Σ.

A.3 Dissipativity

Dissipative systems are of particular interest in engineering and physics. The assumption of dissipation, which distinguishes such systems from general dynamical systems yields to a fundamental additional constraint on their dynamic behavior. For example viscoelastic system are dissipative since viscous friction is responsible for an energy loss. Another group of typical dissipative systems are electrical networks in which a part of the (electrical) energy is dissipated by e.g. resistors in form of heat.

A main result in stability theory states that a feedback system which consists of a passive dynamical system in the forward and the backward loop is itself passive and thus stable (Theorem A.2.1). Furthermore the sum of the stored energy in the forward and backward loop is a Lyapunov function [1],[24].

Dissipativity is a generalization of the passivity concept. In the concept of Dissipativity a very important equation is the so called *dissipation inequality.*

Definition A.3.1 *(from [24]) A dynamical system Σ with the supply rate w defined on $U \times Y$ is said to be dissipative if there exists a nonnegative storage function $S : X \to \mathbb{R}^+$, such that for all $(t_1, t_0) \in \mathbb{R}_2^+$, $\mathrm{x}_0 \in \mathrm{X}$, $u \in U$, and $y \in Y$,*

$$S(x_0) + \int_{t_0}^{t_1} w(t)\mathrm{dt} \geq S(x_1). \tag{A.8}$$

Equation (A.8) is the so called *dissipation inequality.*

The approach taken within equation (A.8) is based on physical considerations. The classification of a system as dissipative implies that a storage function exists. A central question in this analysis isthe nature of such a storage function ([25]). Therefore the quantity named *available storage* is introduced. Available storage is the maximum amount of storage which may at any time have been extracted from the dynamical system. The available storage is a generalization of "available energy".

Definition A.3.2 *(from [24]) The available storage S_a, of a dynamical system Σ with supply rate $w(t)$ is the function X into $\mathbb{R}^{\mathrm{e}}$ defined by*

$$S_x(x) = \sup_{x \to t_1} \Leftrightarrow \int_0^{t_1} w(t)\mathrm{dt}$$

where the notation "$x \to$" denotes the supremum over all motions starting in state x at time 0 and where the supremum is taken over all $u \in U$.

The available storage is an important function in determining whether or not a dynamical system is dissipative. This shows the theorem of [24] below:

Theorem A.3.1 *(from [24]) The available storage S_a is finite for all $x \in X$ if and only if Σ is dissipative. Moreover, $0 \leq S_a \leq S$ for dissipative dynamical systems and S_a is itself a possible storage function.*

For proof see [24].

In this work the concepts of passivity and Dissipativity are only applied to a class of linear systems. The systems are described by the linear, time-invariant vector differential equation

$$\begin{aligned} \dot{x} &= Ax + Bu \\ y &= Cx + Du. \end{aligned} \tag{FDLS}$$

The matrices A, B, C, D of the dynamical system (FDLS)[1] are constant matrices of appropriate dimensions with $x \in \mathbb{R}^{\mathrm{n}}$, $\mathrm{u} \in \mathbb{R}^{\mathrm{m}}$, $\mathrm{y} \in \mathbb{R}^{\mathrm{p}}$. The essential model assumptions in considering this model are linearity, time invariance and a finite number of degrees of freedom. The transfer function of the dynamical system (FDLS) is given by

$$G(s) = D + C(sI \Leftrightarrow A)^{-1}B \tag{A.9}$$

A.3.1 Frequency–Domain Condition for Dissipativeness

In this section, the conditions for Dissipativeness are established in case of frequency–domain. The following theorem for Dissipativeness is given by [24]:

Theorem A.3.2 *(from [24]) Assume that the dynamical system (FDLS) is minimal. Then it is dissipative with respect to the supply rate $w =< u, y >$ if and only if the transfer function (A.9) is positive real, i.e. $G(\sigma + j\omega) + G(\sigma \Leftrightarrow j\omega) \geq 0$ for all $\sigma \geq 0$ and $\omega \in \mathbb{R}$, $\sigma + j\omega \neq \lambda(A)$, or equivalently*

- *(i) $\Re(\lambda(A)) \leq 0$*
- *(ii) $G(j\omega) + G^T(\Leftrightarrow j\omega) \geq 0$ for all $\omega \in \mathbb{R}$, $j\omega \neq \lambda(A)$*
- *(iii) the eigenvalues of A with $\Re(\lambda(A))$ are non–repeated and the residue matrix at those eigenvalues, $\lim_{s \to s_0}(s \Leftrightarrow s_0)C(sI \Leftrightarrow A)^{-1}B$, is Hermitian and nonnegative definite.*

[1] FDLS stands for **F**inite **D**imensional time invariant **L**inear **S**ystems.

This theorem gives a necessary and sufficient condition for there to exist a storage function

$$S : \mathbb{R}^{\mathrm{N}} \to \mathbb{R}^{+}, \qquad \forall \mathrm{x}_0 \in \mathbb{R}^{\mathrm{n}},\ \mathrm{u} \in \mathrm{U}$$

such that the dissipation inequality (A.8) and the solution of the dynamical system (FDLS)

$$\begin{aligned} x_1 &= e^{A(t_1-t_0)}x_0 + \int_{t_0}^{t_1} e^{A(t_1-t_0)}Bu(\tau)d\tau \\ y(t) &= Ce^{A(t-t_0)}x_0 + \int_{t_0}^{t_1} Ce^{A(t-t_0)}Bu(\tau)d\tau + Du(t) \end{aligned}$$

is satisfied. Adopting the normalization convention $\min_{x\in\mathbf{R}^{\mathrm{n}}} S(x) = S(0) = 0$ defines the available storage, S_a, and the required supply, S_r, by

$$S_a(x_0) = \Leftrightarrow \lim_{t_1\to\infty} \inf_{u\in U} \int_0^{t_1} < u(t), y(t) > \mathrm{dt} \tag{A.10}$$

$$S_r(x_0) = \lim_{t_{-1}\to-\infty} \inf_{u\in U} \int_{t_{-1}}^{0} < u(t), y(t) > \mathrm{dt} \tag{A.11}$$

subject to the dynamical system (FDLS) and the initial and terminal conditions $x(t_{-1}) = 0$ and $x(0) = x_0$. As shown in Section 4 in [25], the assumption of invertibility of the matrix $D + D^T$ reduces the evaluation of the available storage and the required supply to a standard optimal control problem which may be solved by considering appropriate solutions of the algebraic Ricatti equation

$$KA + A^TK + (KB \Leftrightarrow C^T)(D + D^T)^{-1}(B^TK \Leftrightarrow C) = 0. \tag{ARE}$$

This yields to Lemma 2 in [25]

Lemma A.3.1 *(from [25]) Assume that the system (FDLS) is minimal and that* $D + D^T$ *is invertible. Then the algebraic Ricatti equation (ARE) has a real symmetric nonnegative definite solution if and only if the system (FDLS) is dissipative with respect to the supply rate* w*. If this is the case, then there exists precisely one real symmetric solution* K^-*, having the additional property* $\Re(\lambda(A^-)) \leq 0$*, where* $A^- = A + B(D + D^T)^{-1}(B^T K^T \Leftrightarrow C)$*, and precisely one real symmetric solution,* K^+*, having the additional property* $\Re(\lambda(A^+)) \geq 0$*. Moreover* $0 < K^- \leq K^+$ *and every real symmetric solution satisfies the inequality* $K^- \leq K \leq K^+$*. Thus, all real symmetric solutions are positive definite. The strict inequalities* $G(j\omega) + G^T(\Leftrightarrow j\omega) > 0$ *for* $\omega \in \mathbb{R}$*,* $\Re(\lambda(A^-)) < 0$*,* $\Re(\lambda(A^+)) > 0$*, and* $K^- < K^+$ *all hold simultaneously.*

Lemma (A.3.1) only holds if the transition matrix D ($D + D^T$ respectively) is non-singular. Since the transition matrix in the later used example of Appendix B is singular, the case D singular has to be considered. In the case when $D + D^T$ ceases to be nonsingular, the simplest way of apporaching this problem is introducing

$$\hat{D} = \lim_{\varepsilon \to 0}(D + \frac{\varepsilon}{2}).$$

Then K_ε^- and K_ε^+ are defined by the Ricatti equation

$$K_\varepsilon A + A^T K_\varepsilon + (K_\varepsilon B \Leftrightarrow C^T)(D + D^T + \varepsilon I)^{-1}(B^T K_\varepsilon \Leftrightarrow C) = 0$$

and $K^- = \lim_{\varepsilon \to 0} K_\varepsilon^-$ and $K^+ = \lim_{\varepsilon \to 0} K_\varepsilon^+$, assumed these limits exist. Using Theorem 2 in [25] defines the available storage as

$$S_a(x) = \frac{1}{2} < x, K^-, x >$$

and the required supply as

$$S_r(x) = \frac{1}{2} < x, K^+, x > .$$

A.3.2 State–Space Definition for Dissipassivity with Quadratic Storage Functions

In this section, the definition in the state–space for dissipativity will be given. This will be done considering the storage function being a quadratic function of the state x

$$\frac{1}{2} < x, Qx > . \tag{A.12}$$

The quadratic storage functions are of a particular interest. Quadratic storage functions reflect internal linearity. Moreover, in these applications it is a good assumption for postulating that dissipative systems exhibit their linear input/output behaviors. Assuming a storage function given by equation (A.12) with $Q = Q^T$ symmetric[2]. This leads to Theorem 3 in [25]

Theorem A.3.3 *(from [25]) Assume that the dynamical system (FDLS) is minimal. Then the matrix inequalitites*

$$\left[\begin{array}{c|c} A^TQ + QA & QB \Leftrightarrow C^T \\ \hline B^TQ \Leftrightarrow C & \Leftrightarrow (D + D^T) \end{array}\right] \leq 0 \qquad \textit{(MIE)}$$

and

$$Q = Q^T \geq 0$$

have a solution if and only if (FDLS) is dissipative with respect to the supply rate $w =< u, y >$*. Moreover, the function* $\frac{1}{2} < x, Qx >$ *defines a quadratic storage function if and only if it satisfies these inequalitites. Consequently,* K^- *and* K^+ *satisfy these inequalities and every solution satisfies* $0 < K^- \leq Q \leq K^+$.

This theorem is proofed in [25]. Theorem A.3.3 states that the external linearity given by the input/output map from u to y is linear implies the existence of a model which is linear in its state variables ([25]). This model (i.e. a model like (FDLS))

[2] As given in [25] this entails no loss of generality.

has, additionally, a storage function which is quadratic in the state variables. The matrix inequality (MIE) will have a very important role later in this work. Usually the storage function of a dynamical system (FDLS) is unknown. Interpreting (MIE) as an optimization problem yields a solution for the matrix Q and also for the storage function.

Appendix B

The IEEE14 bus network

In this appendix the IEEE14 bus network is described. It is the example system, which is exmined in this work. The One–Line diagram of the IEEE14 bus network is shown in Figure B.1. The IEEE14 bus network consist out of 14 buses - 5 generator buses

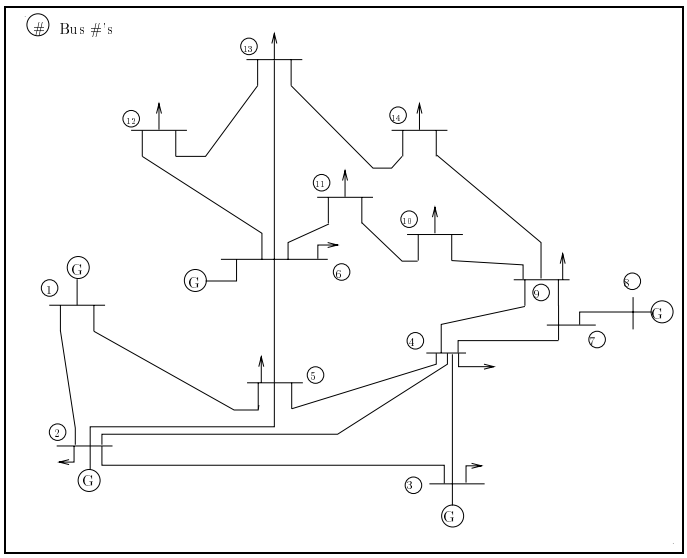

Figure B.1: One–Line Diagram if IEEE14 Bus System.

and 9 load buses. No infinite bus is employed. The generators are the input of the system. They appear at the buses 1, 2, 3, 6, and 8. The state variables for the IEEE14

bus network are given by

$$x = \begin{bmatrix} \omega_{G_1} \\ \vdots \\ \omega_{G_5} \\ \delta_{G_1} \\ \vdots \\ \delta_{G_5} \end{bmatrix}$$

with

$$x \in \mathbb{R}^1 0.$$

B.1 Values of the matrices in Chapter 2

The parameters for the matrices in (2.32) are:

$$A_1 = \begin{bmatrix} 20.7258 & \Leftrightarrow 18.6820 & \Leftrightarrow 0.6050 & \Leftrightarrow 0.9496 & \Leftrightarrow 0.4893 \\ \Leftrightarrow 18.5920 & 29.0662 & \Leftrightarrow 6.9031 & \Leftrightarrow 2.0330 & \Leftrightarrow 1.5382 \\ \Leftrightarrow 0.6134 & \Leftrightarrow 6.9883 & 9.3404 & \Leftrightarrow 0.8235 & \Leftrightarrow 0.9151 \\ \Leftrightarrow 0.9747 & \Leftrightarrow 2.0402 & \Leftrightarrow 0.8159 & 5.4931 & \Leftrightarrow 1.6623 \\ \Leftrightarrow 0.4546 & \Leftrightarrow 1.4054 & \Leftrightarrow 0.8049 & \Leftrightarrow 1.9029 & 4.5678 \end{bmatrix}$$

$$D_{damp} = \begin{bmatrix} \Leftrightarrow 0.0250 & 0 & 0 & 0 & 0 \\ 0 & \Leftrightarrow 0.0250 & 0 & 0 & 0 \\ 0 & 0 & \Leftrightarrow 0.0250 & 0 & 0 \\ 0 & 0 & 0 & \Leftrightarrow 0.0250 & 0 \\ 0 & 0 & 0 & 0 & \Leftrightarrow 0.0250 \end{bmatrix}$$

$$M = \begin{bmatrix} 1 & 0 & 0 & 0 & 0 \\ 0 & 1 & 0 & 0 & 0 \\ 0 & 0 & 1 & 0 & 0 \\ 0 & 0 & 0 & 1 & 0 \\ 0 & 0 & 0 & 0 & 1 \end{bmatrix}$$

The impulse response of the IEEE14 bus network is shown in Figure B.2. The output is the frequency of each generator The parameters are remotely realistic. The system

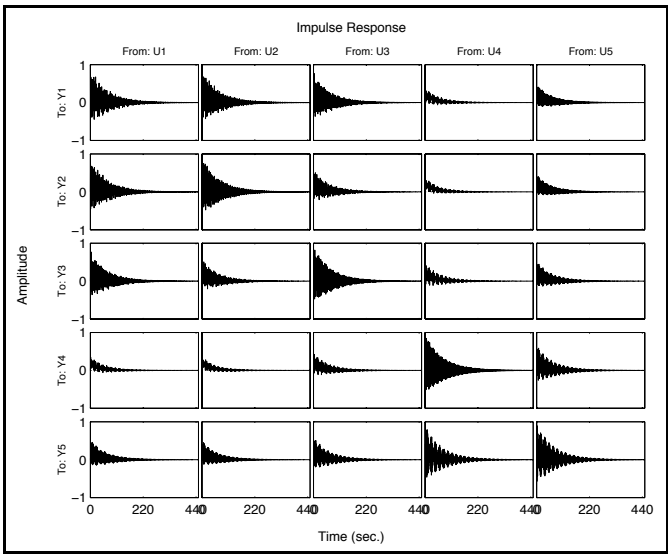

Figure B.2: Impulse Response of the IEEE14 bus network

itself is oscillating, but stable. After a time period of around 5 minutes the oscillations are minimal.

Appendix C

Results of the computations

C.1 RCL-circuit (2)

In this section are the results for the matrices and eigenvalues of section 3.5.1 presented.

```
Matrix =

   1.0e+12 *

  -8.00386624000123   0.00409997075120  -0.00000000100005
   0.00409997075120  -4.00000004956985   0.00000000200000
  -0.00000000100005   0.00000000200000                   0

>> Q

Q =

   1.0e+06 *

   4.00193312000062  -0.00004901881560
  -0.00004901881560   1.99999997576611
```

```
>> eig(Matrix)

ans =

   1.0e+12 *

  -8.00387043837893
  -3.99999585119215
                  0

>> eig(Q)

ans =

   1.0e+06 *

   4.00193312120088
   1.99999997456585

>>
```

C.2 Computations of the IEEE14 system

The matrix $\mathbf{F}(Q)$ is given by

```
>> Matrix

Matrix =

  Columns 1 through 4

   0.03829944526169   0.01428164745350   0.00125112852038   0.00095151080345
```

```
 0.01428164745350   0.00187424399521  -0.02050716099347  -0.01267601197351
 0.00125112852038  -0.02050716099347   0.01428719178563   0.01473287400916
 0.00095151080345  -0.01267601197351   0.01473287400916   0.02642994198135
-0.01376431319851  -0.01870210353131  -0.01156701545458  -0.01551958266321
 0.01260312008653   0.04614701998119   0.04041963961384   0.00873306933092
-0.03786806044551   0.02238455250778  -0.04134321067840   0.01927729242297
 0.02305119376116   0.00006875489713  -0.01219464025044   0.03891826525178
 0.00870319412232   0.01774607435337   0.07506867612215  -0.07558200291193
-0.00615029146618   0.02884733773639  -0.01873731644598  -0.00687473491210
 0.02884733773639  -0.02652950398050  -0.00251471077382  -0.00573697247536
-0.01873731644598  -0.00251471077382   0.01248053249546  -0.01192892388904
-0.00687473491210  -0.00573697247536  -0.01192892388904   0.01076654806802
 0.00558993257288  -0.00250653232736  -0.00138621750030   0.01601457080971

Columns 5 through 8

-0.01376431319851   0.01260312008653  -0.03786806044551   0.02305119376116
-0.01870210353131   0.04614701998119   0.02238455250778   0.00006875489713
-0.01156701545458   0.04041963961384  -0.04134321067840  -0.01219464025044
-0.01551958266321   0.00873306933092   0.01927729242297   0.03891826525178
-0.00755554693344   0.08167958149563  -0.02571963163530   0.11283493896294
 0.08167958149563  -0.41465288836028   0.28217668578933  -0.07512677143076
-0.02571963163530   0.28217668578933  -0.39615051316242  -0.03204783875014
 0.11283493896294  -0.07512677143076  -0.03204783875014  -0.17294479040840
 0.00204665676296  -0.05698995329771   0.09036926154043   0.08043516483051
 0.00558993257288   0.00318817372462  -0.01796768557272  -0.00154901494187
-0.00250653232736   0.00580447447770  -0.01384405464165   0.00603824445843
-0.00138621750030  -0.00668825345955   0.01220599855529  -0.00076361297094
 0.01601457080971  -0.01877162615669   0.01537719774120   0.01826880373102
-0.02182235412860  -0.00934655745386   0.01220469542386   0.00194671675660

Columns 9 through 12
```

```
 0.00870319412232  -0.00615029146618   0.02884733773639  -0.01873731644598
 0.01774607435337   0.02884733773639  -0.02652950398050  -0.00251471077382
 0.07506867612215  -0.01873731644598  -0.00251471077382   0.01248053249546
-0.07558200291193  -0.00687473491210  -0.00573697247536  -0.01192892388904
 0.00204665676296   0.00558993257288  -0.00250653232736  -0.00138621750030
-0.05698995329771   0.00318817372462   0.00580447447770  -0.00668825345955
 0.09036926154043  -0.01796768557272  -0.01384405464165   0.01220599855529
 0.08043516483051  -0.00154901494187   0.00603824445843  -0.00076361297094
-0.14772032388263  -0.00779044438354  -0.00938061140072  -0.02378557305345
-0.00779044438354                  0                  0                  0
-0.00938061140072                  0                  0                  0
-0.02378557305345                  0                  0                  0
-0.01730615371172                  0                  0                  0
 0.00111311476264                  0                  0                  0

Columns 13 through 14

-0.00687473491210   0.00558993257288
-0.00573697247536  -0.00250653232736
-0.01192892388904  -0.00138621750030
 0.01076654806802   0.01601457080971
 0.01601457080971  -0.02182235412860
-0.01877162615669  -0.00934655745386
 0.01537719774120   0.01220469542386
 0.01826880373102   0.00194671675660
-0.01730615371172   0.00111311476264
                 0                  0
                 0                  0
                 0                  0
                 0                  0
                 0                  0
```

```
>>
```

The matrix Q is given by

```
>> Q

Q =

  Columns 1 through 4

   0.99384970853382   0.02884733773639  -0.01873731644598  -0.00687473491210
   0.02884733773639   0.97347049601950  -0.00251471077382  -0.00573697247536
  -0.01873731644598  -0.00251471077382   1.01248053249546  -0.01192892388904
  -0.00687473491210  -0.00573697247536  -0.01192892388904   1.01076654806802
   0.00558993257288  -0.00250653232736  -0.00138621750030   0.01601457080971
   0.00318817372462   0.00580447447770  -0.00668825345955  -0.01877162615669
  -0.01796768557272  -0.01384405464165   0.01220599855529   0.01537719774120
  -0.00154901494187   0.00603824445843  -0.00076361297094   0.01826880373102
  -0.00779044438354  -0.00938061140072  -0.02378557305345  -0.01730615371172

  Columns 5 through 8

   0.00558993257288   0.00318817372462  -0.01796768557272  -0.00154901494187
  -0.00250653232736   0.00580447447770  -0.01384405464165   0.00603824445843
  -0.00138621750030  -0.00668825345955   0.01220599855529  -0.00076361297094
   0.01601457080971  -0.01877162615669   0.01537719774120   0.01826880373102
   0.97817764587140  -0.00934655745386   0.01220469542386   0.00194671675660
  -0.00934655745386  27.83517779529352  -6.73192574545204  -2.03098565584388
   0.01220469542386  -6.73192574545204   9.45518859730408  -0.88592678673031
   0.00194671675660  -2.03098565584388  -0.88592678673031   5.58879885852053
   0.00111311476264  -1.49340777873621  -0.82508323356601  -1.65959194077680
```

```
  Column 9

  -0.00779044438354
  -0.00938061140072
  -0.02378557305345
  -0.01730615371172
   0.00111311476264
  -1.49340777873621
  -0.82508323356601
  -1.65959194077680
   4.44593694573725

>>
```

Appendix D

Optimization via Gershkorim–rings

D.0.1 Restated problem

Since the eigenvalue computation wasunique in MATLAB one decided to approximate the eigenvalues of a system by its Gershkorim–rings around the diagonal elements of the system matrix. The eigenvalues have to ly within these rings as shown in figure D.1. The new optimization problem is finally described by

$$z = \min\left(\max\left(\mathbf{F}_{ii} + \sum_{k\neq i} |F_{ik}|\right)\right), \qquad F_{ii} \leq 0 \tag{D.1}$$

$$G_1(Q) := \Leftrightarrow\min\left(Q_{ii} \Leftrightarrow \sum_{k\neq i} |Q_{ik})\right| \tag{D.2}$$

$$G_2(Q) := Q \Leftrightarrow Q^T \leq 0 \tag{D.3}$$

$$G_3(Q) := \Leftrightarrow G_2(Q). \tag{D.4}$$

$$\tag{D.5}$$

Unfortunately this approach again does not yield to a unique result. As a matter of fact, the results got worse in all the cases. This justifies the assumption, that the restriction on the constraints were too strong.

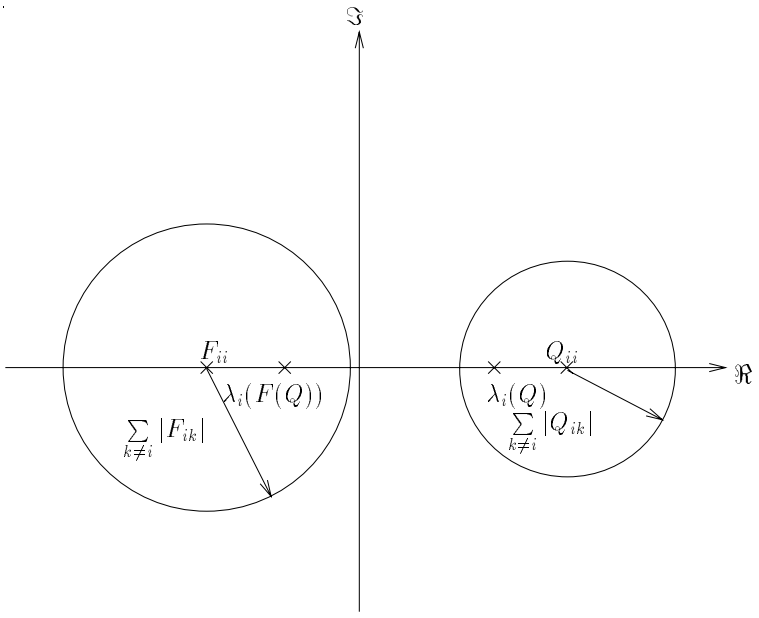

Figure D.1: Gershkorim–rings for the matrices $\mathbf{F}(Q)$ and Q.

Appendix E

Reduction of the modified IEEE14 bus network

In Chapter 6 it has been shown, that a composite system consisting of the the IEEE14 bus network in its present form given by equation (2.32) and a state observer cannot be reduced in the number of its states by applying the balanced realization and eleminating states.

In this section the IEEE14 bus network is modified such that the model reduction via the approach of the balanced realization can be applied.

E.1 Design of a reduced PS-OS system

As we derived earlier in this work the dynamics of the IEEE14 bus network is given by the matrix

$$A = \left[\begin{array}{c|c} \Leftrightarrow D_{damp} & A_1 \\ \hline 0 & I \end{array}\right]. \tag{E.1}$$

Based on this matrix A the eigenvalues of the observer matrix are chosen such that

$$\lambda(A \Leftrightarrow LC) \approx 2 \cdot \lambda(A).$$

To be able to reduce the size of the system consisting of the physical system and the observer system (PS-OS) the damping of the system has to be increased. The new damping matrix is determined by multiplying the old damping matrix by a constant α

$$D_{damp}^{new} = \alpha \cdot D_{damp}. \tag{E.2}$$

The new damping matrix yields a new system matrix A^*

$$A^* = \left[\begin{array}{c|c} \Leftrightarrow D^{new} & A_1 \\ \hline 0 & I \end{array}\right]. \tag{E.3}$$

Based on this system matrix A^* a LQR control can be designed which yields a control matrix of the form $K(A^*)$. As seen before one of the eigenvalues of the closed loop $\lambda(A^* \Leftrightarrow BK)$ is far away from the other eigenvalues of the system. As before, this eigenvalue is replaced by an eigenvalue which is approximatively $\Leftrightarrow 10$. So the new, destinated closed loop eigenvalues are

$$\lambda^*(A^* \Leftrightarrow BK^*) = \left[\begin{array}{c} \Leftrightarrow 10 \\ \lambda_2(A^* \Leftrightarrow BK) \\ \vdots \\ \lambda_9(A^* \Leftrightarrow BK) \end{array}\right] \approx \left[\begin{array}{c} \Leftrightarrow 9.9376 \\ \Leftrightarrow 2.8335 + 5.1587i \\ \Leftrightarrow 2.8335 \Leftrightarrow 5.1587i \\ \Leftrightarrow 2.5497 + 1.4740i \\ \Leftrightarrow 2.5497 \Leftrightarrow 1.4740i \\ \Leftrightarrow 2.5378 + 1.7521i \\ \Leftrightarrow 2.5378 \Leftrightarrow 1.7521i \\ \Leftrightarrow 1.9073 + 1.8648i \\ \Leftrightarrow 1.9073 \Leftrightarrow 1.8648i \end{array}\right] \tag{E.4}$$

Since the eigenvalues of the closed loop system, and the matrices A^*, B are known the matrix K^* can be determined. The dynamics of the new system (PS)-(OS) is given by

$$\left[\begin{array}{c} \dot{x} \\ \dot{\hat{x}} \end{array}\right] = \left[\begin{array}{cc} A^* & \Leftrightarrow BK^* \\ LC & A^* \Leftrightarrow BK^* \Leftrightarrow LC \end{array}\right] \left[\begin{array}{c} x \\ \hat{x} \end{array}\right] \tag{E.5}$$

or in terms of a balanced realization

$$\left[\begin{array}{c} \dot{x} \\ \dot{\hat{x}}^b \end{array}\right] = \left[\begin{array}{cc} A^* & \Leftrightarrow Bk \\ LC & a \Leftrightarrow bk \end{array}\right] \left[\begin{array}{c} x \\ \hat{x}^b \end{array}\right]. \tag{E.6}$$

In the balanced realization (E.6) up to 3 modes (mode $\#'s\ 7, 8, 9$) can be removed without loss of stability. By removing mode #6 the system becomes unstable.

The step response of the (reduced) system is shown in Figure E.1. That the by 3 modes reduced system still provides sufficiently enough precision, is shown by the Figure E.2 The error between $\xi_{10} \Leftrightarrow \xi_{10}^{b}$ is minimal and stable, even in the largest reduction. This is shown in Figure E.2. The bode diagram of the by 3 states reduced model and the full system is shown in Figure E.3. As can be seen in Figure E.3 the I/O properties of the reduced and the full system are almost identical. This yields the conclusion, that the model reduction by eleminating states of the balanced realization is realizable. But this approach is not applicable on such poorly damped systems as the in this work considered IEEE14 bus network.

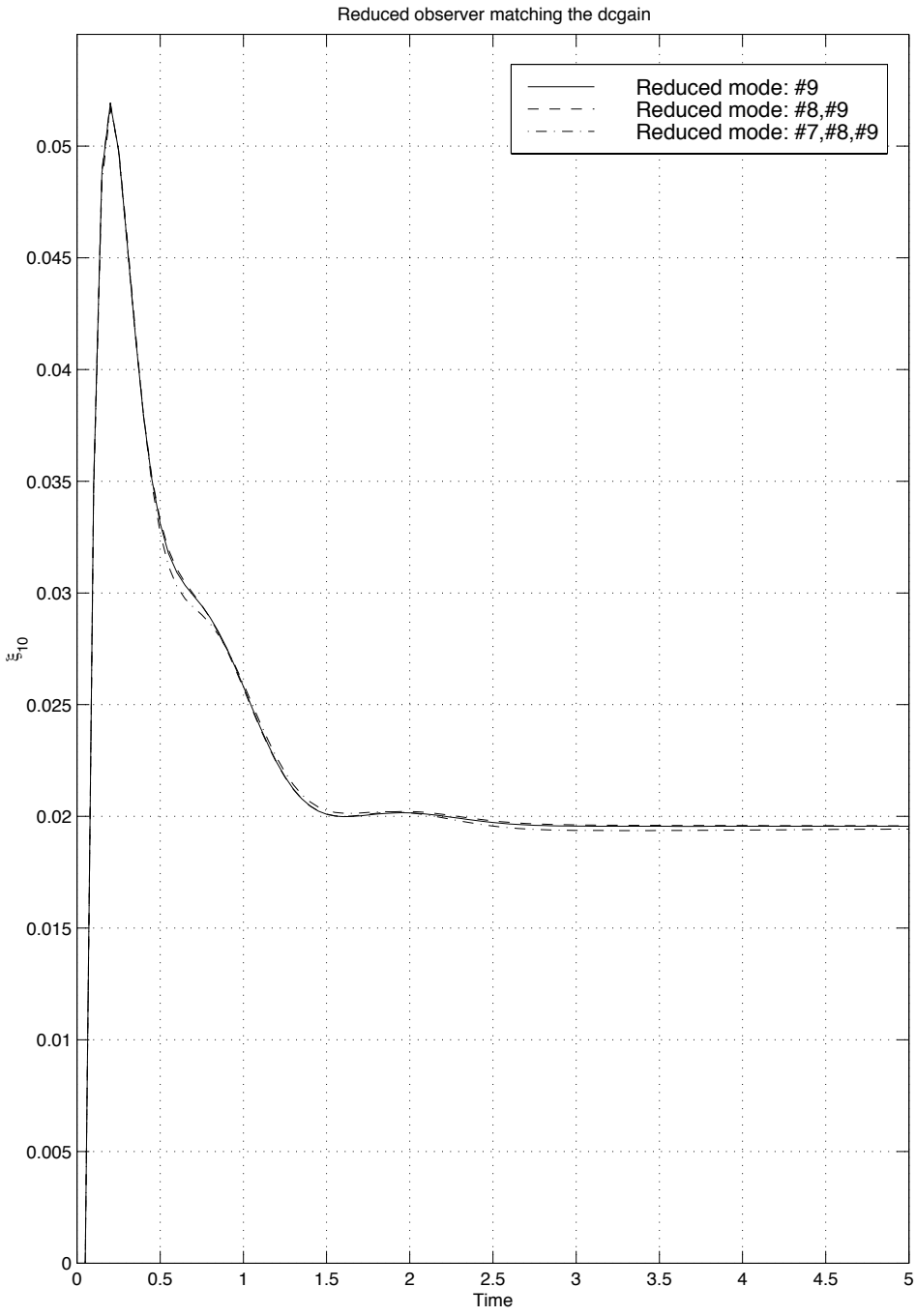

Figure E.1: Step Responses of the Dynamical System (E.6) with different stages of reductions. The state $\xi_{10} = \hat{x}^b$ is shown.

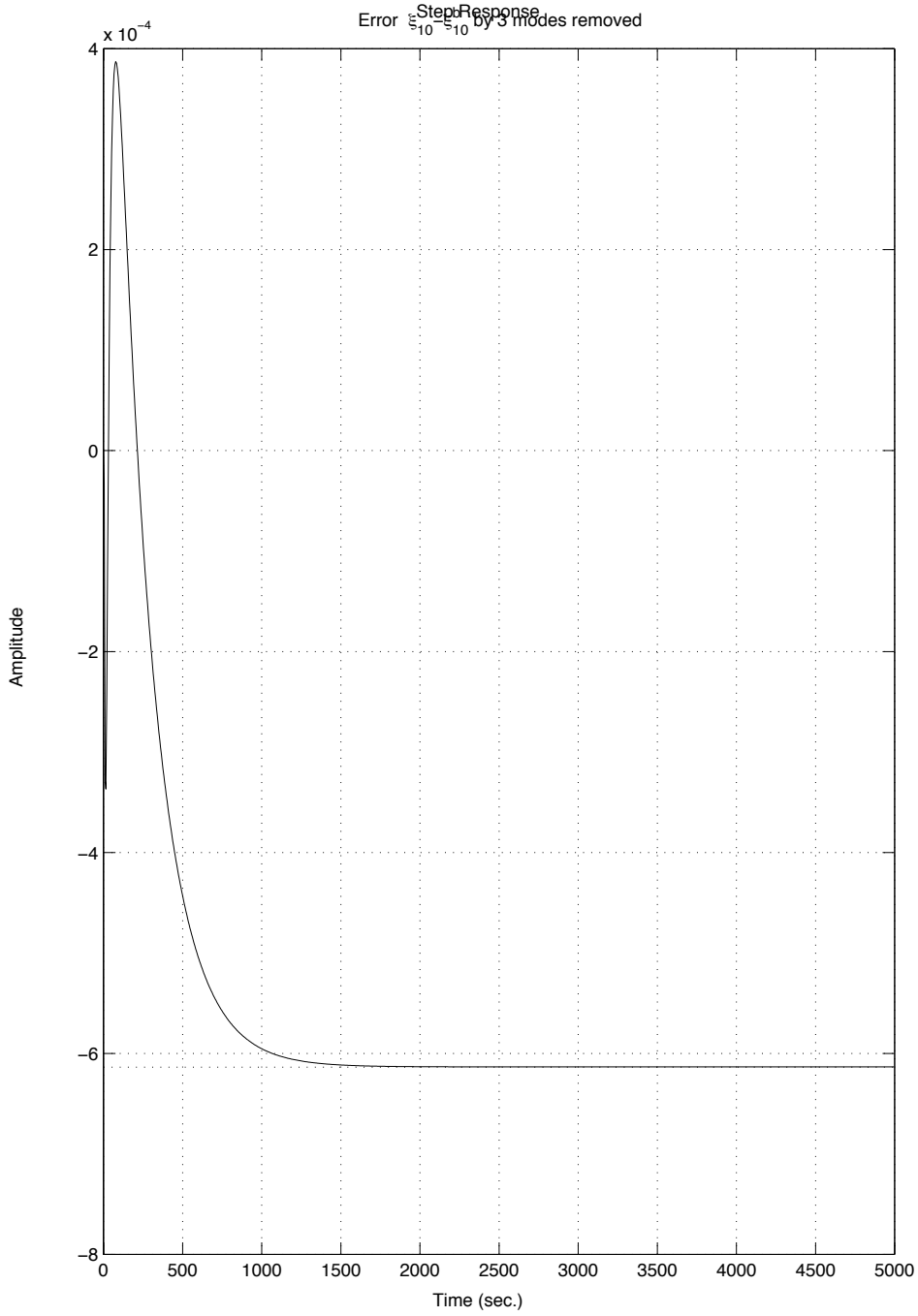

Figure E.2: Error $\xi_{10} \Leftrightarrow \xi_{10}^b$ by 3 removed modes. The occuring error is sufficiently small.

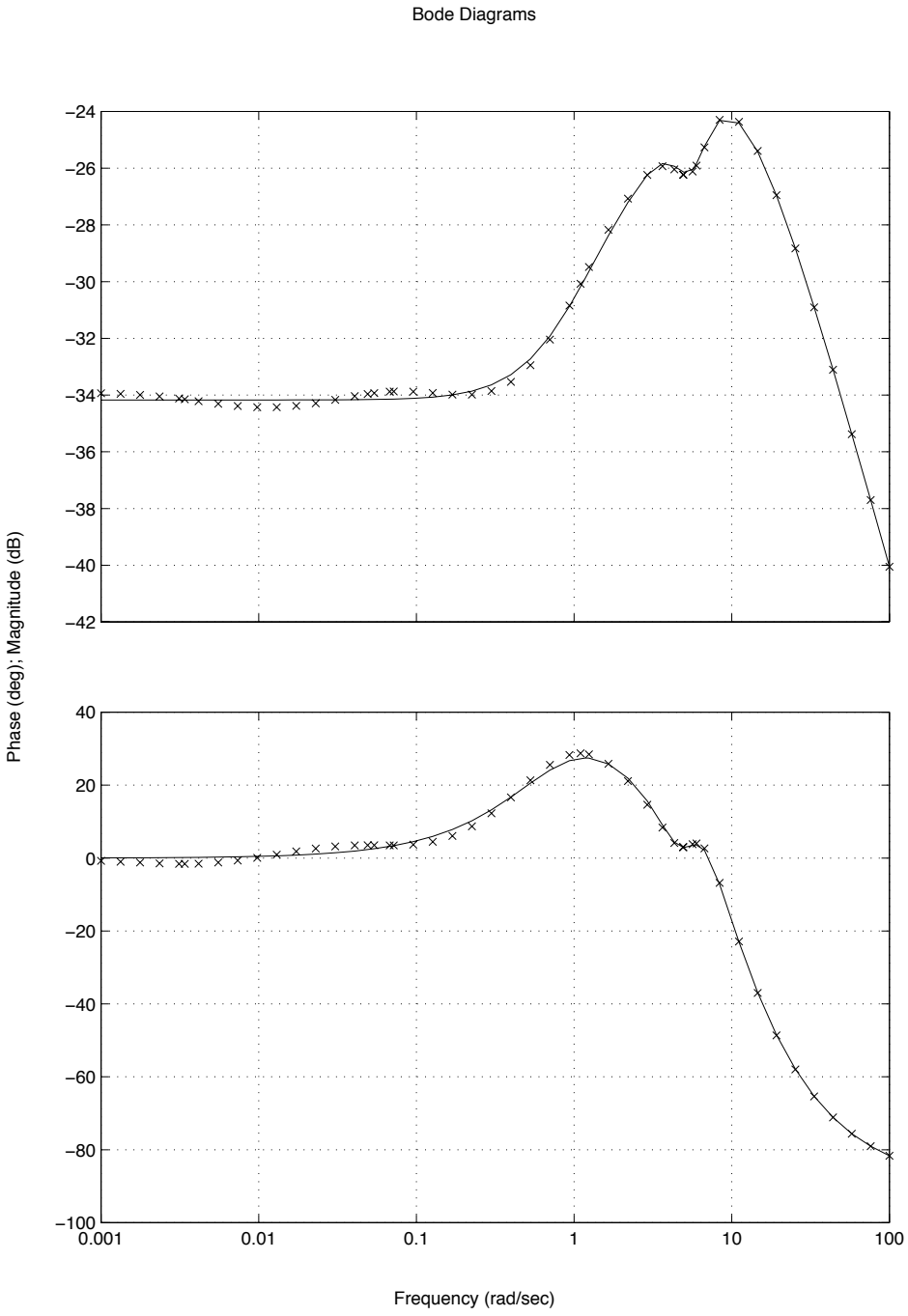

Figure E.3: Bode Diagram of the full system and the by 3 states reduced system.

Appendix F

Documentation of the MATLAB Network Partitioning Code

Tests the RSB and arbitrarily network partitioning algorithms were performed within MATLAB environment [51]. There are 3 main functions and 17 sub-functions in our complete packages briefly described below:

Three main functions:

- RSB.m

separate a given test network into a predetermined parts using the recursive spectral bisection method (RSB)

- Arbitrary.m

prepare OPF data of the arbitrarily cut sub-networks

- find_cost.m

perform the OPF for each individual decomposed sub-network and find each sub-network power generating cost.

17 sub-functions:

- add_Sline.m

add the equivalent fixed demands or injections at both ends of the cutset-links with the values equal the corresponding active/reactive OPF line flows

- bus_ordering.m

re-number all the sub-network bus indices to have "1" as its first index and the rest are 1 incrementally ordered

- bus_reordering.m

re-number bus indices of part 1 and part 2 back to the original numbers

- construct_jacobian.m

construct the network OPF Jacobian

- constructA_Y.m

construct the network incidence matrix, primitive admittance matrix, and admittance matrix

- dataout.m

  display the network bus voltage and line flow OPF results on the monitor screen

- edge_separators.m

  find the indices of the edge separators between the 2 sub-networks

- form_subnetwork.m

  extract the sub-network data from the MATPOWER unreduced network format

- initial_condition.m

  create the state initial values for the *fmincon* command

- network_data.m

prepare the necessary network data to be used during our MATLAB computation

- obj_function.m

  the objective function for the optimization solver *fmincon*

- pf_constraint.m

setup both equality and inequality OPF constraints for the optimization solver *fmincon*

- pflowjac.m

form the matrix of partial derivative of complex power absorbed by the network at each bus with respect to bus voltage angle and voltage magnitude

- pfmiss.m

  form the vector of complex power mismatch at each bus

- separation.m

  perform the optimization routine for the RSB network partitioning

- UPDATESep.m

update the "Sep" matrix (the matrix that contains indices of each sub-network)

- UPDATESm.m

update the matrix "Sm" (the matrix that contains the number of generators and the Fiedler value in each sub-network) and determine the part that is separated in the next step

The main functions RSB.m, Arbitrary.m and find_cost.m are called from the MATLAB command line. Their related sub-functions, then, are automatically invoked. Before the find_cost.m main function is used, either RSB.m (for the RSB partitioning method) or Arbitrary.m (for the arbitrarily partitioning method) are required to be executed.

All above functions and sub-functions are described in more detail in the next section. Note that the data entering in the sub-functions can be either unreduced network data or the sub-network data; the output data are in the same format.

Function “RSB.m”

The function RSB.m is the main program to separate a given test network into the predetermined parts using the recursive spectral bisection method (RSB). This function can be called from the MATLAB command line.

From the study-network data in the MATPOWER format, first, the code extracts all the necessary information (i.e., number of lines and buses, and indices and numbers of all types of buses). The resulting information is used to initialize some values before the code enters the main partitioning loop. The partitioning loop runs until the desired number of parts is met or until every part has only one generator left. To facilitate the construction of the incidence and network admittance matrices, in each iteration, the code needs to re-number all the sub-network bus indices. The function “separation.m” is invoked in each iteration to process the optimization problem. The resulting bus indices of the 2 parts are re-numbered back to the original indices using the function “bus_reordering.m”. The function “add_Sline.m” adds the equivalent fixed demands or injections to both ends of the cutset-links. The number of generator buses in each part is determined.

The code chooses to partition in the next sub-network that has the smaller Fiedler value, and that has more than 1 generator left.

When the main loops end, the monitor screen displays the generating cost, the indices of all separated parts, and the program executed time. The resulting bus data (after adding the equivalent fixed demands or injections), and the indices of all decomposed sub-networks are stored in M-files. These 2 matrices are used as the input data for the function “find_cost.m” to test our method’s performance to check the total cost of power generation and the bus active nodal prices.

{RSB.m - MATLAB code follows:}

```
% Clear the monitor screen.
clc
% Clear all previous variables.
clear all

% Input a predetermined number of desired parts.
parts=input('How many parts to be separated? ')

% Check the total computational time (also see toc command below).
tic

% Choose to test between 9 or 30 bus cases.
  [baseMVA, Bus, gen, Line, area, gencost] = case9;
% [baseMVA, Bus, gen, Line, area, gencost] = case30;

% Prepare necessary data to be processed in the first loop.
[nbus,nline,slacklist,genlist,loadlist,slackUgen,all_list,...
      nslack,ngen,nload,L_sUg]=network_data(Bus,Line);

% Initialize data for the first loop computation.

% First loop set all buses together in one part.
Sep(:,1)=[1:nbus]';
% Number of generators.
Sm(1,1)=ngen;
% Smallest eigenvalue.
Sm(2,1)=0;
% Current part number that is separated.
seppt=1;
% # of buses within current part.
busseppt=nbus;
% Set flag : cost of generating power from each RSB loop.
index_cost=1;

% RSB loop starts here.
while(size(Sep,2)<parts)&(size(Sep,2)<L_sUg)

% Check the buses in the current part.
nonzero_index=length(find(Sep(1:busseppt,seppt)));
bus_list=Sep(1:nonzero_index,seppt);

% Prepare data for the next loop of network partitioning.
[Bus_sub,Line_sub,gen_sub,gencost_sub,nbus_sub,nline_sub]=...
   form_subnetwork(Bus,Line,bus_list,gen,gencost);

% Re-number the network bus indices making them no shift in numbering.
% Otherwise, later loops are not converge.
[Bus_sub_or,Line_sub_or,gen_sub_or,gencost_sub_or] = ...
   bus_ordering(Bus_sub,Line_sub,nbus_sub,nline_sub,gen_sub,gencost_sub);

% Use the re-numbered data for our computations.
[nbus_sub,nline_sub,slacklist_sub_or,genlist_sub_or,loadlist_sub_or,...
   slackUgen_sub_or,all_list_sub_or,nslack_sub,ngen_sub,nload_sub,...
   L_sUg_sub]=network_data(Bus_sub_or,Line_sub_or);

% Construct the network incident matrix and admittance matrix.
[A_sub_or,Yp_sub_or,Ybus_sub_or] = ...
   constructA_Y(nbus_sub,nline_sub,Bus_sub_or,Line_sub_or);
```

```
% The fmincon function require users to set the initial data.
[vbus_sub_or,Pg_sub_or,del_sub_or,vmag_sub_or,x0_sub_or] = ...
    initial_condition(Bus_sub_or,baseMVA,nbus_sub,...
    slacklist_sub_or,genlist_sub_or,slackUgen_sub_or,gen);

% The RSB partitioning is occurred within this sub-function.
[fval,part_1_or,part_2_or,second_smallest_eig,...
    sline,sline_oddindex,sline_evenindex] = separation...
   (del_sub_or,x0_sub_or,Ybus_sub_or,Yp_sub_or,A_sub_or,...
   Bus_sub_or,Line_sub_or,baseMVA,slacklist_sub_or,...
   genlist_sub_or,loadlist_sub_or,nbus_sub,gencost_sub_or,...
   gen_sub_or,slackUgen_sub_or,L_sUg_sub,Bus_sub,Line_sub);

% The value of the objective cost function.
gen_cost(index_cost)=fval;
% Increase flag when complete the first loop.
index_cost=index_cost+1;

% Re-number bus indices in part_1, and part_2 back to the original number.
[part_1,part_2]=bus_reordering(Bus_sub,Bus_sub_or,part_1_or,part_2_or);

% This function locates the cutsets that link between the 2 parts.
[edge_cuts,cut_index] = ...
    edge_separators(part_1,part_2,Bus_sub,Line_sub,nbus_sub,nline_sub)

% This function adds the fixed equivalent demands or injections
%    to the cutset links.
[Bus] = ...
    add_Sline(edge_cuts,cut_index,Bus,sline,...
    sline_oddindex,sline_evenindex,baseMVA)

% Update the Sep matrix.
Sep=UPDATESep(Sep,seppt,part_1,part_2);

% Check # of gen in part1.
gen1=length(find(ismember(part_1,gen(:,1))));

% Check # of gen in part2.
gen2=length(find(ismember(part_2,gen(:,1))));

% Use the same functions as above
%   to determine the Fiedler value for part 1
sm1=0;
if gen1 >1,
[Bus_sub,Line_sub,gen_sub,gencost_sub,nbus_sub,nline_sub]=...
   form_subnetwork(Bus,Line,part_1,gen,gencost);

[Bus_sub_or,Line_sub_or,gen_sub_or,gencost_sub_or] = ...
   bus_ordering(Bus_sub,Line_sub,nbus_sub,nline_sub,...
   gen_sub,gencost_sub);

[nbus_sub,nline_sub,slacklist_sub_or,genlist_sub_or,...
        loadlist_sub_or,slackUgen_sub_or,all_list_sub_or,...
        nslack_sub,ngen_sub,nload_sub,L_sUg_sub]=...
        network_data(Bus_sub_or,Line_sub_or);

[A_sub_or,Yp_sub_or,Ybus_sub_or] = ...
   constructA_Y(nbus_sub,nline_sub,Bus_sub_or,Line_sub_or);
```

```
[vbus_sub_or,Pg_sub_or,del_sub_or,vmag_sub_or,x0_sub_or] = ...
    initial_condition(Bus_sub_or,baseMVA,nbus_sub,...
    slacklist_sub_or,genlist_sub_or,slackUgen_sub_or,gen);

[fval,part_1_1_or,part_1_2_or,second_smallest_eig1,...
    sline1,sline_oddindex1,sline_evenindex1] = separation...
   (del_sub_or,x0_sub_or,Ybus_sub_or,Yp_sub_or,A_sub_or,...
   Bus_sub_or,Line_sub_or,baseMVA,slacklist_sub_or,...
   genlist_sub_or,loadlist_sub_or,nbus_sub,gencost_sub_or,...
   gen_sub_or,slackUgen_sub_or,L_sUg_sub,Bus_sub,Line_sub);

% re-number bus indices of part_1, and part_2 back to the original number

[part_1_1,part_1_2]=bus_reordering(Bus_sub,Bus_sub_or,...
    part_1_1_or,part_1_2_or)


sm1=second_smallest_eig1;

end,

% Use the same functions as above
%   to determine the Fiedler value for part 2
sm2=0;
if gen2 >1,
[Bus_sub,Line_sub,gen_sub,gencost_sub,nbus_sub,nline_sub]=...
   form_subnetwork(Bus,Line,part_2,gen,gencost);

% Re-number network bus indices making them no shift in numbering
[Bus_sub_or,Line_sub_or,gen_sub_or,gencost_sub_or] = ...
   bus_ordering(Bus_sub,Line_sub,nbus_sub,nline_sub,gen_sub,gencost_sub);

[nbus_sub,nline_sub,slacklist_sub_or,genlist_sub_or,loadlist_sub_or,...
   slackUgen_sub_or,all_list_sub_or,nslack_sub,ngen_sub,nload_sub,...
   L_sUg_sub]=network_data(Bus_sub_or,Line_sub_or);

[A_sub_or,Yp_sub_or,Ybus_sub_or] = ...
   constructA_Y(nbus_sub,nline_sub,Bus_sub_or,Line_sub_or);

[vbus_sub_or,Pg_sub_or,del_sub_or,vmag_sub_or,x0_sub_or] =...
    initial_condition(Bus_sub_or,baseMVA,nbus_sub,slacklist_sub_or,...
    genlist_sub_or,slackUgen_sub_or,gen);

[fval,part_2_1_or,part_2_2_or,second_smallest_eig2,...
    sline2,sline_oddindex2,sline_evenindex2] = separation...
   (del_sub_or,x0_sub_or,Ybus_sub_or,Yp_sub_or,A_sub_or,Bus_sub_or,...
   Line_sub_or,baseMVA,slacklist_sub_or,genlist_sub_or,loadlist_sub_or,...
   nbus_sub,gencost_sub_or,gen_sub_or,slackUgen_sub_or,L_sUg_sub,...
   Bus_sub,Line_sub);

% Re-number bus indices of part_1, and part_2 back to the original number
[part_2_1,part_2_2]=bus_reordering(Bus_sub,Bus_sub_or,...
    part_2_1_or,part_2_2_or)


sm2=second_smallest_eig2;

end,

% From the Fiedler values of sub-networks 1 and 2 above,
```

```
%   determine which part (part_1, or part_2)
%   that is separated next.
[Sm,seppt]=UPDATESm(Sm,seppt,gen1,gen2,sm1,sm2);

% # of buses that is separated next
busseppt=length(find(Sep(:,seppt)));

end,

% Show the resulting OPF cost of generation, and the partitioning matrix
gen_cost
Sep

% Save these matrices in M-files formats to proceed next
%   in "find_cost.m" to test the sub-network performances.
save Bus_9buses_RSB_3parts.m -ascii Bus
save Sep_9buses_RSB_3parts.m -ascii Sep

% Stop Timing
toc
```

Function "Arbitrary.m"

The function Arbitrary.m is the main program to prepare OPF data of the arbitrarily cut sub-networks to use further in the “find_cost.m” main program. First, the code finds the OPF optimal operating point of the unreduced IEEE30-bus network. The optimization approach used here is similar to that of “RSB.m” and find_cost.m. The OPF solutions are displayed on the screen. Next, the code creates matrices/vectors “cut_index”(the location of the cutset indices in the "Line" data), “edge_cuts”(the bus indices linking between cutsets), “part_a”, “part_b”, and “part_c”(bus indices of part a, b, and c). These matrices/vectors are the inputs to the function “add_Sline.m” to add the equivalent fixed demands or injections at both ends of the cutset-links with the values equal the corresponding active/reactive OPF line flows. The bus index matrix of the arbitrarily partitioning network and the “Bus” data after added equivalent fixed demands/injections are stored in M-files. As in RSB.m, these 2 matrices are used in the function “find_cost.m” to test this arbitrarily cut partitioning performance.

{Arbitrary.m - MATLAB code follows:}

```
% Clear the monitor screen.
clc
% Clear all previous variables.
clear all

% Check the total computational time (also see toc command below).
tic

% Obtain the IEEE 30-bus data.
[baseMVA, Bus, gen, Line, area, gencost] = case30;

% Prepare data to be processed in the first loop
[nbus,nline,slacklist,genlist,loadlist,slackUgen,all_list,...
      nslack,ngen,nload,L_sUg]=network_data(Bus,Line);

% Construct the network incidence and admittance matrices.
[A,Yp,Ybus] = constructA_Y(nbus,nline,Bus,Line);

[vbus,Pg,del,vmag,x0] = initial_condition...
   (Bus,baseMVA,nbus,slacklist,genlist,slackUgen,gen);

% The lower and upper boundaries for the state solution.
lower_bound=[gen(:,10)./baseMVA;
            -2*pi.*ones(length(del),1);
            Bus(:,13)];

upper_bound=[gen(:,9)./baseMVA;
             2*pi.*ones(length(del),1);
             Bus(:,12)];

% These "options" are the operation modes of the "fmincon".
% See the Optimization toolbox 2.0 manual for more details.
options = optimset('Display','iter','Diagnostics','on');

% The optimization routine begins here.
[x,fval,exitflag,output,lamda]=fmincon('obj_function',x0,[],[],[],[],...
    lower_bound,upper_bound,'pf_constraint',options,Ybus,Yp,A,Bus,...
    Line,baseMVA,slacklist,genlist,loadlist,nbus,gencost,gen);

% These values are the Lagrange multipliers:
% for the lower boundaries of the state variable
lamda_lower=lamda.lower
% for the upper boundaries of the state variable
lamda_upper=lamda.upper
% for the linear inequality constraints
lamda_ineqlin=lamda.ineqlin
% for the linear equality constraints
lamda_eqlin=lamda.eqlin
% for the nonlinear inequality constraints
lamda_ineqnonlin=lamda.ineqnonlin
% for the nonlinear equality constraints
lamda_eqnonlin=lamda.eqnonlin

% Extract the desired values from the resulting "x".
% Bus voltage angles.
del_final=x(L_sUg+1:L_sUg+nbus);
% Bus voltage magnitudes.
vmag_final=x(L_sUg+nbus+1:L_sUg+(2.*nbus));
```

```
% Complex bus voltages.
vbus_final = vmag_final.*exp(j*del_final);

% Display the OPF solutions on the screen.
OPF_Pg=baseMVA.*x(1:size(gen,1));

% Show the power flow solution results.
nline = size(Line,1);
fromto = Line(:,1:2);

% “cline” here is the sline in the "dataout" function
% It is the complex line flow at two ends (from bus to network)
% “Bus”, “Line” here actually are “Bus_sub_or”, “Line_sub_or”
[sline,sline_oddindex,sline_evenindex] = ...
    dataout(vbus_final,A,Yp,fromto,nline,Bus,Line);

% The OPF cost of power generation.
gen_cost=fval

% 3 parts
% The location of the cutset indices in the "Line" data
cut_index=[...
    5;
    6;
    7;
    10;
    12;
    14;
    27;
    28;
    18;
    20;
    22;
    41]

% The bus indices linking between the cutsets.
edge_cuts=[...
    2 5;
    2 6;
    4 6;
    6 8;
    6 10;
    9 10;
    10 21;
    10 22;
    12 15;
    14 15;
    15 18;
    6 28]

% Bus indices of part a
part_a=[...
    1
    2
    3
    4
    10
    12
    13
    14
```

```
    16
    17
    18
    19
    20];

% Bus indices of part b
part_b=[...
    5
    6
    7
    9
    11];

% Bus indices of part c
part_c=[...
     8
    15
    21
    22
    23
    24
    25
    26
    27
    28
    29
    30];

% Check for the accuracy.
% All bus indices.
all_parts=union(part_a,union(part_b,part_c));
% # of all buses.
total_bus=length(all_parts)

% Delete cutset branches and replace them with the equivalent fixed demands or
%   injections at both ends.
[Bus_added] = ...

add_Sline(edge_cuts,cut_index,Bus,sline,sline_oddindex,sline_evenindex,baseMVA)

% Initialize data
Sep=zeros(30,3);
% Assign the first row of "Sep" as bus indices of part a
Sep(1:length(part_a),1)=sort(part_a);
% Assign the second row of "Sep" as bus indices of part b
Sep(1:length(part_b),2)=sort(part_b);
% Assign the third row of "Sep" as bus indices of part c
Sep(1:length(part_c),3)=sort(part_c);
% Display the "Sep" matrix on the screen to check for the correctness again.
Sep

% Save these matrices to proceed next to find the generating cost
%   of sub-networks.
save Bus_30buses_arbitary_3parts2pi.m -ascii Bus_added
save Sep_30buses_arbitary_3parts2pi.m -ascii Sep

% Stop timing.
toc
```

Function “find_cost.m”

The function find_cost.m is the main program to perform the OPF for each decomposed sub-network and to calculate the sub-network power generating cost. This function can be called from the MATLAB command line.

Two input data matrices (Sep_xxx_xxx and Bus_xxx_xxx) created by “RSB.m” or “Arbitary.m” main functions are loaded at the beginning of the program. Users can choose to perform the test either in the unreduced or decomposed sub-network by commenting/un-commenting some specific command lines. All generator bus indices and the equivalent fixed demands or injections at both ends of each cutset-link are displayed on the screen. Next, the code perturbs the active load demand in each load bus as a percentage deviating from its base case. During each iteration, the main-loop of the find_cost.m extracts each column of the matrix Sep (sub-network bus indices), and performs each sub-network OPF computation. The code uses the similar approach as the approach in “RSB.m” and “Arbitary.m”, so the sub-functions to be called from this main-loop are quite the same. The code, then, re-numbers all the sub-network bus indices by the function “bus_ordering.m” to make the construction of the sub-network admittance and incidence matrices possible. Sub-network data and the state solution lower/upper boundaries are set before each optimization loop begins. The resulting Lagrange multipliers and OPF solutions are displayed on the monitor screen. The complex line flows are determined by the function “dataout.m”. Once the main program iterates until all the sub-network state solutions are solved, the generating active powers and their corresponding costs are displayed on the monitor screen.

{find_cost.m - MATLAB code follows:}

```
% Clear the monitor screen.
clc
% Clear all the values of the previous variables.
clear all

% Check the total computational time (also see toc command below).
tic

% Choose between IEEE 9 or 30-bus case.
[baseMVA, Bus, gen, Line, area, gencost] = case9;
%[baseMVA, Bus, gen, Line, area, gencost] = case30;

% For 9 buses:
% These 2 matrices are obtained after the function "RSB.m" or "Arbitary.m"
load Sep_9bus_arbitary1.m;
load Bus_9bus_arbitary1.m;

% If users want to find the gen cost of the original unreduced network,
%   uncomment here.
% Sep=Bus(:,1)
Sep=Sep_9bus_arbitary1;

% Check which buses are the generator buses
Gen_location=Sep;
Gen_location=ismember(Gen_location(:,:),gen(:,1))

% Display the equivalent fixed demands or injections
%   at both ends of the cutsets on the screen.
temp_fixed_S_added=Bus_9bus_arbitary1(:,3:4)-Bus(:,3:4);
fixed_S_added=[Bus(:,1) temp_fixed_S_added]
Padded=temp_fixed_S_added(:,1)
Qadded=temp_fixed_S_added(:,2)

% The code perturbs load demand at each load bus here.
%   Change to the desired percentage value. (70 percent in this case)
temp=0.70.*Bus(:,3);
Bus=Bus_9bus_arbitary1;
Bus(:,3)=Bus(:,3)+temp;

% Initialize data.
temp_Pg=[];

for index_sub_number=1:size(Sep,2);

% # of buses in the current part.
n_sub=length(find(Sep(:,index_sub_number)));
```

```
% Bus indices of the current part.
bus_sub_list=Sep(1:n_sub,index_sub_number);

% Create new data from the current part.
[Bus_sub,Line_sub,gen_sub,gencost_sub,nbus_sub,nline_sub]=...
   form_subnetwork(Bus,Line,bus_sub_list,gen,gencost);

% Re-number the index number of the sub-network
%   making them no shift in numbering.
[Bus_sub_or,Line_sub_or,gen_sub_or,gencost_sub_or] = ...
   bus_ordering(Bus_sub,Line_sub,nbus_sub,nline_sub,gen_sub,gencost_sub);

% Extract some desired data from the previous sub-network information.
% Note : "nbus_sub" and "n_sub" is the same.
[nbus_sub,nline_sub,slacklist_sub_or,genlist_sub_or,loadlist_sub_or,...
   slackUgen_sub_or,all_list_sub_or,nslack_sub,ngen_sub,nload_sub,...
   L_sUg_sub]=network_data(Bus_sub_or,Line_sub_or);

% Construct sub-network incidence matrix and admittance matrix.
[A_sub_or,Yp_sub_or,Ybus_sub_or] = ...
   constructA_Y(nbus_sub,nline_sub,Bus_sub_or,Line_sub_or);

% Function "fmincon" need the initial condition.
[vbus_sub_or,Pg_sub_or,del_sub_or,vmag_sub_or,x0_sub_or] = ...
    initial_condition(Bus_sub_or,baseMVA,nbus_sub,slacklist_sub_or,...
    genlist_sub_or,slackUgen_sub_or,gen);


% The lower and upper boundaries for the state solution.
lower_bound=[gen_sub_or(:,10)./baseMVA;
            -inf.*ones(length(del_sub_or),1);
            Bus_sub_or(:,13)];

upper_bound=[gen_sub_or(:,9)./baseMVA;
             inf.*ones(length(del_sub_or),1);
             Bus_sub_or(:,12)];

% These "options" are operatation modes of the "fmincon".
% See the Optimization toolbox 2.0 manual for more details.
options = optimset('Display','iter','Diagnostics','on');

% The optimization begins here.
[x,fval,exitflag,output,lamda]=fmincon('objective',x0_sub_or,...
    [],[],[],[],lower_bound,upper_bound,'constraints',options,...
    Ybus_sub_or,Yp_sub_or,A_sub_or,Bus_sub_or,Line_sub_or,...
    baseMVA,slacklist_sub_or,genlist_sub_or,loadlist_sub_or,...
    nbus_sub,gencost_sub_or,gen_sub_or);


% These values are the Lagrange multipliers:
% for the lower boundaries of the state variables
lamda_lower=lamda.lower
% for the upper boundaries of the state variables
lamda_upper=lamda.upper
% for the linear inequality constraints
lamda_ineqlin=lamda.ineqlin
% for the linear equality constraints
lamda_eqlin=lamda.eqlin
% for the nonlinear inequality constraints
```

```
lamda_ineqnonlin=lamda.ineqnonlin
% for the nonlinear equality constraints
lamda_eqnonlin=lamda.eqnonlin


% Extract the desired values from the resulting "x".
% Bus voltage angles.
del_sub_final=x(L_sUg_sub+1:L_sUg_sub+nbus_sub);
% Bus voltage magnitudes.
vmag_sub_final=x(L_sUg_sub+nbus_sub+1:L_sUg_sub+(2.*nbus_sub));
% Complex bus voltages.
vbus_sub_final = vmag_sub_final.*exp(j*del_sub_final);


% Display OPF solution on the screen.
OPF_Pg_sub=baseMVA.*x(1:size(gen_sub_or,1))
temp_Pg(length(temp_Pg)+1:length(temp_Pg)+size(gen_sub_or,1))=OPF_Pg_sub;
OPF_v_sub=x((size(gen_sub_or,1)+1):size(x,1));
OPF_solution_sub=[OPF_Pg_sub;
                  OPF_v_sub]

% Show the power flow solution results
nline_sub = size(Line_sub,1);
actual_fromto = Line_sub(:,1:2);
% cline here is the sline in the "dataout" function
% complex line flow at two ends (from bus to network)
% Bus, Line here actually are Bus_sub_or,Line_sub_or
[sline,sline_oddindex,sline_evenindex] = ...
    dataout(vbus_sub_final,A_sub_or,Yp_sub_or,actual_fromto,...
    nline_sub,Bus_sub_or,Line_sub_or,Bus_sub,Line_sub);

% The current sub-network generating cost.
cost_sub(index_sub_number)=fval;

% Go to the next part.
end,

% Display OPF solution on the screen.
% All generating powers.
Pgen=temp_Pg.'
% The generating costs from all parts.
cost_sub
% The total generating cost from all parts.
total_cost=sum(cost_sub)
% Stop timing
toc
```

Function “add_Sline.m”

The function add_Sline.m is invoked from the main routines “RSB.m” and “Arbitrary.m”. This command adds the equivalent fixed demands or injections at both ends of the cutset links with the values equal the corresponding active/reactive OPF line flows. The branch flows “from” the relating buses are assigned positive values, and the flows “to” buses are assigned negative values.

Arguments:

edge_cuts	- bus indices at both ends of the cutsets linking between two separated parts.
cut_index	- indices of lines in the “Line” data that form matrix edge_cuts
Bus	- network “Bus” data
Sline	- active/reactive OPF line flows
sline_oddindex	- Sline “from” buses
sline_evenindex	- Sline “to” buses
baseMVA	- system base MVA (100MVA)

Returns:

Bus_added	- bus data after adding the equivalent fixed

demands or injections at both ends of the cutset-links.

{add_Sline.m - MATLAB code follows:}

```
function [Bus_added] = ...
    add_Sline(edge_cuts,cut_index,Bus,sline,sline_oddindex,...
    sline_evenindex,baseMVA)

% Initialize data.
Bus_added=Bus;

% Replace line flows with equivalent fixed demands "From" bus.

for index=1:length(cut_index),

    % Active line flows.
    Bus_added(edge_cuts(index,1),3)=Bus_added(edge_cuts(index,1),3)+...
        real(sline_oddindex(cut_index(index)))*baseMVA;
    % Reactive line flows.
    Bus_added(edge_cuts(index,1),4)=Bus_added(edge_cuts(index,1),4)+...
        imag(sline_oddindex(cut_index(index)))*baseMVA;

end,


% Replace line flows with equivalent fixed injections "To" bus.
for index=1:length(cut_index),

    % Active line flows.
    Bus_added(edge_cuts(index,2),3)=Bus_added(edge_cuts(index,2),3)+...
        real(sline_evenindex(cut_index(index)))*baseMVA;
    % Reactive line flows.
    Bus_added(edge_cuts(index,2),4)=Bus_added(edge_cuts(index,2),4)+...
        imag(sline_evenindex(cut_index(index)))*baseMVA;

end,
```

Function “bus_ordering.m”

The function bus_ordering.m is invoked from the main routines “RSB.m” and “find_cost.m”. This function is used to facilitate the construction of the incidence and network admittance matrices. The code re-numbers all the sub-network bus indices to have "1" as its first bus index and the rest are 1 incrementally ordered.

First, the code re-numbers the sub-network “Bus” data, and then change the sub-network “Line” and “gen” data to their corresponding indices. No change of the bus index for the sub-network “gencost” data.

Arguments:

Bus_sub	- sub-network “Bus” data
Line_sub	- sub-network “Line” data
nbus_sub	- # of sub-network buses
nline_sub	- # of sub-network lines
gen_sub	- sub-network “gen” data
gencost_sub	- sub-network “gencost” data

Returns:

Bus_sub_or - ordered sub-network “Bus” data

Line_sub_or - ordered sub-network “Line” data

gen_sub_or - ordered sub-network “gen” data

gencost_sub_or - ordered sub-network “gencost” data

{bus_ordering.m - MATLAB code follows:}

```
function [Bus_sub_or,Line_sub_or,gen_sub_or,gencost_sub_or]=...
   bus_ordering(Bus_sub,Line_sub,nbus_sub,nline_sub,gen_sub,gencost_sub)

% Initialize the values.
Bus_sub_or=Bus_sub;
Bus_sub_or(:,1)=[1:nbus_sub].';
Line_sub_or=Line_sub;

% Re-number the "Line" data of sub-network in column 1.
for index1=1:size(Line_sub,1),
   Line_sub_or(index1,1)=find(Bus_sub(:,1)==Line_sub(index1,1));
end,

% Re-number the "Line" data of subnetwork in column 2.
for index1=1:size(Line_sub,1),
   Line_sub_or(index1,2)=find(Bus_sub(:,1)==Line_sub(index1,2));
end,

% List of generator buses of the sub-network ordered data.
gen_sub_list_or1=Bus_sub_or(find(Bus_sub_or(:,2)==2),1);
gen_sub_list_or2=Bus_sub_or(find(Bus_sub_or(:,2)==3),1);
gen_sub_list_or=sort(union(gen_sub_list_or1,gen_sub_list_or2));
for index=1:length(gen_sub_list_or)
   gen_sub_list_or_final(index,1)=gen_sub_list_or(index);
end,


% Re-number the bus number of the sub-network "gen" data
```

```
gen_sub_or=gen_sub;
gen_sub_or(:,1)=gen_sub_list_or_final;

% No re-numbering in gencost_sub
gencost_sub_or=gencost_sub;
```

Function “bus_reordering.m”

The function bus_reordering.m is invoked from the main routines “RSB.m” and “find_cost.m”. Because our RSB partitioning routine uses the input data whose indices are previously ordered by the function “bus_ordering.m”, the part 1 and part 2 indices obtained are not the correct number. This function re-numbers those indices back to the original number.

Arguments:

part_1 - indices of buses in part 1

part_2 - indices of buses in part 2

Returns:

Bus_sub - sub-network “Bus” data

Bus_sub_or - sub-network “Bus” data that is previously ordered by the function “bus_ordering.m”

part_1_or - part 1 bus indices from the computation of the ordered input data

part_2_or - part 2 bus indices from the computation of the ordered input data

{bus_reordering.m - MATLAB code follows:}

```
function [part_1,part_2]=bus_reordering(Bus_sub,Bus_sub_or,...
    part_1_or,part_2_or)

% Locate the indices of "Bus_sub_or" that have the same
%   bus numbers as "part_1_or"
Find the bus indices of the Bus_sub_or
for index1=1:length(part_1_or),
    temp1(index1)=find(Bus_sub_or(:,1)==part_1_or(index1));
end,
% Use that indices to locate the true bus number of part 1
part_1=Bus_sub(temp1,1);

% Locate the indices of "Bus_sub_or" that have the same
%   bus numbers as "part_2_or"
for index2=1:length(part_2_or),
    temp2(index2)=find(Bus_sub_or(:,1)==part_2_or(index2));
```

```
end,
% Use that indices to locate the true bus number of part 2
part_2=Bus_sub(temp2,1);
```

Function "construct_jacobian.m"

The function "construct_jacobian.m" is invoked from the function "separation.m". This function constructs the network OPF Jacobian. It transfers some input data to "pflowjac.m" to formulate the partial derivative of complex powers with respect to voltage angles ($\frac{\partial \vec{S}}{\partial \delta}$) and with respect to voltage magnitudes ($\frac{\partial \vec{S}}{\partial V}$). Blocks of the power flow Jacobian in a standard form are recovered by selecting the appropriate rows and columns of the real or imaginary parts of $\frac{\partial \vec{S}}{\partial \delta}$ or $\frac{\partial \vec{S}}{\partial V}$.

Arguments:

Ybus	- network admittance matrix
vbus_final	- network complex bus voltage
slackUgen	- indices of the network slack buses and generator buses
loadlist	- indices of the network load buses

Returns:

jac_final	- resulting OPF Jacobian (no deletion of the associated slack generator components)

{construct_jacobian.m - MATLAB code follows:}

```
function [jac_final] = construct_jacobian(Ybus,vbus_final,slackUgen,loadlist)

% Use function "pflowjac.m" to create the partial derivatives
%  of COMPLEX power absorbed by the network at each bus, with
%  respect to bus voltage angles and voltage magnitudes.
[dsdd, dsdv] = pflowjac(Ybus,vbus_final);

% Construct the power flow jacobian matrix.
% No deletion of the slack generator components.
jac_final = [ ...
         real(dsdd(slackUgen,slackUgen)) real(dsdd(slackUgen,loadlist)) ...
         real(dsdv(slackUgen,loadlist)); ...

         real(dsdd(loadlist,slackUgen)) real(dsdd(loadlist,loadlist)) ...
         real(dsdv(loadlist,loadlist)); ...

         imag(dsdd(loadlist,slackUgen)) imag(dsdd(loadlist,loadlist)) ...
```

```
        imag(dsdv(loadlist,loadlist)) ];
```

Function “constructA_Y.m”

The function constructA_Y.m is invoked from the main routines “RSB.m”, “Arbitrary.m”, and “find_cost.m”. This function employs sparse matrices to construct the network incidence matrix, primitive admittance matrix, and admittance matrix. Transformers, shunt conductance, and susceptance of the sub-networks are accounted during the matrix construction. Because sparse matrices are not applicable for “fmincon.m” in our case, the resulting matrices are required to transform to the full format.

Arguments:

nbus	- # of buses
nline	- # of lines
Bus	- “Bus” data (MATPOWER format)
Line	- “Line” data (MATPOWER format)

Returns:

A	- incidence matrix
Yp	- primitive admittance matrix
Ybus	- admittance matrix

{construct_A_Y.m - MATLAB code follows:}

```
function [A,Yp,Ybus] = constructA_Y(nbus,nline,Bus,Line)

% Construct system incidence matrix A
A=sparse(nbus,2*nline);
for i=1:nline
    A(Line(i,1),i*2-1)=1;
    A(Line(i,2),i*2)=1;
end

% Construct primitive admittance matrix y,
Yp=sparse(zeros(2*nline));
```

```
for i=1:nline
  if Line(i,9)==0    % transmission block
    Yp(2*i-1,2*i-1)=1/(Line(i,3)+j*Line(i,4))+j*Line(i,5)/2;
    Yp(2*i,2*i)=Yp(2*i-1,2*i-1);
    Yp(2*i-1,2*i)=-1/(Line(i,3)+j*Line(i,4));
    Yp(2*i,2*i-1)=Yp(2*i-1,2*i);
  end
  if Line(i,9)~=0    % transformer block
    Yp(2*i-1,2*i-1)=1/((Line(i,3)+j*Line(i,4))*Line(i,9)^2);
    Yp(2*i,2*i)=1/(Line(i,3)+j*Line(i,4));
    Yp(2*i-1,2*i)=-1/((Line(i,3)+j*Line(i,4))*Line(i,9));
    Yp(2*i,2*i-1)=Yp(2*i-1,2*i);
  end
end

% Compute bus admittance matrix Y
Ybus = A*Yp*A';
for i= 1:length(Bus(:,1))   % Add shunt conductance and susceptance
  Ybus(i,i) = Ybus(i,i)+Bus(i,5)+j*Bus(i,6);
end

% "fmincon.m" solver does not preserve sparsity in solving our problems.
A=full(A);
Ybus=full(Ybus);
```

Function "dataout.m"[1]

The function dataout.m is invoked from the main routines "Arbitrary.m" and "find_cost.m", and the function "separation.m". This function displays the network bus voltage and line flow OPF results on the monitor screen. The bus voltage magnitudes

[1] This code is developed by Professor Christopher L. DeMarco for his MATLAB power flow packages.

and angles are analyzed from the complex bus voltage input data. The OPF complex line flow matrix is calculated from the product of the complex voltage difference across lines and the conjugate of the complex line currents. The branch flows "from"/"to" the relating buses are extracted from this matrix.

Arguments:

vbus	- complex bus voltage of the sub-network
aa	- network incidence matrix
bb	- network primitive admittance matrix
fromto	- matrix of network line indices
nline	- # of lines
Bus	- network "Bus" data that previously ordered by function "bus_ordering.m"
Line	- network "Line" data that previously ordered by function "bus_ordering.m"
Bus_sub	- sub-network "Bus" data
Line_sub	- sub-network "Line" data

Returns:

Sline	- vector of OPF branch flow solutions
sline_oddindex	- branch flows "from" the relating buses
sline_evenindex	- branch flows "to" the relating buses

{dataout.m - MATLAB code follows:}

```
function [sline,sline_oddindex,sline_evenindex] = ...
    dataout(vbus,aa,bb,fromto,nline,Bus,Line,Bus_sub,Line_sub)

% Convert sparse formatted data to full matrix.
fromto = full(fromto);
```

```
% Extract only for first 2 columns of the sub-network Line data.
actual_fromto = full(Line_sub(:,1:2));

disp('The current power flow solution for the study network is:')
disp('    Bus#      V p.u.  Angle-degrees')

% Bus indices.
b_indices=Bus_sub(:,1);
% Display the OPF bus voltage results on the screen.
disp(full([b_indices abs(vbus)  (180/pi)*angle(vbus)]));

% Compute line flows
% Complex voltage difference accross lines
vline=aa'*vbus;
iline=bb*vline;
sline=vline.*conj(iline);
evenindex=2*(1:nline)';
oddindex=evenindex-ones(length(evenindex),1);

% Display the OPF line flow results on the screen.
 disp('Associated Branch Flows')
 disp...
 ('                                        Power Into Line     Power Into
Line')
 disp...
 ('"From"-Bus          "To"-Bus             "From" Bus Side     "To" Bus Side')
 disp(full([actual_fromto sline(oddindex) sline(evenindex)]))

 sline_oddindex=sline(oddindex);
 sline_evenindex=sline(evenindex);


return
```

Function “edge_separators.m”

The function edge_separators.m is invoked from the main routines "RSB.m". This function finds the indices of the edge separators between the 2 sub-networks. It checks whether the bus indices of part 1 and part 2 are the indices of the lines linking between these 2 parts; those links are the edge separators.

Arguments:

part_1	- bus indices of sub-network 1
part_2	- bus indices of sub-network 2
Bus_sub	- sub-network "Bus" data
Line_sub	- sub-network "Line" data
nbus_sub	- # of buses in the Bus_sub data
nline_sub	- # of lines in the Line_sub data

Returns:

edge_cuts	- bus indices of the edge separators
cut_index	- indices of the edge_cuts matrix in the Line_sub matrix

{edge_separators.m - MATLAB code follows:}

```
function [edge_cuts,cut_index] = ...
    edge_separators(part_1,part_2,Bus_sub,Line_sub,nbus_sub,nline_sub)

% Indices of line in the sub-network.
Line_index=Line_sub(:,1:2);

% The edge-separator is the link that its one end locates at
%   part 1 and the other end locates at part 2.
for index=1:nline_sub,
temp1=ismember(Line_index(:,1),part_1);
temp2=ismember(Line_index(:,2),part_2);
end,
cut_index1=find(temp1&temp2);

% In case of reverse order numbering.
for index=1:nline_sub,
temp3=ismember(Line_index(:,1),part_2);
temp4=ismember(Line_index(:,2),part_1);
end,
cut_index2=find(temp3&temp4);

cut_index=union(cut_index1,cut_index2);

% This matrix contains bus indices of both ends of the edge separators
%   that link between the two parts.
edge_cuts=Line_index(cut_index,:);
```

Function “form_subnetwork.m”

The function form_subnetwork.m is invoked from the main routines “RSB.m” and “find_cost.m”. This function extracts the sub-network data from the MATPOWER unreduced network data using the input sub-network indices.

Arguments:

Bus	- “Bus” data (MATPOWER format)
Line	- “Line” data (MATPOWER format)
bus_sub_list	- sub-network bus indices
gen	- “gen” data (MATPOWER format)
gencost	- “gencost” data (MATPOWER format)

Returns:

Bus_sub	- sub-network “Bus” data
Line_sub	- sub-network “Line” data
gen_sub	- sub-network “gen” data
gencost_sub	- sub-network “gencost” data
nbus_sub	- # of bus indices in the Bus_sub data
nline_sub	- # of line indices in the Line_sub data

{form_subnetwork.m - MATLAB code follows:}

```
function [Bus_sub,Line_sub,gen_sub,gencost_sub,nbus_sub,nline_sub]=...
   form_subnetwork(Bus,Line,bus_sub_list,gen,gencost)

% Number of lines in the network before the bisection
nline=size(Line,1);

for index1=1:nline,
% Note: index2 is the line indices in the sub-network that are
%       in the "Line" data.
   index2(index1)=ismember(Line(index1,1),bus_sub_list)&...
                           ismember(Line(index1,2),bus_sub_list);

end,

% # of buses in the sub-network.
nbus_sub=length(bus_sub_list);

% Create new data for the sub-network
%   that contain the sub-network bus data only.
Bus_sub=Bus(bus_sub_list,:);

% Create new data for the sub-network
%   that contain sub-network line data only.
Line_sub=Line(find(index2),:);

% number of lines in sub-network
nline_sub=size(Line_sub,1);

% Find the generator buses in the sub-network (including slack)
gen_sub_list1=Bus_sub(find(Bus_sub(:,2)==2),1);
gen_sub_list2=Bus_sub(find(Bus_sub(:,2)==3),1);
gen_sub_list=sort(union(gen_sub_list1,gen_sub_list2));

% Indices of the sub-network generator buses in the "gen" data
for index=1:length(gen_sub_list),
gen_index_sub(index)=find(gen(:,1)==gen_sub_list(index));
end,

% Create the new data for the sub-network
%   that contain only the sub-network "gen" data
gen_sub=gen(gen_index_sub,:);

% Create the new data for the sub-network
%   that contain only the sub-network "gencost" data
gencost_sub=gencost(gen_index_sub,:);
```

Function “initial_condition.m”

The function initial_condition.m is invoked from the main routines “RSB.m”, “Arbitary.m”, and “find_cost.m”. This function creates the state initial values for the *fmincon* command of the Optimization Toolbox. The bus voltage magnitudes of slack and other generator buses are set to equal the values of the MATPOWER “Bus” data; each load bus voltage magnitude is set to equal 1. All voltage angles are initialized to 0. The initial values of the active power generations are set to equal the values from the MATPOWER “gen” data. The initial value state vector, x0, is created from the above bus voltage magnitudes/angles and the active power generations.

Arguments:

Bus	- “Bus” data (MATPOWER format)
baseMVA	- system base MVA (100MVA)
nbus	- # of buses
slacklist	- indices of slack generators
genlist	- indices of generators
slackUgen	- indices of both slack and generators
gen	- “gen” data (MATPOWER format)

Returns:

vbus	- complex bus voltages
Pg	- active power generations
del	- bus voltage angles
vmag	- bus voltage magnitudes

x0 - initial state vector

{initial_condition.m - MATLAB code follows:}

```
function [vbus,Pg,del,vmag,x0]=initial_condition...
   (Bus,baseMVA,nbus,slacklist,genlist,slackUgen,gen)


% Set the initial values of bus voltage data
vbus=ones(nbus,1);
vbus(slacklist)=Bus(slacklist,8);
vbus(genlist)=Bus(genlist,8);
del=angle(vbus);
vmag=abs(vbus);

% Set the initial values of the power generations
Pg=gen(:,2);

% x0 is used as an state initial value for the "fmincon" MATLAB function
x0=[Pg./baseMVA;
    del;
    vmag];
```

Function “network_data.m”

The function network_data.m is invoked from the main routines “RSB.m”, “Arbitary.m”, and “find_cost.m”. This function prepares the necessary network data for our further computation by extracting these values from the MATPOWER formatted “Bus” and “Line” data.

Arguments:

Bus	- “Bus” data (MATPOWER format)
Line	- “Line” data (MATPOWER format)

Returns:

nbus	- # of buses
nline	- # of lines
slacklist	- indices of slack generators
genlist	- indices of other generators
loadlist	- indices of load buses
slackUgen	- indices of both slack and other generators
all_list	- all bus indices
nslack	- # of slack generators
ngen	- # of other generators
nload	- # of load buses

L_sUg - # of slack and other generators

{network_data.m - MATLAB code follows:}

```
function [nbus,nline,slacklist,genlist,loadlist,slackUgen,all_list,...
      nslack,ngen,nload,L_sUg]=network_data(Bus,Line)

% Data preparation for further computation.

% Extract data from the input "Bus" and "Line" data.
% # of buses
nbus = size(Bus,1);
% # of lines
nline = size(Line,1);
% indices of the slack generators
slacklist = Bus(find(Bus(:,2)==3), 1);
% indices of other generators
genlist   = Bus(find(Bus(:,2)==2), 1);
% Bus type 4 is isolated bus and is treated as a normal load bus.
loadlist1  = Bus(find(Bus(:,2)==1), 1);
loadlist2  = Bus(find(Bus(:,2)==4), 1);
loadlist = union (loadlist1,loadlist2);

% Find indices of all generator buses.
slackUgen=union(slacklist,genlist);
% Find indices of all buses.
all_list=union(slackUgen,loadlist);
% # of slack generators.
nslack=length(slacklist);
% # of other generators.
ngen=length(genlist);
% # of load buses.
nload=length(loadlist);
% # of all generator buses.
L_sUg=length(slackUgen);
```

Function “obj_function.m”

The function obj_function.m is invoked from the main routines “Arbitary.m”, “find_cost.m”, and from the function “separation.m” (check the Optimization Toolbox’s user manual for the formatting of this function.) This function is the objective function for the optimization solver *fmincon*. The active power generations are extracted from the state vector, x. The objective cost (in $/hr) is calculated by the relationship between each active power generation and its corresponding polynomial characteristic cost function.

Arguments:

x	- the resulting state variable: active power generation and bus voltage magnitudes/angles
Ybus	- network admittance matrix
Yp	- network primitive admittance matrix
A	- network incidence matrix
Bus	- “Bus” data (MATPOWER format)
Line	- “Line” data (MATPOWER format)
baseMVA	- system base MVA (100MVA)

slacklist	- indices of slack generators
genlist	- indices of other generators
loadlist	- indices of load buses
nbus	- # of buses
gencost	- “gencost” data (MATPOWER format)
gen	- “gen” data (MATPOWER format)

Returns:

f	- the resulting objective value

{obj_function.m - MATLAB code follows:}

```
function [f] = obj_function(x,Ybus,Yp,A,Bus,Line,baseMVA,slacklist,genlist,...
   loadlist,nbus,gencost,gen)

% Indices of the slack and other generator buses
slackUgen=union(slacklist,genlist);

% Active power generations
Pg=x(1:length(slackUgen),1);

% Characteristic cost functions in quadratic form
c2=gencost(:,5);
c1=gencost(:,6);
c0=gencost(:,7);

% The objective equation
cost=(c2.*((Pg.*baseMVA).^2))+(c1.*(Pg.*baseMVA))+c0;

% The resulting objective value
f=sum(cost);
```

Function “pf_constraint.m”

The function pf_constraint.m is invoked from the main routines “Arbitary.m” and “find_cost.m”, and from the function “separation.m” (check the Optimization Toolbox’s user manual for the format ting of this function.) This function sets up both equality and inequality OPF constraints for the optimization solver “fmincon.m”. The equality constraints are the power flow mismatches that are constructed using “pfmiss.m”, and the inequality constraints are the line flow securities limits. Note that the securities limit on each bus voltage magnitude and bus active power generation is already imposed as a boundary condition in fmincon.m, so it is not considered here.

Arguments:

x	- the resulting state variable: active power generations and bus voltage magnitudes/angles
Ybus	- network admittance matrix

Yp	- network primitive admittance matrix
A	- network incidence matrix
Bus	- “Bus” data (MATPOWER format)
Line	- “Line” data (MATPOWER format)
baseMVA	- system base MVA (100MVA)
slacklist	- indices of slack generators
genlist	- indices of other generators
loadlist	- indices of load buses
nbus	- # of buses
gencost	- “gencost” data (MATPOWER format)
gen	- “gen” data (MATPOWER format)

Returns:

c	- inequality constraints
ceq	- equality constraints

{pf_constraint.m - MATLAB code follows:}

```
function [c,ceq] = pf_constraint(x,Ybus,Yp,A,Bus,Line,baseMVA,slacklist,...
   genlist,loadlist,nbus,gencost,gen)

% # of lines.
nline = size(Line,1);

% Indices of all generator buses including slack.
slackUgen=union(slacklist,genlist);
% Total # of generator buses including slack.
L_sUg=length(slackUgen);
% Indices of all buses.
all_list=union(slackUgen,loadlist);


% Assign the first rows of the state vector "x" as output generating powers.
Pg=x(1:length(slackUgen),1);
% Change the p.u. values to the real values.
gen(:,2)=Pg.*baseMVA;

% Initialize the data
snet=(1+j)*ones(nbus,1);

% Extract complex bus power demand data.
```

```
% The code assigns the negative to the injections, and
%   positive to the demand consumptions.

% Complex power injections at generator buses.
snet(slackUgen)=-(gen(:,2)-Bus(slackUgen,3)) - j*(gen(:,3)-Bus(slackUgen,4));
% Transform to p.u. values.
snet(slackUgen)=snet(slackUgen)/baseMVA;

% Complex bus power demands at load buses.
snet(loadlist)=Bus(loadlist,3)+j*Bus(loadlist,4);
% Transform to p.u. values.
snet(loadlist)=snet(loadlist)/baseMVA;

% Extract some rows of the state vector "x" for the values of
%   the bus voltage angles and magnitudes.
del=x(L_sUg+1:L_sUg+nbus);
vmag=x(L_sUg+nbus+1:L_sUg+(2.*nbus));

% Complex bus voltages.
vbus = vmag.*exp(j*del);

% Calculate power flow mismatches using the "pfmiss" command.
fullmiss = pfmiss(Ybus,vbus,snet);

% Construct the mismatch vector.
rmiss=[real(fullmiss(slackUgen));
       real(fullmiss(loadlist));
       imag(fullmiss(loadlist))];

% These power flow mismatches, actually, are
%   the equality constraints of the optimization problem.
ceq=[rmiss];



% The below section is for constructing the inequality constraints.
% Note that the limits on voltage magnitudes and power generating outputs
%   are already considered in the upper/lower boundary conditions
%   of the "fmincon" function.

% Construct the constraints on the line flow limits.

% Complex voltage differences across lines.
vline=A.'*vbus;
iline=Yp*vline;
pline=vline.*conj(iline);
evenindex=2*(1:nline)';
oddindex=evenindex-ones(length(evenindex),1);

% The code puts constraints at both ends of the lines: leaving and entering.
c=[real(pline(oddindex))-(Line(:,6)./baseMVA);
   real(pline(evenindex))-(Line(:,6)./baseMVA)];
```

Function “pflowjac.m”[2]

The function pflowjac.m is invoked from the function “construct_jacobian.m”. This function forms the matrix of partial derivative of complex power absorbed by the network at each bus with respect to bus voltage angle and voltage magnitude.

The operation of this routine is illustrated as following (see equation (9) and (10) also):

S = diag(vbus)*conj(ibus) = diag(conj(ibus))*vbus;

[2] This code is developed by Professor Christopher L. DeMarco for his MATLAB power flow packages.

Hence:

dS/d(delta) = diag(vbus)*conj(d(ibus)/d(delta)) +
diag(conj(ibus))*d(vbus)/d(delta)

Similarly:

dS/d(vmag) = diag(vbus)*conj(d(ibus)/d(vmag)) +
diag(conj(ibus))*d(vbus)/d(vmag)

Arguments:

Y	- admittance matrix
vbus	- complex bus voltages

Returns:

dSdd	- partial derivatives of complex powers with respect to voltage angles
dSdv	- partial derivatives of complex powers with respect to voltage magnitudes

{pflowjac.m - MATLAB code follows:}

```
function [dSdd , dSdv] = pflowjac(Y,vbus)


% Transform matrices into sparse format.
Y=sparse(Y);
vbus=sparse(vbus);

ibus=Y*vbus;

% Complex power absorbed by the network at each bus, with
%   respect to bus voltage angles.
dSdd =j*diag(conj(ibus).*vbus) ...
```

```
         -j*diag(vbus)*conj(Y)*diag(conj(vbus));

% Complex power absorbed by the network at each bus, with
%   respect to bus voltage magnitudes.
dSdv = diag(conj(ibus).*(vbus./abs(vbus)))+ ...
          diag(vbus)*conj(Y)*diag(conj(vbus)./abs(vbus));
```

Function "pfmiss.m"[3]

The function pfmiss.m is invoked from the function "pf_constraint.m". This function forms the vector of complex power mismatch at each bus. From equation (9)

[3] This code is developed by Professor Christopher L. DeMarco for his MATLAB power flow packages.

$$\vec{S} = \vec{V} .*\text{conj}(\vec{I}) \;=\; \text{conj}(\vec{I}).*(\vec{V})$$

$\vec{V} \in \boldsymbol{C}^n$, $\vec{V}$:= vector of complex bus voltages; note that $\vec{V} = V.*\exp(j\delta)$

$\vec{I} \in \boldsymbol{C}^n$, $\vec{I}$:= vector of externally injected current at buses ($\vec{I} = \vec{Y} * \vec{V}$)

$\vec{Y} \in \boldsymbol{C}^{nxn}$, $\vec{Y}$:= full bus admittance matrix (reference bus rows and column not eliminated)

$\vec{S} \in \boldsymbol{C}^n$, $\vec{S}$:= vector of externally injected power at buses

The function returns mismatches at all buses (no deletion of the slack mismatch component.) Power leaving the bus is treated as positive sign; that entering the bus is treated as negative sign.

Arguments:

Ybus	- complex bus admittance matrix
vbus	- vector of complex bus voltage phasors
s_net_demand	- vector of complex bus power demand

Returns:

nmiss	- a full complex n-vector of power mismatches

{pfmiss.m - MATLAB code follows:}

```
function nmiss = pfmiss(Ybus,vbus,s_net_demand)
```

```
ibus=Ybus*vbus;

% The vector of complex power mismatch at each bus.
nmiss = vbus.*conj(ibus)+s_net_demand;
```

Function “separation.m”

The function separation.m is invoked from the main routines “RSB.m”. The RSB partitioning is occurred here. The function sets the OPF state solutions lower and upper boundaries for the “fmincon” solver. Each resulting Lagrange multiplier and OPF state solution is displayed on the monitor screen. The network Jacobian is constructed using the function “construct_jacobian.m”. The OPF branch flows are determined by “dataout.m”, and the results are displayed on the screen. The code uses “eigs” command to calculate the Fiedler value/vector of the OPF Jacobian. Because the structure of the Jacobian matrix have the components associated with the slack bus in its first rows, each index of the second null is incorrectly numbered. To assign the correct bus indices, this second null is re-numbered during this process. The RSB method assigns buses whose indices above the median value of the Fiedler vector to the one part and the below the median value to the other. Warning message is displayed if any error occurs.

Arguments:

del	- bus voltage angles
x0	- initial state vector
Ybus	- bus admittance matrix
Yp	- primitive bus admittance matrix
A	- incidence matrix
Bus	- “Bus” data (MATPOWER format)
Line	- “Line” data (MATPOWER format)
baseMVA	- system base MVA (100MVA)
slacklist	- indices of slack bus
genlist	- indices of other generator buses
loadlist	- indices of load buses
nbus	- # of buses
gencost	- “gencost” data (MATPOWER format)
gen	- “gen” data (MATPOWER format)
slackUgen	- indices of slack and other generator buses
L_sUg	- # of slack and other generator buses

Bus_sub - sub-network “Bus” data (MATPOWER format)

Line_sub - sub-network “Line” data (MATPOWER format)

Returns:

fval - objective cost value ($/hr)

part_1_or - re-numbered indices of bus in part 1

part_2_or - re-numbered indices of bus in part 2

second_smallest_eig - Fiedler value of the OPF Jacobian

sline - vector of OPF branch flow solutions

sline_oddindex - branch flows “from” the relating buses

sline_evenindex - branch flows “to” the relating buses

{separation.m - MATLAB code follows:}

```
function [fval,part_1_or,part_2_or,second_smallest_eig,...
        sline,sline_oddindex,sline_evenindex]=...
   separation(del,x0,Ybus,Yp,A,Bus,Line,baseMVA,slacklist,...
   genlist,loadlist,nbus,gencost,gen,slackUgen,L_sUg,Bus_sub,Line_sub)

% Set the lower boundaries of the state variables, "x".
lower_bound=[gen(:,10)./baseMVA;
            -inf.*ones(length(del),1);
            Bus(:,13)];

% Set the upper boundaries of the state variables, "x".
upper_bound=[gen(:,9)./baseMVA;
             inf.*ones(length(del),1);
             Bus(:,12)];

% Use "fmincon" in Optimization toolbox 2.0
% See the user manuals for details
options = optimset('Display','iter','Diagnostics','on');
[x,fval,exitflag,output,lamda]=fmincon('obj_function',x0,[],[],[],[],...
    lower_bound,upper_bound,'pf_constraint',options,Ybus,Yp,A,Bus,...
    Line,baseMVA,slacklist,genlist,loadlist,nbus,gencost,gen);

% These values are the Lagrange multipliers:
% for the lower boundaries of the state variables
lamda_lower=lamda.lower
% for the upper boundaries of the state variables
lamda_upper=lamda.upper
% for the linear inequality constraints
lamda_ineqlin=lamda.ineqlin
% for the linear equality constraints
lamda_eqlin=lamda.eqlin
% for the nonlinear inequality constraints
lamda_ineqnonlin=lamda.ineqnonlin
% for the nonlinear equality constraints
lamda_eqnonlin=lamda.eqnonlin

% Extract data from the resulted "x".
```

```
% Bus voltage angles.
del_final=x(L_sUg+1:L_sUg+nbus);
% Bus voltage magnitudes.
vmag_final=x(L_sUg+nbus+1:L_sUg+(2.*nbus));
% Complex bus voltages.
vbus_final = vmag_final.*exp(j*del_final);

% Construct the network Jacobian from this OPF operation.
% This Jacobian contains the elements associated with the slack bus also
[jac_final] = construct_jacobian(Ybus,vbus_final,slackUgen,loadlist);

% Display the resulting OPF solution on the screen.
OPF_Pg=baseMVA.*x(1:size(gen,1));
OPF_v=x((size(gen,1)+1):size(x,1));
OPF_solution=[OPF_Pg;
              OPF_v]

% Show the resulting power flow solutions on the screen.
nline = size(Line,1)
fromto = Line(:,1:2)

% The "cline" is complex line flow at two ends (from bus to network).
% It is the "sline" in the "dataout" function.

% "Bus", "Line" here actually are "Bus_sub_or","Line_sub_or"
[sline,sline_oddindex,sline_evenindex] = ...
    dataout(vbus_final,A,Yp,fromto,nline,Bus,Line,Bus_sub,Line_sub);

% Calculate the 2 smallest eigen-values of the sparse Jacobian matrix.
options.disp = 0;
jac_final=sparse(jac_final);
block_jac_final=jac_final(1:nbus,1:nbus);
[rjac_vec_final,rjac_val_final,FLAG] = eigs(block_jac_final,2,0,options);

% Display below message if not converged.
   if FLAG == 1,
   disp('not converge for the "eigs" command for eigenvector calculation');
      return
   end,
```

```
% The diagonal vector of the resulting eigenvalue matrix.
   diag_rjac_val_2min_final=diag(rjac_val_final)
   rjac_vec_2min_final=rjac_vec_final

% Sometimes, "eigs" command produces the resulting eigenvalues that
%   are not numerically increasing ordered.
   if diag_rjac_val_2min_final(1)>diag_rjac_val_2min_final(2),

       second_null_gl=rjac_vec_2min_final(:,1)
       second_smallest_eig=max(diag_rjac_val_2min_final)
   end

   if diag_rjac_val_2min_final(2)>diag_rjac_val_2min_final(1),

       second_null_gl=rjac_vec_2min_final(:,2)
       second_smallest_eig=max(diag_rjac_val_2min_final)
   end

   % Because the approach constructs the Jacobian matrix
   %    to have the generator and slack buses associated components
   %    in its first rows,
   %    each index of the second null is incorrectly numbered.
   % To assign the correct index number, this second null is re-numbered.
   %
   %    Note:
   %    The results obtained are still needed
   %    to enter to the "bus_reording.m" again.
second_null_or(slackUgen,1)=second_null_gl(1:length(slackUgen),1);
second_null_or(loadlist,1)=...
    second_null_gl(length(slackUgen)+1:length(slackUgen)+length(loadlist),1);

   median_second_null_or=median(second_null_or(1:nbus))

% Assign buses whose indices above the median value of the Fiedler vector
%   to one sub-network, and the below the median value to the other.
   part_1_or=find(second_null_or(1:nbus)>median_second_null_or);
   part_2_or=find(second_null_or(1:nbus)<median_second_null_or);

   % For some cases, some elements are exactly equal to the median value.
   temp_part=find(second_null_or(1:nbus)==median_second_null_or);
```

```
% Check to see whether part 1 contain generator or slack buses
temp_slackUgen_part1=any(ismember(part_1_or,slackUgen));
% Check to see whether part 2 contain generator or slack buses
temp_slackUgen_part2=any(ismember(part_2_or,slackUgen));
% These buses are assigned to the part that contain no gen.
if (temp_slackUgen_part1==0)&(temp_slackUgen_part2==1),
    part_1_or=union(part_1_or,temp_part);
end,
if (temp_slackUgen_part2==0)&(temp_slackUgen_part1==1),
    part_2_or=union(part_2_or,temp_part);
end,

% In case both parts already have generator buses,
%    these elements are arbitrarily assigned to part2
if (temp_slackUgen_part1==1)&(temp_slackUgen_part2==1),
    part_2_or=union(part_2_or,temp_part);
end,

% The code checks again to see
%   whether part 1 contain any generator or slack buses.
new_temp_slackUgen_part1=any(ismember(part_1_or,slackUgen));

% The code checks again to see
%   whether part 2 contain any generator or slack buses.
new_temp_slackUgen_part2=any(ismember(part_2_or,slackUgen));

% Warning if there are no generators in either part
if (new_temp_slackUgen_part1==0)|(new_temp_slackUgen_part2==0),
   warning('error : no gen or slack in either part');
   % Debug if the above warning occurred
   dbstop if warning
end,
```

Function "UPDATESep.m"[4]

The function UPDATESep.m is invoked from the main routines "RSB.m". The new separation matrix "Sepnew" is first obtained as the old separation matrix "Sep". All entries in the column, corresponding to the separated part, are set to zero. Then, in this column the buses of part_1 are entered. The buses of part_2 are assigned to the new column of Sepnew. The part of the network, contained in the column "seppt" of Sep, has been separated in part_1 and part_2. Therefore, Sepnew has one column, i.e., part, more than Sep and as many rows as there are buses in the biggest part of the network after the current separation.

Arguments:

Sep	- separation matrix before current partition
seppt	- part that has been separated
part_1	- bus indices of part 1 after separation of sub-network
part_2	- bus indices of part 2 after separation of sub-network

Returns:

Sepnew	- separation matrix after current partition

[4] This code is developed by Professor Christopher L. DeMarco and Juergen Wassner for their work in [7].

{UPDATESep.m - MATLAB code follows:}

```
function Sepnew=UPDATESep(Sep,seppt,part_1,part_2)

% # of parts.
npart=size(Sep,2);
% Total bus #.
nbus=size(Sep,1);

% # of buses in part1
nbus1=length(part_1);
% # of buses in part2
nbus2=length(part_2);

% Initialize data
Sepnew=Sep(:,1:npart);
Sepnew(:,seppt)=zeros(nbus,1);

% Assign buses in part1 into the same column using for the partition steps.
Sepnew(1:nbus1,seppt)=part_1;
% Create a new column for matrix Sepnew and assign buses in part2
%   into that new column
Sepnew(1:nbus2,npart+1)=part_2;
```

Function "UPDATESm.m"[5]

The function UPDATESm.m is invoked from the main routines "RSB.m". This function updates the matrix "Sm" and determines the part that is separated in the next step. First, the matrix Sm is updated according to the separation matrix Sep (see function UPDATESep.m). The information referring to the new part 1 is entered in the column of the currently separated part seppt. Then, by extending Sm by one column, the values for part 2 are entered. Afterwards, in sep_cand all parts with more than one generator bus are found. Among all these parts in "minidx" the part with the Fiedler value is determined and stored as return variable seppt.

Arguments:

Sm	- contains Fiedler values and the # of generators within every part
seppt	- part that has been separated
gen1	- # of generators within new part 1
gen2	- # of generators within new part 2
sm1	- Fiedler value of part 1

[5] This code is developed by Professor Christopher L. DeMarco and Juergen Wassner for their work in [7].

sm2 - Fiedler value of part 2

Returns:

Sm - updated matrix of Fiedler values

seppt - part that is separated in the next step

{UPDATESm.m - MATLAB code follows:}

```
function[Sm,seppt]=UPDATESm(Sm,seppt,gen1,gen2,sm1,sm2)

% # of parts.
npart=size(Sm,2);

% # of generator buses in part1.
Sm(1,seppt)=gen1;
% The Fiedler value of power flow Jacobian of part1.
Sm(2,seppt)=sm1;

% Create new column for matrix Sm and assign
%   # of generator buses in part2 into the row 1 of that new column.
Sm(1,npart+1)=gen2;
% Assign the Fiedler value of power flow Jacobian of part2
%    into the row 2 of that new column.
Sm(2,npart+1)=sm2;

% The following steps finds the next part to be partitioned next.
% The candidate parts contain more than one generator.
sep_cand=find(Sm(1,:)>1);
% The code selects to partition in the part that has smallest Fiedler value.
[dum,minidx]=min(Sm(2,sep_cand));
seppt=sep_cand(minidx);
```

Bibliography

[1] A.J. van der Schaft. L_2–*Gain and Passivity Techniques in Nonlinear ContRol*. Springer–Verlag, London Berlin Heidelberg New York Barcelona Hong Kong Milan Paris Santa Clara Singapore Tokyo, 1996.

[2] Arthur R. Bergen. *Power System Analysis*. PRENTICE–HALL, Englewood Cliffs, NJ, 07623, 1986.

[3] Bronstein,I.N. und Semendjajew,K.A. *Taschenbuch der Mathematik*. Verlag Harri Deutsch, Frankfurt(Main), 1983.

[4] Chi-Tsong Chen. *Linear System Theory and Design*. Holt, Rinehart and Winston, Inc., New York – Chicago – San Francisco – Philadelphia – Montreal – Toronto – London – Sydney – Tokyo – Mexico City – Rio de Janeiro – Madrid, 1970.

[5] Christopher L. DeMarco, J.V. Sarlashkar, and F.L. Alvarado. The potential for malicous control in a competitive power systems environment. In *Proc. IEEE Conference on Control Applications*, pages 462–467, Dearborn, MI, Sept 18–20 1996. first appearing as University of Wisconsin–Madison, Department of Electrical and Computer Engineering memorandum ECE-95-10, August 1995.

[6] Christopher L. DeMarco. Design of Predatory Generation Control in Electrical Systems. Project note University of Wisconsin–Madison, Department of Electrical and Computere Engineering.

[7] C.A. Desoer. *Notes For A Second Course On Linear Systems*. D. Van Nostrand Company, New York Cincinnati Toronto London Melbourne, 1975.

[8] C.A. Desoer and M. Vidyasagar. *Feedback Systems: Input–Output Properties.* Academic Press, New York San Francisco London, 1975.

[9] Thomas Gorski. Malicious control of a power system through eigenvector placement. Master's thesis, University of Wisconsin–Madison, Department of Electrical and Computer Engineering, 1415 Engineering Drive; Madison, WI 53706, 1995.

[10] H.L. Trentelmann and J.C. Willems. *Essays on control: Perspectives in the theory and its application.* Birkhäuser, Boston Basel Berlin, 1993.

[11] H.Nijmeijer, A.J. van der Schaft. *Nonlinear dynamical control systems.* Springer–Verlag, New York Berlin Heidelberg London Paris Tokyo Hong Kong, 1990.

[12] Alberto Isidori. *Nonlinear Control Systems, 2.Edition.* Springer–Verlag, Berlin, 1989.

[13] Jan.C.Willems. *Stability theory of dynamical systems.* NELSON, London Nairobi Dar es Salaam Accra San Fernando (Trinidad), 1971.

[14] J.C.Willems. *The analysis of feedback systems.* The M.I.T. Press, Cambridge, Massachusetts, and London, England, 1971.

[15] Jörg Raisch. *Mehrgrössenregelung im Frequenzbereich.* R.Oldenburg Verlag München Wien, München Wien, 1994.

[16] Gerald J. Kirwin and Stephen E. Grodzinsky. *Basic Circuit Analysis.* Houghton Mifflin Company, Dallas Geneva, IL Hopewell,NJ Palo Alto London, 1980.

[17] J.M. Maciejowski. *Multivariable Feedback Design.* Addison–Wesley Publishing Company, Wokingham, England – Reading, Massachusetts – Menlo Park, California – New York – Don Mills, Ontario – Amsterdam – Bonn – Sydney – Singapore – Tokyo – Madrid – San Juan, 1989.

[18] B.C. Moore. Principal component analysis in linear systems: controllability, observability, and model reduction. *IEEE Transactions on Automatic Control*, AC(27):17–27, 1981.

[19] R.D. Strum and J.R. Ward. *Electric Circuits and Networks.* Quantum Publishers, Inc., 257 Park Avenue South, New York, NY 10010, 1973.

[20] Thomas E. Fortmann and Darrell Williamson. Design of low–order observers for linear feedback control laws. *IEEE Transactions on Automatic Control*, 1972.

[21] Thomas Kailath. *Linear Systems.* Prentice–Hall, Englewood Cliffs, 1980.

[22] E.D. Gilles und U. Knöpp. *Skriptum zur Vorlesung Regelungstechnik II, Analyse und Synthese von Regelsystemen im Zustandsraum.* Universität Stuttgart, Institut für Systemdynamik und Regelungstechnik (ISR), Stuttgart, Germany, 1993.

[23] Uwe Helmke and John B. Moore. *Optimization and Dynamical Systems.* Springer–Verlag, London Berlin Heidelberg New York Paris Tokyo Hong Kong Barcelona Budapest, 1994.

[24] Jan C. Willems. Dissipative Dynamical Systems Part I: General Theory. *Archive for Rational Mechanics and Analysis*, 45(5):321–351, 1972.

[25] Jan C. Willems. Dissipative Dynamical Systems Part II: Linear Systems with quadratic Suply Rates. *Archive for Rational Mechanics and Analysis*, 45(5):352–393, 1972.

[26] Willems, Bittanti, Laub. *The Ricatti Equation.* Springer–Verlag, London Berlin Heidelberg New York Paris Tokyo Hong Kong Barcelona Budapest, 1980.